CONTROLLED HEPARIN-BASED DELIVERY STRATEGIES TO PROMOTE MUSCULOSKELETAL TISSUE REGENERATION AFTER INJURY

A Dissertation
Presented to
The Academic Faculty

By

Liane Elizabeth Tellier

In Partial Fulfillment
Of the Requirements for the Degree
Doctor of Philosophy in Biomedical Engineering

Georgia Institute of Technology
& Emory University

December 2018

CONTROLLED HEPARIN-BASED DELIVERY STRATEGIES TO PROMOTE MUSCULOSKELETAL TISSUE REGENERATION AFTER INJURY

Approved by:

Dr. Johnna S. Temenoff, PhD, Advisor
Department of Biomedical Engineering
Georgia Institute of Technology & Emory University

Dr. Claude D. Jarrett, MD
Wilmington Health Orthopedic Medical Center

Dr. Edward A. Botchwey, PhD
Department of Biomedical Engineering
Georgia Institute of Technology & Emory University

Dr. Nick J. Willett, PhD
Department of Biomedical Engineering
Georgia Institute of Technology & Emory University

Dr. Robert E. Guldberg, PhD
Department of Mechanical Engineering
Georgia Institute of Technology

Date Approved: July 26, 2018

ACKNOWLEDGEMENTS

I'd like to thank my advisor, Johnna, who encouraged me to aim high from the very beginning and supported me in accomplishing great things throughout my five years at Georgia Tech. My committee members were also instrumental in my graduate work. Dr. Nick Willett and Dr. Claude Jarrett spent many hours helping to establish the animal models used in my work, and Dr. Bob Guldberg and Dr. Ed Botchwey provided expertise to better my thesis. All four committee members made themselves available whenever needed, and their support was incredibly encouraging over the years.

To the "T lab": Dr. Song Seto and Dr. Tobias Miller were the older, wiser lab mates and Melissa Goude was my mentor in my 1st year, and they were all willing to share their knowledge and expertise with me. Dr. Jen Lei and Dr. Torri Rinker became my close friends after an initial phase where they wouldn't speak to me but would talk to each other by shouting over my cubicle. We were and still are a sisterhood where I can ask scientific questions, share ridiculous stories, and vent about anything, and I cherish these friendships. Jennifer McFaline-Figueroa, Elda Trevino, and I spent many hours together working on our animal models during my 3rd and 4th year, and I enjoyed being a part of that well-oiled team. Dr. Molly Ogle also joined the lab as a post-doc and has offered so much knowledge and guidance in the short time I have known her. We need more people like her as professors and faculty in academia. Finally, Gilad Doron and Leah Anderson have also joined in the past few years, and are both extremely bright and hardworking which makes me excited to see where their work takes them over the next few years.

To my friends: My closest undergraduate friends, Maggie Phillips, Meghan Kellett, and Dr. Sam Stuek remind me of our more care-free times as college students and provide a good laugh whenever I need it. We are all across the country now and they are all doing amazing things in science and medicine. I am lucky to have them. My Georgia Tech friends, Iris, Jose, David, Shannon, Casey, Marissa, Chad, Michael, Kristin, and especially Ali Brimeyer and Muaz Rushdi have all helped me get to the end in some way. Thank you.

To my family: My mom is the brightest person I know, extremely intelligent but also bubbly and positive, and I have tried to emulate those qualities in her all my life. My pragmatism, dedication to work and family, and (at times) my stubbornness has all come from my dad, and those qualities have been instrumental in getting to where I am today. I'm happy to be a little like both of my parents, and I am grateful to them for encouraging me to pursue a PhD. Over the years, I've also come to realize my brother, Kevin, and I are very similar. He is brilliant and passionate, and has been a genuine source of support for me.

Finally, to my fiancé Dan: Dan and I met in my first semester at Georgia Tech, and I'm lucky to have had him by my side ever since. I've been fortunate to meet his entire extended family many times in Florida, Ohio, and Utah, and have always felt so welcome for holidays, weddings, skiing, and Mucky Duck crunchy grouper consumption. Though Dan has many qualities that I greatly admire, his happy and care-free attitude towards life has brightened mine more than I could imagine, and he makes me confident that we can conquer anything together. Thank you bud.

TABLE OF CONTENTS

LIST OF TABLES

LIST OF FIGURES

LIST OF ABBREVIATIONS

^{1}H NMR	*Proton nuclear magnetic resonance*
AcCl	*Acryloyl chloride*
ACL	*Anterior cruciate ligament*
ALP	*Alkaline phosphatase*
AM	*Anti-inflammatory monocyte*
ANOVA	*Analysis of variance*
APMAm	*N-(3-Aminopropyl) methacrylamide hydrochloride*
BMP-2	*Bone morphogenetic protein-2*
BSA	*Bovine serum albumin*
C4S	*Chondroitin-4 sulfate*
CCRC	*University of Georgia Complex Carbohydrate Research Center*
CS	*Chondroitin sulfate*
CT	*Computed tomography*
CUB	*C1r/C1s-, uEGF-, BMP-1-like*
CXCR4	*CXC chemokine receptor type 4*
DCM	*Dichloromethane*
DMD	*Duchenne muscular dystrophy*
DMEM	*Dulbecco's modified eagle medium*
DMOADS	*Disease modifying osteoarthritis drugs*
DMSO	*Dimethyl sulfoxide*
DsDNA	*Double stranded DNA*

DT	*Dithiothreitol*
ECM	*Extracellular matrix*
EDC	*1-Ethyl-3-(3-dimethylaminopropyl)-carbodiimide*
EGF	*Epidermal growth factor*
eMHC	*Embryonic myosin heavy chain*
EPIC-uCT	*Equilibrium partitioning of an ionic contrast agent – microcomputed tomography*
ESC	*Embryonic stem cells*
FBS	*Fetal bovine serum*
FGF	*Fibroblast growth factor*
G-CSF	*Granulocyte colony stimulating factor*
GAG	*Glycosaminoglycan*
GPCR	*G-protein coupled receptor*
HA	*Hyaluronic acid*
Hep	*Natively sulfated heparin*
Hep-	*Fully desulfated heparin*
$Hep^{-6O,N}$	*6O,N-desulfated heparin*
Hep^{-N}	*N-desulfated heparin*
HGF	*Hepatocyte growth factor*
HGH	*Human growth hormone*
HHGS	*Histological/Histochemical Grading System*
HIV	*Human immunodeficiency virus*
HOBt	*Hydroxybenzotriazole*
HSPC	*Hematopoietic stem and progenitor cells*

IGF-1	*Insulin-like growth factor-1*
IL	*Interleukin*
IM	*Inflammatory monocyte*
I.P.	*Intraperitoneal injection*
Iαl	*Inter-alpha-inhibitor*
LSK	*$Lin^{neg}Sca\text{-}1^{+}c\text{-}Kit^{+}$*
MAm	*Methacrylamide*
MCP-1	*Monocyte chemoattractant protein-1*
MDSC	*Muscle-derived stem cells*
MIA	*Monosodium iodoacetate*
MMP	*Matrix metalloproteinase*
MMT	*Medial meniscal transection*
MP	*Microparticle*
MRI	*Magnetic resonance imaging*
MSC	*Mesenchymal stem cells*
NGF	*Nerve growth factor*
NMP	*N-methylpyrrolidone*
NSAIDS	*Non-steroidal anti-inflammatory drugs*
OA	*Osteoarthritis*
OARSI	*Osteoarthritis Research Society International*
OCT	*Optimum cutting temperature*
PCA	*Principal component analysis*
PBS	*Phosphate buffered saline*
PDGF-BB	*Platelet derived growth factor-BB*

PEDF	*Pigment epithelium-derived factor*
PEG	*Poly (ethylene glycol)*
PEGDA	*PEG-diacrylate*
PFA	*Paraformaldehyde*
PHD	*HIF prolyl 4-hydroxylases*
PLGA	*Poly(lactic-co glycolic acid)*
PLSDA	*Partial least squares discriminate analysis*
PRP	*Platelet rich plasma*
RA	*Rheumatoid arthritis*
ROI	*Region of interest*
S1P	*Sphingosine 1 phosphate*
SAX-HPLC	*Strong anion exchange high performance liquid*
SDF-1α	*Stromal cell-derived factor-1alpha*
SIS-ECM	*Porcine-derived small intestinal submucosa*
SMC	*Smooth muscle cell*
Sulfo-NHS	*N-hydroxysulfosuccinimide*
TCEP	*Tris-(2-carboxyethyl)-phosphine*
TEA	*Triethylamine*
TGF-B	*Transforming growth factor-beta*
TNF-α	*Tumor necrosis factor-alpha*
TSG-6	*Tumor necrosis factor-alpha stimulated gene-6*
VEGF	*Vascular endothelial growth factor*

SUMMARY

Despite the prevalence of musculoskeletal disorders, one of the leading causes of work-related disability in the United States, effective therapeutic delivery to the affected musculoskeletal tissues such as bone, cartilage, and muscle remains a significant challenge. Thus, the long term goal of this research was to develop a tunable biomaterial-based system for the delivery of regenerative therapeutics to musculoskeletal tissues. This goal was approached through the engineering of a heparin-based microparticle (MP) system with tunable heparin sulfation, heparin content, and hydrolytic degradation, which was subsequently employed for *in vitro* release of an osteoinductive growth factor and *in vivo* delivery of a chondroprotective anti-inflammatory protein and a chemokine capable of recruiting pro-regenerative cells to muscle.

In aim 1, hydrolytically-degradable, heparin-based MPs were fabricated containing heparin derivatives of varying levels of sulfation, and N-desulfated heparin MPs were found to efficiently load and release an osteoinductive growth factor, bone morphogenetic protein-2 (BMP-2), *in vitro*. In aim 2, heparin-based MPs were loaded with tumor necrosis factor-α stimulated gene-6 (TSG-6), an anti-inflammatory protein known to inhibit plasmin, and delivered via intra-articular injection to rat knees in the context of post-traumatic osteoarthritis. After 21 days, TSG-6 loaded MPs reduced cartilage damage following injury, whereas a 3X higher dose of soluble TSG-6 did not, suggesting that Hep^{-N} can enhance TSG-6 bioactivity *in vivo* and that Hep^{-N}-based MPs can effectively deliver a chondroprotective protein for cartilage regeneration. Finally, in aim 3, heparin-based MPs were loaded with the chemokine stromal cell-derived factor-1α (SDF-1α) and delivered via local injection to the supraspinatus muscle in combination

with systemic delivery of the bone marrow mobilizing agent, VPC01091, following severe rotator cuff injury in rats. Co-delivery of SDF-1α loaded MPs and VPC01091 led to significant modulation of the inflammatory cellular milieu and mesenchymal stem cell population in muscle 3 and 7 days following injury, along with significantly more regenerating muscle fibers compared to either treatment alone.

Overall, in this thesis, heparin-based MPs were utilized to deliver therapeutics capable of stimulating endogenous healing processes in two unique contexts of cartilage and muscle degeneration. Given the tunability of the MP system and the ability for heparin to bind and interact with a myriad of proteins, the application of heparin-based MPs extends beyond cartilage and muscle, and may be used for a wide range of applications where controlled release of bioactive positively-charged therapeutics is required.

CHAPTER 1

1.1 MOTIVATION

Despite the prevalence of musculoskeletal disorders, one of the leading causes of work-related disability in the United States [1], effective therapeutic delivery to the affected musculoskeletal tissues such as bone, cartilage, and muscle remains a significant challenge [2]. Though systemic drug delivery may be an option for some conditions, supraphysiological doses are often required which can be costly and result in adverse side effects for the patient [3–6]. Local delivery strategies may alleviate these shortcomings, but methods that require additional invasive surgical procedures may have limited clinical application as well. Moreover, in many musculoskeletal disorders, the affected and degenerating musculoskeletal tissues lie within the joint space, which presents an additional challenge to effectively target and treat these tissues [7].

Once delivered to the site of injury or disease, controlled and sustained release of drugs for many musculoskeletal conditions is also critical. Though dependent on many factors, soluble proteins and small molecules are often rapidly cleared from the site of delivery [6–8], limiting therapeutic efficacy, and for chronic and progressive disorders, sustained release of therapeutics may be beneficial and reduce the number of repeat injections required. For these reasons, among others, treatment strategies are in high demand for degenerating tissues in many musculoskeletal conditions.

The research presented in this thesis strives to develop a tunable biomaterial-based platform for the facile delivery of regenerative therapeutics for musculoskeletal tissues including bone, cartilage, and muscle. Though a myriad of hydrogel-based drug delivery

systems exist [9–12], microparticles are advantageous as they are injectable using standard needles and syringes without an invasive surgical procedure, which may facilitate clinical translation of these biomaterials [13–16]. Furthermore, particularly advantageous for musculoskeletal diseases, microparticles can be injected directly into muscle, tendon, or into the joint space for treatment of articular cartilage and bone.

Furthermore, our laboratory and others have focused on the development of microparticles containing heparin, a highly sulfated glycosaminoglycan (GAG) that can bind with a myriad of positively-charged proteins through sequence-specific interactions and, primarily due to heparin's sulfate groups, electrostatic interactions [9,14,17–19]. That said, though we and others have previously employed heparin-based biomaterials to load and release positively-charged proteins, varying heparin sulfation may be a method to further tune heparin-protein electrostatic interactions and, in turn, modulate protein release. Thus, alteration and assessment of heparin sulfation level, as well as heparin content and hydrolytic degradation of microparticles, may be a novel approach to develop a more tunable therapeutic delivery platform.

Through binding and interacting with proteins, heparin has also shown to protect and even enhance protein bioactivity, potentially enhancing their therapeutic efficacy *in vivo* [20–22]. However, few studies have investigated how heparin sulfation affects protein bioactivity, especially in the context of musculoskeletal tissue regeneration. Furthermore, varying heparin content and heparin sulfation within microparticles may further modulate protein release and bioactivity, which has never been assessed previously. Thus, the development of a heparin-based microparticle platform may

facilitate systematic evaluation of how heparin sulfation, among other variables, affects therapeutic release and bioactivity when delivered *in vitro* and *in vivo*.

1.2 Research Objectives

Overall, the ***long term goal*** of this research was to develop a tunable biomaterial-based system for the delivery of regenerative therapeutics for musculoskeletal tissue including bone, cartilage, and muscle. This goal was achieved through the engineering of a heparin-based microparticle system with tunable heparin sulfation, heparin content, and hydrolytic degradation, which was subsequently employed for *in vitro* release of an osteoinductive growth factor and *in vivo* delivery of a chondroprotective anti-inflammatory protein and a chemokine capable of recruiting pro-regenerative cells to muscle.

First, a tunable heparin-based microparticle system was developed through the modulation of hydrolytic degradation, heparin sulfation, and heparin content within microparticles to, in turn, vary the *in vitro* loading, release, and bioactivity of an osteoinductive growth factor, BMP-2. Then, a single formulation, hydrolytically degradable N-desulfated heparin-based microparticles, was assessed as an *in vivo* delivery vehicle for two musculoskeletal tissues, cartilage and muscle, in two unique injury contexts. First, heparin-based microparticles were utilized to deliver the anti-inflammatory protein TSG-6 to reduce cartilage degeneration in a rat model of post-traumatic osteoarthritis and second, to deliver the chemokine SDF-1α alone or in combination with systemic delivery of a bone marrow mobilizing agent, VPC01091, to recruit pro-regenerative cells to muscle in a rat model of severe rotator cuff tear.

The ***overarching rationale*** for this project is that the engineering of a heparin-based drug delivery platform can be utilized to deliver bioactive therapeutics for musculoskeletal tissues including cartilage and muscle. The ***overall hypothesis*** of this work is that heparin-based microparticles can be tuned to efficiently deliver bioactive proteins *in vitro* and *in vivo*, thereby preventing cartilage degeneration in the context of post-traumatic osteoarthritis via an anti-inflammatory protein and promoting a pro-regenerative cellular milieu within muscle in the context of rotator cuff tear via a chemokine. This hypothesis was investigated in the following three specific aims:

Specific Aim 1: Develop hydrolytically-degradable heparin-based microparticles and evaluate their ability to act as a drug delivery vehicle for a positively-charged osteoinductive protein *in vitro*.

The ***hypothesis*** for this aim is that altering heparin sulfation level, heparin content, and degradation properties of heparin-based microparticles, three approaches to control BMP-2 release from microparticles, will allow for tunable growth factor delivery kinetics from these materials. The ***rationale*** for this aim is that heparin has been shown to bind positively-charged BMP-2 in part through its negatively-charged sulfate groups [15]. Thus, release of BMP-2 from microparticles may be tuned by systematically altering heparin sulfation and content within microparticles, as well as hydrolytic degradation rate of microparticles. First, hydrolytically-degradable heparin-based microparticles of varying sulfation levels (fully sulfated, N-desulfated, 6O,N-desulfated, and fully desulfated), heparin content (1 and 10 wt%), and hydrolytic degradation rate (7 to 14 days) were fabricated. Subsequently, loading and release of BMP-2 from microparticles

was assessed over 10 days via ELISA, followed by evaluation of the bioactivity of released BMP-2 via a cell-based C2C12 alkaline phosphatase (ALP) bioactivity assay. Lastly, to further probe the effect of heparin sulfation on BMP-2 denaturation, BMP-2 was incubated with each soluble heparin derivative of varying total sulfation and analyzed via ELISA.

Specific Aim 2: Evaluate the ability of an anti-inflammatory protein delivered via heparin-based microparticles to reduce cartilage degeneration in a rat model of post-traumatic osteoarthritis.

The ***hypothesis*** for this aim is that heparin of greater total sulfation will enhance TSG-6 bioactivity and, subsequently, TSG-6 loaded onto heparin-based microparticles with the appropriate sulfation level and delivered via intra-articular injection will reduce cartilage damage significantly more than soluble TSG-6 treatment in a model of post-traumatic osteoarthritis (OA). The ***rationale*** for this aim is, first, that heparin has previously shown to bind and enhance TSG-6 bioactivity, potentially by maintaining TSG-6 in a "closed" conformation [22,23], though the effect of heparin sulfation on TSG-6 bioactivity has yet to be assessed. Second, TSG-6 has been shown to possess anti-inflammatory properties through the inhibition of plasmin, an enzyme present in OA joints and capable of activating matrix metalloproteinases (MMPs) and degrading extracellular matrix (ECM) [24–27]. Therefore, as plasmin may be a key factor in the cartilage degeneration seen in OA joints, TSG-6 delivery may be a method to ameliorate the cartilage degeneration observed. To that end, heparin derivatives of varying sulfation level between 0-100% total sulfation were incubated with TSG-6 to assess their effect on TSG-6 bioactivity

using a plasmin inhibition assay. The results of the *in vitro* studies subsequently informed the development of degradable, N-desulfated heparin-based microparticles to release bioactive TSG-6 via intra-articular injection to the knee of rats following post-traumatic OA injury. Medial meniscal transection (MMT) injury was induced in the knee of rats at day 0, followed by 3 weekly injections of TSG-6 loaded microparticles, soluble TSG-6, or no treatment. After 21 days, animals were euthanized to assess cartilage proteoglycan content (histology and safranin-O staining) and cartilage thickness, volume, and attenuation (Equilibrium Partitioning of an Ionic Contrast agent via μCT analysis, EPIC-μCT).

Specific Aim 3: Evaluate the ability for bone marrow-derived cell mobilization and subsequent bone marrow-derived cell recruitment to synergistically increase the pro-regenerative cellular milieu within muscle following rotator cuff injury.

The ***hypothesis*** for this aim is that systemic delivery of a bone marrow mobilizing agent, VPC01091, in combination with intra-muscular delivery of a chemokine, SDF-1α, loaded onto microparticles, will synergistically enhance the number of pro-regenerative bone marrow-derived cells in the muscle compared to either treatment alone. The ***rationale*** for this aim is that SDF-1α has previously shown to attract immune cells such as monocytes [7,8], stem cells such as hematopoietic [30] and mesenchymal stem cells (MSCs) [31], and progenitor cell populations [12,32], among others [33,34]. Furthermore, through sphingosine 1 phosphate receptor 1 ($S1PR_1$) agonism and $S1PR_3$ antagonism [35], VPC01091 has previously shown to increase LSK cell ($Lin^{neg}Sca\text{-}1^{+}c\text{-}Kit^{+}$, early hematopoietic stem cells) and MSC migration [36], ultimately resulting in significantly

more CXCR4+ cells (cells possessing the primary receptor for SDF-1α) in circulation [36]. Thus, through VPC01091-mediated mobilization of CXCR4+ cells, and subsequent SDF-1α-mediated recruitment of CXCR4+ cells into the muscle, co-delivery of VPC01091 and SDF-1α may be a method to recruit pro-regenerative cell populations to the muscle following severe rotator cuff injury and prevent muscle degeneration. First, SDF-1α release kinetics from heparin-based microparticles was monitored *in vitro* via ELISA and *in vivo* via near-infrared protein tracking. Next, VPC01091 was delivered via intraperitoneal injection and SDF-1α loaded microparticles were delivered via intra-muscular injection immediately following tendon transection and denervation in rats. Following injury and treatment, pro-regenerative cell mobilization was assessed in blood over 7 days and cell recruitment was assessed in muscle at day 3 and 7 via flow cytometry. Finally, muscle fiber regeneration and angiogenesis were assessed at day 7 and 14 via immunohistochemistry for embryonic myosin heavy chain (eMHC and H&E) and CD31, respectively. Finally, after 14 days muscle degeneration was assessed via muscle fiber regeneration (eMHC and H&E), muscle atrophy (muscle weight), functional testing (isometric torque testing).

1.3 Significance and Scientific Contribution

Musculoskeletal disorders, including arthritis and rotator cuff tears, are among the most common chronic conditions affecting the US population today [1,37], yet methods to effectively treat the associated degenerating tissues remains an unsolved problem. Thus, to develop a delivery method for therapeutics following musculoskeletal injuries, a heparin-based microparticle system was first engineered and assessed *in vitro*. The

tunability of the microparticle system was validated by modulating heparin content (1 and 10 wt%), heparin sulfation (0 to 100% total sulfation), and hydrolytic degradation (8 to 30 days) of microparticles to, in turn, modulate the *in vitro* loading, release, and bioactivity of a positively-charged protein, BMP-2. Though BMP-2 loading was unaffected by these variables, microparticles with greater heparin content and greater heparin sulfation released significantly more BMP-2 and enhanced BMP-2 bioactivity *in vitro*. Finally, given the diminished anti-coagulant properties of desulfated heparin derivatives compared to fully sulfated heparin (Hep), N-desulfated heparin (Hep^{-N}, 80% sulfation compared to Hep) was chosen for the fabrication of microparticles used for subsequent *in vivo* therapeutic delivery.

Next, heparin-based microparticles were employed to deliver a anti-inflammatory protein, TSG-6, in the context of osteoarthritis, a condition which affects more than 60% of Americans over 65 years of age and is characterized by significant articular cartilage degeneration [4,38,39]. While OA is a multi-factorial disease, at stages of disease progression both cartilage-resident chondrocytes and synoviocytes in the joint capsule have been found to secrete increased levels of inflammatory factors known to promote or be directly involved in cartilage degradation [39–41]. Additionally, components of the plasminogen activation pathway [24–27] have been shown to be upregulated in OA joints, which can in turn activate MMPs and degrade ECM [42,43]. Thus, TSG-6, which exhibits both anti-inflammatory and anti-plasmin activity, was delivered as a method to ameliorate the cartilage degeneration exhibited in OA joints [26,44]. Degradable, 10 wt% Hep^{-N} microparticles were found to release and enhance TSG-6 bioactivity *in vitro*, and *in vivo* TSG-6 was significantly more chondroprotective than a 3x dose of soluble

TSG-6. Ultimately, a novel, heparin-based biomaterial system was developed and validated as a method to load, release, and enhance the therapeutic efficacy of a therapeutic for musculoskeletal tissue.

Finally, heparin-based microparticles were validated as a method to delivery therapeutics to muscle in the context of severe rotator cuff injury. Though nearly 300,000+ rotator cuff repairs occur annually [45], the current standard of surgical treatment involves only the reattachment of the tendons to the humeral head, resulting in continued degeneration of the supraspinatus and infraspinatus muscles of the rotator cuff, an increased likelihood of re-tear, and poor patient prognoses. Thus, the work described in this thesis is significant, first, because the timeline of cell inflammatory cell and stem cell recruitment following rotator cuff injury is investigated using an animal model of severe rotator cuff injury. Using a rat model of severe rotator cuff tear, though no significant changes in inflammatory cells were observed 3 days following injury, a significant increase in total leukocytes and macrophages were observed in injured supraspinatus muscles compared to uninjured contralateral controls after 7 days. Subsequently, though no significant differences were observed at 1 week, by 3 and 6 weeks significant muscle atrophy and fibrosis was observed in injured supraspinatus muscles compared to uninjured muscles. Fatty infiltration was also investigated via histology, though no significant differences were observed between injured and uninjured supraspinatus muscles in our studies. Ultimately, the results of this work elucidated the timeline of inflammatory and stem cell recruitment following tendon transection and denervation in rats, providing a platform to further investigate and modulate the cellular milieu following rotator cuff injury.

Following characterization of muscle degeneration in the animal model, 10 wt% Hep^{-N} microparticles were ultimately employed to deliver the chemokine SDF-1α to the supraspinatus muscle alone and in combination with systemic delivery of a bone marrow mobilizing agent, VPC01091, following rotator cuff tear. After 7 days post-injury and treatment, significantly more anti-inflammatory, M2-like macrophages and MSCs were detected with SDF-1α MPs alone, and when in combination with VPC010191, the M2:M1 macrophage ratio was also significantly increased compared to injury by day 3 and 7 in muscle. By day 7 significantly more eMHC+ regenerating muscle fibers were observed in the dual treatment group than any treatment or injury alone. Thus, this work is significant in that our novel microparticle platform was utilized to deliver therapeutics to modulate the cellular milieu of muscle toward a more pro-regenerative state following rotator cuff injury.

Overall, in this thesis, a biomaterial-based drug delivery system was developed to effectively treat degenerating musculoskeletal tissues following injury or disease. A naturally derived glycosaminoglycan, heparin, and poly (ethylene glycol) (PEG), a polymer that is FDA-approved as PEG-conjugated drugs, were utilized to reduce the likelihood of an undesired immune response and to increase the potential for clinical translation in the future. Furthermore, injectable biomaterial-based microparticles were fabricated, enabling delivery of therapeutics to the articular cartilage and muscle without invasive surgical procedures. Once developed, heparin-based microparticles were assessed as a drug delivery vehicle, and were shown to release multiple positively-charged proteins over several days *in vitro* and *in vivo* and enhance the bioactivity of each protein compared to soluble controls. Finally, the ability of the microparticle

system to treat degenerating musculoskeletal tissues was validated through the delivery of an anti-inflammatory protein to reduce articular cartilage damage following post-traumatic OA and through the delivery of a chemotactic protein to recruit pro-healing cells to the muscle following rotator cuff tear. Given the tunability of the microparticle system and the ability for heparin to bind and interact with a myriad of proteins, the application of heparin-based microparticles extends far beyond cartilage and muscle, and may be used for a wide range of applications where controlled release of bioactive positively-charged therapeutics is required.

CHAPTER 2

LITERATURE REVIEW

2.1 BIOMATERIALS FOR DRUG DELIVERY

2.1.1 MICROPARTICLES FOR DRUG DELIVERY

For biomaterial-based drug delivery strategies, a wide range of microparticle (MP) systems have been developed and exhibit significant advantages compared to bulk hydrogels. First, MPs are advantageous as they are injectable using standard needles and syringes, allowing for clinical translation in the future [13–16]. Though some hydrogel systems are also injectable, the free radicals or initiators required for crosslinking once in the body may be detrimental to the patient or denature the delivered protein [46–48]. Particularly advantageous for certain musculoskeletal diseases, MPs can also be injected directly into muscle, tendon, or into the joint space for treatment of articular cartilage [49] and bone [50]. Finally, MPs can be made with a myriad of materials, including synthetic, bioinert polymers such as poly (ethylene glycol) (PEG) and naturally-derived materials [15,51].

2.1.2 HEPARIN-BASED BIOMATERIALS

Though MPs have been fabricated with a variety of materials, a major consideration in the use of MPs for drug delivery is their ability to efficiently load and release the therapeutic of interest in a controlled manner. Previously, materials including chitosan, collagen, gelatin, and PEG have been used to deliver a myriad of proteins [52–55]. However, our laboratory and others have explored the use of glycosaminoglycans (GAGs) within our biomaterials to better control the loading and release kinetics of each

therapeutic [9,14,21,56]. GAGs are linear polysaccharides found within the extracellular matrix (ECM) either as free chains or covalently bound to a polypeptide core, collectively known as proteoglycans [57,58]. Heparin in particular is a highly sulfated GAG species found mainly in mast cells of connective tissues, although heparan sulfate, a similar GAG species, is abundantly found on cell surfaces throughout the body [59]. Native heparin is well-known for its anti-coagulant properties, but other biological functions include tumor growth inhibition and antiviral activity [60]. Furthermore, heparin is capable of binding with proteins through carbohydrate sequence-specific interactions and through electrostatic interactions with positively-charged proteins, primarily due to heparin's negatively-charged sulfate groups [58,61,62].

Harnessing these protein-binding properties, significant research has focused on the development of heparin-based drug delivery systems [63–67]. As bulk hydrogels, heparin-based materials have been used to deliver basic fibroblast growth factor (bFGF) [68], bone morphogenetic protein-2 (BMP-2) [69–71], epidermal growth factor (EGF) [72], human growth hormone (HGH) [73], stromal cell-derived factor-1alpha (SDF-1α) [11], and vascular endothelial growth factor (VEGF), among others. In our lab specifically, heparin-based hydrogels have been used to release proteins and small molecules *in vitro* [17] and *in vivo* [9,10], as well as to encapsulate mesenchymal stem cells (MSCs) [56]. Though fewer systems exist to date, injectable heparin-based biomaterials have become increasingly more prevalent for a wide variety of applications. Injectable heparin-based hydrogel systems have been used to encapsulate cells including primary chondrocytes [74], hepatocytes [75] and fibroblasts [76] and to release a model protein as a proof-of-concept study [77], hepatocyte growth factor (HGF) [75], and FGF-

2 [78]. Finally, though heparin-decorated hyaluronic particles exhibited near zero order release of BMP-2 after an initial burst release [16], few other heparin-based MP systems currently exist.

In our work, we have collaborated with other labs to develop 100% heparin MPs, which have previously shown to modulate release of BMP-2 *in vitro* [15] and bone regeneration *in vivo* [50,79]. Furthermore, 100% heparin MPs have been incorporated within core-shell MPs to modulate BMP-2 release [13], while 10 wt% heparin-based MPs have been incorporated within ATDC5 cell aggregates to control cell differentiation [80]. Ultimately, several heparin-based drug delivery systems have been developed with varying levels of success, and these results indicate that heparin-based materials may be an effective and tunable drug delivery method.

2.1.3 Heparin Sulfation

To further probe the interactions between heparin and heparin-binding proteins, heparin sulfation has been investigated in several contexts. Given that heparin's negatively-charged sulfate groups are primarily responsible for the electrostatic interactions between heparin and positively-charged molecules, several labs have investigated how altering heparin sulfation levels and patterns may affect binding to proteins. In the Werner lab, hydrogels composed of heparin derivatives of varying sulfation level were used to tune loading and release of several proteins from the biomaterial [66,81]. For VEGF, the less sulfated, less negatively-charged heparin hydrogels were found to load significantly less protein. However, these less sulfated heparin-based hydrogels released a significantly higher percentage of their loaded cargo, indicating that these hydrogels may have had decreased affinity toward the positively-charged VEGF. Similar results were also seen

using FGF-2, whereby the amount of protein released from heparin-based hydrogels increased as the heparin was more desulfated [81]. In our lab as well, heparin can be systematically desulfated resulting in fully sulfated (Hep), N-desulfated (Hep^{-N}), 6O,N-desulfated ($Hep^{-6O,N}$) and fully desulfated (Hep-) heparin derivatives with 100, 80, 20, and 0% total sulfation, respectively [21]. When these heparin derivatives were incorporated within 10 wt% heparin hydrogels, it was found that significantly more crystal violet, a cationic small molecule, was loaded onto the more sulfated Hep and Hep^{-N} hydrogels compared to the more desulfated heparin hydrogels. Furthermore, the release of crystal violet from the more sulfated heparin hydrogels was more linear and sustained than from the more desulfated heparin hydrogels, where significantly more burst release was observed. Thus, utilizing heparin within biomaterials has shown to enable efficient protein loading and release, and altering heparin sulfation may offer a means to further tune this loading and release.

HEPARIN AND BMP-2

Aside from altering binding and release, heparin sulfation has shown to play a significant role in the bioactivity of proteins as well [14,21,82,83]. As described above, heparin's negatively charged sulfate groups allow for binding to many positively-charged proteins, but heparin sulfation also contributes to heparin's sequence-specific binding to certain proteins [58]. These interactions have been studied extensively for many proteins. For example, with BMP-2 it was found that heparin likely can bind to two locations on an electropositive surface of BMP-2, where specific sulfate groups are involved, and possibly required, for complete binding between heparin and BMP-2 [62,84]. It has also been determined that heparin does not affect BMP-2 binding to its receptor, which eliminates this possible mechanism by which heparin can enhance BMP-2 bioactivity.

However, other hypotheses have been published, including the conjecture that heparin acts as a continuous ligand for BMP-2 [85]. In *in vitro* culture, heparin suppressed the accumulation of BMP-2 onto the cell layer, and rather maintained the BMP-2 and BMP-2 bioactivity within the culture media and overall these studies indicates that heparin could protect BMP-2 homodimer and heterodimer activity. It has also has been shown that heparin sulfate proteoglycans increase the recruitment of type II receptor units to BMP-2 type 1 receptor heteromeric complexes, which can subsequently regulate signaling [84]. In another study, BMP-2 was able to prolong the half-life of BMP-2 by 20-fold, indicating that heparin can protect BMP-2 from denaturation. Furthermore, when in the presence of heparin, noggin failed to inhibit BMP-2 activity, which also suggests that heparin may out-compete for binding to BMP-2 compared to certain inhibitors, further enhancing BMP-2 activity [86]. Finally, the effect of selective desulfation of heparin on BMP-2 bioactivity was assessed *in vitro* and *in vivo* [87]. 2O-desulfated heparin was the most effective in enhancing BMP-2-mediated MSC proliferation, whereas 6O-desulfated heparin was least effective, and 2O-desulfate heparin enhanced BMP-2-mediated bone formation *in vivo* significantly more than native heparin. A similar pattern was found with BMP-2 binding to heparin, whereby 2O-desulfated heparin bound the most BMP-2 and 6O-desulfated heparin bound the least, which all collectively suggest that specific sulfate groups are differentially required for protein binding and modulation of protein bioactivity.

HEPARIN AND TSG-6

Heparin interactions with the anti-inflammatory protein tumor necrosis factor-alpha stimulated gene-6 (TSG-6) have also been studied. TSG-6 is comprised primarily of link and complement C1r/C1s-, uEGF-, BMP-1-like (CUB) modules, and the link module in

particular has shown to bind to GAGs such as chondroitin-4 sulfate (C4S),[14] chondroitin-6 sulfate (C6S), dermatan sulfate, heparin [18,19], and the non-sulfated GAG, hyaluronic acid (HA) [15-17]. Though several GAG species bind within the link modules of TSG-6, the binding domains for heparin and HA, for example, were found to be distinct and non-overlapping [14,18,23]. Unlike HA which binds to the link module of TSG-6 at a 1:1 molar ratio, the stoichiometry for heparin and TSG-6 was found to be ~0.46±0.06. As this value is close to 0.5, it is hypothesized that two TSG-6 link modules may bind to heparin to form a protein dimer [23]. Importantly, once bound to heparin, TSG-6 does not undergo a conformational change as with HA, and therefore remains in a "closed" state [20,23]. Furthermore, TSG-6 binding to heparin has previously shown to enhance TSG-6 anti-plasmin activity *in vitro*, whereas TSG-6 anti-plasmin activity was unaffected or even inhibited by HA [23]. Thus, it is hypothesized that heparin's ability to maintain TSG-6 in a closed conformation may be a contributing factor to the enhanced bioactivity observed. To begin to understand the role of heparin sulfation, one study investigated chondroitin sulfate (CS) derivatives with varying sulfation patterns. It was found that chondroitin-4-sulfate (C4S) could bind to TSG-6 while chondroitin-6-sulfate (C6S) could not [88], suggesting that specific sulfate groups may significantly affect GAG binding to TSG-6 and subsequent bioactivity. However, heparin sulfation has yet to be studied any further in the context of TSG-6 binding and bioactivity.

HEPARIN AND SDF-1α

The binding site and importance of heparin sulfation has also been investigated for SDF-1α. It has been shown that SDF-1α dimerizes when crystallized, and the number of SDF-1α molecules capable of binding to a single 9 kDa heparin chain, 6 in total, also

suggests that SDF-1α may dimerize when bound to heparin [89,90]. In fact, heparin has shown to enable and stabilize dimerization of SDF-1α which may be one method by which heparin enables SDF-1α bioactivity *in vivo* [91]. It was also determined that heparin binding involves the N-terminus of SDF-1α, which is critical for SDF-1α's bioactivity [89]. Furthermore, in one study heparin was also shown to bind the C-terminus of SDF-1α, which in turn enhanced the biological activity of the SDF-1α N-terminus [92]. Thus, it has been hypothesized that heparin may stabilize the SDF-1α N-terminus, thereby protecting or enhancing SDF-1α bioactivity. Finally, it was also found that heparin binding to SDF-1α decreased with 2O [93] and N-desulfated heparin, whereas only a modest decrease in binding was exhibited with 6O-desulfated heparin, which indicates that 2O and N-sulfate groups may be more critical to complete heparin binding to SDF-1α [89].

HEPARIN AND OTHER PROTEINS

Though heparin interactions have been examined with many proteins, the importance of heparin sulfation is not as well established and the most characterized example is with the FGF family of proteins. First, it has previously been found that the transmembrane tyrosine kinase for FGF is activated by heparin, which induces FGF-2 and activates FGF-2 bioactivity [58]. In understanding the role of heparin sulfation in this process, it has been found that 6O-desulfated heparin promoted FGF-2 binding while 2O-sulfate groups were essential for FGF-2/heparin binding. However, in other work it was found that partially 2O and 6O-sulfated heparin was the minimum binding motif for FGF-1 and FGF-4, which suggests that heparin binding may be slightly different dependent on the specific FGF protein [58,94]. Finally, it was also found that FGF-2 incubated with 6O-

desulfated heparin showed significantly diminished bioactivity compared to FGF-2 incubated with fully sulfated heparin, which indicates that incomplete heparin binding to proteins, through loss of specific sulfate groups, may result in diminished protein bioactivity as well [95]. Overall, this work collectively indicates that heparin binds differentially to many proteins, and heparin sulfation plays a unique and critical role in binding and protecting or enhancing protein bioactivity.

2.1.4 Heparin In Vivo

Finally, when using heparin materials *in vivo* it is important to consider its anti-coagulation properties, which have been observed and utilized clinically since as early as 1935 [60]. Normally, anti-thrombin, a serine protease inhibitor, is inactive in the body [60]. Once bound to heparin or heparan sulfate, however, anti-thrombin undergoes a conformational change, binds to serine protease thrombin and factor Xa, another serine protease inhibitor, and this complex is free to activate additional anti-thrombin. This pathway of binding ultimately results in an anti-coagulation cascade, and is beneficial in many clinical applications. However, if implanted *in vivo*, the heparin-mediated anti-coagulation may cause excessive bleeding and ultimately prevent successful drug delivery. Instead, it has been found that desulfated heparin derivatives have significantly diminished anti-coagulation properties compared to the natively sulfated heparin [57,66,96,97]. In fact, even Hep^{-N}, which has ~80% total sulfation compared to native heparin, exhibited significantly less anti-coagulant activity using a standard *in vitro* assay [66]. In our lab, Hep and Hep^{-N}-based biomaterials have also exhibited similar loading and release efficiency of BMP-2 and crystal violet, and both have been shown to protect BMP-2 bioactivity [14]. Overall, when incorporated into biomaterial systems, heparin

derivatives which possess reduced anti-coagulant properties while maintaining the ability to bind proteins, such as N-desulfated heparin, may be an effective method of *in vivo* drug delivery.

2.2 OSTEOARTHRITIS

2.2.1 OSTEOARTHRITIS

Osteoarthritis (OA) affects more than 60% of Americans over 65 years of age and is characterized by significant articular cartilage and subchondral bone degeneration [4,38,39]. Though complete etiology has yet to be fully understood, OA is correlated with increasing age, increased body mass index, and is more commonly observed in women [98]. Furthermore, while OA most commonly affects the knee joint, hands, feet, hips, and the spine may also be affected [99]. Ultimately, OA is the leading cause of disability in the United States [99], highlighting the significant healthcare burden and the need for effective treatment strategies.

2.2.2 CARTILAGE DEGENERATION IN OSTEOARTHRITIC JOINTS

CARTILAGE DEGENERATION

OA is characterized by significant cartilage degeneration within the joint space, which evolves as the disease progresses. In early stages of OA, cartilage thickness decreases and cartilage fibrillation develops on the cartilage surface. Chondrocytes in OA joints do exhibit slightly elevated levels of proliferation when compared to healthy patients, which may be the cause of chondrocyte clustering often exhibited in OA joints [100]. However, chondrocyte apoptosis has also been observed in many studies to varying degrees, which is at least partially responsible for the decreased chondrocyte population within the

cartilage tissue [101,102]. Due to the decreased chondrocyte population, proteoglycan and collagen synthesis decreases as well, leading to thinning of cartilage and decreased cartilage integrity [103]. As OA progresses, factors such as matrix metalloproteinases (MMPs) and pro-inflammatory cytokines including interleukins and tumor necrosis factor-alpha [39–41], among others, have been shown to be upregulated in OA joints, which likely further contributes to cartilage degradation and erosion. Ultimately, hallmarks of articular cartilage degeneration in OA joints include cartilage fibrillation, fissures, and loss of proteoglycan and collagen content within the cartilage ECM, ultimately leading to significant pain and poor joint function [4,38,39].

SCORING METHODS OF CARTILAGE DEGENERATION IN OSTEOARTHRITIS

Many scoring methods exist to evaluate cartilage degeneration in the context of OA. Of the more commonly utilized systems, Mankin scoring (also known as Histological/Histochemical Grading System (HHGS) was developed earliest in the 1971. The Mankin scoring approach utilized histological images to identify cartilage structure, cell distribution, safranin-O proteoglycan staining, and cartilage tidemark integrity. Also commonly used, the Osteoarthritis Research Society International (OARSI) created a scoring system that, unlike other systems, emphasized the extent of cartilage damage over the articular surface. OARSI scoring includes evaluation of cartilage matrix architecture, including fibrillation and proteoglycan depletion, cartilage cell viability, including proliferation, hypertrophy, and death, and bone remodeling, including the development of microfractures and osteophyte formation [104–106].

With the development of more sophisticated analysis techniques such as magnetic resonance imaging (MRI) and computed tomography (CT), these techniques have been used increasingly more frequently to assess cartilage degeneration in patients [107].

With MRI-based methods, certain systems are semi-quantitative and assess cartilage volume, thickness, surface area, percent cartilaginous joint surface area, cartilage surface curvature, among others [107]. With CT imaging, contrast agents are employed to better visualize cartilage compared to bone and surrounding air, which allows for scoring of cartilage contour and the level of contrast agent penetration into the cartilage, indicative of cartilage degeneration [108].

2.2.3 Plasminogen activation pathway in osteoarthritic joints

Central to the fibrinolytic system is the plasminogen activation pathway, in which the proenzyme plasminogen is converted to the fibrin-degrading enzyme plasmin [24]. In addition to fibrin, plasmin is capable of cleaving and degrading most other extracellular matrix (ECM) proteins, and has previously shown to activate both metalloproteinase precursors and matrix metalloproteinases (MMPs) [42,43,109]. As components of the plasminogen activation pathway including plasminogen and plasminogen activators, receptors, and inhibitors [24–27] have all shown to be upregulated in OA joints when compared to healthy patients [26,44], it is postulated that the plasminogen activation pathway may play a significant role in the cartilage degeneration exhibited in OA joints [25,27]. Thus, plasmin-inhibiting therapeutics may be a promising method to ameliorate cartilage degeneration in the context of OA.

2.2.4 Current clinical treatment strategies

As no disease modifying OA drugs (DMOADs) are clinically approved, current treatment strategies first include exercise and weight loss [106], followed by pain reduction with non-steroidal anti-inflammatory drugs (NSAIDs) [110], COX-2 selective inhibitors [111], or corticosteroid injections, all of which often provide only temporary relief [106,112].

More recently, intra-articular injections of HA, a non-sulfated GAG, have become a more common treatment option [112]. HA was FDA-approved as a method to increase the viscosity of synovial fluid, and though some clinical trials have shown efficacy compared to placebo controls, others have not [112]. Furthermore, for intra-articular delivery of these treatments, injections are typically limited to ~4 injections per year given the invasiveness of the procedure, and the rapid clearance of these treatments from the joint space likely limits their therapeutic efficacy [4]. Finally, in advanced cases of OA, surgery may be required and is most commonly a full joint replacement which, though costly, has shown to be cost effective compared to recurring drug alternatives [113].

2.2.5 Treatment strategies in development

Therapeutics in clinical trials

Given the lack of FDA-approved DMOADs, significant research has focused on development of such treatments. Treatments targeting inflammatory mediators that are upregulated in OA joints may be one approach, and options such as doxycycline and diacerein which inhibit MMPs and interleukin-1 (IL-1), respectively, and have shown to lower OA progression when analyzed via x-ray imaging in human trials [111]. In other cases, however, MMP inhibitors have shown to cause musculoskeletal side effects leading to failure in their clinical trials. Alternatively, other work has investigated the use of drugs which promote chondrocyte activity or MSC differentiation toward a chondrogenic phenotype. The GAG CS, which stimulates chondrocyte RNA synthesis, has previously shown to lower OA progression in human trials [99] and a small molecule inhibitor of the Wnt pathway, SM04690, has shown to induce MSC differentiation into functional chondrocytes and is now in a Phase 2 clinical trial [114]. Despite these

promising options, these treatment strategies are still in development, and important considerations such as the frequency of injections, side effects, and cost have yet to be fully assessed.

PARTICLE-BASED DELIVERY STRATEGIES

Micro and nano-scale biomaterials have also been employed for drug delivery to the osteoarthritic joint space, particularly due to their injectability into the joint space. Biomaterials including gelatin [115,116], C6S [117], chitosan [118], polymers [119,120], and others have been used alone and in combination with drugs primarily to enhance their retention in the joint space [121,122]. In several cases, gelatin hydrogel microspheres were used to deliver platelet rich plasma (PRP) and FGF into OA-induced rabbit knees [115,116]. OA score was significantly lower in PRP microsphere animals than animals treated with PRP alone [115], and microspheres retained FGF within the joint space for at least 7 days, leading to a reduction in OA progression compared to soluble FGF [116]. Diclofenac sodium loaded albumin microspheres were also injected into OA-induced rabbit knees [123], while gelatin/C6S microspheres were injected into OA-induced mouse knees [117], and results indicated that microspheres could retain the drug of interest locally within the joint [123] with minimal inflammatory response [117]. Poly(lactic-co glycolic acid) (PLGA) microspheres loaded with paclitaxel were delivered into the knee or rats with antigen induced arthritis, and it was found that indicators of cartilage degeneration were diminished with specific sized microspheres [120]. Nanoparticle systems composed of copolymers [119,124], chitosan [49], superparamagnetic iron oxide [125], among others, have also been used for delivery of IL-1receptor agonist (IL-1Ra) [124], bethamethasone sodium phosphate [119], kartogenin [49], and dexamethasone 21-acetate [125], respectively. In many cases, nanoparticles

improved the retention of drug in the joint space [49,124] and maintained drug bioactivity *in vivo* [119,126]. Thus, both microparticle and nanoparticle systems may enable controlled delivery of therapeutics to OA joints and these systems primarily focus on the delivery of corticosteroids [119,125] and anti-inflammatory proteins/molecules [123,124].

2.2.6 Animal models of osteoarthritis

Due to the moderate cost and relatively rapid onset of degenerative changes compared to other animals, rat models of osteoarthritis have become prevalent for research purposes. Chemically induced OA models are one option, and the most common approach is the injection of monosodium iodoacetate (MIA), which induces chondrocyte apoptosis and joint inflammation [127,128]. However, it is difficult to compare chemically-induced OA models to the human condition, as each chemical works through a particular pathway to induce degeneration [129]. Instead, the knee joint can also be surgically destabilized by transecting tissues including the anterior cruciate ligament (ACL), medial collateral ligament (MCL), meniscus, or a combination, the most common of which includes medial meniscal transection, often referred to as the MMT model [4]. In this model, cartilage degeneration is commonly observed through proteoglycan loss, fibrillation, and osteophyte formation within 3 to 6 weeks following the initial injury [38,127,130,131].

In these animal models, cartilage degeneration has been historically assessed via histological scoring using the Osteoarthritis Research Society International (OARSI) scoring system. However, with the development of more sophisticated analysis techniques such as microcomputed tomography (μCT) in combination with contrast agents, the Guldberg and Willett labs have established Equilibrium Partitioning of an

Ionic Contrast agent via μCT (EPIC-μCT) as another method to evaluate cartilage degeneration in OA joints [38,127,131–134]. In one study, histological analysis with OARSI scoring and EPIC-μCT were directly compared using the MMT rat model of post-traumatic OA [131]. In this work, it was determined that EPIC-μCT and histological scoring provided similar results, but using power analysis it was found that EPIC-μCT was more powerful and sensitive than histology, requiring fewer animals to achieve significant results. Therefore, EPIC-μCT is an alternative approach to the assessment of articular cartilage in animal models of OA.

2.2.7 TSG-6 AS A THERAPEUTIC FOR OSTEOARTHRITIS

TNF-α-stimulated gene-6 (TSG-6) is a positively charged 35 kDa protein with anti-plasmin and anti-inflammatory properties [42]. In particular, TSG-6 has been studied extensively for its ability to potentiate inter-alpha-inhibitor (IalphaI)-mediated inhibition of plasmin [42,43] and more recently, its ability to suppress the response of chondrocytes to inflammatory factors such as interleukin-1 and TNF-α [135]. In the context of OA, while little constitutively expressed TSG-6 has been observed in healthy patients, TSG-6 protein expression was found to be upregulated in OA joints and greater TSG-6 levels were observed in patients where OA symptoms had advanced over a three year period compared to non-progressing OA patients [136–138].

Despite the increased production of endogenous TSG-6, however, tissues within OA joints continue to degenerate, leading to studies on the effect of adding exogenous TSG-6 on arthritis progression. In rheumatoid arthritis (RA) mouse models, soluble TSG-6 treatment led to a significant improvement in joint swelling [139] and cartilage damage [139,140], assessed via joint diameter and histology, respectively; but these

effects were often short-lived, and by day 12 [139] or day 35 [140] no differences were observed between treated and untreated animals. Most recently, soluble TSG-6 treatment was also investigated in a rat OA model induced by anterior cruciate ligament and meniscus transection [135]. In this work, a portion of the TSG-6 molecule was delivered via intra-articular injection weekly up to 21 days following injury. After 28 days, histology indicated that cartilage fibrillation and ulceration were significantly diminished with TSG-6 treatment compared to untreated controls, indicating that TSG-6 or TSG-6 derivatives may be an effective OA treatment strategy [135].

2.3 ROTATOR CUFF INJURY

2.3.1 ROTATOR CUFF

The rotator cuff is made up of the subscapularis, supraspinatus, infraspinatus, and teres minor muscles, all of which originate at the scapula and insert onto the humeral head [141]. Each muscle is functionally unique, allowing for specific movements including abduction and rotation of the humerus. Collectively, the tendons of these muscles also form the rotator cuff around the humeral head, and ultimately stabilize the glenohumeral joint. Unlike other ball and socket joints, the socket of the glenoid is shallow, leading to decreased stability of the humeral head within the glenohumeral joint space [142]. Thus, functionally the rotator cuff provides both stability to the glenohumeral joint, as well range of motion to the shoulder [142,143].

2.3.2 SEVERE ROTATOR CUFF INJURY

Rotator cuff tear is one of the most common injuries of the shoulder, accounting for nearly 50% of major shoulder injuries [141,144,145]. Moreover, the prevalence of

rotator cuff tears continues to increase with age, as up to 50% of adults over 70 will suffer from some degree of rotator cuff injury [145,146]. In severe rotator cuff injury, which involves a significant tear of the rotator cuff, the size or shape of the tear is typically used to classify the injury through arthroscopic examination or imaging modalities such as ultrasonography and MRI [147]. While small to medium-sized tears can range between 0 to 3 cm, large and massive tears, indicative of a severe rotator cuff injury, are generally characterized as greater than 3 to 4 cm [141,147]. After such injury, symptoms typically include substantial pain and poor shoulder function, and these symptoms often progress with time [148,149]. Furthermore, the surrounding tissue of the joint space including cartilage, bone, and muscle have all shown to be significantly affected after severe rotator cuff injury, which surgical interventions for rotator cuff injury do not currently address. Specifically, Mankin scoring of cartilage tissue has indicated increased structural disorganization, hypocellularity, decreased GAG content and tide marks crossed by blood vessels, all of which are indicators of cartilage degeneration [148]. For the surrounding bone tissue, the disrupted kinematics of the glenohumeral joint after rotator cuff injury can often lead to osteoarthritis, where the subchondral bone of the humeral head collapses and the surrounding bone tissue erodes [148]. Finally, severe rotator cuff tears are often accompanied by supraspinatus and infraspinatus muscle atrophy and fatty infiltration, often referred to as "fatty degeneration" [149,150].

2.3.3 Muscle degeneration following rotator cuff tear

The unique degeneration of the supraspinatus and infraspinatus muscles after rotator cuff tear has been investigated extensively in humans. Conventionally, muscle atrophy is

assessed using sagittal plane MRI of the supraspinatus and infraspinatus to appropriately measure the size, and therefore the atrophy, of each muscle [150]. To assess fatty infiltration, a system first established by Goutallier et al. is often used, where either CT scans or MRI are used to measure fatty streaking within the muscle belly [147,151]. Using these methods, supraspinatus and infraspinatus muscle atrophy and fatty infiltration have been established as hallmarks of rotator cuff injury, and have shown to negatively correlate with range of motion [152] and muscle strength [153] and positively correlate with the size of the tear [146,149,150,152,154,155]. Muscle fibrosis, though not as well characterized in rotator cuff injuries due to limitations in imaging techniques, is a hallmark of skeletal muscle injury and disease, and leads to decreased muscle fiber diameter, contractility and function in other muscle injury contexts [152,156]. In the context of rotator cuff tears, muscle fibrosis has been observed in many animal studies, and certain work has even correlated poor muscle function with increased expression of fibrotic markers [157,158]. Ultimately, though initially a tendon injury, rotator cuff tears result in a unique profile of supraspinatus and infraspinatus muscle degeneration, which includes muscle atrophy, fatty infiltrate, and fibrous infiltrate, that ultimately leads to decreased muscle function [159].

2.3.4 Current clinical treatment strategies

Treatment strategies prior to surgical intervention

Among non-operative treatment options for rotator cuff injuries, NSAIDS, physical therapy, subacromial corticosteroid injections, and other more moderate options such as heat and ice are common [146]. However, in a longitudinal study of patients receiving non-operative care for their injury, over half of patients with a full-thickness tear

exhibited an increase in tear size over 1 year despite their treatment [160]. Thus, surgical intervention is more commonly suggested as the size and severity of the tear increases. PRP injections have also become a popular option, as PRP contains numerous factors that are essential for recruitment and proliferation of cells required for healing [161]. In one meta-analysis study, 70% of patients self-reported either mostly complete or completely improved perceived symptoms of their injury, but other studies indicated no difference between PRP-treated and placebo patients [161]. Thus, non-operative treatment options may be promising, but provide either highly variable results or may become ineffective as the severity of the tear increases.

SURGICAL INTERVENTION

Due to the limitations of non-operative treatment strategies for massive rotator cuff tears, surgical treatment has continued to increase as much as 140% from 1996 to 2006, with over 250,000 surgeries now occurring every year in the United States [146,155]. When surgery is performed, two options exist to reattach the torn tendons back to the humeral head; in traditional open surgery, a surgical incision is made through the shoulder to access the tendon and view the humeral head [162]. Alternatively, an arthroscopic procedure may be used, where a camera is inserted into a small incision in the skin, along with the tools necessary to repair the tendon. In both open and arthroscopic procedures, anchors are screwed into the humeral head, while sutures attached to these anchors are threaded through the tendon tissue and tightened to reapproximate the tendons and humeral head [163].

MUSCLE DEGENERATION BEFORE AND AFTER SURGICAL INTERVENTION

Historically, significant improvement in range of motion and strength has been observed in patients following tendon reattachment, and thus surgical rotator cuff repair

has become the standard of care for severe tears [37,162,164]. However, it has also been observed that surgical prognosis diminishes with increasing muscle degeneration and tear size [165–167], leading to a re-tear rate of up to 94% according to one study [168]. In another study, it was observed that supraspinatus muscle fatty infiltration and atrophy positively correlated with tear size (R^2 values of 0.745 and 0.819, respectively), and ultimately those patients with moderate to severe muscle fatty infiltration or atrophy had a ~70% probability of re-tear, significantly greater than the ~30% probability for patients with mild or no muscle degeneration [150]. Moreover, significant muscle degeneration has now been used to indicate irreparability of the rotator cuff tear even prior to surgery [169]. Fatty infiltrate affecting more than 50% of the musculature or MRI indicating fatty infiltrate of the supraspinatus muscle are both predictors that a patient should not receive surgery, primarily due to the unlikelihood that the shoulder will heal [169]. Thus, treatment strategies targeting muscle degeneration before or after surgical intervention may be a method to improve patient prognoses.

2.3.5 Animal models of severe rotator cuff tear

Animal models of acute, severe rotator cuff injury

To mimic acute, severe rotator cuff injury, tendon transection is the most common surgical technique used. In 1996, the Soslowsky lab investigated 33 animal species and, based on the similarity in anatomy and range of motion of the rotator cuff as well as ease of use and care, the rat was chosen as the most appropriate animal to mimic the human condition of rotator cuff injury [170]. Several labs have since developed tendon transection models, often in rats and mice, and several variations of the procedure exist. In the Soslowsky lab, only the supraspinatus tendon is transected [171], whereas in the

Feeley [172–174] and Mendias [175,176] labs both the supra and infraspinatus tendons are transected. In one instance, the Feeley lab also transected an additional tendon, the teres minor [177]. To avoid spontaneous reattachment, in certain cases the Feeley lab has removed a 5 mm portion of each tendon [177] and in other labs tubing is sutured around the transected ends of each transected tendon [178].

In rats with transection of 2 tendons, significant muscle weight loss was observed after ~4 weeks in supraspinatus and infraspinatus muscle, and in the infraspinatus muscle fiber cross sectional area was significantly reduced as well as fiber contractility [175,176]. In a separate study, supraspinatus muscle length significantly decreased and the number of Evans Blue Dye + muscle fibers, indicative of permeable and nonviable fibers, significantly increased compared to uninjured controls [179]. Similar results were observed in mice, whereby supraspinatus muscle fiber cross-sectional area was significantly reduced after 3 and 14 weeks compared to sham contralateral controls [174]. In rats with transection of 3 tendons, significant muscle weight loss was observed after 2 and 6 weeks in both the supra and infraspinatus muscles and a significant increase in fatty infiltrate was observed after 6 weeks in the infraspinatus muscle [177].

To add to the degeneration observed, in many studies the suprascapular nerve was also transected in addition to tendon transection [172,173,180–182]. Though concomitant suprascapular denervation is relatively uncommon in humans, suprascapular neuropathy due to compression or impingement has been observed [152,183,184]. With this surgical procedure, an additional significant decrease in muscle weight of the supraspinatus was observed, though infraspinatus muscle weight and fatty infiltrate did not differ from a tendon transection only group [177]. In a separate study, significant

muscle weight loss was observed after 6 weeks compared to sham contralateral controls, and fibrous and fatty infiltrate was observed via histological imaging [173]. Ultimately, these models recapitulate several hallmarks of muscle degeneration following rotator cuff injury, including muscle atrophy, fatty and fibrous infiltration, and allow for a testbed to ameliorate the muscle degeneration commonly observed after rotator cuff tears.

REATTACHMENT MODELS

To recapitulate the current standard of care, several labs have adapted a reattachment procedure following tendon transection in their animal models. In the Rodeo and Mendias labs, two crossing bone tunnels are made through the humerus, and sutures attached to the transected supraspinatus tendon are fed through these bone tunnels and pulled taught [163,179,185–187]. In some cases, the tendon(s) may be reattached immediately or after several weeks to allow for tissue degeneration to occur. In one such study with mice, mechanical testing of the transected and immediately reattached tendon indicated that while tendon failure force and stiffness was decreased after 2 weeks compared to uninjured tendon, both measurements improved over time. Similarly, in our own work both muscle weight, indicative of atrophy, and fibrosis, both improved following reattachment, suggesting that some level of tissue healing occurs as a result of tendon repair (data not published). It is important to note, however, that tissue regeneration, particularly of the muscle, is not common in human rotator cuff repairs, indicating that animal models of rotator cuff repair may not fully recapitulate the human conditions.

2.3.6 THERAPEUTIC INTERVENTIONS FOR ROTATOR CUFF TEAR

THERAPEUTIC INTERVENTIONS IN ANIMAL MODELS OF ROTATOR CUFF TEAR

Utilizing variations of the tendon transection animal model, many studies have focused on treatment strategies for severe rotator cuff injuries. However, these studies primarily focus on the treatment and regeneration of the bone, cartilage, tendon, and enthesis. For example, platelet derived growth factor – BB (PDGF-BB) has been combined with type 1 collagen scaffolds [188], gelatin hydrogel sheets, or fiberwire sutures [189] and placed near the tendon-to-bone insertion following rotator cuff injury in sheep and rat animal models. In these studies, higher ultimate load to failure measurements were observed in some cases [188] but not others [189]. FGF-2 has also been delivered via gelatin hydrogel sheets or electrospun PLGA fibrous membrane in rat and rabbit models, which resulted in significantly improved mechanical strength [190] of the tendon-to-bone insertion as well as improved collagen organization. Other therapeutics including a COX-1, COX-2, and LOX-5 inhibitor, which are fundamental enzymes in the inflammatory cascade, and a MMP inhibitor, doxycycline, significantly increased the load to failure of the enthesis compared to uninjured controls [186,191]. Focusing on bone regeneration, BMP-2 and an antibody to sclerostin, a negative regulator of bone formation, have been delivered within rat and rabbit animal models. Both treatment strategies resulted in significantly more humerus bone formation and significantly increased ultimate tensile load of the tendon-to bone insertion [192]. Ultimately, many therapeutics have been utilized with or without scaffolds to augment rotator cuff repair, but the focus of these treatment strategies included cartilage, tendon, and the enthesis [193,194].

THERAPEUTIC INTERVENTIONS FOR OTHER MUSCLE INJURIES: CELL-BASED STRATEGIES

Many therapies have been investigated to improve muscle healing after injury, albeit not typically in the unique context of rotator cuff injury. For example, cell-based therapies

have included the use of MSCs [185,195–197], embryonic stem cells (ESCs) [198], muscle-derived stem cells (MDSCs) [199], and satellite cells [200], among others [201] in a variety of animal models for muscle injury, and MDSCs have have even been tested in clinical trials with patients [195]. In a mouse model of Duchenne muscular dystrophy (DMD), MSCs derived from the synovial membrane restored sarcolemmal expression of dystrophin, reduced central nucleation, and returned the expression of mechano growth factor within muscle [197]. In other work, highly myogenic ESCs were first identified as Pax3+, PDGF-alpha receptor+, and Flk-1^{neg} [198]. Then, this ESC subpopulation was transplanted into dmx mice, resulting in enhanced contractile function of the tibialis anterior muscle without formation of teratomas [198]. Finally, other work has investigated the induction of myogenic differentiation in bone marrow stromal cells, also referred to as MSCs, through a 14 day *in vitro* process, after which time the induced "skeletal muscle cells" were implanted *in vivo* and resulted in the generation of muscle fibers in mdx mice [196].

THERAPEUTIC INTERVENTIONS FOR OTHER MUSCLE INJURIES: VOLUMETRIC MUSCLE LOSS

Though certain cell-based therapies are promising, these methods are often accompanied by significant disadvantages, including locating an abundant and viable cell source, heterogeneity and characterization of the cell populations, and significant time and cost [202]. Thus, significant work has focused on engineering drug-based therapies instead, including the stimulation of existing muscle cells and tissue to regenerate. Several growth factors have shown to improve muscle regeneration through a variety of mechanisms: insulin-like growth factor-1 (IGF-1) is highly mitogenic for myoblasts and may be a key player in mediating skeletal muscle growth, while FGF, PDGF, and nerve growth factor (NGF) are capable of stimulating satellite cell proliferation [203,204]. In

the context of volumetric muscle loss specifically, experimental treatments primarily focus on scaffolds [205–208], and examples include muscle-derived decellularized ECM scaffolds [205], porcine-derived small intestinal submucosa (SIS)-ECM scaffolds [207], bladder-derived acellular matrices[206,209], and skeletal muscle autografts [208]. Furthermore, minced or fragments options were also investigated including adipose-derived microvascular fragments [210] and a minced form of skeletal muscle autografts [208]. Though less common, drug-based strategies have included losartan administration [211], which reduced fibrosis but did not improve functional recovery, and delivery of hepatocyte growth factor (HGF) on fibrin matrices, which improved muscle force production after 60 days following injury and treatment [212].

THERAPEUTIC INTERVENTIONS FOR OTHER MUSCLE INJURIES: ISCHEMIC MUSCLE INJURY

In ischemic muscle injury, a primary focus is the development of new vasculature to, in turn, promote muscle regeneration. Therefore, current treatment strategies have included the delivery of VEGF alone [213] and in combination with IGF-1 [214], FGF gene delivery [215], and transplantation of human adipose stromal cells and bone marrow stromal cells to promote neovascularization [216,217]. The combinatorial delivery of VEGF and IGF-1 lead to angiogenesis reinnervation, and myogenesis, specifically stimulating satellite cells proliferation [214], while certain cell-based treatment strategies resulted in improved blood flow in the ischemic muscle [216].

THERAPEUTIC INTERVENTIONS FOR MUSCLE FOLLOWING ROTATOR CUFF INJURY

In one study, a HIF prolyl 4-hydroxylases (PHD) inhibitor was used to enhance the activity of HIF-1α, a transcription factor that activates many genes important to skeletal muscle regeneration [178]. The supraspinatus tendon was transected and reattached after 4 weeks in rats, with daily oral delivery of the PHD inhibitor and after 2 weeks post-

reattachment, muscle mass was significantly higher in the PHD inhibitor treated groups, but maximum isometric force of the muscle had significantly decreased compared to injury alone [178]. In separate studies, a TGF-B small molecule inhibitor, SB431542 [218], and simvastatin [158], were both utilized for their potential to reduce muscle fibrosis, among other factors. After daily IP injection of the TGF-B inhibitor for 2 or 6 weeks following tendon transection and denervation in mice, a significant decrease in muscle fibrosis was observed compared to injured controls [218], though treated muscles were still only ~25% the weight of uninjured controls [218]. Furthermore, with daily oral delivery of simvastatin, though a significant increase in specific force (maximum isometric force / muscle fiber cross sectional area) after 4 weeks, no significant difference in absolute maximum isometric force was observed with treatment [158]. Ultimately, though these studies offer some promise, novel delivery strategies and therapeutics for muscle healing in the context of rotator cuff injury are in high demand.

2.3.7 Therapeutics to modulate cellular milieu in rotator cuff muscle

Chemotactic proteins

One potential approach for muscle regeneration is chemotactic therapeutics such as SDF-1α have previously been used to recruit endogenous, pro-regenerative cell populations in the context of other muscle injuries. Primarily through its G protein-coupled receptor, CXC chemokine receptor type 4 (CXCR4), SDF-1α has previously shown to attract a myriad of cell populations including monocytes [28,29], lymphocytes [29,219], stem cells such as hematopoietic [30] and MSCs [31], and progenitor cell populations [12,32], among others [33,34]. Previously in our laboratory, we subcutaneously implanted SDF-1α loaded hydrogels into a murine dorsal skinfold window chamber model to enable the

visualization of cell recruitment and vascular remodeling and after 2-3 days, more bone marrow-derived cells [9] and significantly more anti-inflammatory monocytes were detected near the SDF-1α loaded hydrogels [9,10] compared to unloaded gels. After 7 days, significantly more anti-inflammatory, M2-like macrophages, were observed near SDF-1α loaded gels compared to unloaded controls [10], which suggests that SDF-1α delivery may be an effective approach to modulate the cellular milieu during disease states involving tissue degeneration.

BONE MARROW MOBILIZING AGENTS

Bone marrow mobilizing agents, including clinically approved granulocyte colony stimulating factor (G-CSF) and AMD3100, are most commonly used to treat neutropenia or lymphopenia following chemotherapy treatment [220–223]. Through indirect signaling, G-CSF has been shown to promote chemotaxis of hematopoietic stem and progenitor cells (HSPCs) from the bone marrow into circulation, and increased progenitor cells of all lineages have been subsequently detected in the spleen of G-CSF treated mice [224]. Furthermore, through initial studies utilizing AMD3100 as a human immunodeficiency virus (HIV) inhibitor, significantly more circulating leukocytes were also observed in treated patients, leading to the approval of AM3100 as a hematopoietic cell mobilization agent in 2008 [222]. Among other mechanisms of actions, both G-CSF and AMD3100 have shown to antagonize CXCR4, an essential mediator of cell trafficking [33], which may also disrupt CXCR4 signaling with SDF-1α [221]. Despite these promising effects, G-CSF and AMD3100 can lead to significant complications and specifically through CXCR4 inhibition, AMD3100 has shown to impair the ability for

cells to return to the bone marrow niche. Thus, bone marrow mobilizing agents with non-CXCR4 targets may be advantageous [36,225,226].

Sphingosine-1-phosphate (S1P) is a structurally simple lipid with a class of corresponding G-protein coupled receptors (GPCRs) $S1PR_{1-5}$, found in abundance in the plasma and serum [226]. During homeostasis, a steep gradient of S1P is maintained between the blood and bone marrow [227], and the disruption of this gradient leads to the sequestration of HSPCs, indicating the importance of S1P in the mobilization of bone marrow-derived cell populations. Though structurally similar, $S1PR_{1-5}$ possess unique functions, both related and unrelated to cell mobilization. For example, $S1PR_1$ is required for the egress of lymphocytes from secondary lymphoid organs and antagonism of $S1PR_1$ has been shown to induce lymphopenia [35,228–230]. In contrast, antagonism of $S1PR_3$ has been shown to promote egress of HSPCs from bone marrow to peripheral blood, ultimately suggesting that $S1PR_1$ agonists and $S1PR_3$ antagonists may be methods to promote cell mobilization.

Among a host of drugs targeting S1P receptors, VPC01091 is both an $S1PR_1$ agonist and $S1PR_3$ antagonist [35,231]. *In vitro*, VPC01091 induced a reduction in LSK ($Lin^{neg}Sca\text{-}1^{+}c\text{-}Kit^{+}$, early hematopoietic stem cells) cell adhesion and an increase in LSK cell migration. Furthermore, when delivered via intraperitoneal (I.P.) injection in rats, significantly more MSCs were observed in blood 1.5 and 24 hours after delivery [232] while in mice, significantly more circulating LSK cells were observed in blood 1.5 hours after delivery [36]. Interestingly, of the mobilized LSK cells, significantly more cells were CXCR4+, the primary receptor for SDF-1α, compared to untreated controls [36].

Thus, SDF-1α and VPC01091 may synergistically increase the number of pro-regenerative cells in the supraspinatus muscle following rotator cuff injury.

CHAPTER 3

HYDROLYSIS AND SULFATION PATTERN EFFECTS ON RELEASE OF BIOACTIVE BONE MORPHOGENETIC PROTEIN-2 FROM HEPARIN-BASED MICROPARTICLES [14]

3.1 INTRODUCTION

Bone morphogenetic protein-2 (BMP-2) is an osteoinductive growth factor that is FDA-approved for use in specific orthopaedic procedures including spinal fusions and tibial fracture repairs [3,233]. Currently supraphysiological levels of BMP-2 are required to induce bone repair, primarily due to the inability of biomaterial delivery vehicles to maintain growth factor bioactivity or spatiotemporally control growth factor release [234,235]. These high and costly doses of BMP-2 ultimately result in undesirable side effects, including inflammation and bone formation with cyst-like voids or poor mechanical properties [236,237]. Therefore, a novel strategy to maintain BMP-2 bioactivity while releasing it in a controlled manner is in high demand.

Previous efforts to fabricate BMP-2 delivery vehicles have employed alginate, chitosan, collagen, gelatin, and synthetic polymers derived from polyethylene glycol (PEG) or poly(lactic acid) [53,238–241]. However, we and other laboratories [56,242–245] are exploring the use of glycosaminoglycans (GAGs) to potentially reduce burst release of BMP-2 and prolong growth factor bioactivity [239,241,246]. GAGs are linear polysaccharides found within the extracellular matrix (ECM) either as free chains or, more often, covalently bound to a polypeptide core, collectively known as proteoglycans [57,58]. GAGs can bind growth factor through carbohydrate sequence-specific

interactions and sulfated GAGs can also bind positively-charged growth factors via their negatively-charged sulfate groups [58]. Therefore, sulfation pattern can be adjusted experimentally to further alter the binding and release of growth factor from GAG molecules [96,97,247,248]. Ultimately, GAGs can immobilize growth factors near cells and prevent growth factor degradation, making GAGs a promising biomaterial for growth factor delivery [56,61,249].

Heparin is a highly sulfated GAG species found mainly in mast cells, although heparan sulfate, a similar GAG species, is abundantly found on cell surfaces throughout the body [59]. Heparin is capable of non-covalent and reversible binding to a wide variety of positively charged growth factors including BMP-2, transforming growth factor-β (TGF-β), vascular endothelial growth factor (VEGF), fibroblast growth factors (FGFs) and insulin-like growth factors (IGFs) [58,61,62]. Our laboratory and others have incorporated heparin into bulk hydrogels for improved BMP-2 loading and release [56,242–245], but microparticles (MPs) are advantageous to efficiently load growth factors with little excess material due to the MP's high surface area-to-volume ratio [239,250]. Therefore, microgels and MPs with heparin have also been fabricated as BMP-2 carriers [16,251,252], and we have demonstrated that 100 wt% heparin MPs can bind significant amounts of BMP-2 with up to 95-100% loading efficiency and enhanced BMP-2 bioactivity [15].

The potential drawback of including large amounts of heparin in MPs, however, is that little BMP-2 release was observed from 100% heparin MPs due to sequestration of growth factor, limiting the efficiency of these MPs as soluble growth factor delivery vehicles [15,16]. Therefore, in this study we explored two methods to facilitate more

complete growth factor release from MPs while maintaining their ability to bind and preserve growth factor bioactivity. First, by incorporating a hydrolytically degradable crosslinker and varying heparin content within heparin-based MPs, we hypothesized that the release of growth factor could be enhanced as the MP degrades. Secondly, given that heparin sulfation is primarily responsible for electrostatic growth factor-GAG binding and release, we hypothesized that systematically reducing the degree of heparin sulfation may promote the release of BMP-2 from heparin MPs. Furthermore, since desulfated GAGs have been shown to have diminished anti-coagulation properties, desulfated heparin MPs may be safer for future *in vivo* therapies [57,96,253]. Therefore, we fabricated a series of MPs with selectively desulfated heparin derivatives to further control BMP-2 release. Overall, we hypothesized that altering the degradation properties and sulfation pattern of heparin MPs, two orthogonal approaches to control BMP-2 release from MPs, would allow for tunable growth factor delivery kinetics from these materials.

3.2 Materials and Methods

3.2.1 Preparation of heparin derivatives

Preparation of desulfated Hep^{-N}, $Hep^{-6O,N}$, and Hep- species was carried out as described previously [21]. Briefly, heparin sodium salt from porcine intestinal mucosa (Sigma Aldrich, St. Louis, MO) was reconstituted at ~10 mg/mL in water and passed through Dowex 50WX4 resin (mesh size 100-200, Sigma Aldrich). Pyridine was added drop-wise to the desalted heparin until the pH of the solution was ~6.0. Excess water and

pyridine were removed on a rotary evaporator (Buchi). The heparin pyridinium salt solution was flash frozen in liquid nitrogen, lyophilized to a powder, and stored at -20°C.

For Hep^{-N} preparation, heparin pyridinium salt was dissolved at 1 mg/mL in 90% DMSO/10% water (v/v) and mixed at 50°C for 2 hours [254,255]. For $Hep^{-6O,N}$, heparin pyridine was dissolved at 10 mg/mL in 90% N-methylpyrrolidone (NMP, Acros Organics, Belgium)/10% water (v/v) and maintained at 90°C for 48 hours [247]. Hep- was prepared under identical conditions to $Hep^{-6O,N}$ but the reaction proceeded at 100°C for 24 hours. Following each reaction, each heparin solution was cooled on ice and precipitated with 95% ethanol saturated with sodium acetate. The heparin precipitates were stirred for 2 hours on ice and centrifuged to remove excess ethanol and water. The resulting material was dissolved in water, dialyzed for 3 days, lyophilized to a powder, and stored at -20°C.

3.2.2 THIOLATION OF HEPARIN DERIVATIVES

400 mg of each heparin derivative was dissolved in water with 0.2-4.0 molar excess hydroxybenzotriazole (HOBt, Ark Pharm, Libertyville, IL) and cystamine. After adjusting the pH to 5.0, 0.2-4.0 molar excess 1-Ethyl-3-(3-dimethylaminopropyl)-carbodiimide (EDC, Sigma Aldrich) was added and the reaction was allowed to proceed for 2 hours (see Table 3.1). Following the reaction, the solution was dialyzed for 3 days, lyophilized to a powder, and stored at -20°C [76,256].

Table 3.1. Molar excesses of reagents used for thiolation of heparin derivatives.

Heparin species	**EDC** [x molar]	**HOBt** [x molar]	**Cystamine** [x molar]
Hep	0.2	0.2	0.2

Hep^{-N}	1.0	1.0	1.0
$Hep^{-6O,N}$	2.0	2.0	2.0
Hep-	4.0	4.0	2.0

3.2.3 Material characterization

Proton nuclear magnetic resonance (^{1}H NMR) was performed to determine the degree of thiolation and sulfation of the various chemically modified heparin species. Heparin derivatives were dissolved in deuterated water (10 mg/mL) and ^{1}H NMR spectra were recorded on a Bruker Avance III 400 spectrometer at 400 MHz as described previously [21].

3.2.4 Microparticle fabrication and size analysis

To functionalize 4-arm polyethylene glycol (PEG, 10 kDa, Creative PEGWorks, Chapel Hill, NC), PEG was reacted with acryloyl chloride (AcCl, Sigma Aldrich) in an 8:1 AcCl to PEG molar ratio in dichloromethane (DCM) solution [257]. Triethylamine (TEA, Sigma Aldrich) was added drop-wise in a 1:1 TEA to AcCl molar ratio as a catalyst to yield 4-arm PEG acrylate (PEG-4Ac). To prepare the aqueous phase for 10 wt% heparin MPs, 5.6 mg thiolated heparin, 50 mg PEG-4Ac, and 16 μL 50 mM tris-(2-carboxyethyl)-phosphine (TCEP, pH 9, Calbiochem, Germany) were dissolved in 200 μL water. For 1 wt% heparin MPs, 0.6 mg thiolated heparin, 55 mg PEG-4Ac, and 16 μL 50 mM TCEP were dissolved in 220 μL water. After all heparin/PEG-4Ac solutions incubated for 15 minutes at 37°C, water (pH 3) and 25 mM D,L-dithiothreitol (DTT, Sigma Aldrich) were added to yield a final aqueous phase volume of 320 μL.

A homogenizer (Polytron PT 3100, Kinematica, Bohemia, NY) was set to 3,100 RPM and a water bath set to 26°C was configured underneath the homogenizer probe. The oil phase, 15 mL mineral oil (Amresco, Solon, OH) + 0.05% v/v Span 80 (TCI, Cambridge, MA), was placed under the homogenizer and the aqueous phase was subsequently added via pipette. After 2 minutes, 5 mL mineral oil containing between 5-13 μL TEA was added to the emulsion via syringe and homogenized for 10 minutes (Table 3.2).

Table 3.2. TEA amounts added for each MP formulation.

MP formulation	TEA (μl)
10 wt% Hep	13.0
10 wt% Hep^{-N}	12.0
10 wt% Hep$^{-6O,N}$	9.5
10 wt% Hep-	13.0
1 wt% Hep	8.0
1 wt% Hep^{-N}	7.4
1 wt% Hep$^{-6O,N}$	5.2
1 wt% Hep-	8.0

After homogenizing, 25 mL 0.8 mM Pluronic F 127 (Pluronic buffer, Sigma Aldrich) + 0.5% v/v acetic acid (VWR) was added to the emulsion and this solution was centrifuged at 4100 RPM for 10 minutes. The oil phase was removed, MPs were washed with Pluronic buffer two additional times and then stored at 4°C. MP average size and distribution analysis were performed on newly formed MPs via phase contrast imaging (Nikon i80 microscope), with Image J and Origin 9 software. A minimum of 150 MPs were measured per experimental group.

3.2.5 MICROPARTICLE DEGRADATION

MP degradation was monitored by incubating 0.1 mg of all MP formulations in 0.5 mL 0.5% v/v BSA (Thermo Scientific, Norcross, GA) + 0.5% NaN_3 (Alfa Aesar, Ward Hill, MA) phosphate buffered saline (PBS) solution at 37°C. To capture MP degradation over time, 30 μL of each sample was removed and imaged via phase microscopy at day 1, 2, 4, 7, 10, and 14. Approximately 25 MPs were captured per image at Day 1 and a minimum of 12 images were taken per group at each time point.

3.2.6 BMP-2 LOADING AND RELEASE

Recombinant human BMP-2 (R&D Systems, Minneapolis, MN) was dissolved at 100 μg/mL in sterile water and single-use aliquots were frozen until use. For loading and release studies, 0.1 mg of each MP formulation and 100 ng BMP-2 were incubated in 0.5 mL 0.5% BSA PBS solution for 16 h at 4°C. The amount of BMP-2 was chosen to ensure that the concentration of BMP-2 released from the MPs falls within the linear range of the BMP-2 bioactivity assay. After 16 hours, MPs were centrifuged at 15,000 RCF for 3 min, the supernatant was removed, and MPs were re-suspended in 0.5 mL fresh 0.5% BSA solution. The supernatant removed at 16 and 19 h was used to quantify loading onto MPs via BMP-2 ELISA (R&D Systems). Assuming that BMP-2 released over the initial 3 h was not specifically bound to the MPs, the BMP-2 in the supernatant at 16 and 19 h was subtracted from the amount of BMP-2 in BMP-2 samples that had been incubated for the same time without MPs to determine the amount of BMP-2 bound/loaded onto MPs. Following this loading procedure, MPs were incubated at 37°C and supernatant was collected on days 1, 2, 4, 7, and 10 to quantify BMP-2 release (n = 3-5).

3.2.7 BMP-2 BIOACTIVITY AFTER MICROPARTICLE LOADING AND RELEASE

Using an established cell-based BMP-2 bioactivity assay, 1.92 $x10^4$ C2C12 myoblasts/cm^2 (ATCC) were plated into 96-well plates with 100 μL media consisting of 4.5 g/mL glucose Dulbecco's Modified Eagle Medium (DMEM, Cellgro, Manassas, VA), 10% v/v fetal bovine serum (FBS, Atlanta Biologics, Atlanta, GA), 1% v/v 10000 IU penicillin/10000 μg/mL streptomycin (Mediatech, Manassas, VA), and 1% v/v 200 mM L-glutamine (Cellgro) [258]. After 6 h of attachment, cells were treated with media only, 75 ng soluble BMP-2, 0.1 mg unloaded 10% Hep MPs, or 0.1 mg of all MP formulations loaded with BMP-2. After MPs were loaded with BMP-2 as described above, all groups were maintained for 3 days at 37°C and 95% O_2, 5% CO_2, after which cells were lysed with 100 μL lysis buffer for alkaline phosphatase (ALP) activity and double stranded DNA (dsDNA) quantification.

ALP activity in C2C12 cells was assessed via production of p-nitrophenol (Sigma Aldrich). All lysed cell samples were frozen, thawed and sonicated three times to completely dissociate the cells. 20 μL of sample or p-nitrophenol standards was combined with 5 μL 1.5 M 2-amino-2-methyl-1-propanol (pH 10.25, Sigma Aldrich) in each well of a 96-well plate. Then, 100 μL of a 1:1 mixture 20 mM p-nitrophenol phosphate disodium salt hexahydrate (Sigma Aldrich) and 10 mM $MgCl_2$ was added to each well. All samples and standards were incubated for 1 hour at 37°C, at which point the reaction was terminated by adding 100 μL 1 M NaOH and absorbance was read at 405 nm (n = 3-5). The ALP activity (nmol of p-nitrophenol/mL/min) of each sample was normalized to its respective dsDNA concentration (μg/mL, Figure A.1).

3.2.8 STATISTICAL ANALYSIS

All data are presented as mean ± standard deviation. One-way analysis of variance (ANOVA) and Tukey's post hoc multiple comparison test with a significance value set at $p \leq 0.05$ were used to identify significant differences. Statistical analysis was performed with Minitab (v15.1).

3.3 RESULTS

3.3.1 HEPARIN MP FABRICATION AND CHARACTERIZATION

Prior to MP fabrication, four heparin derivatives were prepared through desulfation, including fully sulfated (Hep), N-desulfated (Hep^{-N}), 6O,N-desulfated ($Hep^{-6O,N}$), and fully desulfated (Hep-) heparin. Total sulfation was quantified via ^{1}H NMR for each heparin derivative and ranged from 0% for Hep- to 100% for Hep (Table 3.3). Additionally, ^{1}H NMR indicated that all heparin derivatives were successfully thiolated with 10-14% thiolation per disaccharide unit (Table 3.3).

Table 3.3. Sulfation and thiolation degrees of synthesized heparin derivatives.

Heparin species	Total sulfation [%]	Thiolation [%] per disaccharide units
Hep	100 ± 1	14 ± 2
Hep^{-N}	87 ± 2	14 ± 2
$Hep^{-6O,N}$	20 ± 2	10 ± 1
Hep-	0 ± 0	12 ± 2

10 wt% heparin and 1 wt% heparin MPs were formed with each heparin derivative (Figure 3.1) and based upon phase contrast imaging, most MP formulations appeared similar in size, transparency and spherical morphology (Figure 3.2). Size distribution

analysis indicated that a majority of MPs in all formulations were less than 20 μm in diameter and specifically for 1% Hep^{-N} MPs, most were less than 10 μm in diameter (Figure 3.2Aii). The average diameter of all MPs ranged between 11-14 μm and 1% Hep^{-N} MPs were only significantly smaller than 10% Hep$^{-6O,N}$ MPs (Table 3.4).

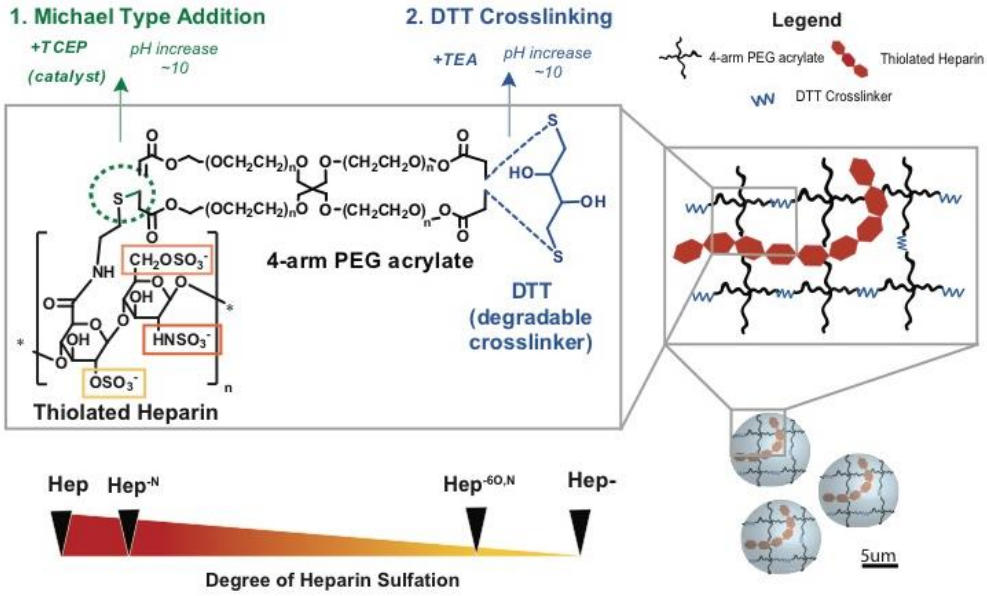

Figure 3.1. Schematic of microparticle fabrication with thiolated heparin, 4-arm PEG acrylate, and DTT crosslinker.

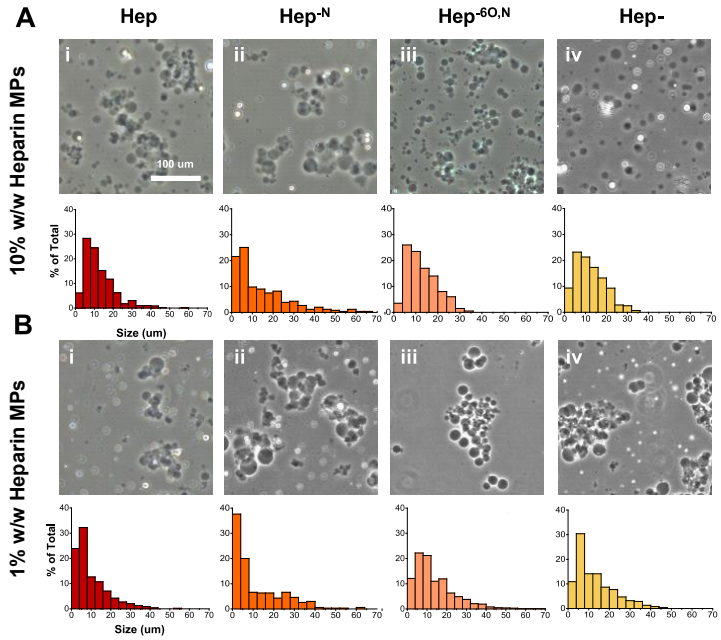

Figure 3.2. Heparin microparticle size distribution. Microparticles contain either 10 wt% heparin (A) or 1 wt% heparin (B) of differing sulfation patterns (i-iv). Scale bar is 100 μm.

Table 3.4. Average size of microparticle formulations. $^{\$}$Significantly different from each other; $p \leq 0.05$; $n > 150$.

	Hep	**Hep^{-N}**	**Hep$^{-6O,N}$**	**Hep-**
10 wt% heparin MPs	12.3 ± 7.7	13.2 ± 11.4	13.5 ± 9.7$^{\$}$	12.3 ± 7.0
1 wt% heparin MPs	11.3 ± 9.3	11.8 ± 10.9$^{\$}$	12.8 ± 6.4	13.3 ± 6.8

3.3.2 Heparin MP degradation

In the MP degradation study, all MP formulations remained present at day 4 (Figure 3.3). By day 7, 10% Hep MPs had degraded and all other 10% heparin MPs appeared to have swelled. Finally by day 10, all remaining 10% heparin MP formulations had degraded. In contrast, though 1% Hep- MPs degraded by day 10, all other 1% heparin MP formulations degraded by day 14 (Table 3.5). Throughout the degradation process, based

on the phase-contrast microscopy images, all MPs appeared to remain similar in shape over time.

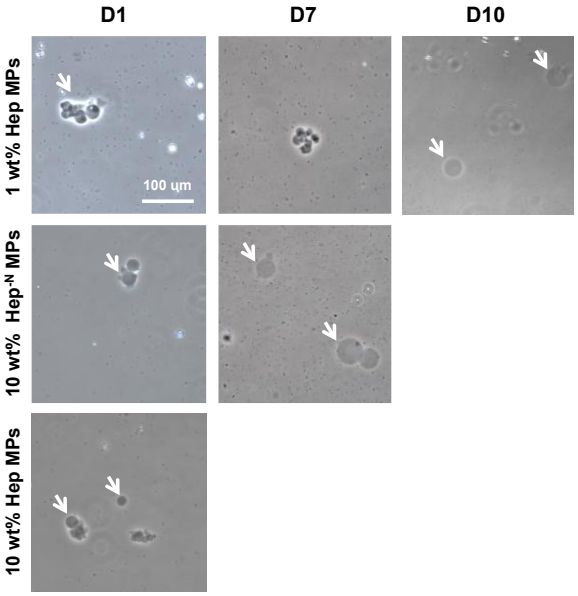

Figure 3.3. Microparticle degradation time course. First row shows representative images that were similar for 1 wt% Hep, 1 % Hep^{-N} and 1% Hep^{-6ON} microparticles. Second row shows representative images that were similar for 10 wt% Hep^{-N}, 10% Hep^{-6ON}, 10% Hep- microparticles, and 1% Hep- microparticles. White arrows indicate microparticles and scale bar is 100 µm.

Table 3.5. Degradation time (days) for all microparticle formulations.

	Hep	**Hep^{-N}**	**$Hep^{-6O,N}$**	**Hep-**
10 wt% heparin MPs	7	10	10	10
1 wt% heparin MPs	14	14	14	10

3.3.3 BMP-2 LOADING AND RELEASE FROM MPS

All MP formulations loaded 46-50% of the 100 ng BMP-2, except 1% Hep- MPs, which loaded 56% (Figure 3.4A). Furthermore, all heparin MPs loaded significantly more BMP-2 than 100% PEG MPs. BMP-2 release from MPs was monitored over 10 days and

found to be significantly different dependent on heparin sulfation pattern and amount of heparin in MPs. 10% and 1% heparin MPs with more sulfated heparin derivatives, Hep and Hep^{-N}, released significantly more BMP-2 (at least five-fold) than 10% and 1% heparin MPs with Hep$^{-6O,N}$ and Hep- (Figure 3.4B-C). Moreover, the 10% Hep and 10% Hep^{-N} MPs released significantly more BMP-2 than 1% Hep and 1% Hep^{-N} MPs. However, similar release kinetics were observed from all MP formulations. More than 95% of the cumulative release occurred between days 1-4 for all MPs, and after day 7 no detectable levels of additional BMP-2 were observed in any MP group.

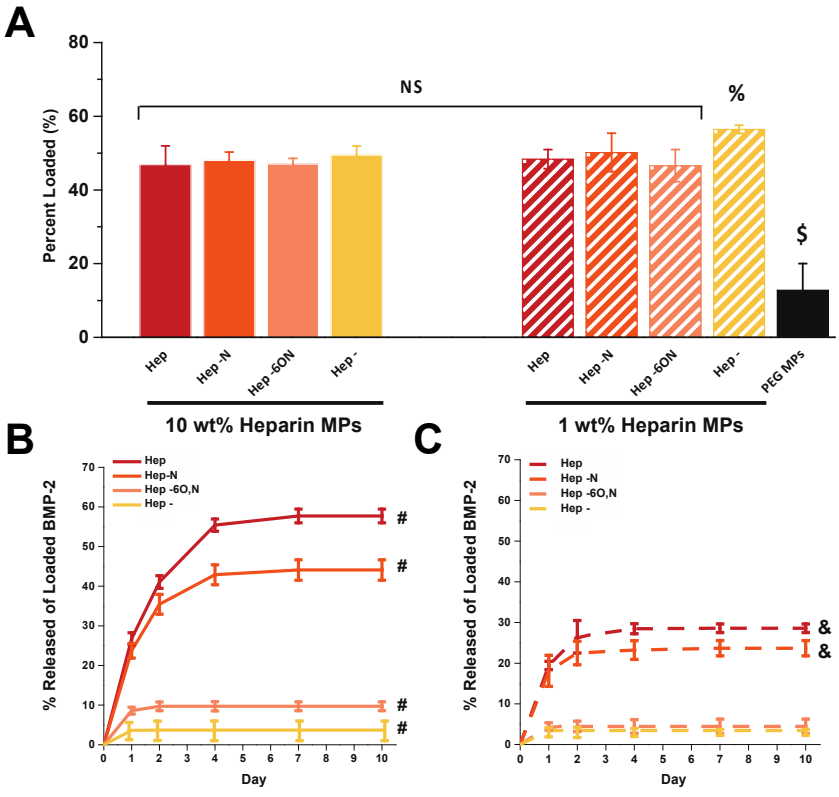

Figure 3.4. BMP-2 loading and release from all microparticle formulations. (A) BMP-2 loading was similar for most microparticle formulations whereas (B-C) BMP-2 release was significantly higher for more sulfated heparin microparticles with higher heparin content. $^{\$}$Significantly different than all other groups; $p \leq 0.05$. $^{\%}$Significantly different than 10 wt% Hep, 10% Hep$^{-6O,N}$, and 1% Hep$^{-6O,N}$ microparticle groups; $p \leq 0.05$. $^{\#}$All groups significantly different from each other; $p \leq 0.05$. $^{\&}$Significantly different from 1% Hep$^{-6O,N}$ and 1% Hep- microparticles; $p \leq 0.05$; n = 3-5.

3.3.4 Cell-Based BMP-2 Bioactivity Assay

For these experiments, the ALP activity of each group was normalized to its dsDNA content (Figure A.1). After 3 days, BMP-2-loaded 10% Hep and 10% Hep^{-N} MPs stimulated significantly more ALP activity than all other groups, including control groups of unloaded 10% Hep MPs (no observable ALP activity; data not shown) and 75 ng soluble BMP-2 (Figure 3.5). Moreover, since the release studies indicated that 10% Hep and 10% Hep^{-N} MPs released less than 20 ng BMP-2 of the ~50 ng loaded over 3 days, these results suggested that BMP-2 bioactivity was enhanced compared to soluble BMP-2. Similarly, 1% Hep and 1% Hep^{-N} MPs stimulated comparable levels of ALP activity to 75 ng soluble BMP-2, though the release studies indicated that these MPs had released less than 10 ng BMP-2 over 3 days. In contrast, the more desulfated heparin MPs, including Hep$^{-6O,N}$ and Hep- MPs, stimulated little to no ALP activity over the 3 day time period regardless of heparin content (10% or 1%).

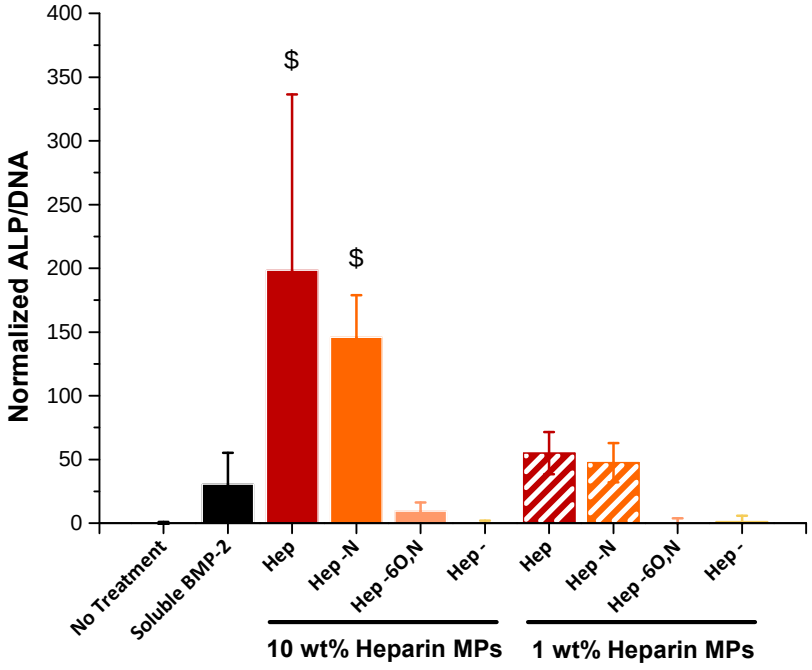

Figure 3.5. C2C12 ALP assay for BMP-2 bioactivity. BMP-2 bioactivity is significantly enhanced in the more sulfated heparin microparticle groups. $^{\$}$Significantly different than all other groups; $p \leq 0.05$; n = 3-5.

3.4 DISCUSSION

In these studies, a series of heparin-based MPs were fabricated for the purpose of controlling release of bioactive BMP-2. In future *in vivo* applications we envision that these MPs could be combined with gels or mesh-like carriers as an effective orthopaedic therapy. Towards this goal, we investigated (1) the incorporation of hydrolytically degradable crosslinker and alteration of heparin content in MPs to vary MP degradation and (2) the desulfation of heparin within MPs to vary the release of BMP-2 from MPs. Though we have previously developed 100 wt% heparin MPs, to our knowledge the incorporation of degradable crosslinker and desulfated heparin into MPs to further control BMP-2 release has yet to be investigated. Furthermore, the use of Michael Type addition crosslinking within MPs is a novel approach and allows for controlled crosslinking by tuning pH (Figure 3.1). We deliberately chose to incorporate heparin within PEG MPs because the PEG could be functionalized to include a degradable crosslinker, as well as the fact that it is relatively inert [259]. Altogether, we examined eight different MP formulations, including 10 wt% heparin and 1 wt% heparin MPs with four heparin species.

After fabrication, all MPs exhibited spherical morphology, little MP aggregation, and similar size distributions (Figure 3.2). Overall, the size of our MPs were similar to those made previously with 100 wt% heparin [15] to facilitate direct comparisons of growth factor loading and release. To vary MP degradation, we initially sought to

modify the DTT concentration in MPs, but found that MPs only formed within a small range of DTT concentrations (15-25 mM DTT) and MP degradation was not significantly altered by DTT content. Instead, we modified the heparin content in MPs and found that 10% heparin MPs degraded sooner than most 1% heparin MPs (Figure 3.3). With 10-fold less negatively charged heparin within 1% heparin MPs, this may have resulted in less water attraction into the MPs and subsequently slower hydrolysis of the MPs. Similarly, other studies have found that with increasing sulfation, the hydrolytic degradation of sulfated cellulose fibers occurred at lower temperatures, suggesting that more negatively charged materials are increasingly susceptible to hydrolytic degradation [260]. Finally, it was observed that the 10% Hep MPs were first to degrade of the 10% heparin MPs whereas 1% Hep- MPs were the first to degrade of the 1% heparin MPs. The faster degradation of 1% Hep- MPs may indicate that these MPs were not as stable or did not crosslink as well, and therefore degraded more quickly. Ultimately, we have demonstrated that by reducing the heparin content within MPs the time course of MP degradation was increased by ~4 days for most formulations, thus providing a means to modulate the degradation time of these materials.

In order to produce degradable MPs, the heparin content was reduced compared to the 100 wt% heparin MPs fabricated previously in our laboratory [15]. However, even with significantly reduced heparin content, most MP formulations exhibited a loading efficiency of ~50% (Figure 3.4A). Based on these results and previous data from our laboratory, 100%, 10%, and 1% heparin MPs loaded 90, 500, and 5000 ng BMP-2 per 0.1 mg heparin, respectively, though the efficiency of loading can vary depending upon the amounts of growth factor and MPs used [15]. These differences in growth factor-to-

heparin loading efficiency may result from the increasing availability of heparin as the heparin content within MPs is reduced. For 100% heparin MPs, the high density of heparin binding sites may sterically hinder some sites from being occupied, whereas within 10% and 1% heparin MPs, the increased distance between heparin binding sites could potentially allow for more efficient BMP-2 binding. Previous studies in our laboratory found that positively charged protein penetration into heparin-based hydrogels decreased with increasing heparin content, again supporting the idea that MPs with less heparin could load growth factors more efficiently than 100% heparin MPs [56]. Taken together, these results suggest that reduced heparin content within MPs is still adequate for efficient BMP-2 loading.

Over 10 days, nearly 60% of loaded BMP-2 was released from 10% Hep MPs, substantially more than 100% Hep MPs, which released only 20% in previous studies from our laboratory (Figure 3.4B) [15]. In our system, it is possible that the 100% Hep MPs, which are crosslinked along the heparin backbone, are more tightly crosslinked than the 10% Hep MPs, which crosslink only at the ends of each PEG-4Ac arm. Therefore, one rationale for the difference in BMP-2 release is the less tightly crosslinked network of 10% Hep MPs in comparison to 100% Hep MPs, allowing for greater diffusion and more abundant release of BMP-2. Prior studies with heparin-containing hydrogels resulted in a large range of release, between 20-80% of loaded BMP-2 [70,71,245]. In studies more similar to our system, heparin-containing MPs released 40-60% of loaded BMP-2 [16,252], which is consistent with our findings from 10% Hep MPs. In these cases, however, heparin was either covalently attached to hyaluronic acid MPs or coated

onto the alginate MP surface, rather than crosslinked into PEG-based MPs as in our system.

To further tune BMP-2 release from MPs we varied the degradation of MPs between ~10-14 days. However, regardless of the time course of MP degradation, similar release kinetics were observed from all MPs (Figure 3.4). These findings suggest that BMP-2 release was governed by diffusion rather than exclusively on the degradation of the MPs and led us to simultaneously alter sulfation pattern within the degradable MPs. Specifically, we hypothesized that with decreased heparin sulfation and concomitant reduction in electrostatic interactions within the MPs, more desulfated heparin MPs would release greater amounts of BMP-2 and thus provide a means to further tune BMP-2 release. Instead, as heparin sulfation levels within MPs decreased, the total BMP-2 release recorded also significantly decreased (Figure 3.4B-C). Additionally, C2C12 ALP activity indicated that MPs with more sulfated heparin derivatives, Hep and Hep^{-N}, enhanced the bioactivity of BMP-2 over soluble BMP-2, whereas little ALP activity was stimulated by less sulfated heparin MPs. For the MPs that had not fully degraded by Day 10 (1 wt% Hep, Hep^{-N}, and $Hep^{-6O,N}$) it is possible that some BMP-2 was still entrapped beyond the timeframe of the 10 day release study, however, this does not explain the trends in ALP activity and BMP-2 release observed in the majority of the MP formulations. Interpreting our BMP-2 release and bioactivity results collectively, we hypothesized that BMP-2 was significantly more protected by more sulfated heparin MPs, resulting in greater detected levels of BMP-2 and enhanced BMP-2 bioactivity in these MP groups. This interpretation also applies to the differences between 10% and 1%

heparin MPs, whereby the MPs with greater amounts of heparin (10 wt%) protected more BMP-2 than 1 wt% MPs with the same heparin species.

To test our hypothesis, we incubated all the heparin derivatives with BMP-2 in solution to investigate the effect of heparin on BMP-2 detection. After 24 hours at 4°C, the detected levels of BMP-2 remained between 90-100 ng in Hep and Hep^{-N} samples but decreased significantly in $Hep^{-6O,N}$, Hep-, and no heparin samples, suggesting that more sulfated heparin derivatives may protect BMP-2 from denaturation in this time frame (Figure A.2). Similar trends were also seen previously in our laboratory after heat treatment, where more BMP-2 protection was found with more sulfated soluble heparin derivatives, although these experiments were carried out with non-glycosylated BMP-2, unlike the glycosylated form used in these studies [21]. It is important to note, however, that even in the most sulfated heparin MP groups, some BMP-2 denaturation may have occurred over time, resulting in less than 100% detected release of loaded BMP-2

Applying our bioactivity results to our MP studies, more desulfated heparin MPs were likely unable to protect the bound BMP-2, resulting in little release of detectable BMP-2 and minimal BMP-2 bioactivity after as little as 24 hours. In contrast, more sulfated heparin MPs, and particularly those with higher heparin content, were able to maintain BMP-2 bioactivity during release. However, in our MP experiments it is still unclear whether the source of BMP-2 protection lies in BMP-2 interactions with heparin within and on the surface of MPs or interactions with soluble heparin released from MPs. Therefore, quantifying the amount of heparin released from MPs over time may shed light on how BMP-2 is protected in this system.

Previous experiments have demonstrated that the FGF family of growth factors is protected by heparin [82,83]. However, compared with FGF, relatively few studies have investigated how sulfation pattern may contribute to heparin's role in protecting BMP-2 bioactivity, and the results have been inconsistent [21,85]. One group has demonstrated that BMP-2 bioactivity was enhanced after incubating with a desulfated heparin derivative. This work used soluble 2O-desulfated heparin, which is distinct from any of our derivatives, and mesenchymal stem cells (MSCs) were used to assess BMP-2 bioactivity rather than C2C12 cells [87]. On the other hand, a separate set of studies have corroborated our findings where BMP-2 was bioactive after incubation with fully sulfated heparin and inactive with fully desulfated heparin, as determined via C2C12 ALP activity [47]. It should be noted, however, that only soluble heparin was used and the fully desulfated heparin was further altered to be N-acetylated or N-sulfated, unlike the Hep- used for our studies. In our studies, because multiple sulfate groups were removed simultaneously, we were unable to completely decouple the effects of sulfation level and sulfation pattern, although this may be an interesting avenue for future investigation. Thus, based on reported results as well as our findings in these experiments, heparin sulfation pattern/level may be an important consideration in fabrication of GAG-based delivery systems for BMP-2 in the future.

3.5 Conclusions

Hydrolytically-degradable, heparin-based MPs were fabricated containing heparin derivatives with varying levels of sulfation. It was demonstrated that MP degradation time in vitro can be adjusted by varying the heparin content (weight %) within MPs.

Furthermore, our results indicate that most MP formulations load equivalent amounts of BMP-2, whereas more sulfated heparin MPs, Hep and Hep^{-N}, are able to release significantly greater detectable levels of intact BMP-2 than more desulfated heparin MPs, $Hep^{-6O,N}$ and Hep-. Similarly, presentation of BMP-2 from more sulfated heparin MPs can enhance BMP-2 bioactivity compared to growth factor in solution, whereas heavily desulfated heparin MPs maintain little to no BMP-2 bioactivity. Therefore, we have identified 10 wt% Hep and Hep^{-N} MPs as viable growth factor carriers capable of efficient loading and release of bioactive BMP-2, and demonstrated that heparin sulfation level may be an important consideration for any future heparin-based biomaterials approach for bioactive growth factor delivery.

CHAPTER 4

INTRA-ARTICULAR TSG-6 DELIVERY FROM HEPARIN-BASED MICROPARTICLES REDUCES CARTILAGE DAMAGE IN A RAT MODEL OF OSTEOARTHRITIS [261]

4.1 INTRODUCTION

Osteoarthritis (OA) affects more than 60% of Americans over 65 years of age and is characterized by significant articular cartilage degeneration including cartilage fibrillation, fissures, and loss of proteoglycan and collagen content within the cartilage extracellular matrix (ECM) [4,38,39]. While OA is a multi-factorial disease, at stages of disease progression both cartilage-resident chondrocytes and synoviocytes in the joint capsule have been found to secrete increased levels of soluble factors including interleukins, tumor necrosis factor-alpha (TNF-α), and matrix metalloproteinases (MMPs), among others, which are known to promote or be directly involved in cartilage

degradation [39–41]. Additionally, components of the plasminogen activation pathway including plasminogen and plasminogen activators, receptors, and inhibitors [24–27] have also been shown to be upregulated in OA joints when compared to healthy patients [26,44]. As plasmin, the active form of plasminogen, has been shown to activate MMPs and degrade ECM [42,43], it is postulated that the plasminogen activation pathway plays a significant role in the cartilage degeneration exhibited in OA joints [25,27]. Thus, plasmin-inhibiting therapeutics may be a promising method to ameliorate cartilage degeneration in the context of OA.

TNF-α-stimulated gene-6 (TSG-6) is a positively charged 35 kDa protein with anti-plasmin and anti-inflammatory properties [42]. In particular, TSG-6 has been studied extensively for its ability to potentiate inter-alpha-inhibitor (IalphaI)-mediated inhibition of plasmin [42,43] and more recently, its ability to suppress the response of chondrocytes to inflammatory factors such as interleukin-1 and TNF-α [135]. In the context of OA, while little constitutively expressed TSG-6 has been observed in healthy patients, TSG-6 protein expression was found to be upregulated in OA joints and greater TSG-6 levels were observed in patients where OA symptoms had advanced over a three year period compared to non-progressing OA patients [136–138].

Despite the increased production of endogenous TSG-6, however, tissues within OA joints continue to degenerate, leading to studies on the effect of adding exogenous TSG-6 on arthritis progression. In rheumatoid arthritis (RA) mouse models, soluble TSG-6 treatment led to a significant improvement in joint swelling [139] and cartilage damage [139,140], assessed via joint diameter and histology, respectively; but these effects were often short-lived, and by day 12 [139] or day 35 [140] no differences were

observed between treated and untreated animals. Most recently, soluble TSG-6 treatment was also investigated in a rat OA model induced by anterior cruciate ligament and meniscus transection [135]. In this work, a portion of the TSG-6 molecule was delivered via intra-articular injection weekly up to 21 days following injury. After 28 days, histology indicated that cartilage fibrillation and ulceration were significantly diminished with TSG-6 treatment compared to untreated controls, indicating that TSG-6 or TSG-6 derivatives may be an effective OA treatment strategy [135].

Despite these promising results, one drawback to soluble treatments are the high doses often required and short retention due to rapid clearance from the joint space [4,5]. Therefore, in this study we explored the use of heparin, a naturally derived and highly sulfated GAG that can bind to a myriad of positively charged proteins including TSG-6 [10,12,14,16,17,20], as an injectable biomaterial carrier. Heparin is of particular interest in this application because previous work has demonstrated that soluble complexes of heparin and TSG-6 resulted in enhanced TSG-6 anti-plasmin activity [22,43]. Although desulfated heparin derivatives have been explored as a safer *in vivo* therapeutic delivery strategy due to their diminished anti-coagulant properties compared to fully sulfated heparin [14,17,66,96], the effect of heparin desulfation on TSG-6 binding and bioactivity has yet to be determined. Therefore, investigating the ability for desulfated heparin derivatives to maintain or enhance TSG-6 bioactivity is important to the development of an efficacious delivery strategy for TSG-6.

In this work, we first assessed the ability for desulfated heparin derivatives ranging from 0 to 100% total sulfation to enhance TSG-6 bioactivity *in vitro*. Next, though heparin-based hydrogels have been utilized extensively for protein delivery

[65,66,81,262–265], hydrogel volume may be prohibitive for drug delivery to joint spaces,[4]. Therefore, we have developed hydrolytically degradable heparin-based microparticles (MPs) based on our *in vitro* results and delivered TSG-6 loaded heparin-based MPs via intra-articular injection following medial meniscal transection (MMT) injury in a rat model. We hypothesized that heparin of greater total sulfation would enhance TSG-6 bioactivity and, ultimately, that TSG-6 loaded on MPs with the appropriate sulfation level and delivered via intra-articular injection would reduce cartilage damage following MMT injury significantly more than soluble TSG-6 treatment.

4.2 Materials and Methods

4.2.1 Heparin modifications

N-desulfated (Hep^{-N}) and fully desulfated (Hep-) heparin were prepared as described previously, whereby 10 mg/mL heparin sodium salt (Hep) from porcine intestinal mucosa (Sigma) was dissolved in dH_2O and passed through Dowex 50WX4 resin (mesh size 100-200, Sigma) [14,21]. Pyridine was added until the heparin solution reached pH 6, after which time excess dH_2O and pyridine were removed via rotatory evaporator (Buchi), flash frozen, and lyophilized. For Hep^{-N}, the heparin pyridinium was then dissolved at 1 mg/mL in 9:1 v/v dimethyl sulfoxide (DMSO)/ dH_2O at 50°C for 2 hours.[254,255] For Hep-, heparin pyridinium was dissolved at 10 mg/mL in 9:1 v/v N-methylpyrrolidone (NMP, Acros Organics)/ dH_2O at 100°C for 24 hours [247]. Subsequently, Hep^{-N} and Hep- were precipitated with 95% ethanol saturated with sodium acetate, collected via centrifuge, dissolved in dH_2O, dialyzed, lyophilized, and stored at -20°C.

Hep^{-N} methacrylamide (Hep^{-N} MAm) functionalization was performed as described previously.[13] Briefly, 1.1 mM Hep^{-N}, 83.0 mM N-hydroxysulfosuccinimide (sulfo-NHS, Sigma), 101.0 mM N-(3-Aminopropyl) methacrylamide hydrochloride (APMAm, Polysciences Inc.), and 156.0 mM (N-3-Dimethylaminopropyl)-N'-ethylcarbodiimide hydrochloride (EDC, Sigma) were combined in 10 mL phosphate buffer saline (PBS, Teknova). After stirring on ice for 6 hours, Hep^{-N} MAm was dialyzed, lyophilized, and stored at -20°C.

4.2.2 Poly (ethylene glycol) diacrylate synthesis

Poly (ethylene glycol) (PEG, 3.4 kDa, Sigma) was reacted in a 8:1 molar ratio of acryloyl chloride (AcCl, Sigma) to PEG in dichloromethane (DCM) solution.[33] Next, a 1:1 molar ratio of triethylamine (TEA, Sigma) to AcCl was added as a catalyst resulting in linear PEG-diacrylate (PEGDA).

4.2.3 Proton nuclear magnetic resonance

Proton nuclear magnetic resonance (^{1}H NMR) was performed whereby 10 mg/mL Hep^{-N} MAm and PEGDA samples were each dissolved in deuterated H_2O (Sigma), run on a Bruker Avance III spectrometer at 400 Hz, and analyzed using iNMR software [21]. Percent modification was determined by dividing the integral of the methacrylamide peak by the heparin peak for Hep^{-N} MAm and the acrylate peaks by the PEG peak for PEGDA.

4.2.4 Plasmin inhibition assay

Plasmin inhibition via TSG-6 was determined as described previously.[43] Briefly, clear 96-well plates were blocked for 1 hour with 0.5 wt% bovine serum albumin (BSA, Thermo) PBS solution. For TSG-6 with soluble heparin derivatives, 108 nM TSG-6 was

added with 108 nM of Hep, Hep^{-N} or Hep- in a pH 7.4 buffer of 10 mM HEPES, 150 mM NaCl, and 0.02% v/v Tween20 in dH_2O for 30 mins at 37°C. Next, 24 nM IalphaI (Athens Research & Technology) was added and allowed to incubate for an additional 30 mins at 37°C. Finally, 3.4 nM plasmin (Sigma) and 197 μM plasmin substrate (N-p-Tosyl-Gly-Pro-Lys 4-nitroanilide acetate salt, Sigma) were added and incubated for 20 mins at RT and 20 mins at 37°C, at which time the plate was analyzed on a plate reader at 405 nm every ~40 mins for a total of 180 mins; n = 3.

4.2.5 MICROPARTICLE FABRICATION

To fabricate 10 wt% Hep^{-N} MPs, 50.0 mg PEGDA and 1.61 mg dithiothreitol (DTT, 35 mM, Sigma) were added to 273 μL 10 wt% BSA PBS solution and incubated at 37°C for 30 mins to allow for Michael Type addition between PEGDA and DTT. Then, 5.6 mg Hep^{-N} MAm was added and the aqueous solution was incubated again at 37°C for 30 mins.

Next, an oil phase of 5 mL mineral oil (Amresco) with 3.0-3.2 μL Span80 (TCI) was placed under a homogenizer (Polytron PT 3100, Kinematica) set to 4000 RPM. After adding 27 μL of 0.05 wt% Irgacure 2959 photoinitiator (Ciba) to the aqueous phase, the solution was added drop-wise to the oil phase and the water-and-oil emulsion was allowed to homogenize for 5 mins. Subsequently, the water-and-oil emulsion was nitrogen purged for 1 min and crosslinked under UV (~15 mW/cm^2) via free radical polymerization between PEGDA and Hep^{-N} MAm. MPs were then washed through 3 iterations of the following procedure: MPs were combined with 35 mL dH_2O, centrifuged at 4000 RPM for 5 mins, and the supernatant consisting of water and oil was removed. In the final wash, MPs were pipetted through 40 μm cell strainers to remove MPs under 40

μm in diameter. To sterilize MPs, each MP batch was incubated with 70% ethanol on rotary platform at 4°C for 30 mins, followed by 3 30-min washes in sterile PBS. Phase microscopy and ImageJ software were used to image and determine the size distribution of each MP batch. MPs were stored in sterile PBS at 4°C until use.

4.2.6 TSG-6 LOADING AND RELEASE FROM MICROPARTICLES

To load TSG-6 onto MPs, 1.0 μg human TSG-6 (R&D Systems) was added to 0.6 mg MPs in 50 μL 0.1 wt% BSA solution. TSG-6 and MPs were incubated for 2 hours at 4°C, after which time MPs were rinsed by adding an additional 450 μL 0.1 wt% BSA solution. The MPs were centrifuged for 3 mins at 10,000 RCF and 495 μL supernatant was removed. For all *in vitro* and *in vivo* studies, MP loading was completed on the day of the experiment to reduce variability and avoid potential protein denaturation prior to the start of the experiment.

For *in vitro* TSG-6 release studies, the removed supernatant was replaced with 495 μL fresh 0.1 wt% BSA solution and samples were incubated at 37°C. MPs were centrifuged and 495 μL supernatant was removed and replaced 3 hours, 1, 3, 7, and 10 days following TSG-6 loading until MPs degraded. TSG-6 protein levels were quantified using a human TSG-6 sandwich ELISA with the following steps: 10 μg/mL monoclonal capture antibody (Santa Cruz Biotechnology) overnight, 100-10,000 pg/mL recombinant human TSG-6 used as standards and samples for 2 hours, 0.5 μg/mL biotinylated secondary detection antibody (R&D Systems) for 2 hours, streptavidin-horseradish peroxidase enzyme (R&D Systems) for 20 mins, substrate solution (R&D Systems) for 20 mins, and lastly a stop solution of 2 N sulfuric acid (Ricca) that was read at 450 nm; n = 3-5.

To assess TSG-6 bioactivity after release from MPs, the plasmin inhibition assay protocol was followed with day 1 TSG-6 release supernatant (11 ng/mL) and compared to a soluble TSG-6 control at the same concentration (11 ng/mL); n= 3-5.

4.2.7 MEDIAL MENISCAL TRANSECTION MODEL

Animal use was reviewed and approved by the Georgia Institute of Technology Institutional Animal Care and Use Committee which follows the "Public Health Service Policy on Humane Care and Use of Laboratory Animals" and uses the National Guidelines outlined in the "Guide for the Care and Use of Laboratory Animals, 8th Ed." as its basis. In addition, experiments followed all institutional guidelines, personnel were enrolled in the Georgia Institute of Technology Occupational Health & Safety Program and experiments were reviewed by Environmental Health & Safety and Radiation Safety Committee. MMT injury was induced using a similar method to previously established protocols with male Sprague-Dawley rats (11 total animals used for all *in vivo* experiments, 250-300 g initial weight, 8-10 weeks old from Charles River).[38] Prior to surgery animals were anesthetized by 5% isoflurane (Isothesia), followed by 2-3% isoflurane during surgery and were administered sustained release buprenorphine as an analgesic. Next, a small incision was made through the skin on the medial aspect of the left femoro-tibial joint. The medial collateral ligament was exposed by blunt dissection and transected to visualize the joint space and medial meniscus. The meniscus was then transected completely at its narrowest point. The skin was sutured with 4.0 silk sutures (Ethicon) and then closed using wound clips.

4.2.8 IN VIVO TSG-6 DELIVERY

For TSG-6 loaded MP treatment, MPs were loaded as described above but 3.6 mg MPs were resuspended in a total volume of 50 μL sterile 0.1 wt% BSA PBS solution and subsequently loaded into sterile syringes. 1, 7, and 15 days following MMT injury, MPs were delivered via intra-articular injection through the infrapatellar ligament and into the stifle joint of the left leg. For soluble TSG-6 controls, 16.7 μg TSG-6 was dissolved in a total volume of 50 μL sterile 0.1 wt% BSA PBS solution, loaded into sterile syringes, and delivered using the same method as TSG-6 loaded MPs. Overall, *in vivo* experimental groups included TSG-6 loaded MPs (18 μg TSG-6 loaded onto 10.8 mg MPs delivered over 3 time points; n = 4), soluble TSG-6 (50 μg TSG-6 delivered over 3 time points; n = 4) or injury only (no TSG-6 or MPs; n = 3). The same animals were used for all subsequent outcome measures. Contralateral tibiae served as uninjured controls.

4.2.9 MicroCT analysis

21 days following MMT injury, rats were euthanized and tibiae were harvested and fixed in 10% neutral buffered formalin (EMD Chemicals) for 7 days. Tibiae were then immersed in a 30% Hexabrix (Covidien) PBS solution at 37°C for 30 mins and scanned using a μCT40 (Scanco Medical) at 45 kVp, 177 μA, 200 ms integration time, and 16 μm voxel size.

For cartilage assessment via μCT, Equilibrium Partitioning of an Ionic Contrast agent-μCT (EPIC-μCT) and Scanco evaluation software (Scanco μCT evaluation software V6.5-3) was used as described previously [132]. First, raw scan data were automatically reconstructed to 2D grayscale tomograms, which were subsequently rotated to sagittal sections. Next, cartilage (gray in images) was manually contoured on the head of the tibiae to separate it from trabecular bone (white in images) and surrounding area

(black in images). Fixed threshold values were used to separate cartilage from air and bone: a lower threshold of 458 mg HA/cm^3 was used to separate cartilage from air and a higher threshold of 635 mg HA/cm^3 was used to separate cartilage from bone. The threshold values were globally applied for both the left and right tibiae of all animals. After manually defining the cartilage region of interest (ROI), Scanco evaluation software was used to measure cartilage thickness (distance transformation of stacked 2D images), volume (# of voxels * voxel volume), attenuation (inversely proportional to proteoglycan content), osteophyte volume, and lesion volume within the medial third of the medial tibial plateau, which is the characteristic region of damage in MMT injuries; n = 3-4 [38,127,131].

4.2.10 Histology

Following μCT, tibiae were decalcified in Cal-Ex II (Fisher) for 10 days, then processed for frozen histology sectioning as described previously [266]. Sections were stained in 0.1% fast green (Sigma) and 0.25% safranin-O solution (Sigma) and imaged at 20x magnification with a Nikon Eclipse 80i; n = 3-4.

4.2.11 Statistical analysis

All data are presented as mean ± standard deviation. One-way analysis of variance (ANOVA) and Tukey's post hoc multiple comparison test (significance value of $p \leq 0.05$) were run using Prism software.

4.3 Results

4.3.1 Materials characterization

^{1}H NMR indicated that PEGDA was ~55% functionalized while Hep^{-N} MAm was between 20-28% functionalized (Figure B.1).

4.3.2 Plasmin inhibition assay with soluble heparin derivatives

Hep and Hep^{-N} both significantly enhanced TSG-6 anti-plasmin activity (57.3 ± 1.2% and 66.1 ± 1.7% plasmin activity compared to plasmin control, respectively) compared to TSG-6 alone (74.6 ± 0.2%), though Hep enhanced TSG-6 activity significantly more than Hep^{-N}. In contrast, Hep- had no significant effect (69.6 ± 1.2%) compared to TSG-6 alone (Figure 4.1).

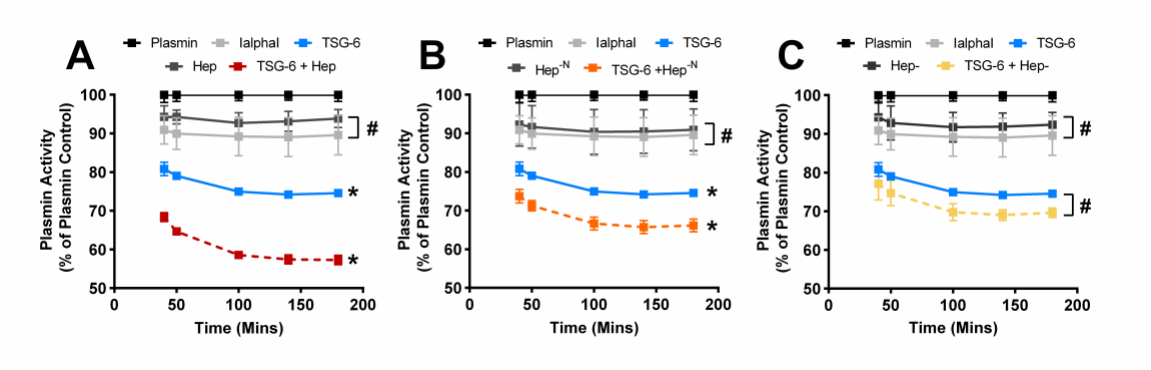

Figure 4.1. Degree of heparin sulfation affects TSG-6 bioactivity *in vitro*. (A-B) Fully sulfated and N-desulfated heparin significantly enhanced TSG-6 anti-plasmin activity whereas (C) fully desulfated heparin had no effect on TSG-6 activity compared to soluble TSG-6 controls. *Significantly different than all other groups; $p \leqq 0.05$. #Not significantly different from each other but significantly different than all other groups; $p \leqq 0.05$; n = 3; data shown as mean ± SD.

4.3.3 Microparticle fabrication, loading, and release

Degradable 10 wt% Hep^{-N} MPs were found to be 80 ± 60 μm in diameter (Figure 4.2) and have previously been shown to degrade within 10-16 days *in vitro* [266]. *In vitro*, 6.0 μg TSG-6 was loaded onto MPs and over 1-3 days ~1 μg TSG-6 was released (Figure 4.3A). Therefore, over 3 injections *in vivo*, 18.0 μg TSG-6 was originally added to MPs and ~3 μg TSG-6 was released. In comparison, for soluble TSG-6 treatment, 16.7 μg

TSG-6 was delivered per injection, resulting in a total dosage of 50.0 μg soluble TSG-6 over three injections. Importantly, TSG-6 released from MPs after 1 day exhibited significantly greater anti-plasmin activity (65.7 ± 3.0% plasmin activity compared to plasmin control) than soluble TSG-6 (96.4 ± 3.1%) at the same concentration (Figure 4.3B).

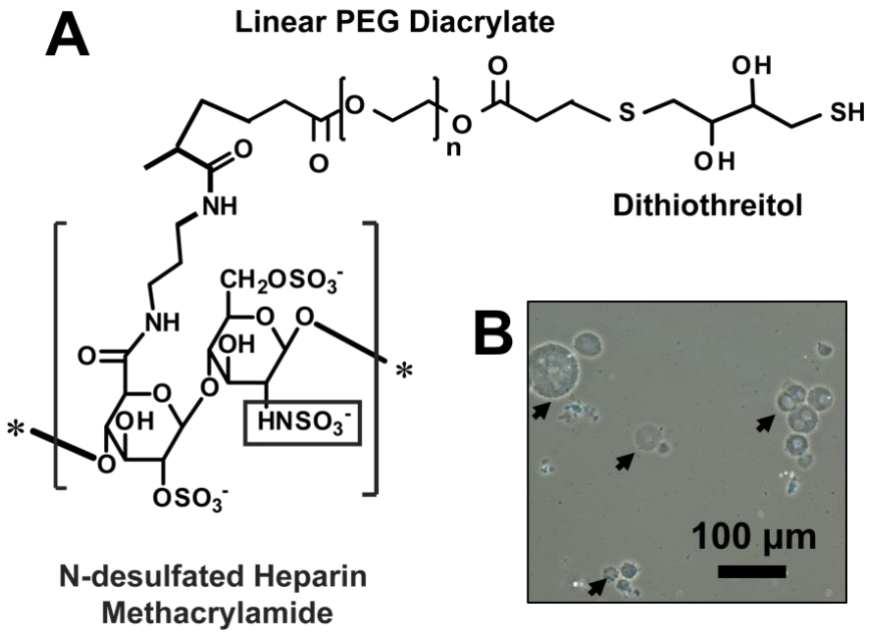

Figure 4.2. Degradable, 10 wt% N-desulfated heparin microparticles were fabricated via Michael type addition and free radical polymerization. (A) Microparticles were fabricated with 10 wt% N-desulfated heparin methacrylamide, 90 wt% linear poly (ethylene glycol) diacrylate and 35 mM dithiothreitol (DTT). (B) Phase image analysis indicated that microparticles were 80±60 μm in diameter; black arrows indicate microparticles; scale bar is 100 μm.

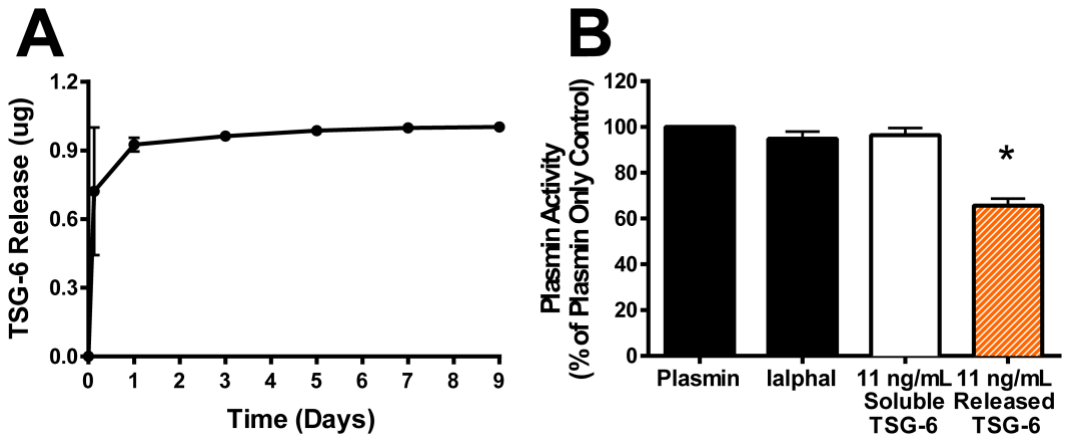

Figure 4.3. 10 wt% Hep^{-N} MPs released TSG-6 over ~3 days and enhanced TSG-6 bioactivity. (A) Over 5 days, ~1.0 µg TSG-6 was released from MPs; n = 3-4 ± SD. (B) TSG-6 released from MPs exhibited significantly more anti-plasmin activity than soluble TSG-6 at the same concentration. *Significantly lower than all other groups; $p \leq 0.05$; n = 3-4; data shown as mean ± SD.

4.3.4 MicroCT analysis

µCT images 21 days following MMT injury were quantified to assess changes in cartilage thickness, volume, and attenuation (Figure 4.4E-H). After 21 days following MMT injury, cartilage thickness (1.9 ± 0.4X compared to uninjured control) and volume (2.0 ± 0.6X) increased significantly compared to uninjured contralateral controls (Figure 4.4I-J). Soluble TSG-6 treated samples also exhibited significantly increased cartilage thickness (1.5 ± 0.2X) and volume (1.9 ± 0.5X) as well as increased attenuation (1.6 ± 0.2X) (Figure 4.4I-K) compared to uninjured controls. In contrast, neither cartilage thickness, volume, nor attenuation were increased in the TSG-6 loaded MP group compared to uninjured controls (Figure 4.4I-K). Osteophyte volume, focal lesion volume, and surface roughness were not significantly different between each experimental group or compared to respective contralateral controls (data not shown).

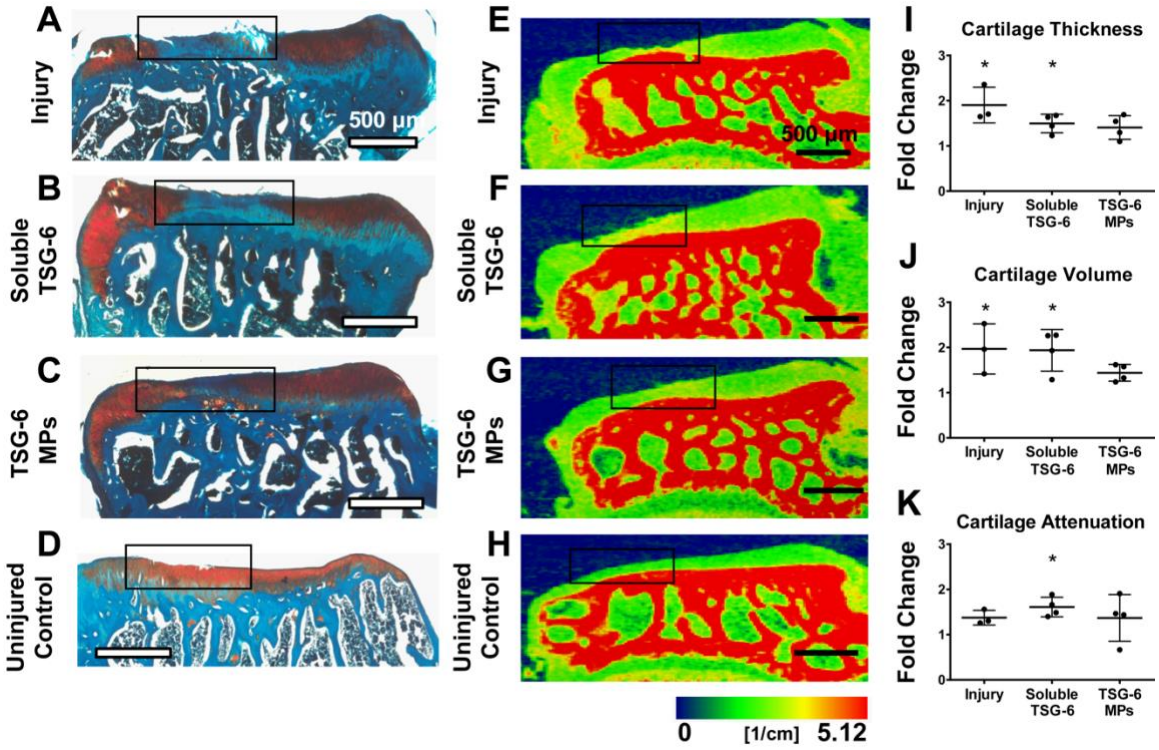

Figure 4.4. TSG-6 loaded MPs reduce cartilage damage 3 weeks following MMT injury. (A-D) Safranin-O stained coronal sections of tibiae 3 weeks following injury and treatment indicated that GAG loss was observed in the (A) injured and (B) soluble TSG-6, but not in the (C) TSG-6 loaded MP group. (E-H) Contrast-enhanced µCT imaging of the same samples indicated that cartilage fibrillation was present in the (E) injured and (F) soluble TSG-6 groups but was not present in the (G) TSG-6 loaded MP group. Scale bars are 500 µm; n = 3-4 ± SD. (I-K) Quantified evaluation of articular cartilage indicated that (I) cartilage thickness and (J) volume were significantly increased compared to uninjured controls after injury and soluble TSG-6 treatment, and (K) cartilage attenuation was significantly increased after soluble TSG-6 treatment. In contrast, no significant increase in cartilage thickness, volume, or attenuation was observed in the TSG-6 loaded MP group compared to uninjured controls. *Significantly different than contralateral control; $p \leqq 0.05$; n = 3-4; data shown as mean ± SD.

4.3.5 HISTOLOGY

Safranin-O staining of GAG within cartilage was observed in TSG-6 loaded MP treated tibiae (Figure 4.4C) and in uninjured controls (Figure 4.4D). Qualitatively, less intense safranin-O staining was observed in the medial one-third of the injured and soluble TSG-6 treated tibiae (Figure 4.4A-B).

4.4 DISCUSSION

The objectives of this work were to elucidate the effect of heparin sulfation on TSG-6 bioactivity and, utilizing this information, to develop heparin-based biomaterials for the intra-articular delivery of TSG-6. To this end, soluble heparin derivatives including Hep, Hep^{-N}, and Hep-, found to have 100%, ~80% and ~0% sulfation compared to natively sulfated heparin [14,21], were incubated with TSG-6 and results indicated that Hep and Hep^{-N} significantly enhanced TSG-6 anti-plasmin activity compared to soluble TSG-6 alone, whereas Hep- had no effect (Figure 4.1). For Hep specifically, these results parallel previous work, and it is hypothesized that the ability for Hep to maintain TSG-6 in a "closed" conformation upon binding, unlike other GAGs such as HA, may have contributed to the enhanced anti-plasmin activity observed [22,23]. Secondly, as Hep can bind to both TSG-6 and IalphaI, it is possible that Hep increased the proximity of the two proteins, thereby enabling TSG-6 to potentiate IalphaI-mediated plasmin inhibition [22].

In comparison to Hep, Hep^{-N} enhanced TSG-6 activity to a significantly less degree, whereas Hep- showed no enhancement over soluble TSG-6, indicating that heparin desulfation reduced heparin-mediated enhancement of TSG-6 anti-plasmin activity (Figure 4.1). One possible explanation may be that the sulfate groups removed from Hep^{-N} and Hep-, the N sulfate group for Hep^{-N} as well as the 2O and 6O sulfate groups for Hep-, are necessary for complete heparin binding to TSG-6 and the subsequent enhancement of TSG-6 bioactivity. In a study with derivatives of another GAG, chondroitin sulfate, with varying sulfation patterns, it was found that chondroitin-4-

sulfate (C4S) could bind to TSG-6 while chondroitin-6-sulfate (C6S) could not,[88] suggesting that specific sulfate groups may significantly affect GAG binding to TSG-6. Alternatively, as Hep- is ~0% sulfated, it is possible that Hep- bound to TSG-6 in a similar manner as HA, a naturally non-sulfated GAG which binds to TSG-6 at a distinct and non-overlapping binding site from heparin, and which did not enhance TSG-6 bioactivity in previous work [22,23].

Finally, more sulfated heparin derivatives have also been shown to protect proteins from denaturation, providing an additional mechanism by which Hep and Hep^{-N} may have maintained TSG-6 bioactivity in this study. For example, when Hep, Hep^{-N}, and Hep- were incubated with bone morphogenetic protein-2 (BMP-2) and exposed to 65°C heat treatment for 15 mins, Hep was significantly more effective in protecting BMP-2 than all other desulfated heparin derivatives [14,21]. As our *in vitro* studies were conducted at 37°C over ~4 hours, it is possible that Hep and Hep^{-N}, due to binding with TSG-6, could protect TSG-6 from denaturation over this time course, thereby protecting TSG-6 bioactivity. In summary, these findings indicate that Hep and Hep^{-N} can enhance TSG-6 anti-plasmin activity, potentially due to interactions with specific sulfate groups which may enable binding to TSG-6, through the protection of TSG-6 from denaturation when bound to heparin, or through a combination of mechanisms. Ultimately, given its diminished anti-coagulant properties compared to Hep, Hep^{-N}-based MPs were chosen as the biomaterial carrier for intra-articular delivery of TSG-6.

To determine the ability for Hep^{-N}-based MPs to enhance TSG-6 treatment *in vivo*, we first assessed the effect of soluble TSG-6 and injury alone via EPIC-μCT, an analysis technique which utilizes a contrast agent to better distinguish cartilage from bone

in μCT images [132,267]. Our results following injury alone parallel previous findings whereby cartilage thickness, volume, and attenuation (which is inversely proportional to proteoglycan content) were all significantly increased after 21 days following MMT injury in rats (Figure 4.4I-K) [127]. Furthermore, these results also parallel findings from human OA joints, where chondrocytes have been shown to proliferate, produce ECM, and undergo hypertrophy potentially resulting in increased cartilage thickness and volume, whereas the upregulation of proteinases in OA patients is known to cause cartilage proteoglycan loss [38,127,130,268].

However, our results also indicate that soluble TSG-6 was unable to improve cartilage degeneration following injury (Figure 4.4B,F,I-K). In contrast, in a recent study the intra-articular injection of soluble TSG-6 link modules, a portion of TSG-6 that has been shown to retain certain TSG-6 anti-inflammatory properties [269], over 3 weeks within a rat OA model led to a significant reduction in cartilage fibrillation and ulceration when analyzed via histology [135]. It is important to note, however, that several differences exist between this study and our work, including the OA animal model, which included both anterior cruciate ligament transection and MMT compared to MMT alone in our work, and the methods for analyzing cartilage degeneration, which included only histology. Furthermore, the doses of TSG-6 used in the study were not reported, which may be an explanation for the results of soluble TSG-6 treatment observed in this case.

In our experiments, in contrast to injury and soluble TSG-6, EPIC-μCT revealed that neither cartilage thickness, volume, nor attenuation were increased in the TSG-6 loaded MP group compared to uninjured controls (Figure 4.4G,I-K), indicating that cartilage swelling and proteoglycan loss were reduced by TSG-6 loaded MP treatment.

Histological analysis similarly showed that cartilage safranin-O staining remained qualitatively similar to uninjured controls, again suggesting that proteoglycan loss was reduced by TSG-6 loaded MP treatment (Figure 4.4C). As TSG-6 treatment was only effective when delivered with Hep^{-N}-based MPs, even with a 3X lower dose than soluble TSG-6, our results indicate that the Hep^{-N}-based carrier played a significant role in the efficacy of TSG-6 *in vivo*. Combining these findings with our *in vitro* studies, it is possible that Hep^{-N} MPs enhanced TSG-6 anti-plasmin activity, thereby reducing plasmin-mediated MMP activation and ECM degradation, or protected TSG-6 against denaturation, further improving the efficacy of TSG-6 treatment. Importantly, our findings indicate that Hep^{-N}-based MPs may reduce the amount of TSG-6 required for therapeutic effect by at least 3-fold, providing a more efficacious approach to TSG-6-mediated OA treatment.

However, in our system TSG-6 is still released from MPs over a relatively short period of time, within 1-3 days after loading (Figure 4.3A). Moreover, given the relatively fast degradation rate of MPs (between 9-16 days *in vitro* [266]), we delivered TSG-6 loaded MPs in weekly injections which is unsuitable for direct clinical translation. Thus, future optimization of this carrier may include extending the degradation rate of MPs over several weeks by decreasing the concentration of DTT within MPs [14,17,266], potentially extending the release of TSG-6 from MPs. Furthermore, in other work, by increasing the heparin content within heparin-PEG hydrogels from 3 to 6 wt%, a ~20% reduction in the amount of protein released after the first 7 days was observed [270], suggesting that increasing heparin content may provide another mechanism to prolong the release of TSG-6 from our MPs.

Ultimately, in this system, TSG-6 loaded onto Hep^{-N}-based MPs was significantly more chondroprotective than a 3X dosage of soluble TSG-6. While, based on our soluble GAG experiments, TSG-6 anti-plasmin activity is likely one potential mechanism through which TSG-6 displayed a chondroprotective effect following MMT injury, TSG-6 has also been shown to interact with a number of cell populations potentially found within the injured joint space, including leukocytes [269], neutrophils [43], macrophages [271], and MSCs [272,273]. Thus, in the future, additional studies designed to fully elucidate which functions of TSG-6 are responsible for the results seen in these experiments and how Hep^{-N} may enhance these capabilities may further improve TSG-6-mediated OA treatment.

4.5 CONCLUSIONS

In this chapter, we assessed the effect of heparin sulfation on TSG-6 bioactivity to inform the development of heparin-based MPs for the intra-articular delivery of TSG-6 in post-traumatic osteoarthritis. More sulfated heparin derivatives (Hep and Hep^{-N}) significantly enhanced TSG-6 anti-plasmin activity *in vitro,* whereas fully desulfated heparin (Hep-) had no effect, indicating that heparin sulfation plays a significant role in modulating TSG-6 bioactivity. Based on this data, hydrolytically degradable TSG-6 loaded Hep^{-N}-based MPs were delivered via intra-articular injection following MMT injury. After 21 days, EPIC-μCT analysis indicated that TSG-6 loaded MPs reduced cartilage damage following MMT injury, whereas a 3X higher dose of soluble TSG-6 did not. These results suggest that Hep^{-N} can enhance TSG-6 bioactivity *in vivo* and, ultimately, that

Hep^{-N}-containing MPs may be an effective method for delivery of TSG-6 for OA treatment in the future.

CHAPTER 5

LOCALIZED SDF-1α DELIVERY INCREASES PRO-HEALING BONE MARROW-DERIVED CELLS IN THE SUPRASPINATUS MUSCLE FOLLOWING SEVERE ROTATOR CUFF INJURY [266]

5.1 INTRODUCTION

The chemotactic protein stromal cell-derived factor-1alpha (SDF-1α), primarily through its G protein-coupled receptor, CXC chemokine receptor type 4 (CXCR4), has previously shown to attract a myriad of cell populations including immune cells such as monocytes [28,29] and lymphocytes [29,219], stem cells such as hematopoietic [30] and mesenchymal stem cells (MSCs) [31], and progenitor cell populations [12,32], among others [33,34]. Previously in our laboratory, we subcutaneously implanted SDF-1α loaded hydrogels into a murine dorsal skinfold window chamber model to enable the visualization of cell recruitment and vascular remodeling [9,274]. After 2-3 days following implantation, more bone marrow-derived cells [9] and significantly more anti-inflammatory monocytes were detected near the SDF-1α loaded hydrogels [9,10] compared to unloaded gels. Moreover, after 7 days significantly more anti-inflammatory, M2-like macrophages, were observed near SDF-1α loaded gels compared to unloaded controls [10]. Thus, as SDF-1α can recruit certain potentially pro-regenerative cell populations, including MSCs and anti-inflammatory monocytes and macrophages, SDF-1α delivery may be an effective approach to modulate the cellular milieu during disease states involving tissue degeneration.

Despite these prior findings, SDF-1α treatment has yet to be explored in the unique context of muscle degeneration following rotator cuff tear. Though rotator cuff tear begins primarily as a tendon injury, significant muscle degeneration often accompanies rotator cuff tears, which can include muscle atrophy as well as fatty and fibrous infiltration into the muscle [149,150]. To fully understand the degenerative changes in muscle following rotator cuff tear, several laboratories have investigated the cellular milieu within rotator cuff muscles following injury [159,175,176,275]. In our work, significantly more mononuclear phagocytes, monocytes, and M2 macrophages, among others, were detected in the supraspinatus muscle 7 days following transection of two rotator cuff tendons in mice [275]. Furthermore, using a rat model with a similar tendon transection approach, it was found that macrophages were specifically observed near areas of fat accumulation [176] and, in patients with chronic full-thickness tears, lipid-laden macrophages were observed surrounding muscle fibers [159]. Collectively, these results suggest that specific inflammatory cell populations may play a role in muscle degeneration following rotator cuff tear, and further investigation and manipulation of these cell populations through the delivery of SDF-1α may enable a better understanding of the muscle degeneration observed as well as potential treatment strategies following rotator cuff tear.

For the facile delivery of SDF-1α to muscle following rotator cuff injury, we have developed a degradable, injectable microparticle platform. First, our laboratory and others have developed biomaterials containing heparin, a highly sulfated glycosaminoglycan (GAG) that can bind and interact with a myriad of proteins to maintain or enhance protein bioactivity, including SDF-1α [9,14,17–19]. Second, as

natively sulfated heparin possesses potent anti-coagulant properties and may present safety issues *in vivo*, we have incorporated N-desulfated heparin (Hep^{-N}) within our biomaterials, which exhibits diminished anti-coagulant properties while maintaining the ability to bind protein and protect protein bioactivity [14,96]. Lastly, though heparin and heparin derivatives have been successfully incorporated within bulk hydrogels for SDF-1α delivery [9–12], we and others have developed heparin-based microparticles (MPs) [13–16] as an injectable protein delivery method without exposure to free radicals that are required for *in situ* radically-polymerized hydrogels [46–48]. Furthermore, building on our previous work [17], we have incorporated dithiothreitol (DTT) within the MPs to vary the rate of hydrolytic degradation [276] and ultimately allow for more complete release of protein over time.

In the present study, we have developed SDF-1α loaded 10 wt% Hep^{-N} MPs comprised of Hep^{-N} methacrylamide, poly (ethylene glycol) diacrylate (PEGDA), and DTT and injected them into the supraspinatus muscle immediately following rotator cuff tendon transection and denervation in rats. Based on previous results [14,261], 10 wt% Hep^{-N} MPs due to their ability to efficiently release protein, protect protein bioactivity, and degrade within 1-2 weeks *in vitro*. The tendon transection and denervation model utilized in these studies recapitulates many hallmarks of muscle degeneration exhibited in the human condition of rotator cuff tear in as little as 3 weeks following injury [171,176,177] and thus provides an excellent platform to investigate and modulate the cellular milieu via SDF-1α treatment. Specifically, after 3 and 7 days, the supraspinatus muscles were harvested and analyzed for changes in cellular composition by quantifying the number of myeloid cells, macrophages, macrophage subpopulations and MSCs

present via flow cytometry. We hypothesized that significantly more pro-regenerative bone marrow-derived cells would be observed in muscle treated with SDF-1α loaded Hep^{-N} MPs than untreated muscle after rotator cuff tendon transection.

5.2 Materials and Methods

5.2.1 Heparin modifications

N-desulfated heparin (Hep^{-N}) was prepared as described previously [14,21,254,255]. Briefly, heparin sodium salt (Hep) from porcine intestinal mucosa (Sigma) was dissolved at 10 mg/mL in dH_2O and passed through Dowex 50WX4 resin (mesh size 100-200, Sigma). Pyridine was added drop-wise to the heparin until the solution reached pH 6 and the solution was placed on a rotatory evaporator (Buchi) to remove excess dH_2O and pyridine. Heparin pyridinium salt solution was frozen in liquid nitrogen, lyophilized, and then dissolved at 1 mg/mL in 9:1 v/v dimethyl sulfoxide (DMSO)/ dH_2O at 50°C for 2 hours. Following the reaction, the Hep^{-N} was cooled on ice and precipitated with 95% ethanol saturated with sodium acetate, then collected by centrifugation. The resulting material was dissolved in dH_2O, dialyzed for 3 days, lyophilized, frozen in liquid nitrogen, and stored at -20°C.

For methacrylamide (MAm) functionalization, 1.1 mM Hep^{-N}, 83.0 mM N-hydroxysulfosuccinimide (sulfo-NHS, Sigma), 101.0 mM N-(3-Aminopropyl) methacrylamide hydrochloride (APMAm, Polysciences Inc.), and 156.0 mM (N-3-Dimethylaminopropyl)-N'-ethylcarbodiimide hydrochloride (EDC, Sigma) were dissolved in 10 mL phosphate buffer saline (PBS, Teknova) solution. After stirring on

ice for 6 hours, the Hep^{-N}MAm was dialyzed for 2 days, lyophilized, frozen in liquid nitrogen, and stored at -20°C.

To fluorescently label Hep^{-N}MAm, Hep^{-N}MAm was dissolved at 10 mg/mL in 0.1 M Na_2HPO_4 solution at pH 6. Next, 10 mM EDC and 5.7 μM AlexaFluor633 hydrazide (AF633, Invitrogen) were added and the reaction proceeded in the dark for 90 mins at RT. AF633 Hep^{-N}MAm was dialyzed for 2 days, frozen in liquid nitrogen, lyophilized, and stored at -20°C.

5.2.2 Poly (ethylene glycol) diacrylate synthesis

Poly (ethylene glycol) (PEG, 3.4 kDa, Sigma) was reacted with acryloyl chloride (AcCl, Sigma) in an 8:1 AcCl to PEG molar ratio in dichloromethane (DCM) solution [276]. Triethylamine (TEA, Sigma) was added drop-wise in a 1:1 TEA to AcCl molar ratio as a catalyst to yield linear PEG-diacrylate (PEGDA).

5.2.3 Proton nuclear magnetic resonance

Proton nuclear magnetic resonance (^{1}H NMR) was performed to determine the degree of PEGDA and Hep^{-N}MAm functionalization, whereby each material was dissolved at 10 mg/mL in deuterated H_2O (Sigma), run on a Bruker Avance III spectrometer at 400 Hz, and analyzed using iNMR software [21,261].

5.2.4 Strong anion exchange high performance liquid chromatography

Strong anion exchange high performance liquid chromatography (SAX-HPLC) was performed at the University of Georgia Complex Carbohydrate Research Center (CCRC) to determine the disaccharide composition of Hep and Hep^{-N}. Hep and Hep^{-N} were dissolved at 12.5 mg/mL in a heparinase mixture of 0.5 U/mL heparinases I, II, and III

for 24 hours at 37°C. The reaction was then quenched by heating the mixture for 2 mins at 100°C.

SAX-HPLC was carried out on an Agilent system using a Waters Spherisorb analytical column (4.6×250 mm; 5 μm particle size) at 25°C. Analytes were detected by their UV absorbance at 232 nm using a buffer system consisting of 2.5 mM sodium phosphate (Na_3PO_4) and pH 3.5, which was gradually transitioned from 0 to 1.2 M NaCl. The flow rate was 1.0 mL/min and detection was performed by post-column derivatization and fluorescence detection. Commercial standard disaccharides (Dextra Laboratories) were used for identification of each disaccharide based on elution time and calibration.

5.2.5 Size exclusion chromatography

Size exclusion high performance liquid chromatography (SEC-HPLC) was performed at the University of Georgia CCRC to analyze the average molecular weight and desulfation characteristics of Hep and Hep^{-N}. Hep and Hep^{-N} were dissolved at 20 mg/mL in a 0.5 M lithium nitrate buffer. Separations were carried out using two TSKGel G2000SWXL columns (7.8 mm ID x 30 cm), connected in series, on an Agilent 1200 LC instrument using refractive index detection and a sample flow rate and injection volume of 0.6 mL/min and 10 μL, respectively. Cirrus GPC software was used to construct 3rd order polynomial standard curves with the molecular weights and elution times of USP enoxaparin sodium molecular weight calibrants and broad standard USP heparin molecular weight calibrants. Weight molecular weights were calculated in Cirrus using the raw chromatograms exported from the SEC-HPLC instrument software.

5.2.6 Microparticle fabrication

10 wt% Hep^{-N} microparticles (MPs) were fabricated via water-and-oil emulsion. First, 50.0 mg PEGDA and 0.92-1.85 mg dithiothreitol (DTT, 20-40 mM, Sigma) were added to 273 μL 10 wt% bovine serum albumin (BSA, Thermo) PBS solution, consistent with previous studies in our laboratory [9,10], and incubated at ~ pH 7 and 37°C for 30 mins to allow for Michael Type addition between PEGDA and DTT. Next, 5.6 mg Hep^{-N}MAm was added and the aqueous phase was incubated for an additional 30 mins. For fluorescently tagged Hep^{-N} MPs (AF633 Hep^{-N} MPs), a 1:1 ratio of AF633 Hep^{-N}MAm to Hep^{-N}MAm was used and for non-degradable MPs, no DTT was added during fabrication.

After 27 μL of 0.05 wt% Irgacure 2959 photo initiator (Ciba) was added, the aqueous phase described above was added drop-wise to an oil phase of 5 mL mineral oil (Amresco) with 3.0-3.2 μL Span80 (TCI) and allowed to homogenize at 4000 RPM (Polytron PT 3100, Kinematica) for 5 mins. The amount of Span80 in the oil phase was varied to ensure that MPs with different DTT concentrations were maintained at the same average diameter. The water-and-oil emulsion was nitrogen purged for 1 min then placed into a petri dish under UV (~15 mW/cm^2) for 10 mins to allow for free radical polymerization between PEGDA and Hep^{-N}MAm. Finally, the MP solution was added to 35 mL dH_2O, centrifuged at 4000 RPM for 5 mins, and the oil phase was removed. MPs were washed once more with dH_2O, then pipetted through 40 μm cell strainers to remove most MPs under 40 μm in diameter.

Once fabricated, MPs were sterilized in 70% ethanol on rotary at 4°C for 30 mins, followed by 3 30-min washes in sterile PBS. MPs were imaged via phase microscopy

and size distribution was measured using ImageJ software. MPs were stored in sterile PBS at 4°C and used within 2 weeks of fabrication.

5.2.7 *In vitro* SDF-1α loading and release from microparticles

To load SDF-1α onto MPs, 1.0-1.2 μg sterile human SDF-1α (R&D Systems) was added to 0.6 mg MPs in 50 μL 0.1 wt% sterile BSA solution. SDF-1α and MPs were incubated for 2 hours at 4°C, after which time MPs were rinsed by adding an additional 450 μL 0.1 wt% sterile BSA solution. The MPs were centrifuged for 3 mins at 10,000 RCF and 495 μL supernatant was removed.

For *in vitro* SDF-1α release studies, the removed supernatant was replaced with 495 μL fresh 0.1 wt% sterile BSA solution and samples were incubated at 37°C. MPs were centrifuged and 495 μL supernatant was removed and replaced 3 hours, 1, 3, 7, 10 and 15 days following SDF-1α loading. SDF-1α protein levels were quantified with a human SDF-1α ELISA kit (R&D Systems) using the manufacturer's protocol, except for standard curves which were made with recombinant human SDF-1α rather than the provided standard. To ensure equivalent cumulative SDF-1α release for each *in vivo* study, an *in vitro* SDF-1α release study from MPs was conducted prior to each individual surgery; n = 3-5 per release study.

5.2.8 *In vivo* fluorescently-tagged microparticle injection and imaging

Non-degradable (0 mM DTT) and degradable (35 mM DTT) AF633 Hep^{-N} MPs were suspended in 120 μL sterile dH_2O (4.3 mg MPs) and subsequently loaded into sterile syringes with 20-gauge 1.5 in. hypodermic needles (BD Precision Glide). Immediately following tendon transection and denervation, the MPs were injected into the supraspinatus muscle located posterior to the scapula. Uninjured contralateral

supraspinatus muscles were not injected with MPs and served as negative controls. After 3 and 7 days, supraspinatus muscles were dissected from the scapula, sliced in half length-wise, stained with a 1:1000 dilution Hoechst cellular stain (Thermo) in PBS for 5 mins, and remained unfixed for imaging. Muscles were whole-mounted and single fluorescent images were obtained using a Zeiss LSM 700 confocal microscope with a 20x objective to visualize AF633 Hep^{-N} MPs (red) within the muscle tissue (blue); n = 2 animals per group per time point.

5.2.9 ROTATOR CUFF INJURY MODEL

Rotator cuff injury was induced using a similar method to previously established protocols [177]. Male Sprague-Dawley rats (250-300 g initial weight and 8-10 weeks old) were used in accordance with protocols approved by the Georgia Institute of Technology Institutional Animal Care and Use Committee. Prior to surgery animals were anesthetized by 5% isoflurane (Isothesia), followed by 2-3% isoflurane during surgery and were administered sustained release buprenorphine as an analgesic. The left chest and arm were shaved, wiped with alcohol/chlorhexidine, and a ~2 cm incision was made through the skin and deltoid, parallel to and just below the clavicle. To induce injury, a ~5 mm portion of the suprascapular nerve was resected and, after orienting the humerus to expose the supraspinatus and infraspinatus tendon insertions, both tendons were sharply transected. The deltoid and skin were closed using Vicryl 4-0 absorbable sutures (Ethicon) and wound clips, respectively. The right rotator cuff of each animal served as an internal uninjured contralateral control.

5.2.10 IN VIVO SDF-1α LOADED MICROPARTICLE INJECTION

For *in vivo* SDF-1α loaded MP delivery, we based our dosage of SDF-1α on previous results in mouse models whereby 15-20 ng SDF-1α released from 10 wt% Hep^{-N} hydrogels over ~7 days resulted in significant cell recruitment after 7 days [9]. As male Sprague Dawley rats used in our studies were approximately 10X the weight of the mice used in previous studies, we used a dosage of ~155 ng SDF-1α released from 0.6 mg 10 wt% Hep^{-N} MPs. For *in vivo* injection, MPs were loaded with SDF-1α as described above but after centrifugation, MPs were resuspended in a total volume of 120 μL sterile 0.1 wt% BSA solution. MPs were then loaded into sterile syringes with 20-gauge 1.5 in. hypodermic needles and injected into the supraspinatus muscle immediately following tendon transection and denervation. Unloaded MPs were prepared in the same way, except that the maximum concentration of MPs that could be delivered in 120 uL was used (4.3 mg, 36 mg/mL).

5.2.11 FLOW CYTOMETRY

For flow cytometry experiments, groups included SDF-1α loaded MPs (0.6 mg MPs which released ~155 ng SDF-1α *in vitro*), unloaded MPs (4.3 mg MPs), and injury only (no SDF-1α or MPs). Supraspinatus muscles were harvested 3 and 7 days following injury and treatment, digested with collagenase 1A (Sigma) for 45 mins at 37º C, and passed through a 40 μm cell strainer (Corning). One-half of each sample was stained with the inflammatory cell panel that included FITC-conjugated anti-CD11b (AbD Serotec), PE-conjugated anti-CD163 (BioRad), and APC-conjugated anti-CD68 (BioRad) and the other one-half was stained with the MSC panel that included PE-conjugated anti-CD29 (BioLegend), APC-conjugated anti-CD44 (BioLegend), and BV421-conjugated anti-CD90 (BioLegend). Samples were stained for 30 mins with the appropriate

antibodies and fixed in 2% PFA for 20 mins, then analyzed using a FACS-AriaIIIu flow cytometer (BD Biosciences). Inflammatory cells were identified as CD11b+ myeloid cells, CD11b+CD68+ macrophages, and CD163 was used to differentiate M2-like (CD11b+CD68+CD163+) from M1-like macrophages (CD11b+CD68+CD163-) [277,278]. MSCs were identified as triple positive for CD29, CD44, and CD90 [279]; n = 4-9 animals per group per time point. For data analysis, each cell population was first calculated as a percentage of single cells:

$$\%\ \text{of single cells} = \frac{\#\ \text{of cells in subpopulation}}{\#\ \text{of single cells}}$$

Then, each % of single cell value was divided by the % of single cells in the uninjured contralateral control of the same animal:

$$\text{Fold-change over contralateral control} = \frac{\%\ \text{of single cells in experimental group}}{\%\ \text{of single cells in contralateral control}}$$

5.2.12 VASCULAR STAINING OF WHOLE-MOUNTED SUPRASPINATUS MUSCLE

After 7 days following injury and treatment, supraspinatus muscles were fixed in 4% PFA for 30 mins at RT, rinsed in PBS, permeabilized in 0.2% saponin (Sigma) PBS solution for 24 hours at 4ºC, and blocked in 10% BSA solution for 24 hours at 4ºC. For vascular staining, muscles were incubated in 5 µg/mL anti-mouse/rat CD31/PECAM-1 primary antibody (R&D Systems) in a 1.0% BSA, 0.3% Triton X-100 (Amresco), 0.01% sodium azide solution (incubation buffer) overnight at 4ºC, followed by 4 30-min washes in 0.2% saponin solution. Muscles were then stained in a 1:200 dilution of NL557-

conjugated anti-goat IgG secondary antibody (R&D Systems) in incubation buffer for 4 hours at RT, then washed in 0.2% saponin solution and PBS twice each for 30 mins. As a negative control, samples were stained using the same protocol but with polyclonal goat IgG isotype control (R&D Systems) in place of the primary antibody. Finally, muscles were incubated in a 1:1000 dilution of Hoechst cellular stain in PBS for 5 mins. Muscles were whole-mounted and single fluorescent images were obtained using a Zeiss LSM 700 confocal microscopy with a 10x objective to visualize vasculature (green) within muscle tissue (blue); n = 2 animals per group.

5.2.13 STATISTICAL ANALYSIS

All data are presented as mean ± standard deviation. One-way analysis of variance (ANOVA) and Tukey's post hoc multiple comparison test with a significance value set at $p \leq 0.05$ were used to identify significant differences. Statistical analysis was performed with Prism software.

5.3 RESULTS

5.3.1 MATERIALS CHARACTERIZATION

Using ^{1}H NMR analysis, PEGDA was determined to be ~55% functionalized and Hep^{-N} methacrylamide was determined to be 22-28% functionalized [261]. SAX-HPLC analysis was also used to assess Hep and Hep^{-N} disaccharide composition. Disaccharide elution patterns showed evidence of N-desulfation when comparing Hep^{-N} against Hep samples (Table 5.1). Finally, using SEC-HPLC, the weight average molecular weight was determined to be ~13.5 kDa for Hep^{-N} compared to ~18.4 kDa for Hep.

5.3.2 MICROPARTICLE FABRICATION

Degradable 10 wt% Hep^{-N} MPs were found to be 62 ± 65 μm in diameter (Figure 5.1B and C.1). Additionally, by varying DTT concentration within MPs, MP degradation ranged between 30 days for 20 mM DTT to 8 days for 40 mM DTT (Figure C.3). MPs used in all subsequent studies contained 35 mM DTT, which degraded within 16 days *in vitro* (Figure C.3).

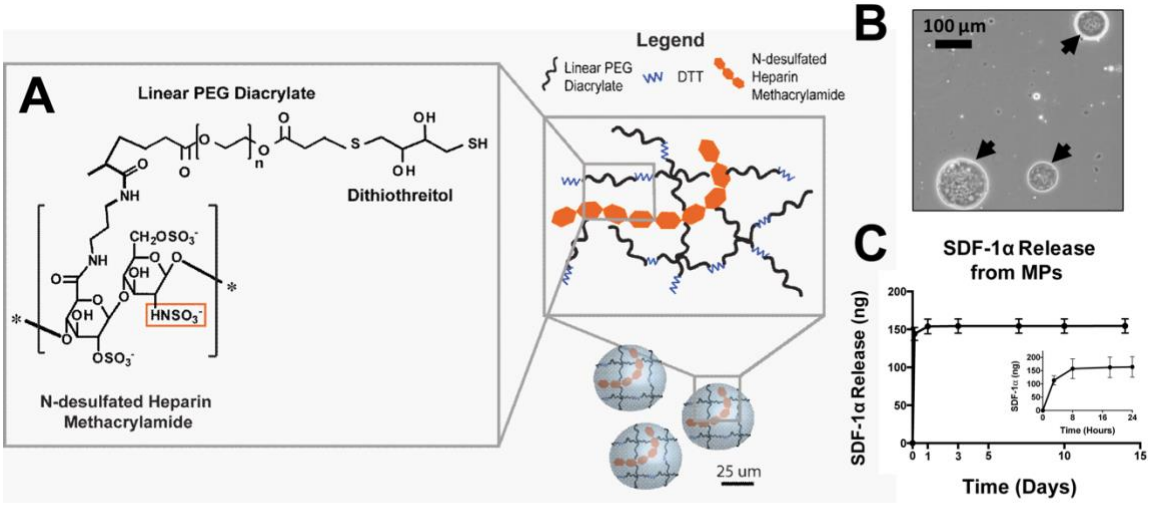

Figure 5.1. Degradable 10 wt% N-desulfated heparin microparticles released SDF-1α over 24 hours *in vitro*. (A) Microparticles were fabricated with 10 wt% N-desulfated heparin methacrylamide, 90 wt% linear poly (ethylene glycol) diacrylate and 35 mM dithiothreitol (DTT). (B) Phase image analysis indicated that microparticles were ~62±65 μm in diameter; black arrows indicate microparticles; scale bar is 100 μm. (C) Microparticles released ~155 ng SDF-1α over ~3 days *in vitro*; n = 3-5 ± SD.

5.3.3 In vitro SDF-1α loading and release from microparticles

For all MP batches, 370 ± 50 ng was loaded onto MPs and 155 ± 10 ng SDF-1α was released from MPs over ~24 hours *in vitro* (Figure 5.1C). Using the ~155 ng dose of SDF-1α, a small *in vivo* pilot study was conducted and results indicated that ~155 ng SDF-1α induced significant cell recruitment compared to injury alone. Once ~155 ng SDF-1α was determined to be an effective dose, we ensured that ~155 ng SDF-1α was

released from all subsequent batches of MPs by varying the initial mass of SDF-1α added to each batch of MPs between 1.0-1.2 µg SDF-1α and by conducting an *in vitro* release study prior to each surgery. The pilot study and additional data was combined and is shown in Figure 5.3 and 5.4.

5.3.4 In vivo injection of microparticles

Intact, non-degradable AF633 Hep^{-N} MPs (red) were visible within the supraspinatus muscle (blue) 3 and 7 days following injection (Figure 5.2Bi-ii), whereas degradable AF633 Hep^{-N} MPs were present at day 3 but no longer detectable by day 7 (Figure 5.2Biii-iv).

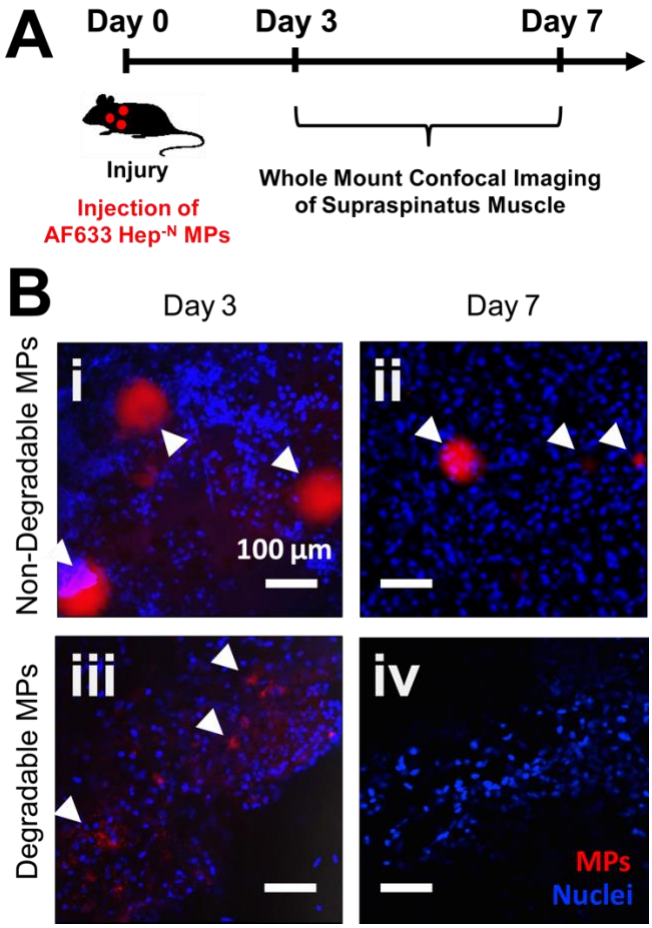

Figure 5.2. Injected 10 wt% Hep^{-N} microparticles were retained within the supraspinatus muscle for up to 7 days. (A) Experimental design: AlexaFluor633 tagged Hep^{-N} was

crosslinked within 10 wt% Hep^{-N} microparticles and injected into the supraspinatus muscle immediately following injury, then tracked at day 3 and 7 via confocal microscopy. (Bi-ii) Non-degradable microparticles (red) remained within the muscle (nuclei in blue) for at least 7 days while (Biii-iv) degradable microparticles appeared to have degraded by day 7; white arrow heads indicate microparticles; scale bar is 100 μm.

5.3.5 Inflammatory Cell Analysis

Supraspinatus muscles were analyzed for inflammatory cell infiltration via flow cytometry at days 3 and 7. For unloaded MPs, there was small but significant elevation in total myeloid cells (1.8 ± 0.6X compared to contralateral control) and macrophages (1.7 ± 0.6X) compared to the uninjured contralateral controls after 3 days (Figure 5.3A-B). For all other groups, there were no significant differences in myeloid cells (1.3-2.1X), macrophages (1.2-1.9X), or macrophage subpopulations (1.1-2.6X) between the experimental groups and the uninjured contralateral controls after 3 days (Figure 5.3A-D). There were also no differences between any of the experimental groups including SDF-1α loaded MPs, unloaded MPs, and injury only at the day 3 time point.

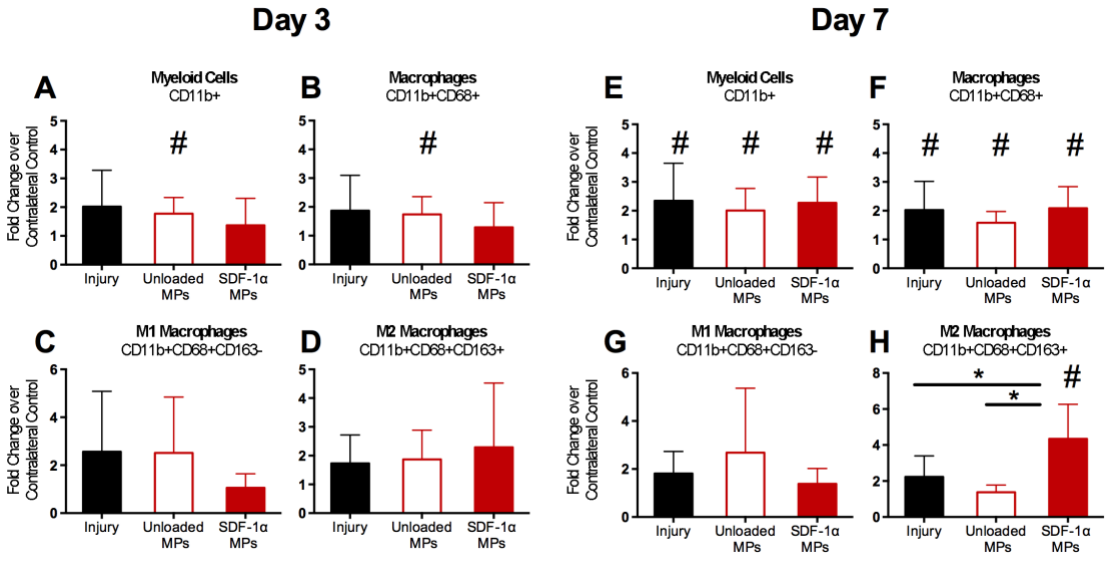

Figure 5.3. SDF-1α loaded microparticles recruited significantly more M2-like macrophages 7 days following injury and treatment. (A-D) No significant increase in cell

recruitment was observed after 3 days except in (A) total myeloid cells and (B) total macrophages after treatment with unloaded microparticles compared to uninjured controls. (E-F) By day 7, significantly more total myeloid cells and macrophages were recruited to all experimental groups compared to uninjured controls. (G) While there were no differences in M1-like macrophage recruitment between any of the experimental groups, (H) SDF-1α loaded microparticles recruited significantly more M2-like macrophages than all other groups. #Significantly greater than contralateral control at that time point; *Significantly different; $p \leqq 0.05$; n = 4-9 ± SD.

In contrast, 7 days following injury, significantly more M2-like macrophages were observed in muscle treated with SDF-1α loaded MPs than uninjured controls (4.3 ± 1.9X), unloaded MPs (1.4 ± 0.4X) and injury alone (2.2 ± 1.2X, Figure 5.3H). There were also no significant differences in M1-like macrophages between groups (Figure 5.3G). Notably, significantly more total myeloid cells (2.0-2.3X) and macrophages (1.6-2.1X) were detected in each experimental group compared to the respective uninjured contralateral controls (Figure 5.3E-F), though experimental groups were not significantly different from each other. Background fluorescence from antibody binding to inflammatory cell Fc receptors was tested by incubating separate samples with Fc blocker (CD16/32, BioLegend), and no significant differences were observed with any inflammatory cell population between Fc blocked and non-Fc blocked samples (Figure C.6). Therefore, Fc blocking was not used for the experiments and data presented in Figure 5.3.

5.3.6 MESENCHYMAL STEM CELL ANALYSIS

Similar to the trends seen in inflammatory cell analysis, there were no significant differences in MSC recruitment between any experimental group or between each experimental group and the uninjured contralateral controls at day 3 (1.1-1.4X, Figure 5.4A). However, by day 7 there were significantly more MSCs in both the SDF-1α

loaded MP group (3.0 ± 0.8X) and the unloaded MP group (1.7 ± 0.6X) compared to their respective uninjured contralateral controls, and significantly more MSCs were recruited to the SDF-1α loaded MP group than unloaded MPs and injury alone (Figure 5.4B).

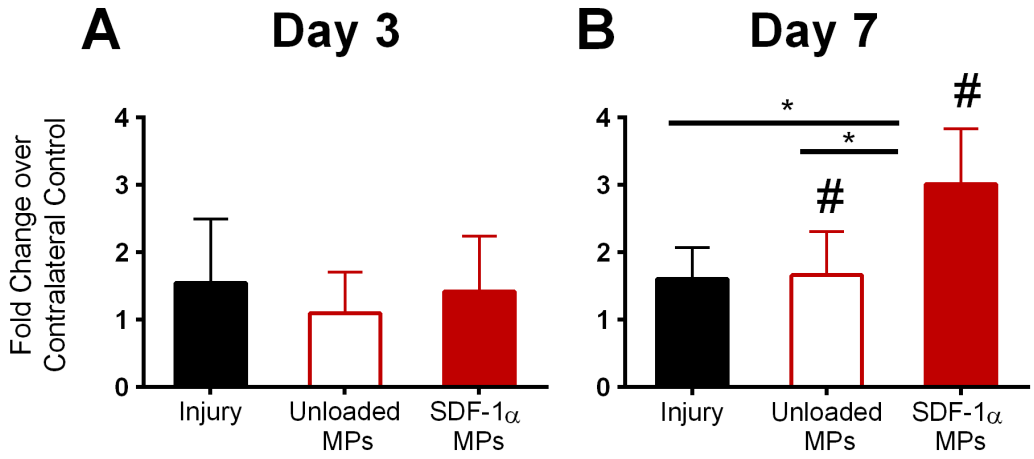

Figure 5.4. SDF-1α loaded microparticles recruited significantly more mesenchymal stem cells 7 days following injury and treatment. (A) No significant increase in mesenchymal stem cell (MSC, CD29+CD44+CD90+) recruitment was observed after 3 days but (B) by day 7, significantly more MSCs were recruited to the SDF-1α loaded microparticle group than all other groups. #Significantly greater than contralateral control; *Significantly different; $p \leqq 0.05$; n = 4-11 ± SD.

5.3.7 Vascular staining of whole-mounted supraspinatus muscle

Compared to uninjured contralateral controls that had little CD31+ vascular staining (Figure 5.5A), CD31+ vascular staining was present in the injury only control (Figure 5.5B). Furthermore, CD31+ vascular looping, a product of rapid angiogenesis whereby vessels elongate and form loops of vasculature [280], also appeared to be present in muscles treated with SDF-1α loaded MPs (Figure 5.5C). No staining was observed in samples prepared with isotype controls (data not shown).

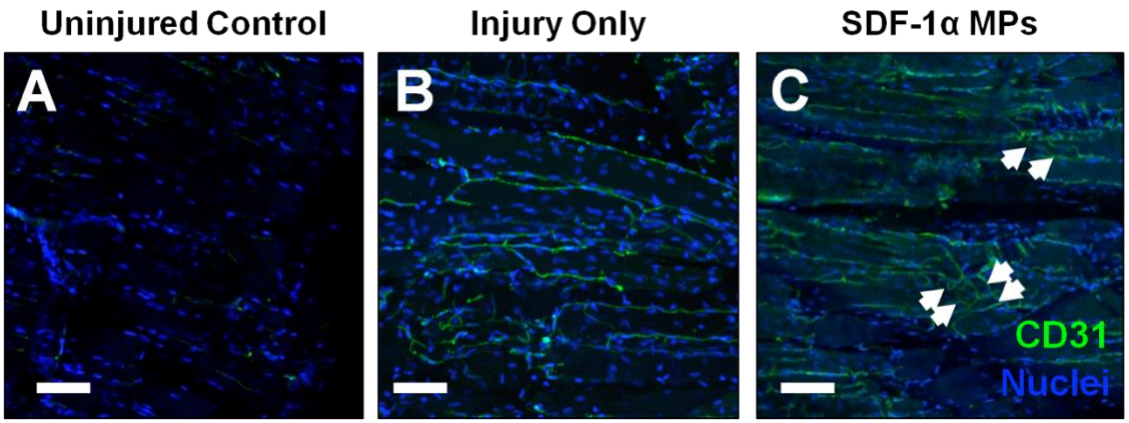

Figure 5.5. Vascular looping was observed in SDF-1α loaded MP treated supraspinatus muscle. Supraspinatus muscles treated with SDF-1α loaded MPs (C) appear to exhibit CD31+ vascular looping 7 days following injury and treatment compared to uninjured (A) or injured (B) controls; blue = Hoechst stained nuclei, green = CD31+ vasculature; white arrows indicate vascular loops; scale bar is 50 μm; n = 2.

5.4 Discussion

Despite the well-documented ability for SDF-1α to induce chemotaxis of pro-regenerative cell populations, SDF-1α treatment has yet to be explored in the unique cellular context of muscle degeneration following rotator cuff tear. Furthermore, as current standard-of-care reattachment surgery for rotator cuff tear largely neglects the muscle tissue, leading to further degeneration and an increased likelihood of re-tear [149,150], SDF-1α may be a promising strategy to recruit pro-regenerative cell populations to the degenerating muscle for improved rotator cuff repair prognoses in the future. We therefore developed injectable 10 wt% Hep^{-N} MPs capable of releasing bioactive SDF-1α and subsequently degrading within 1-2 weeks (Figure 5.1A-B) to enable further investigation and manipulation of cell populations within the rotator cuff muscle.

By incorporating varying concentrations of DTT within the MP crosslinking network, it is thought that the thioether group established between PEGDA and DTT increases the atomic charge of the carbonyl carbon within the PEGDA molecule, thereby increasing its reactivity with water and ultimately resulting in ester hydrolysis [17,281]. Thus, DTT concentrations of 20-40 mM, all of which were previously shown to be non-toxic in *in vitro* studies [282], were incorporated within 10 wt% Hep^{-N} MPs and resulted in degradation within 8 to 30 days *in vitro* (Figure C.3). Furthermore, while non-degradable MPs (0 mM DTT) remained intact over 7 days *in vivo*, degradable MPs (35 mM DTT) were no longer observable 7 days following injection in the supraspinatus muscle (Figure 5.2). Though we observed that MPs with 35 mM DTT degraded within 16 days *in vitro*, MP degradation rate can be concentration-dependent (data not shown) which may account for the differences observed between our *in vitro* and *in vivo* results. Furthermore, upon activation following injury or biomaterial implantation, cells including macrophages may secrete acids which reduce pH and accelerate ester hydrolysis [283], reactive oxygen intermediates which promote oxidation-mediated cleavage of the PEG ether backbone [284], and enzymes including esterases which catalyze the cleavage of PEGDA ester bonds [285], all which may have contributed to the accelerated MP degradation observed *in vivo*. Ultimately, 10 wt% Hep^{-N} MPs with 35 mM DTT degraded within 16 days *in vitro* and 7 days *in vivo*, and these particles were utilized in all subsequent *in vivo* studies to enable release of SDF-1α.

Next, we assessed *in vitro* and *in vivo* SDF-1α release from the Hep^{-N}-based MPs. In our system, though MP degradation occurred over 1-2 weeks *in vitro*, most of the ~155 ng SDF-1α released from MPs within 3 days *in vitro* (Figure 5.1C). *In vivo*,

fluorescently labelled SDF-1α was observed for at least 3 days following SDF-1α loaded MP injection, whereas little to no SDF-1α signal was observed after 3 days following soluble SDF-1α injection (Appendix A), which may indicate that MPs can retain SDF-1α at the site of injury for a longer period of time than soluble SDF-1α alone. It is important to note, however, that since the dose of MPs required for the *in vivo* tracking study was significantly higher due to sensitivity of the instrument, direct comparison with *in vitro* studies is not possible. Overall, this general release profile is similar to many other SDF-1α hydrogel and MP delivery systems, whereby more than 60% of all SDF-1α released over the time course of the experiment occurred within the first 1-3 days in all but one of these systems [11,12,19,31,34,286]. However, to improve the release kinetics of SDF-1α in future studies, one method may be to adjust the heparin-SDF-1α molar ratio, as increasing the heparin-to-protein molar ratio has previously been shown to reduce the release rate of basic fibroblast growth factor (bFGF) in a theoretical model of bFGF and heparin-containing biomaterials [67].

To assess the ability for SDF-1α loaded MPs to modulate the cellular milieu within the supraspinatus muscle, we first assessed how injury alone affected the muscle and its inflammatory cell and MSC populations. First, a significant decrease in supraspinatus muscle weight was observed after 6 weeks and a significant increase in fibrous infiltration was observed after only 3 weeks, both of which mimic symptoms of the human condition and indicate that significant muscle degeneration was induced within our animal model (Figure C.4) [149,150]. Concurrently, we assessed changes in the cellular milieu following injury and while no significant differences in the inflammatory cell populations were observed at day 3, significantly more myeloid cells

and macrophages were observed in the muscle from injured rotator cuffs compared to uninjured controls by day 7 (Figure 5.3E-F). Similar findings were also observed in our previous characterization of rotator cuff injury in mice, where significantly more mononuclear phagocytes, monocytes, macrophages, and dendritic cells were observed in the muscle from injured rotator cuffs compared to uninjured controls after 7 days [275]. Similar to injury alone, significantly more myeloid cells and total macrophages were also recruited following unloaded MP treatment at day 3 and day 7 (Figure 5.3A-B, E-F), and in no case was the unloaded MP group significantly different from the injury only group, which indicates that unloaded MPs did not elicit an additional inflammatory response. Overall, tendon transection and denervation resulted in significant total myeloid cell and macrophage recruitment after 7 days, and this characterization provided a baseline to further interrogate effect of SDF-1α release on the supraspinatus cellular milieu.

In this injury model, after SDF-1α loaded MP treatment, little change to inflammatory cell populations was observed after 3 days and, while significantly more total myeloid cells and macrophages were detected compared to uninjured controls after 7 days, this cell recruitment was not significantly different from unloaded MPs or injury alone (Figure 5.3). In analyzing macrophage subpopulations, however, significantly more M2-like macrophages were present at day 7 in muscle treated with SDF-1α loaded MPs than all other groups, including uninjured, injured, and unloaded MPs (Figure 5.3H). To understand the timing of cell recruitment observed, it is important to note that while much of the SDF-1α was released over 1-3 days, additional time may be required for a significant cellular response to be observed. For example, monocyte migration to sites of muscle injury typically peaks 7 days following injury [287] and monocyte to macrophage

differentiation can require up to 10 days depending on the microenvironment [288,289]. Furthermore, our present findings parallel our previous work using a mouse backpack model, whereby significantly more M2-like macrophages were located near a subcutaneously implanted SDF-1α loaded hydrogel after 7 days compared to unloaded hydrogels [10]. Finally, as our *in vivo* study of SDF-1α release from MPs indicates that a small percentage of SDF-1α may remain near the site of injection for at least 3 days, it is possible that this residual SDF-1α observed at later time points may have contributed to the significant differences in cell recruitment observed at day 7.

The selective recruitment of M2 macrophages in this system may be explained by the fact that studies have found that as monocytes underwent *in vitro* macrophage differentiation, CXCR4 (the primary SDF-1α receptor) gene expression increased 10-fold after 7 days [290], and in our recent work, anti-inflammatory monocytes exhibited higher CXCR4 surface expression than inflammatory monocytes [9]. In the same study, SDF-1α loaded 10 wt% Hep^{-N} hydrogels enabled a shift in monocyte composition, whereby significantly more anti-inflammatory monocytes and fewer pro-inflammatory monocytes were present compared to unloaded gels. Thus, it is possible that while SDF-1α release was unable to significantly affect the broader, more heterogeneous population of leukocytes, SDF-1α loaded MP treatment could lead to significant enrichment of high CXCR4-expressing M2-like macrophages.

In the context of muscle regeneration, it is important to note that M1 and M2 macrophages, which exist on a spectrum between pro and anti-inflammatory phenotypes, possess unique and critical functions to muscle repair. While M1 macrophages have been shown to infiltrate quickly following muscle injury and act to phagocytose cellular debris

and secrete pro-inflammatory proteins [277,291], M2 macrophages secrete anti-inflammatory proteins [277,292] and enhance the proliferation and differentiation of satellite cells [293], a muscle-derived stem cell subpopulation and the primary contributor to the reparative phase of muscle regeneration [199]. Thus, while significantly more anti-inflammatory, M2-like macrophages were observed in the muscle following SDF-1α loaded MPs treatment, additional studies are required to fully elucidate the optimal balance between M1 and M2 macrophages for muscle regeneration following rotator cuff injury.

SDF-1α loaded MPs also recruited significantly more MSCs compared to unloaded MPs, injury only, and uninjured contralateral controls 7 days following treatment (Figure 5.5). As MSCs have been previously utilized as a potential therapeutic in a variety of muscle injury types, several studies have investigated the potential mechanisms by which MSCs exhibit their muscle-regenerating capacity. Among these studies, some have shown that MSCs undergo myogenic differentiation *in vivo* [196], while others suggest that the MSC protein secretion profile may be primarily responsible for the regenerative effects of MSCs [294]. Specifically, MSCs possess many immunomodulatory functions, such as secreting proteins that mediate macrophage recruitment, mitigating the inflammatory response to injury, and promoting the polarization of pro-inflammatory, M1 macrophages into a more anti-inflammatory, M2 macrophage phenotype [295]. This immunomodulatory relationship is reciprocal as well, as macrophages have been shown to regulate MSC differentiation and promote MSC secretion of anti-inflammatory proteins such as TNF-α stimulated gene-6 (TSG-6) and pro-angiogenic proteins such as angiopoietin-1 [295,296]. Thus, while SDF-1α loaded

MPs may have initiated the enrichment of M2-like macrophages and the recruitment MSCs, it is possible that the reciprocal and synergistic relationship between these cell populations will enable additional modulation of the cellular milieu toward a more pro-regenerative microenvironment.

Both MSCs and M2 macrophages have previously shown to facilitate vascular remodeling and, in addition, it is well known that SDF-1α can recruit other pro-angiogenic cells including HSCs and smooth muscle cell progenitors [297] which can lead to collateralization, sprouting, looping, and splitting of new microvasculature [280,298,299]. In our studies, whole-mount imaging of the supraspinatus muscle 7 days following injury suggested that while CD31+ vascular staining was present in injured muscle, CD31+ vascular looping appeared present in the SDF-1α loaded MP group (Figure 5.5). As vascular looping is known to be a step of mature vessel formation, which can in turn support the regeneration of injured tissue [300,301] including muscle [214], the recruitment of pro-regenerative and pro-angiogenic cells to the supraspinatus muscle via SDF-1α loaded MPs may ultimately improve muscle healing in the context of rotator cuff injury.

5.5 CONCLUSIONS

In this aim, we developed a heparin-based microparticle platform to recruit pro-regenerative cells to the supraspinatus muscle following severe rotator cuff injury. To locally present SDF-1α, degradable 10 wt% Hep^{-N} microparticles were fabricated and subsequently injected within the supraspinatus muscle. After 7 days, significantly more anti-inflammatory, M2-like macrophages (4.3X increase compared to no injury) and

MSCs (3.0X increase compared to no injury) were detected in muscle treated with SDF-1α loaded MPs compared to unloaded MPs or injury alone. While no prior studies have investigated the use of chemotactic therapeutics such as SDF-1α to treat muscle following rotator cuff injury, our results indicate that SDF-1α loaded MPs can shift the cellular composition of the supraspinatus muscle, which may provide a platform to improve muscle repair after rotator cuff injury in the future.

CHAPTER 6

INTRA-MUSCULAR CHEMOKINE RELEASE AND SYSTEMIC BONE MARROW MOBILIZING AGENT DELIVERY ENHANCES EARLY SUPRASPINATUS MUSCLE REGENERATION FOLLOWING ROTATOR CUFF INJURY

6.1 INTRODUCTION

In Chapter 5, SDF-1α loaded microparticles (MPs) were found to recruit significantly more anti-inflammatory M2-like macrophages and mesenchymal stem cells (MSCs) to the supraspinatus muscle 7 days following rotator cuff injury. Still, it has yet to be determined what amount or what timescale of endogenous cell recruitment may be required for muscle regeneration in this unique context of supraspinatus muscle degeneration [141,144,145,159]. Therefore, delivering therapeutics that synergize with SDF-1α may be, first, a method to further modulate the inflammatory cellular milieu and recruit pro-regenerative cells to muscle and, second, a platform to examine how cell recruitment may result in muscle regeneration following rotator cuff tear.

Bone marrow mobilizing agents, including clinically approved granulocyte colony stimulating factor (G-CSF) and AMD3100, are most commonly used to treat neutropenia or lymphopenia following chemotherapy treatment [220–223]. Through indirect signaling, G-CSF has been shown to promote chemotaxis of hematopoietic stem and progenitor cells (HSPCs) from the bone marrow into circulation, and mice lacking G-CSF demonstrate chronic neutropenia which highlights its biological significance in cell mobilization [221]. Furthermore, through initial studies utilizing AMD3100 as a human immunodeficiency virus (HIV) inhibitor, significantly more circulating leukocytes were also observed in treated patients, leading to the approval of AM3100 as a hematopoietic

cell mobilization agent in 2008 [222]. Among other mechanisms of actions, both G-CSF and AMD3100 have shown to antagonize CXC chemokine receptor type 4 (CXCR4), an essential mediator of cell trafficking [33], which may also disrupt CXCR4 signaling with stromal cell-derived factor 1-α (SDF-1α/CXCL12) [221]. Despite these promising effects, G-CSF and AMD3100 can lead to significant complications and specifically through CXCR4 inhibition, AMD3100 has shown to impair the ability for cells to return to the bone marrow niche. Thus, bone marrow mobilizing agents with non-CXCR4 targets may be advantageous [36,225,226].

Sphingosine-1-phosphate (S1P) is a structurally simple lipid with a class of corresponding G-protein coupled receptors (GPCRs) $S1PR_{1-5}$, found in abundance in the plasma and serum [226]. During homeostasis, a gradient of S1P is maintained between the blood and bone marrow (Schematic 6.1) [227], and the disruption of this gradient leads to the sequestration of HSPCs, indicating the importance of S1P in the mobilization of bone marrow-derived cell populations. Though structurally similar, $S1PR_{1-5}$ possess unique functions, and even play opposing roles in cell mobilization. For example, $S1PR_1$ agonism is required for the egress of lymphocytes from bone marrow and lymphoid organs (Schematic 6.1) [35,228–230], while antagonism of $S1PR_3$ has been shown to promote egress of HSPCs from bone marrow to blood, ultimately suggesting that $S1PR_1$ agonists and $S1PR_3$ antagonists may be methods to promote cell mobilization.

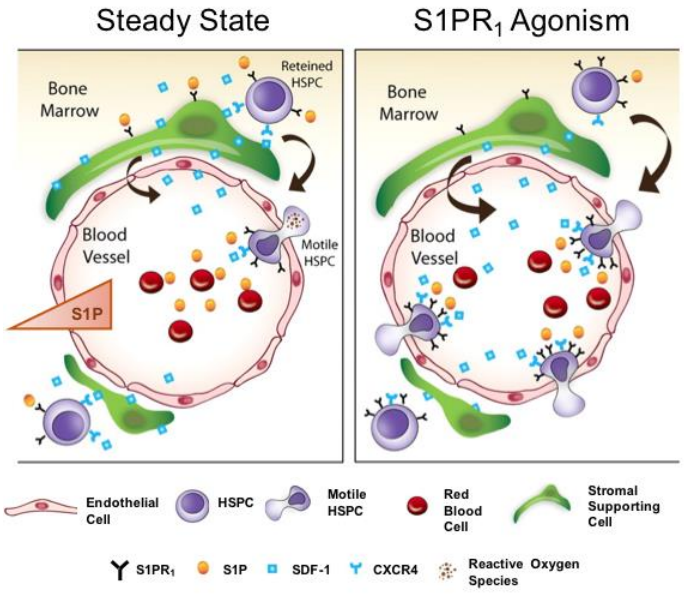

Schematic 6.1 S1P gradient at steady state and after $S1PR_1$ agonism. At steady state, a higher concentration of S1P is present in blood compared to bone marrow and tissue. $S1PR_1$ agonism in blood promotes egress of cells into circulation. Figure adapted from Golan et al [302].

Among a host of drugs targeting S1P receptors, VPC01091 (VPC) is both an $S1PR_1$ agonist and $S1PR_3$ antagonist [35,231]. *In vitro*, VPC induced a reduction in LSK ($Lin^{neg}Sca\text{-}1^{+}c\text{-}Kit^{+}$, early hematopoietic stem cells) cell adhesion and an increase in LSK cell migration. Furthermore, when delivered via intraperitoneal (I.P.) injection in rats, significantly more mesenchymal stem cells (MSCs, CD29+CD44+CD90+Sca1+) were observed in blood 1.5 and 24 hours after delivery [232] while in mice, significantly more circulating LSK cells were observed in blood 1.5 hours after delivery [36]. Interestingly, of the mobilized LSK cells, significantly more cells were CXCR4+ (the primary receptor for SDF-1α), compared to untreated controls [36].

SDF-1α, primarily through its GPCR, CXCR4, has previously shown in our work and others to attract a myriad of cell populations including immune cells such as

monocytes [9,10,28,29] and lymphocytes [29,219,266], stem cells such as hematopoietic [30] and mesenchymal stem cells (MSCs) [31], and progenitor cell populations [12,32], among others [33,34]. Most recently, we have shown that SDF-1α loaded microparticles (MPs) delivered to the supraspinatus muscle following severe rotator cuff injury could recruit significantly more M2-like macrophages and MSCs 7 days following injury and treatment [266]. Building from these findings and previous work indicating that VPC can mobilize CXCR4+ cells responsive to SDF-1α we hypothesized that the co-delivery of VPC via systemic I.P. injection and SDF-1α loaded MPs via intra-muscular injection, would synergistically increase the number of pro-regenerative cell populations in the supraspinatus muscle following rotator cuff injury more than either treatment alone.

6.2 METHODS

6.2.1 ANIMAL MODEL

Rotator cuff injury was induced using a similar method to previously established protocols [177,266]. Male Sprague-Dawley rats (250-300 g initial weight and 8-10 weeks old) were used in accordance with protocols approved by the Georgia Institute of Technology Institutional Animal Care and Use Committee. Prior to surgery animals were anesthetized by 5% isoflurane (Isothesia), followed by 2-3% isoflurane during surgery and were administered sustained release buprenorphine as an analgesic. The left chest and arm were shaved, wiped with alcohol/chlorhexidine, and a ~2 cm incision was made through the skin and deltoid, parallel to and just below the clavicle. To induce denervation, a ~0.5 mm portion of the suprascapular nerve was resected. Next, after orienting the humerus to expose the supraspinatus and infraspinatus tendon insertions,

both tendons were sharply transected, then encased in a 0.3 mm portion of PharMed BPT tubing (Tygon, 1.6 mm inner diameter) to prevent spontaneous reattachment of either tendon. The deltoid and skin were closed using Vicryl 4-0 absorbable sutures (Ethicon) and wound clips, respectively. The right rotator cuff of each animal served as an internal uninjured contralateral control.

6.2.2 MICROPARTICLE FABRICATION

10 wt% Hep^{-N} microparticles (MPs) were fabricated via water-and-oil emulsion as previously described [266]. Briefly, 50.0 mg PEGDA and 35 mM dithiothreitol (DTT) were added to 273 μL 10 wt% BSA PBS solution and incubated at ~ pH 7 and 37°C for 30 mins. Next, 5.6 mg Hep^{-N}MAm was added and the aqueous phase was incubated for an additional 30 mins. After 27 μL of 0.05 wt% Irgacure 2959 photo initiator (Ciba) was added, the aqueous phase described above was added drop-wise to an oil phase of 5 mL mineral oil (Amresco) with 3.0-3.2 μL Span80 (TCI) and allowed to homogenize at 4000 RPM (Polytron PT 3100, Kinematica) for 5 mins. The water-and-oil emulsion was nitrogen purged for 1 min then placed into a petri dish under UV (~15 mW/cm^2) for 10 mins to allow for free radical polymerization between PEGDA and Hep^{-N}MAm. Finally, the MP solution was added to 35 mL dH_2O, centrifuged at 4000 RPM for 5 mins, and the oil phase was removed. MPs were washed once more with dH_2O, then pipetted through 40 μm cell strainers to remove most MPs under 40 μm in diameter. MPs were sterilized in 70% ethanol on rotary at 4°C for 30 mins, followed by 3 30-min washes in sterile PBS. MPs were imaged via phase microscopy and size distribution was measured using ImageJ software. MPs were stored in sterile PBS at 4°C and used within 2 weeks of fabrication.

6.2.3 SDF-1α LOADED MICROPARTICLE ADMINISTRATION

To load SDF-1α onto MPs, 1.0-1.2 μg sterile human SDF-1α (R&D Systems) was added to 0.6 mg MPs in 50 μL 0.1 wt% sterile BSA solution. SDF-1α and MPs were incubated for 2 hours at 4°C, after which time MPs were rinsed by adding an additional 450 μL 0.1 wt% sterile BSA solution. The MPs were centrifuged for 3 mins at 10,000 RCF and 495 μL supernatant was removed. MPs were then resuspended in a total volume of 120 μL sterile 0.1 wt% BSA solution, loaded into sterile syringes with 20-gauge 1.5 in. hypodermic needles, and injected into the supraspinatus muscle immediately following rotator cuff injury.

6.2.4 VPC01091 ADMINISTRATION

VPC (Avanti Polar Lipids) was dissolved at 1 mg/mL in 2% 2-hydroxypropyl-B-cyclyodextrin H_2O solution and placed in a sonicating bath for 1 hr to fully dissolve. VPC was then filtered sterilized and stored at -20°C until use. Immediately following rotator cuff injury, VPC was administered via intraperitoneal (I.P.) injection at either 1 mg or 5 mg/kg animal weight using a 1 mL leur lock syringe and 25-guage 1.5 in. hypodermic needle.

6.2.5 COLLECTION AND FLOW CYTOMETRY ANALYSIS OF BLOOD

To avoid disruption of the cell populations within blood, animals remained awake but restrained for blood collection. After 1.5 hrs, 3 hrs, 1, 3, and 7 days following rotator cuff injury and treatment, a scalpel was used to create a small incision perpendicular to the tail, ~3 cm from the tail tip. No more than 150 μL blood was collected in a 1.7 mL low binding tube containing 10 μL 500 AU/mL heparin to prevent blood coagulation. Next, erythrocytes were lysed by adding 10x ammonium chloride by volume compared to the volume of blood for 10 mins at RT. Samples were centrifuged for 5 mins at 500

RCF, and supernatant was removed. One-half of each sample was stained with the inflammatory cell panel that included FITC-conjugated anti-CD11b (AbD Serotec), PE-conjugated anti-CD163 (BioRad), and APC-conjugated anti-CD68 (BioRad) and the other one-half was stained with the MSC panel that included PE-conjugated anti-CD29 (BioLegend), APC-conjugated anti-CD44 (BioLegend), BV421-conjugated anti-CD90 (BioLegend), and APC/Fire750 anti-CD45 (BioLegend). Samples were stained for 30 mins with the appropriate antibodies and fixed in 2% PFA for 10 mins, then analyzed using a FACS-AriaIIIu flow cytometer (BD Biosciences). Inflammatory cells were identified as CD11b+ myeloid cells, CD11b+CD68+ macrophages, and CD163 was used to differentiate M2-like (CD11b+CD68+CD163+) from M1-like macrophages (CD11b+CD68+CD163-) [277,278]. MSCs were identified as negative for CD45 and triple positive for CD29, CD44, and CD90 [279]; n = 6. For data analysis, each cell population was calculated first as a percentage of single cells:

$$\%\ \text{of single cells} = \frac{\#\ \text{of cells in subpopulation}}{\#\ \text{of single cells}}$$

Then, each % of single cell value was divided by the % of single cells at the 1.5 hour time point from the same animal:

$$\text{Fold-change over 1.5 hour time point:}\ \frac{\%\ \text{of single cells at each time point}}{\%\ \text{of single cells at 1.5 hours}}$$

6.2.6 FLOW CYTOMETRY ANALYSIS OF MUSCLE

Supraspinatus muscles were harvested 3 and 7 days following injury and treatment, digested with collagenase 1A (Sigma) for 45 mins at 37º C, and passed through a 40 μm

cell strainer (Corning). One-half of each sample was stained with the inflammatory cell panel described in Methods Section 6.2.3; n = 5-7. For data analysis, each cell population was first calculated as a percentage of single cells:

$$\%\ \text{of single cells} = \frac{\#\ \text{of cells in subpopulation}}{\#\ \text{of single cells}}$$

Then, each % of single cell value was divided by the % of single cells in the uninjured contralateral control of the same animal:

$$\text{Fold-change over contralateral control} = \frac{\%\ \text{of single cells in experimental group}}{\%\ \text{of single cells in contralateral control}}$$

6.2.7 PROTEIN PRODUCTION IN MUSCLE

Portions of muscle harvested at day 7 were digested with Tissue Extraction Reagent 1 (Invitrogen) and stored at -80ºC prior to use for Luminex analysis with the MILLIPLEX MAP rat cytokine/chemokine immunology magnetic bead panel (EMD Millipore). First, 12.5 µL of sample and standard (EMD Millipore) was combined with 12.5 µL assay buffer (EMD Millipore) and 12.5 µL pre-mixed magnetic beads (EMD Millipore) in a 96-well plate. The plate was incubated overnight at 4ºC on a 750rpm shaker plate. Next, the plate was washed 3 times by placing the plate on a magnet for 2 mins, decanting the plate, adding 200 µL wash buffer (EMD Millipore), and allowing the plate to shake at RT for 2 mins. After washing was repeated 3 times, 12.5 µL of detection antibody (EMD Millipore) was added and the plate was incubated for 1 hr shaking at 750 RPM in RT. Next, 12.5 µL strep-phyco (EMD Millipore) was added and the plate was incubated for 30 mins shaking at 750 RPM in RT. After washing 3 times, 110 µL drive fluid was

added, the plate was shaken for 5 mins at RT, and then analyzed on the Luminex System (MAGPIX Instruments). Individual samples were normalized to total protein content (in mg/mL) which was determined using a BCA assay (Thermo Scientific); n = 4-6.

6.2.8 VASCULAR STAINING OF MUSCLE

After 7 days following injury and treatment, supraspinatus muscles were fixed in 4% PFA for 30 mins at RT, rinsed in PBS, permeabilized in 0.2% saponin (Sigma) PBS solution for 24 hours at 4ºC, and blocked in 10% BSA solution for 24 hours at 4ºC. For vascular staining, muscles were incubated in 5 µg/mL anti-mouse/rat CD31/PECAM-1 primary antibody (R&D Systems) in a 1.0% BSA, 0.3% Triton X-100 (Amresco), 0.01% sodium azide solution (incubation buffer) overnight at 4ºC, followed by 4 30-min washes in 0.2% saponin solution. Muscles were then stained in a 1:200 dilution of NL557-conjugated anti-goat IgG secondary antibody (R&D Systems) in incubation buffer for 4 hours at RT, then washed in 0.2% saponin solution and PBS twice each for 30 mins. As a negative control, samples were stained using the same protocol but with polyclonal goat IgG isotype control (R&D Systems) in place of the primary antibody. Finally, muscles were incubated in a 1:1000 dilution of Hoechst cellular stain in PBS for 5 mins. Muscles were whole-mounted and single fluorescent images were obtained using a Zeiss LSM 700 confocal microscopy with a 10x objective to visualize vasculature (green) within muscle tissue (blue). First, CD31+ vascular loops were quantified manually in 3 10x images per animal. CD31+ vasculature was then quantified using ImageJ and color thresholding; n = 5-7:

$$\%\ \text{CD31+ vasculature} = \frac{\text{total green fluorescent signal}}{\text{total area of muscle}}$$

6.2.9 HISTOLOGY OF MUSCLE

After 7 days following injury and treatment, supraspinatus muscles were harvested and incubated in 10% v/v optimum cutting temperature (OCT, Sakura Finetek) PBS solutions with 0, 10, and 20% sucrose for 10 mins each. Muscles were placed in histology blocks with 100% OCT under vacuum overnight and then frozen in 190 proof ethanol cooled by liquid nitrogen. Muscles were sectioned with a cryostat (Thermo Scientific CryoStar NX70) into 10 μm sections perpendicular to the muscle to create tissue cross-sections.

Prior to hematoxylin and eosin (H&E) staining, muscle cross-sections were rinsed in distilled water (dH_2O) for 2 minutes then stained in hematoxylin (Fisher) for 2 mins. Subsequently, slides were rinsed in dH_2O until excess stain was removed, dipped in 0.5% acid alcohol once, rinsed in dH_2O for 1 min, Scott's tap water (Electron Microscope Science) for 30 seconds, dH_2O for 2 mins, and 95% ethanol for 1 min. Sections were then stained in eosin (VWR) for 30 seconds. Following eosin staining, slides were rinsed in 95% ethanol for 30 seconds, dehydrated in 100% ethanol 3 times for 1 min, and cleared in xylene 3 times for 1 min. Sections were then covered with cytoseal (Richard Allen Scientific) and coverslipped for imaging via phase contrast imaging (Nikon i80 microscope); n = 5-7.

6.2.10 IMMUNOHISTOCHEMISTRY OF EMHC, DYSTROPHIN, AND CD163+ MACROPHAGES IN MUSCLE

Muscle cross-sections were first prepared as described in Methods Section 6.2.7. For immunohistochemical staining, sections were outlined using a hydrophobic pen, then blocked with blocking buffer (2% bovine serum albumin, 0.5% goat serum, 0.5% Triton X in PBS solution) for 30 mins at RT. Between each step, slides were washed 3 times for 2 mins each with 0.1 wt% Tween20 PBS solution. Primary antibodies included

embryonic myosin heavy chain (eMHC) primary antibody (Developmental Studies Hybridoma Bank, 1:10 dilution), dystrophin (Abcam, 1:200), PE-conjugated anti-CD163 (BioRad, 1:10), and APC-conjugated anti-CD68 (BioRad, 1:10) in blocking buffer. Primary antibodies were pipetted onto slides, allowed to incubate for 1 hr at RT, then washed. Secondary antibody for eMHC (Goat anti-mouse AlexaFluor555, Thermo Fisher) and for dystrophin (Goat anti-rabbit AlexaFluor 488) were diluted 1:250 in blocking buffer, pipetted onto slides, allowed to incubate in the dark for 30 mins at RT, then washed. Finally, Hoechst cellular stain was diluted 1:1000 in PBS, pipetted onto slides, allowed to incubate for 5 mins, and washed. Sections were fixed with 4% paraformaldehyde (PFA) for 10 mins at RT, washed, then mounted with cytoseal (Richard Allen Scientific) and coverslipped for imaging using a Zeiss LSM 700 confocal microscopy with a 10x objective to visualize eMHC (red) and CD163+ macrophages (yellow) within outlined muscle fibers (dystrophin, green) with cell nuclei (blue); n = 5-7.

6.2.11 Muscle weight 2 and 3 weeks post-injury and treatment

To assess muscle degeneration at later time points following rotator cuff tear, injury was induced following Methods Section 6.2.1. SDF-1α loaded MPs and VPC were administered as described in Methods Section 6.2.3 and 6.2.4 at day 0, but were also administered weekly such that SDF-1α loaded MPs, injected via percutaneous injection, and VPC were delivered at day 0 and 7 for 2 week animals and day 0, 7, and 14 for 3 week animals. At each designated time point, supraspinatus muscles were harvested, weighed, and its mass was divided by the mass of the uninjured contralateral control; n = 6-8 per group per time point.

6.3 RESULTS

6.3.1 INFLAMMATORY CELL ANALYSIS IN BLOOD AND MUSCLE

After 3 hrs, 24 hrs, 3 and 7 days following injury and treatment, VPC+SDF-1α treatment resulted in significantly more myeloid cell mobilization in blood than injury alone (Figure 6.1A). VPC alone significantly increased the number of circulating myeloid cells at 3 and 24 hrs, whereas SDF-1α alone was significantly higher than injury at day 7. After 3 days, both VPC+SDF-1α and VPC significantly increased the number of myeloid cells in muscle compared to SDF-1α and injury, whereas by day 7 all treated muscles had significantly more myeloid cells than injury alone (Figure 6.1B-C).

Though no significant differences were observed at 3 and 24 hours in blood, after 3 days VPC+SDF-1α treatment resulted in significantly more monocyte mobilization than all other groups, and after 7 days both VPC+SDF-1α and SDF-1α treatment resulted in significantly more monocyte mobilization than VPC and injury (Figure 6.1D). In muscle, significantly more macrophages were observed in VPC+SDF-1α and VPC treated groups after 3 days, whereas significantly more macrophages were presented in VPC+SDF-1α and SDF-1α treated groups after 7 days compared to injury alone (Figure 6.1E-F).

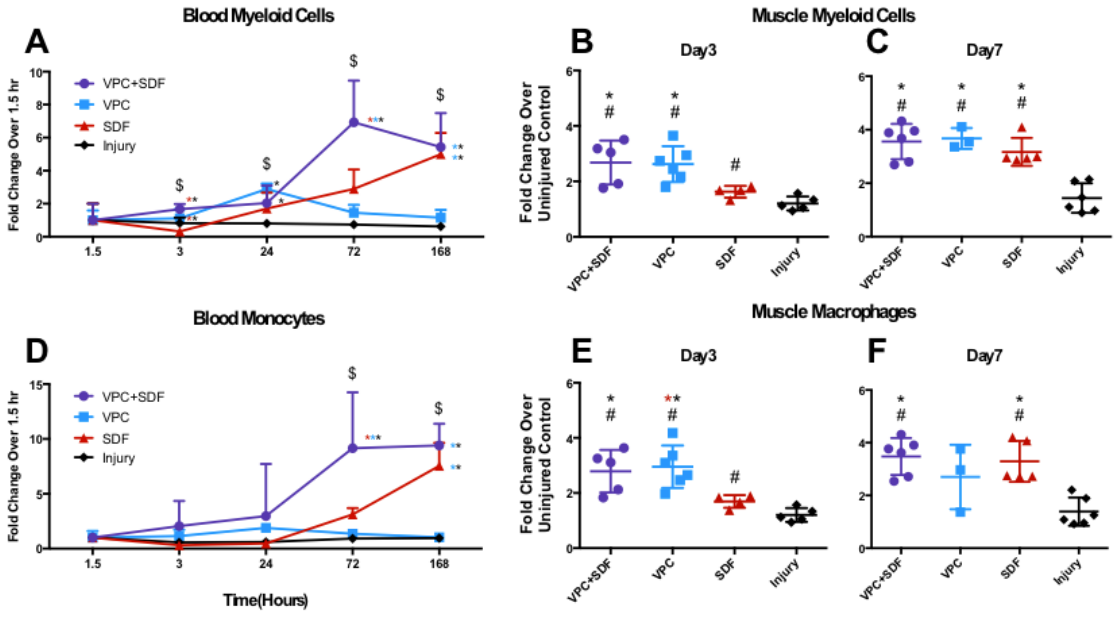

Figure 6.1. Mobilization of myeloid cells and monocytes in blood corresponds to an increase in myeloid cells and macrophages in muscle. (A) VPC+SDF and VPC treatment exhibited significantly more myeloid cell recruitment after 3 hrs, 24 hrs, and 3 days compared to injury, (B-C) leading to a significant increase in myeloid cells in muscle after 3 and 7 days with VPC+SDF and VPC compared to injury. (D) VPC+SDF treatment exhibited significantly more monocyte mobilization after 3 days compared to all groups, whereas both VPC+SDF and SDF exhibited more monocyte mobilization at day 7. (E-F) At day 3, significantly more macrophages were observed in VPC+SDF and VPC treated muscle compared to injury, whereas at day 7 VPC+SDF and SDF treated groups were significantly higher than injury. $^{\$}$VPC+SDF significantly different than injury at designated time point; Significantly different than: $^{\#}$uninjured; * injury; **SDF and injury; **VPC and injury; ***VPC, SDF, and injury; $p \leq 0.05$; n = 6 in blood; n = 4-6 in muscle.

When assessing macrophage subpopulations in muscle, VPC+SDF-1α and VPC treatment resulted in significantly more M2-like and M1-like macrophages compared to injury (Figure 6.2A-B), and a significantly higher M2:M1 macrophage ratios than both SDF-1α and injury (Figure 6.2C). By day 7, all treatments significantly increased the number of M2 macrophages in muscle, though no significant differences were observed in M1 macrophages, except between SDF-1α and VPC treatment (Figure 6.2D-E). However, only VPC+SDF-1α and VPC treatments significantly increased the M2:M1

ratio at day 7, a ~5x increase from uninjured controls (Figure 6.2F). Parallel to our flow cytometry findings, after 7 days more CD163+ staining was observed in treated muscles than in injury alone (Figure 6.2G-J).

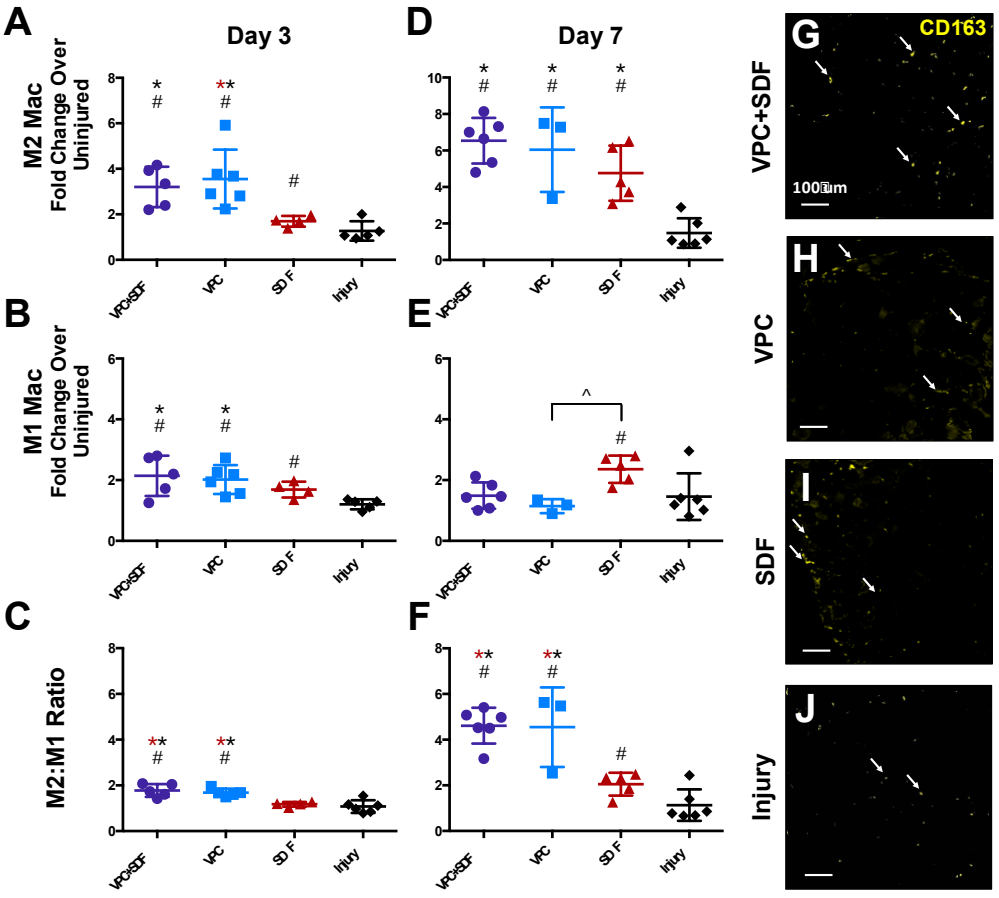

Figure 6.2. More M2-like macrophages were observed in all treated muscles at day 7 compared to injury, but only VPC+SDF and VPC treatment increased the M2:M1 ratio at day 3 and 7 compared to SDF and injury. (A-C) After 3 days, more M2-like and M1-like macrophages were observed with VPC+SDF and VPC treatment compared to injury, resulting in a significantly higher M2:M1 macrophage ratio compared to SDF and injury. (D-F) By 7 days, more M2-like macrophages were observed in all treatment groups compared to injury, though the M2:M1 ratio was only increased in the VPC+SDF and VPC groups compared to SDF injury. ^SDF is significantly different than VPC; Significantly different than: #uninjured; * injury; **SDF and injury; $p \leq 0.05$. (G-J) Similarly, more CD163+ staining (yellow) was observed in treated muscle than in injured

muscle via immunohistochemistry; white arrows indicate example CD163+ cells; scale bar is 100 μm; n = 4-6.

6.3.2 Mesenchymal stem cell analysis in blood and muscle

After 3 hrs, significantly more MSCs were observed in blood with VPC treatment compared to SDF-1α treatment and injury, and with VPC+SDF-1α treatment compared to injury (Figure 6.3A). By 24 hrs, significantly more MSCs were mobilized in VPC+SDF-1α and SDF-1α treated animals compared to VPC treatment and injury, while VPC treatment was only significantly greater than injury alone. At day 3, similar trends were observed as at 24 hrs, whereby VPC+SDF-1α and SDF-1α treated animals exhibited the greatest MSC mobilization. MSC mobilization was significantly higher in SDF-1α treatment compared to VPC treatment and injury, whereas VPC+SDF-1α was only significantly higher than injury. Finally, by day 7 in blood, MSC mobilization via VPC+SDF-1α and SDF-1α treatment was no longer significantly different from injury, and was only significantly higher than VPC treatment alone.

In muscle, after 3 days significantly more MSCs were observed with VPC+SDF-1α and VPC treatment (Figure 6.3B), whereas all treatments, VPC+SDF-1α, VPC, and SDF-1α, led to significantly more MSCs in muscle by day 7 compared to injury (Figure 6.3C).

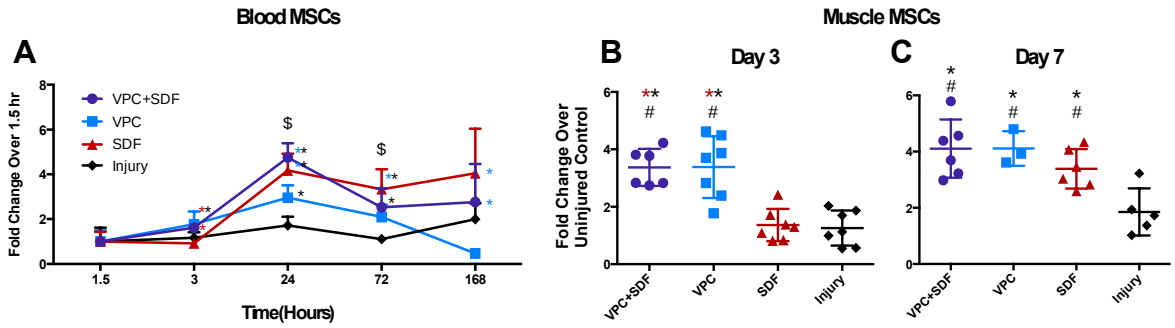

Figure 6.3. Increased MSC mobilization in blood by all treatment groups after 3 hours to 3 days compared to injury led to significantly more MSCs in VPC+SDF and VPC treated muscle after 3 days and all treated muscles at day 7. (A) MSC mobilization was greater than injury with VPC+SDF and VPC after 3 hrs, all treatments after 24 hrs, and VPC+SDF and SDF 3 days. (B) In muscle, MSC recruitment was greater than injury with VPC+SDF and VPC after 3 days, and all treatments after 7 days. $^{\$}$VPC+SDF significantly different than injury at designated time point; Significantly different than: $^{\#}$uninjured; * injury; **SDF and injury; **VPC and injury; ***VPC, SDF, and injury; $p \leq 0.05$; n = 6 in blood; n = 4-6 in day 3 muscle; n = 3-6 in day 7 muscle.

6.3.3 Inflammatory Protein Production in Muscle

Principal component analysis (PCA) was first utilized to assess the muscle secretome after 7 days. Treated, injured, and uninjured groups were not well-discriminated from each other using PCA, suggesting that the global secretome was not significantly altered by injury or treatment at day 7 (Figure D.1). We also analyzed significant differences between groups with each analyte. Due to injury, the pro-inflammatory protein IL-5 was significantly increased compared to all groups, IL-18 and RANTES were significantly increased compared to uninjured controls, and LIX was significantly increased compared to VPC (Figure 6.4A-D). In contrast, analyzing muscles with VPC+SDF-1α, VPC, or SDF-1α treatment, average production of IL-5, IL-18, and RANTES were not significantly different from uninjured muscle. Leptin, an adipogenic mediator, was also significantly increased in injured muscle compared to uninjured, while Leptin production in all treated muscles was not significantly different from uninjured (Figure 6.4E).

Finally, VEGF, a pro-angiogenic factor, was significantly decreased in injured compared to uninjured muscles, while VEGF production in treated muscles were not significantly different than uninjured muscles (Figure 6.4F).

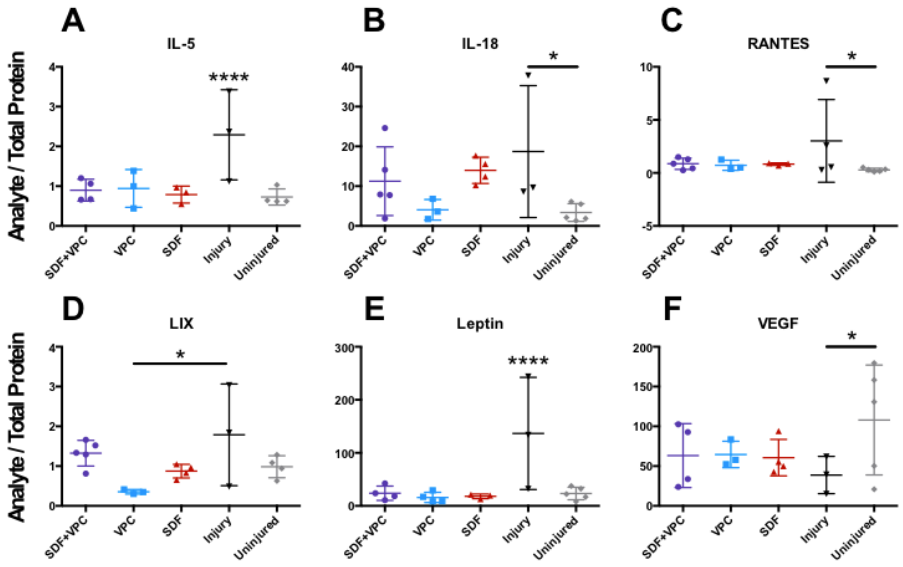

Figure 6.4. Pro-inflammatory mediators were increased in injured muscles compared to uninjured controls after 7 days. (A) Pro-inflammatory protein IL-5 was significantly increased compared to all groups, (B-C) IL-18 and RANTES were significantly increased compared to uninjured controls, and (D) LIX was significantly increased compared to VPC. (E) Leptin production, an adipogenic mediator, was significantly higher in injured muscle than all others and (F) VEGF production, an angiogenic mediator, was significantly lower in injured than uninjured muscle. ****Significantly different than all other groups; *Significantly different than designated group; $p \leq 0.05$; n = 3-6.

On a single analyte basis, certain treatments also significantly altered protein production. SDF-1α treated significantly increased IP-10 production compared to VPC+SDF-1α and uninjured muscle, whereas VPC and SDF-1α treatment significantly reduced IL-13 production compared to uninjured muscles (Figure 6.5).

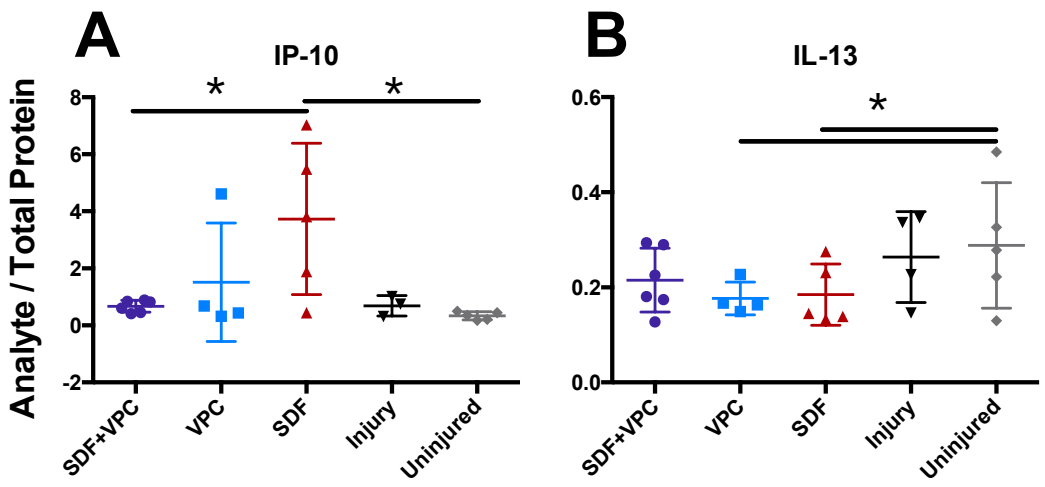

Figure 6.5. VPC and SDF significantly modulated the production of chemoattractive and macrophage polarizing proteins compared to uninjured controls. (A) IP-10 production was significantly higher in SDF treated muscle than SDF+VPC and uninjured, (B) while IL-13 production was significantly decreased in VPC and SDF groups compared to uninjured muscle. *Significantly different than designated group; $p \leq 0.05$; n = 4-6.

6.3.4 Vascular staining of muscle

After 7 days, significantly more CD31+ vasculature was observed in VPC+SDF-1α treated muscles compared to uninjured controls, while no other groups were significantly different from each other (Figure 6.6). Vascular looping, indicative of rapid angiogenesis was also quantified but high variance was observed and no significant differences were found between groups (Figure 6.7).

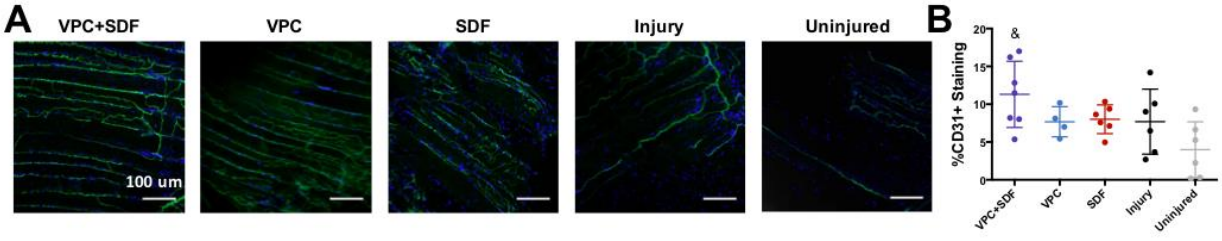

Figure 6.6. Significantly more CD31+ vasculature was present in VPC+SDF treated muscle compared to uninjured controls after 7 days. (A) Whole-mounted muscles were stained for CD31+ vasculature (green) and nuclei (blue); scale bar is 100 µm. (B) Image analysis indicated that significantly more CD31+ staining was observed in VPC+SDF

treated muscles compared to uninjured controls; &Significantly different than uninjured; $p \leq 0.05$; n = 6-7.

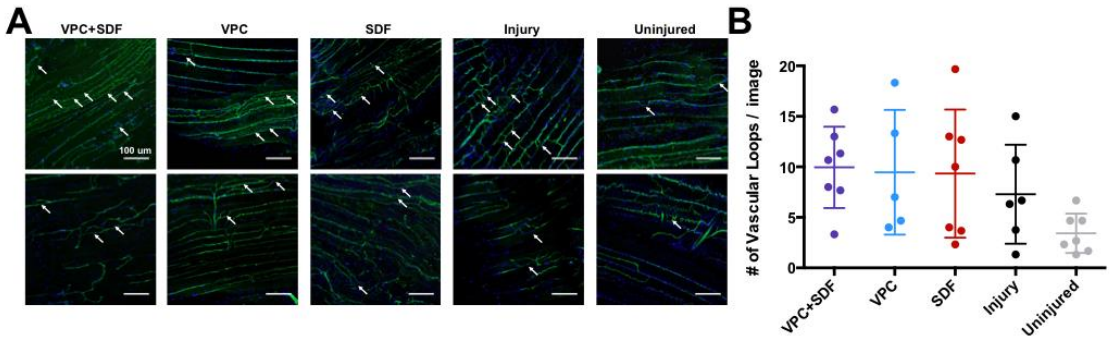

Figure 6.7. CD31+ vascular looping was present in all muscle after 7 days. (A) Whole-mounted muscles were stained for CD31+ vasculature (green) and nuclei (blue) and two images were included per group to accurately portray variability of CD31+ vascular looping; white arrows indicate example CD31+ vascular loops; scale bar is 100 µm. (B) Image analysis indicated that no significant differences were observed between groups; n = 6-7.

6.3.5 Embryonic Myosin Heavy Chain (eMHC) and Dystrophin Staining of Muscle

After 7 days, supraspinatus muscle cross-sections were stained for eMHC+ regenerating muscle fibers (Figure 6.8). With all treatments, significantly more eMHC+ muscle fibers were observed than in untreated injury muscles (Figure 6.8B). However, significantly more eMHC+ fibers were observed in muscles treated with VPC+SDF-1α than either treatment alone (Figure 6.8B).

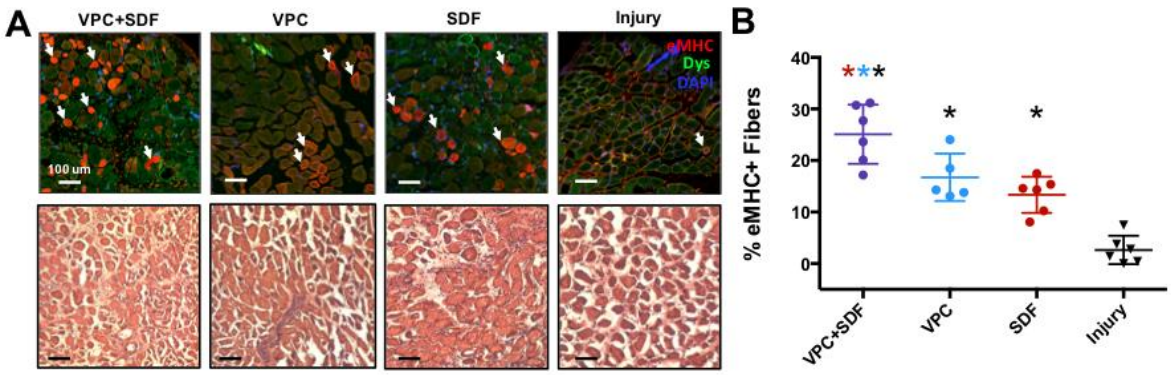

Figure 6.8. Significantly more eMHC+ regenerating muscle fibers were observed in VPC+SDF treated muscles than all other groups after 7 days. (A) Representative images of muscle cross-sections stained with eMHC (red), dystrophin (green), and DAPI (blue) on top, and hematoxylin & eosin on bottom. White arrows indicate example eMHC+ muscle fibers; Scale bar is 100 μm. (B) Quantification of eMHC images indicated that more eMHC+ fibers were observed in VPC+SDF muscle compared to all groups, and more eMHC+ fibers were observed in VPC and SDF muscle than injury. Significantly different than: * injury; ***VPC, SDF, and injury; $p \leq 0.05$; n = 5-7.

6.3.6 Muscle weight 2 and 3 weeks post-injury and treatment

After 1 week, no significant decrease in muscle weight was observed with VPC+SDF-1α muscles or injured muscles (Figure 6.9). However, by 2 and 3 weeks a significant reduction in muscle weight was observed in injured muscles untreated or treated with VPC+SDF-1α compared to uninjured controls. No significant difference was observed at any time point between VPC+SDF-1α treated muscles and injured muscles.

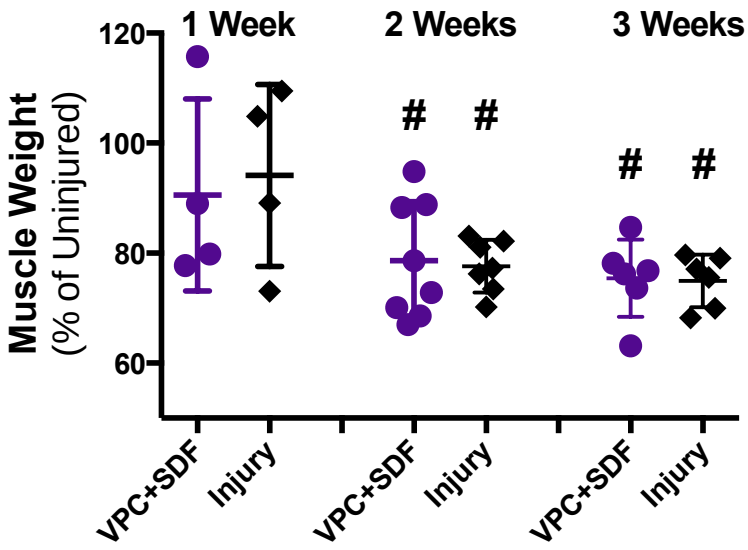

Figure 6.9. Muscle weight was not significantly different between VPC+SDF treated muscle and injured muscles 1, 2, and 3 weeks post-injury. # Significantly different than uninjured contralateral controls; $p \leq 0.05$; n = 4 for 1 week, n = 6-8 for 2 and 3 weeks.

6.4 Discussion

Combining the results of previous work that identified the ability for VPC to mobilize CXCR4+ cells [232] and the ability for SDF-1α loaded MPs to recruit CXCR4+ cells to the supraspinatus muscle, we hypothesized that the co-delivery of VPC via systemic injection and SDF-1α loaded MPs via intra-muscular injection would synergistically increase the number of pro-regenerative cell populations in muscle following rotator cuff injury more than either treatment alone. Therefore, we investigated the ability for VPC and SDF-1α to mobilize inflammatory cells and MSCs within blood and, subsequently, to increase these cell populations in muscle to promote regeneration following rat tendon transection and denervation.

We first investigated inflammatory cell mobilization and recruitment in blood and muscle, respectively, following rotator cuff injury. In blood, the fold-change in myeloid cells and monocytes compared to the 1.5 hour time point was less than 1 at all time points

for injury alone, indicating that cell mobilization generally decreased after the initial response to injury (Figure 6.1A,D). In muscle at day 3, a 1.2 to 1.3-fold increase in myeloid cells, macrophages, and macrophage subpopulations was observed in injury compared to uninjured controls, which increased to a 1.4 to 1.5-fold increase for all inflammatory cell populations by day 7 (Figure 6.1). Furthermore, at both day 3 and 7 the M2:M1 macrophage ratio was ~1.1, though overall no significant differences were observed between injury and uninjured controls. These results parallel our previous findings in mice, where monocytes and macrophages were only slightly skewed toward a more anti-inflammatory phenotype 7 days after rotator cuff injury [275]. In other skeletal muscle injuries, a typical inflammatory response includes an initial influx of neutrophils, then pro-inflammatory M1 macrophages and finally, within 7 to 14 days, recruitment and polarization toward a more anti-inflammatory M2 macrophage phenotype [303,304]. At day 3 and 7 in our work, however, no substantial shift in the M2:M1 ratio was observed, which may indicate that the inflammatory response is dysregulated and may ultimately contribute to the muscle degeneration observed following rotator cuff tear.

Following treatment with VPC and SDF-1α, we investigated the timeline of cell mobilization in blood and recruitment in muscle. VPC+SDF-1α and VPC treatment generally elicited more myeloid cell and monocyte mobilization in blood between 3 and 24 hours after treatment and, subsequently, significant increases in these cell populations were observed in muscle after 3 days compared to SDF-1α or injury alone (Figure 6.1B,E). Similarly, VPC+SDF-1α treatment elicited more myeloid cell and monocyte mobilization at day 3 in blood, though SDF-1α alone induced similar levels of cell mobilization by day 7, resulting in greater myeloid cell populations in VPC+SDF-1α and

SDF-1α treated muscle by day 7 (Figure 6.1C,F). As expected, these results collectively indicate that inflammatory cell mobilization in blood precedes the increase in these same cell populations in muscle. Additionally, the ability for VPC+SDF-1α and VPC to elicit cell mobilization in blood in as little as 3 hours and increase cell populations in muscle after only 3 days may indicate that VPC can evoke a cellular response more rapidly than SDF-1α treatment, which required ~7 days to elicit significant cell recruitment in muscle. One possible explanation for these differences is the method of delivery, whereby VPC was injected systemically while SDF-1α loaded MPs were delivered locally to the supraspinatus muscle. Additionally, as SDF-1α was previously shown to release from MPs over ~1-3 days *in vivo*, this may have delayed the cellular response to SDF-1α treatment as well [266]. Ultimately, these findings suggest that cell mobilization in blood precedes the increase of these cell populations in muscle, and that modulating bone marrow cell mobilization may be a method to increase pro-regenerative cell populations in injured rotator cuff muscle.

We further analyzed how VPC and SDF-1α treatment could modulate macrophage subpopulations and found that after 3 days, VPC+SDF-1α and VPC treatment significantly increased the number of M2-like and M1-like macrophages in muscle compared to injury, which resulted in a significant increase in the M2:M1 ratio compared to SDF-1α and injury (Figure 6.2A-C). By day 7, significantly more M2-like macrophages were observed in all treatment groups compared to injury, which was determined quantitatively via flow cytometry (Figure 6.2D) and observed via immunohistochemistry (Figure 6.2G-J). However, only VPC+SDF-1α and VPC treatments significantly increased the M2:M1 ratio compared to SDF-1α and injury

(Figure 6.2F). In understanding how VPC may increase the M2:M1 macrophage ratio, S1P has shown to induce mouse macrophage IL-4 and IL-13 gene expression [305] and downregulate TNF-α, IL-12, and MCP-1 [306], resulting in M2 macrophage polarization *in vitro*. FTY720 treatment, an $S1PR_1$ and $S1PR_3$ agonist, has also shown to reduce M1 macrophage-associated cytokines and increase IL-1–receptor antagonists, a marker of M2 macrophage activation in mice [307] and in the Botchwey lab, too, FTY720 treatment led to significantly more anti-inflammatory monocytes (AMs) after 3 days in blood and tissue, while inflammatory monocyte (IM) migration was unaffected [308].

Lastly, while most inflammatory cells express $S1PR_1$ [309], certain subpopulations have shown to express these S1PRs to different magnitudes; AMs have shown to exhibit higher $S1PR_3$ expression than IMs, while M2 macrophages exhibit higher $S1PR_1$ and $S1PR_3$ expression than M1 macrophages [308]. In fact, FTY720 further increased the expression of $S1PR_3$ in monocytes and macrophages [308]. Thus, the inherent differences in S1PR expression by inflammatory cells and the potential for VPC to modulate anti-inflammatory monocyte/macrophage polarization may account, in part, for the increased M2:M1 macrophage ratio with VPC treatment in our studies.

Additionally, the selective recruitment of M2-like macrophages with SDF-1α loaded MPs may be explained by previous findings showing that as monocytes underwent *in vitro* macrophage differentiation, CXCR4 (the primary SDF-1α receptor) gene expression increased 10-fold after 7 days [290], and in our recent work, AMs exhibited higher CXCR4 surface expression than IMs [9]. Thus, SDF-1α may be able to recruit high CXCR4 expressing cell populations, including anti-inflammatory M2 macrophages, which would in turn increase the M2:M1 macrophage ratio, though not to

the same magnitude as VPC+SDF-1α treatment. Overall, it is possible that VPC, through $S1PR_1$ agonism and $S1PR_3$ antagonism, promoted M2-like macrophage polarization to increase the M2:M1 macrophage ratio, whereas SDF-1α recruited significantly more high CXCR4-expressing M2-like macrophages to the muscle.

MSCs were also quantified, and significantly more MSCs were observed in muscle treated with VPC+SDF-1α and VPC than SDF-1α and injury after only 3 days whereas by day 7, all treatment groups recruited significantly more MSCs than injury alone, between ~3 to 4-fold change over uninjured controls (Figure 6.3). These results parallel previous work, where VPC treatment induced acute MSC migration in blood 1.5 hours after administration, and loss of the $S1PR_3$ altogether induced MSC circulation as well [232]. Though VPC treatments significantly affected both the M2:M1 macrophage ratio and MSC population, these cell populations exhibit significantly different S1PR expression patterns which may have altered their interaction with VPC. It has been previously shown that VPC is a potent $S1PR_3$ antagonist with an EC_{50} similar to S1P, whereas VPC is only a partial $S1PR_1$ agonist and is about 50% as effective as S1P [231]. In the Botchwey lab, while LSK HSPCs and MSCs have both shown to express $S1PR_1$ and $S1PR_3$ to some extent, LSK HSPCs expressed significantly more $S1PR_3$ than MSCs, while MSCs expressed significantly more $S1PR_1$ [36]. In other work, too, $S1PR_1$ and $S1PR_2$ were found to be critical in MSC migration whereas $S1PR_3$ inhibition had no effect on MSC migration *in vitro* [310]. Given these differences, it is plausible that VPC acted on inflammatory cell populations through both $S1PR_1$ and $S1PR_3$ to enable cell recruitment and polarization, whereas VPC was only able to act on MSCs primarily through $S1PR_1$.

We next sought to understand how the modulation of cell populations affected protein secretion within muscle using a multiplex protein assay, but no global differences were observed between groups when using principal component analysis (Figure D.1). To more fully interpret these results, secretome analysis at additional time points both before and after day 7 may help to capture the time course of protein expression due to injury and treatment. Supervised multivariate analysis such as partial least squares discriminate analysis (PLSDA) and multivariate analyses that are coupled with our other outcome measures such as the quantity of eMHC+ muscle fibers may also help to discriminate between groups. Through individual protein analysis, it was observed that IL-18 [311], RANTES [312], LIX [313], and Leptin [314], all of which have shown to play a role in the acute inflammatory response to injury, were upregulated in injured muscle but not in treated or uninjured muscle (Figure 6.4), which may suggest that VPC and SDF-1α can modulate the initial pro-inflammatory response to injury. Additionally, SDF-1α significantly increased IP-10 production, a chemoattractant for monocytes and macrophages, while VPC and SDF-1α significantly decreased IL-13 production compared to uninjured muscle, which plays a role in M2 macrophage polarization (Figure 6.5) [315]. As VPC and SDF-1α treatments have shown to modulate inflammatory cell recruitment and polarization in our work, these findings generally coincide with our current findings and ultimately, additional multivariate analysis may allow us to further elucidate if these factors, or others, are critical to modulating the muscle microenvironment.

We next assessed angiogenesis in muscle after 7 days, and observed significantly more CD31+ vasculature in VPC+SDF-1α treated muscle than uninjured controls (Figure

6.6A-B). The highest number of vascular loops, a marker of rapid angiogenesis [214,300], was also observed in VPC+SDF-1α treated muscle but no significant differences were observed given the variability within each group (Figure 6.7). VEGF production was also significantly reduced in injured muscle, though not in treated muscles, compared to uninjured controls (Figure 6.4F). It is known that M2 macrophages and MSCs can secrete VEGF and facilitate vascular remodeling, and these cell populations likely played a role in the angiogenesis observed in VPC+SDF-1α muscles [316,317]. However, VPC and SDF-1α have shown to contribute to vascular remodeling and angiogenesis through mechanism independent of M2 macrophages and MSCs as well. For example, $S1PR_1$ agonism has led to increased endothelial cell and smooth muscle cell (SMC) proliferation and migration, thereby increasing vascular diameter and length [274] and VPC treatment has shown to increase SMC proliferation leading to increased arterial thickening [318]. SDF-1α has also shown to mobilize pro-angiogenic cells such as hematopoietic cells, endothelial progenitor cells, and SMCs [297] and can also retain and localize cell populations near vasculature, which may further promote angiogenesis [9,297]. Overall, markers of angiogenesis were observed in treated muscle, which has previously shown to support further cell recruitment and, ultimately, the regeneration of injured muscle [214,298,299,301].

Towards understanding how the modulation of the cellular and vascular microenvironment may affect muscle regeneration, we observed significantly more eMHC+ regenerating muscle fibers in VPC+SDF-1α treated muscle compared to all other groups, though significantly more regenerating muscle fibers were observed in VPC and SDF-1α treated muscle than injury alone as well (Figure 6.8). Given our collective

findings, it is possible that the increased angiogenesis observed in VPC+SDF-1α treated muscles as well as the recruitment of MSCs by all treatments contributed to the muscle regeneration observed. MSCs have shown in many studies to undergo myogenic differentiation *in vitro* [319,320] and contribute to regenerating muscle fibers *in vivo* [197]. In fact, in previous studies, the MSC secretome alone reduced fatty infiltration and increased muscle weight after 8 weeks following rotator cuff injury, possibly due to the MSC secretion of pigment epithelium-derived factor (PEDF) and follistatin which have shown to induce satellite cell proliferation [321].

But in addition, the modulation of the inflammatory profile within muscle due to VPC+SDF-1α treatment may have played an important role in muscle regeneration as well. Along with the significantly increased M2:M1 macrophage ratio that was observed due to VPC+SDF-1α and VPC treatment, individual analyte protein analysis suggested that most treatments may reduce the production of early pro-inflammatory mediators such as IL-18, RANTES [322], LIX [313], some of which have shown to be increased following skeletal muscle and tendon injury [322,323]. Furthermore, M2 macrophages have shown to localize with regenerating skeletal muscle fibers [324], and secrete IL-1 which promotes muscle fusion and MyoD expression [325] and IL-10 which promotes myoblast proliferation [326]. In our work, we observed more CD163+ M2-like macrophages within regenerating muscle, although analysis is ongoing to determine if these macrophages co-localize with eMHC+ regenerating muscle fibers. Furthermore, though we did not observe a significant increase in IL-1 or IL-10 with treatment at day 7, VPC+SDF-1α and VPC treatment significantly increased the M2:M1 macrophage ratio as early as 3 days after injury, so it is possible that production of these factors peaked at

an earlier time point. Overall, it is possible that MSCs, M2-like macrophages, and CD31+ vasculature within muscle all partly contributed to the early muscle regeneration observed with VPC+SDF-1α treated muscle, and future work could focus on elucidating the specific role of each factor, and others, in this context.

Though neither VPC nor SDF-1α have been utilized to mobilize or recruit cells to degenerating muscle, cell recruitment has been observed and employed to promote muscle regeneration through other methods. For example, ß-catenin overexpression in mice resulted in, among other outcomes, significant angiogenic progenitor mobilization to injured skeletal muscle, which may have contributed to the muscle regeneration observed [327]. Additionally, IGF-1 is known to promote anti-inflammatory cell recruitment and in one case, local IGF-1 expression promoted expression of chemokines responsible for monocyte/macrophage recruitment and muscle regeneration was ultimately observed after CTX-induced tibilias anterior injury [322]. It is important to note, however, that many other mechanisms of regeneration were activated in these studies, and in this work and our own, further investigation would be required to determine the specific role of cell recruitment in promoting muscle regeneration.

It is also important to note that we have yet to investigate the effect of VPC and SDF-1α treatment on the satellite cell population within muscle. In previous studies of rotator cuff injury, satellite cell proliferation was decreased in patients with rotator cuff tears [45,328], and satellite cell differentiation capacity was reduced with increasing tear size in another study [329]. In mice with rotator cuff tears, while the satellite cell population with the supraspinatus muscle initially increased and was transiently activated, the population size returned to baseline levels by 14 weeks after injury [174].

In contrast, it has previously been shown in mice that SDF-1α can enhance satellite cell migration [28], and though VPC has not been explored in the context of satellite cells, S1P has shown to enhance satellite cell proliferation in an $S1PR_2$-dependent manner in mdx mice [330], whereas S1P promoted the mitogenic and migratory activities of satellite cells in an $S1PR_2$/$S1PR_4$ and $S1PR_1$/$S1PR_4$-dependent manner, respectively [331].

Beyond the direct signaling between S1P and SDF-1α, immune cells including M2 macrophages which were recruited to muscle in the present work, have also shown to interact with and affect satellite cell behavior. Immune cells have been shown to secrete growth factors and ECM chemoattractive fragments which help satellite cells escape from the basal lamina of myofibers and protect satellite cells from apoptosis [332]. M2 macrophages in particular, through secretion of IL-10 among other factors, can promotes satellite cell commitment to terminal differentiation, cell fusion, and formation of large myotubes [324,333]. Interestingly, satellite cell progeny have also shown to migrate more efficiently toward M2 macrophages compared to M1 macrophages [324] and satellite cell progeny have even shown to attract monocytes themselves, which further highlights the cross-talk between satellite cells and immune cells [325]. Thus, it is evident that satellite cell activity may be dysregulated following rotator cuff injury, and that our co-delivery treatment may directly or, through the modulation of the M2:M1 macrophage ratio, indirectly impact satellite cell behavior to promote muscle regeneration. As Pax7 is becoming increasingly more commonplace as a marker for rat satellite cells, a future direction of this work may be investigating the localization and activity of satellite cells following VPC and SDF-1α treatment.

Though we have now observed early muscle regeneration 1 week following injury, studies are ongoing to examine the efficacy of weekly VPC and SDF-1α injections in promoting muscle regeneration over time. After 2 and 3 weeks, no significant differences in muscle weight, indicative of muscle atrophy, were observed in injured muscles that were untreated or treated with VPC and SDF-1α (Figure 6.9). However, given that this model of rotator cuff injury is degenerative and does not include reattachment of the tendons, it is understandable that muscle atrophy may have continued despite VPC and SDF-1α treatment. Instead, it is possible that other aspects of muscle quality may be affected by VPC and SDF-1α treatment, and ongoing work will analyze regenerating muscle fibers via image analysis of eMHC+ muscle fibers and centrally located nuclei within fibers, muscle fibrosis via histology and Masson's trichrome staining, and muscle function via muscle twitch or tetanic force testing 2 and 3 weeks post-injury. Ultimately, these studies will evaluate whether VPC and SDF-1α, potentially due to the modulation of the cellular milieu, angiogenesis, and early muscle fiber regeneration, can result in functional recovery of muscle following severe rotator cuff injury.

Current standard of care for severe rotator cuff injury involves reattachment of the torn tendons, resulting in continued muscle degeneration and an increased likelihood of re-tear. Our current results indicate that systemic delivery of VPC and local injection of SDF-1α loaded MPs may stimulate endogenous healing mechanisms, leading to increased MSC recruitment, polarization of macrophages toward an anti-inflammatory phenotype, increased angiogenesis and early muscle regeneration in the context of rotator cuff injury. Thus, a promising application of our treatment strategy could be improving

muscle quality following reattachment surgery, potentially reducing the likelihood of re-tear. In realizing the translation of this approach to the clinic, however, it is important to note that the animal model used in this work did not include tendon reattachment, meaning that the muscle degeneration and response to treatment observed in our studies may differ from that of a patient following surgical repair. Nevertheless, our results indicate that harnessing endogenous healing mechanisms may be a novel approach to promote muscle regeneration and could be employed in the future to improve patient prognoses after rotator cuff repair.

6.5 Conclusions

In this work, the synergy between systemic delivery of the bone marrow mobilizing agent VPC and intra-muscular delivery of the chemokine SDF-1α was assessed in the supraspinatus muscle following severe rotator cuff tear in rats. Co-delivery of VPC and SDF-1α loaded MPs led to significant mobilization of inflammatory cells and MSCs in blood, which was followed by a significant increase in the M2:M1 macrophage ratio and number of MSCs in muscle 3 and 7 days following injury. After 7 days, VPC+SDF-1α treatment resulted in significantly more CD31+ vasculature than uninjured controls, indicative of angiogenesis, and significantly more eMHC+ muscle fibers compared to all other groups, indicative of early muscle regeneration. Collectively, these results suggest that the combination of VPC to induce bone marrow cell mobilization and SDF-1α loaded MPs to recruit these bone marrow-derived cell populations to muscle stimulated early endogenous repair processes, and may be a promising method to promote rotator cuff muscle regeneration and improve patient prognoses following repair in the future.

CHAPTER 7

CONCLUSIONS AND FUTURE DIRECTIONS

7.1 SUMMARY

In this work, a tunable heparin-based microparticle (MP) system was developed for the delivery of regenerative therapeutics for musculoskeletal tissues including bone, cartilage, and muscle. Though biomaterial-based drug delivery systems exist, MPs are advantageous for injection to a wide range of injury locations. Furthermore, due to heparin's ability to bind via electrostatic interactions carbohydrate sequence-specific interactions to positively-charged proteins, heparin was employed to load and release proteins of interest in a controlled manner, and to protect and even enhance protein bioactivity. Ultimately, heparin-based MP tunability was validated by modulating heparin content, heparin sulfation, and hydrolytic degradation of MPs, and subsequently investigating the effect of these variable on loading, release, and bioactivity of an osteoinductive growth factor *in vitro*. Subsequently, a single MP formulation was validated as a method to deliver bioactive heparin-binding proteins *in vivo* for the ultimate purpose of regenerating musculoskeletal tissues in two unique injury contexts. These findings were delineated in 4 chapters of this thesis:

In Chapter 3, hydrolytically-degradable, heparin-based MPs were fabricated containing heparin derivatives with varying levels of sulfation. First, it was shown that MP degradation could be modulated between 7-14 days *in vitro*. Furthermore, most MP formulations loaded equivalent amounts of an osteoinductive protein, BMP-2, whereas more sulfated Hep and Hep^{-N} MPs released significantly more BMP-2 than more

desulfated heparin MPs. Similarly, BMP-2 bioactivity was enhanced by more sulfated Hep and Hep^{-N} MPs compared to soluble BMP-2. Collectively, 10 wt% Hep and Hep^{-N} MPs were selected as viable therapeutic carrier capable of efficient loading and release of bioactive BMP-2, and this work ultimately demonstrated that heparin sulfation level may be an important consideration for any future heparin-based biomaterials approach for bioactive therapeutic delivery.

In Chapter 4, the effect heparin sulfation on TSG-6 bioactivity was first determined to inform the development of heparin-based MPs for TSG-6 intra-articular delivery. More sulfated Hep and Hep^{-N} derivatives significantly enhanced TSG-6 anti-plasmin activity *in vitro,* whereas fully desulfated heparin (Hep-) had no effect, indicating that heparin sulfation plays a significant role in modulating TSG-6 bioactivity. Next, hydrolytically degradable TSG-6 loaded 10 wt% Hep^{-N}-based MPs were delivered via intra-articular injection in a rat model of post-traumatic osteoarthritis (OA). After 21 days, EPIC-µCT analysis indicated that TSG-6 loaded MPs reduced cartilage damage following post-traumatic OA injury, whereas a 3X higher dose of soluble TSG-6 did not. These results suggest that Hep^{-N} can enhance TSG-6 bioactivity *in vivo* and, ultimately, that Hep^{-N}-containing MPs may be an effective method to deliver a chondroprotective protein for cartilage regeneration.

In Chapter 5, the same formulation selected in Chapter 3 and utilized in Chapter 4, hydrolytically degradable 10 wt% Hep^{-N} MPs, were utilized and injected within the supraspinatus muscle of rats with severe rotator cuff injury to modulate the cellular milieu within muscle. First, MPs were tracked *in vivo* and were found to be retained within muscle for at least 3 days and appeared to have degraded by day 7. Furthermore,

tracking of SDF-1α released from MPs *in vivo* indicated that SDF-1α may be retained at the site of injection for at least 1-3 days when delivered to the supraspinatus muscle. After 7 days following rotator cuff injury and SDF-1α loaded MP treatment, significantly more anti-inflammatory, M2-like macrophages and MSCs were detected in muscle treated with SDF-1α loaded MPs compared to unloaded MPs or injury alone. As no prior studies have investigated the use of chemotactic therapeutics such as SDF-1α to treat muscle following rotator cuff injury, our results indicate that SDF-1α loaded MPs can shift the cellular composition of the supraspinatus muscle, which may provide a platform to improve muscle repair after rotator cuff injury in the future.

Finally, in Chapter 6, building on the findings of Chapter 5, SDF-1α loaded MPs were delivered via intra-muscular injection to the supraspinatus muscle in combination with systemic injection of a bone marrow mobilizing agent, VPC01091 (VPC), to further modulate the supraspinatus muscle cellular milieu. Co-delivery of VPC and SDF-1α led to significant mobilization of inflammatory cells and MSCs in blood, which was followed by a significant increase in the M2:M1 macrophage ratio and number of MSCs in muscle 3 and 7 days following injury. After 7 days, VPC+SDF-1α treatment resulted in significantly more CD31+ vasculature than uninjured controls, indicative of angiogenesis, and significantly more eMHC+ muscle fibers compared to all other groups, indicative of early muscle regeneration. Collectively, these results suggest that the combination of VPC to induce cell mobilization and SDF-1α loaded MPs to recruit these cell populations to muscle stimulated endogenous healing processes, and may be a promising method to promote muscle regeneration and improve patient prognoses in the future.

7.2 CONCLUSIONS

Overall, the long term goal of this research was to develop a tunable biomaterial-based system for the delivery of regenerative therapeutics for musculoskeletal tissue including bone, cartilage, and muscle. This goal was first achieved through the engineering of a heparin-based microparticle system with tunable hydrolytic degradation, heparin content, and heparin sulfation. To first tune MP degradation, we developed heparin-based MPs with varying concentrations of dithiothreitol (DTT), which accelerates the hydrolytic degradation of the ester linkage within PEGDA molecules. As the concentration of DTT was increased within MPs, MP degradation accelerated, and overall MPs could be fabricated to degrade between 7 to 30 days *in vitro*, and ~7 days within muscle *in vivo*. Interestingly, in studies with heparin of varying degradation rates, between 7-14 days *in vitro*, BMP-2 release rates were unaffected by the degradation rate of MPs, which may indicate that BMP-2 release was governed more by diffusion than MP degradation. It is also important to note that several confounding variables existed within these studies. First, the heparin MPs in this study were composed of varying heparin derivatives making direct comparisons of BMP-2 release rate challenging and second, BMP-2 denaturation likely reduced the ability for the BMP-2 ELISA to detect all released BMP-2 from MPs. In contrast to this study, in previous work it has been found that 10 wt% heparin hydrogels could release the more stable small molecule, crystal violet, with varying release kinetics through modulation of hydrogel degradation [17]. Nevertheless, this work collectively validated the ability to modulate hydrolytic

degradation of heparin MPs, which can be adjusted to accommodate the specific *in vivo* application in the future.

MPs were also developed with varying heparin content to further modulate protein loading and release. In collaboration with other laboratories, we previously developed 100% heparin MPs, but due to the high heparin content, 100% heparin MPs sequestered protein and only released up to ~10% of the originally loaded protein *in vitro* [15]. In contrast, we found that though heparin content did not affect BMP-2 loading, 10% heparin MPs released up to 60% of the originally loaded protein while 1% heparin MPs released up to 30% *in vitro.* As heparin has previously shown to protect BMP-2 from denaturation, it is postulated that greater heparin content within 10% heparin MPs protected more BMP-2 than 1% heparin MPs, thereby enabling more BMP-2 release in this study.

Finally, heparin sulfation has shown to play a critical role in protein binding and, in certain cases, bioactivity. Therefore, we synthesized heparin derivatives of varying sulfation level, between 0 to 100% total sulfation, to further tune protein release, and bioactivity. In *in vitro* studies with BMP-2, more sulfated heparin MPs, Hep and Hep^{-N} which are 100 and 80% sulfated, respectively, released more BMP-2 and enhanced BMP-2 bioactivity compared to more desulfated heparin derivatives, $Hep^{6O,N}$ and Hep- which are 20% and 0% sulfated, respectively. It has been found that heparin sulfate groups are involved, and potentially even required, for complete binding to BMP-2 [62,84]. When desulfated heparin derivatives were incubated with TSG-6, similar results were observed whereby Hep and Hep^{-N} enhanced TSG-6 anti-plasmin activity compared to Hep- and to soluble TSG-6 controls. Heparin has previously shown to enhance TSG-6 plasmin

activity, and it has previously been hypothesized that this is due to heparin's ability to maintain TSG-6 is a "closed" conformation. Ultimately, these results indicate that heparin MPs can be fabricated and utilized to modulate protein release and bioactivity.

Following the validation of the heparin-based MP platform, the system was then employed to deliver therapeutics to musculoskeletal tissues in two injury contexts. Given our *in vitro* findings whereby more sulfated heparin derivatives could release more protein and enhance protein bioactivity, and due to the diminished anti-coagulant properties of desulfated heparin derivatives, 10 wt% Hep^{-N} MPs were chosen for further *in vivo* drug delivery application in this thesis. First, in Chapter 4 the anti-inflammatory protein TSG-6 was loaded onto MPs, which were then delivered via intra-articular injection using standard needles and syringes for treating cartilage in the context of post-traumatic osteoarthritis. Second, the chemokine SDF-1α was loaded onto MPs via intra-muscular injection to the supraspinatus muscle following severe rotator cuff injury. Following intra-muscular injection, MPs were visualized *in vivo* over time, and it was determined that non-degradable MPs were retained within the muscle for at least 7 days, whereas degradable MPs were retained within MPs for at least 3 days and appeared to have degraded by day 7. Furthermore, SDF-1α loaded MPs were shown to release SDF-1α over at least 1-3 days *in vivo*. Lastly, unloaded MPs were also delivered to the supraspinatus muscle after rotator cuff injury and did not elicit any significant inflammatory cell response compared to injury alone, indicating a lack of any undesired immune response at the MP concentration and injection location studied in this work. Thus, MPs were validated as a method to locally deliver therapeutics to degenerating musculoskeletal tissues.

Once it was determined that MPs could be delivered via injection to the joint space and muscle to release therapeutics of interest, MPs were assessed for their ability to enhance the efficacy of these therapeutics to promote musculoskeletal tissue regeneration. First, TSG-6 loaded heparin-based MPs were delivered via intra-articular injection in a rat model of post-traumatic osteoarthritis. In this work, TSG-6 loaded onto MPs was significantly more chondroprotective than a 3x dose of soluble TSG-6, which indicates the ability for MPs to enhance therapeutic efficacy in this context. First, it is possible that MPs were able to retain TSG-6 within the joint space for a longer period of time than soluble TSG-6, which was likely cleared from the joint space rapidly. Secondly, given that heparin could enhance TSG-6 bioactivity *in vitro*, it is possible that heparin-based MPs enhanced the TSG-6 released *in vivo* as well. Ultimately, for the first time, heparin-based MPs were used to more effectively deliver TSG-6 to an osteoarthritic joint, which subsequently protected cartilage from OA-induced degeneration.

Apart from the development of heparin-based MPs, another significant component of this work was the first, elucidation of the cellular milieu in muscle and subsequently, the degenerative state of muscle following severe rotator cuff injury. Though nearly 300,000+ rotator cuff repairs occur annually [45], current standard of surgical repair involves only tendon reattachment, allowing for continued muscle degeneration and an increased likelihood of re-tear. Thus, understanding and altering the cellular milieu within muscle following rotator cuff injury may be a method to improve patient prognoses following rotator cuff repair. After injury in blood, the fold-change in myeloid cells and monocytes compared to the 1.5 hour time point was less than 1 at all time points for injury alone, indicating that cell mobilization generally decreased after the

initial response to injury. In muscle at day 3, a 1.2 to 1.3-fold increase in myeloid cells, macrophages, and macrophage subpopulations was observed in injury compared to uninjured controls, which increased to a 1.4 to 1.5-fold increase for all inflammatory cell populations by day 7. Furthermore, at both day 3 and 7 the M2:M1 macrophage ratio was ~1.1, though overall no significant differences were observed between injury and uninjured controls. Following skeletal muscle injuries, a typical inflammatory response includes an initial response by neutrophils in the first several hours, followed by an influx of pro-inflammatory M1 macrophages and finally, within 7 to 14 days, a shift toward an anti-inflammatory M2 macrophage-dominant cellular milieu [303,304]. However, at the day 3 and 7 time point in our work, no substantial shift in the M2:M1 ratio was observed, which may indicate that the inflammatory response in muscle following rotator cuff tear may be unique or dysregulated compared to other muscle injuries. Additionally, rotator cuff injury begins primarily as a tendon injury, so the inflammatory response in muscle may be delayed compared to other direct muscle injuries. Overall, these results suggest that treatments designed to modulate the M2:M1 macrophage ratio may be a method to significantly alter the regenerative state of muscle following rotator cuff injury.

As a measure of muscle degeneration, we also assessed muscle atrophy and fibrosis 1, 3, and 6 weeks following tendon transection and denervation. Though no differences were apparent after 1 week following rotator cuff injury, supraspinatus muscle weight significantly decreased by 50-60% compared to uninjured controls after 3 and 6 weeks. Similarly, Masson's trichrome staining showed that fibrous infiltration was significantly greater in the injured supraspinatus muscles compared to uninjured controls at both 3 and 6 weeks as well. These results confirm that this is a model of degenerative

muscle injury and thus is an appropriate *in vivo* platform to test effects of release of SDF-1α on altering the cellular milieu in a degenerative environment. These results collectively indicate that a unique inflammatory response occurs in muscle occurs within 1 week following rotator cuff injury, which leads to significant muscle degeneration as early as 3 weeks following tendon transection and denervation in rats.

MPs were also utilized to deliver the chemokine SDF-1α to the supraspinatus muscle alone and in combination with systemic delivery of the bone marrow mobilizing agent, VPC01091, to enhance the pro-regenerative cellular milieu within muscle after rotator cuff injury. SDF-1α loaded MPs significantly increased the number of anti-inflammatory M2-like macrophages and MSCS within muscle compared to injury, and when co-delivered with VPC01019, the M2:M1 ratio was also significantly increased as early as 3 days following injury and treatment. After 7 days, co-delivery of VPC01091 and SDF-1α loaded MPs led to significantly more regenerating muscle fibers within the supraspinatus than any other treatment and injury alone.

With this foundation, we then modulated the muscle's cellular composition with the chemokine SDF-1α and bone marrow mobilizing agent VPC. Co-delivery of VPC+SDF-1α resulted in a significantly increased M2:M1 macrophage ratio and MSC population compared to SDF-1α and injury alone as early as 3 days following injury and treatment. After 7 days, VPC+SDF-1α treatment resulted in significantly more CD31+ vasculature than uninjured controls and significantly more eMHC+ regenerating muscle fibers compared to all other groups. Though cell recruitment has been observed in several muscle injury contexts, few treatment strategies have harnessed endogenous cell recruitment as a method to regenerate muscle. In one case, ß-catenin overexpression

resulted in, among other outcomes, significant angiogenic progenitor mobilization to injured skeletal muscle, which may have contributed to the muscle regeneration observed [327]. Additionally, local IGF-1 expression promoted expression of chemokines responsible for monocyte/macrophage recruitment, and muscle regeneration was ultimately observed after CTX-induced tibilias anterior injury [322]. It is important to note, however, that many other mechanisms of healing and regeneration were activated in these studies, and in this work and ours, further investigation would be required to determine the specific role of cell recruitment in promoting muscle regeneration. Overall, as SDF-1α and VPC have never before been utilized in the context of muscle regeneration following rotator cuff injury, these results indicate a novel approach to enhancing musculoskeletal tissue regeneration may be the modulation of endogenous cell recruitment, which may ultimately improve patient outcomes following rotator cuff repair in the future.

7.3 Future Directions

7.3.1 TSG-6 loaded MPs in the context of osteoarthritis

In Chapter 4, TSG-6 was implemented as a chondroprotective anti-inflammatory protein capable of reducing cartilage degeneration within the context of post-traumatic osteoarthritis. In particular, it was found that TSG-6 delivered via heparin-based MPs was significantly more chondroprotective than a 3x dose of soluble TSG-6. In analyzing these results, it was postulated that heparin-based MPs may have retained TSG-6 within the intra-articular joint space for a longer period of time than soluble TSG-6 and/or heparin within MPs was able to enhance TSG-6 bioactivity compared to soluble TSG-6

alone *in vivo*. To test the first hypothesis, *in vivo* fluorescent imaging could be employed to track both fluorescently-tagged heparin MPs and fluorescently-tagged TSG-6 once delivered via intra-articular injection. By comparing the release kinetics and subsequent clearance rate of both MPs and TSG-6 to a soluble TSG-6 control, we may better understand the importance of heparin MPs in retaining TSG-6 locally within the intra-articular joint space. To test the second hypothesis, in two *in vitro* studies it was previously observed that soluble heparin derivatives, including Hep and Hep^{-N}, could enhance TSG-6 anti-plasmin activity and that TSG-6 released from Hep^{-N}-based MPs exhibited significantly more anti-plasmin activity than soluble TSG-6 at the same concentration. Despite these results, however, we have yet to validate that TSG-6 delivered to an osteoarthritic joint *in vivo* exhibits anti-plasmin activity to, in turn, reduce cartilage degeneration in this context. Therefore, to probe this hypothesis, synovial fluid samples could be collected from treated and untreated knees of rats with post-traumatic osteoarthritis to determine if TSG-6 loaded MP delivery impacts the plasminogen activation pathway within the joint space. Overall, by more fully understanding the mechanism of action by which TSG-6 loaded MPs reduce cartilage degeneration, we may also elucidate specific pathways to explore for effective treatment of cartilage degeneration in osteoarthritic joints in the future.

7.3.2 Cell behavior following VPC and SDF-1α loaded MP treatment

In Chapter 5 and 6, the cellular milieu within muscle was modulated with the chemokine SDF-1α and bone marrow mobilizing agent VPC. It was found that co-delivery of SDF-1α loaded MPs and systemic delivery of VPC treatment led to a significant increase in the M2:M1 macrophage ratio and the MSC population after 3 and

7 days post-injury and treatment. Furthermore, by day 7 VPC+SDF-1α treated muscles exhibited significantly more eMHC+ regenerating muscle fibers than all other groups and significantly more CD31+ vasculature than uninjured controls. Though it is known that cell populations including anti-inflammatory M2 macrophages and MSCs may play a role in angiogenesis and muscle regeneration, it remains unclear what specific cell populations may be directly involved in the increased muscle regeneration in our studies.

One method to further elucidate cell behavior once recruited to the supraspinatus muscle could be to sort each cell population of interest for secretome analysis. We have previously established with flow cytometry that M2-like macrophage and MSC population are significantly increased following VPC and SDF-1α treatment, though it is unclear what proteins and factors these cells are secreting, and if their secretion is differentially affected by each treatment. Therefore, cell populations of interest could be sorted as CD11b+CD68+ for macrophages, CD11b+CD68+CD163- for M1-like macrophages, CD11b+CD68+CD163+ M2-like macrophages, and CD29+CD44+CD90+ MSCs. In situ hybridization studies could be employed to look at each cell population within the muscle, alone with the RNA expression profiles of each cell population. In particular, these studies may elucidate how each individual cell populations contributes to the modulation of the inflammatory profile within muscle, as well as to the angiogenesis and muscle regeneration previously seen 7 days following rotator cuff injury in our studies.

Additionally, to more fully confirm the role of inflammatory cell mobilization and recruitment, monocyte depletion experiments could be conducted by administering clondronate liposome to animals prior to rotator cuff tear and treatment. In previous

work, clondronate liposome administration to mice caused complete depletion of blood monocytes within 6 hours followed by recovery of some monocyte populations at day 2 [334]. As we observed VPC-mediated mobilization in blood during this time frame and VPC-mediated inflammatory cell changes in muscle at day 3, clondronate liposome treatment may eliminate these responses and allow us to decouple the effects of inflammatory cell populations from the effects of other cell populations such as MSCs.

As described in Chapter 6, in our work we have yet to analyze how satellite cells are affected in the context of rotator cuff tear alone and with VPC and SDF-1α treatment. In previous studies of rotator cuff injury, satellite cell proliferation was decreased in patients with rotator cuff tears [45,328], and satellite cell differentiation capacity was reduced with increasing tear size in another study [329]. In mice with rotator cuff tears, while the satellite cell population with the supraspinatus muscle initially increased and was transiently activated, the population size returned to baseline levels by 14 weeks after injury [174]. In contrast, it has previously been shown in mice that SDF-1α can enhance satellite cell migration [28], and though VPC has not been explored in the context of satellite cells, S1P has shown to enhance satellite cell proliferation in an $S1PR_2$-dependent manner in mdx mice [330], whereas S1P promoted the mitogenic and migratory activities of satellite cells in an $S1PR_2$/$S1PR_4$ and $S1PR_1$/$S1PR_4$-dependent manner, respectively [331]. Thus, it is evident that satellite cell activity may be dysregulated following rotator cuff injury, and that our co-delivery treatment strategy may enable improved satellite cell activity in this context.

Until recently, the availability of reliable rat antibodies to identify satellite cells have been limited. However, Pax7 antibodies have become increasingly more available

and more readily used as a marker in immunohistochemistry and flow cytometry experiments to identify satellite cells in rat samples. Therefore, Pax7 could be employed in future experiments to first, determine how the quantity of satellite cells within muscle changes over time with rotator cuff tear. Next, *in situ* hybridization could be employed to visualize satellite cells and their RNA expression profile. Finally, immunohistochemistry experiments could be employed to observe the co-localization of satellite cells with regenerating muscle fibers, newly formed vasculature, and other cell populations that we have shown are present in muscle following injury. As both VPC and SDF-1α have shown to affect satellite cell behavior in other contexts, assessing how these treatments affect satellite cell population using these same experiments may also elucidate if our treatment strategies are a method to improve satellite cell function and enable muscle regeneration.

7.3.3 Advantages & disadvantages of endogenous repair

In Chapter 4, 5, and 6, endogenous repair mechanisms were harnessed to promote cartilage and muscle regeneration. TSG-6 is naturally upregulated in osteoarthritic joints as an anti-inflammatory agent, and we therefore employed TSG-6 loaded MPs to prevent cartilage degeneration after post-traumatic osteoarthritic injury in rats. In our studies with VPC and SDF-1α loaded MPs, VPC was utilized to mobilize endogenous cell populations while SDF-1α loaded MPs were employed to recruit those endogenous cell populations to the muscle following rotator cuff injury. Ultimately, promoting endogenous healing mechanisms for tissue regeneration is advantageous compared to transplants which may be more costly, more difficult to prepare and deliver, and may be rejected once delivered. Scaffolds are another common approach to replace degenerated

tissue, but significant research and development is often required to create materials which mimic the properties of natural tissue and these materials may evoke a negative immune response once implanted.

Still, employing endogenous healing mechanisms also has its disadvantages. For instance, these treatment strategies primarily target a single mechanism to promote tissue regeneration, such as the recruitment of M2-like macrophages and MSCs to the muscle via VPC and SDF-1α. Despite the recruitment of these cell populations, this mechanism alone may not enable complete muscle recovery after rotator cuff injury. Furthermore, in injury contexts including osteoarthritis and rotator cuff tear, among many others, endogenous healing processes are often dysregulated, which may make these mechanisms poor treatment targets. For example, satellite cell proliferation and differentiation has shown to be affected by rotator cuff tear, meaning therapeutics targeting satellite cells specifically may be ineffective as the satellite cell population decreases or loses function.

To improve on our current work and to ensure the efficacy of future treatments which promote endogenous repair processes, it is important to consider the time course of tissue degeneration in each injury context. In osteoarthritic joints and rotator cuff muscles after cuff tear, tissue degeneration progresses over time and may require long-term treatment to, ideally, return the tissue to a healthy state. In fact, dependent on the injury, it may be that life-long treatment is required to maintain the health of each tissue. Therefore, our current work could be improved upon by extending therapeutic delivery in a controlled manner that matches the requirements of the disease state. Though therapeutic delivery of biomaterials over a lifetime is unrealistic, a step towards this goal

would be utilizing biomaterials to decrease the frequency of injections, which can often be inconvenient and costly to patients.

7.3.4 Clinical considerations for treating rotator cuff injury

There are many factors when considering how our treatments may be translated to the clinic. First, significantly larger doses of both VPC and SDF-1α would be required for the human rotator cuff, and both therapeutics are currently too costly to be a reasonable option for patients. Large scale production of both products would be required to ensure affordability and availability. Furthermore, especially for VPC which is delivered systemically, many side effects may occur due to the increased mobilization of bone marrow-derived cells into circulation. Though this has been studied with other S1PR agonists/antagonists, clinical trials focused on the appropriate dosages and the potential risks of systemic VPC administration would be necessary. Finally, the translation of manipulated biomaterials can be time-consuming and costly, and would be a significant component to the translation of our treatment to the clinic. Given the ability for our microparticle platform to improve release and bioactivity of proteins, it is an important component to the treatment strategy, but would likely extend the time and capital required for full clinical translation of our technology.

Beyond the selection and development of therapeutics for musculoskeletal tissue regeneration, timing of intervention is a critical component to successful translation of these treatment strategies. In the case of rotator cuff injuries, it is known that muscle degeneration continues after surgical intervention, and correlates with an increased likelihood of re-tear. Therefore, a potential timeline of intervention with muscle regenerating therapeutics could be immediately following surgical reattachment, thereby

promoting muscle regeneration and reducing the likelihood of re-tear. However, certain patients have shown to exhibit such significant muscle degeneration that they become ineligible for surgery. For these patients, earlier intervention may promote muscle regeneration and potential improve their eligibility for surgery in the future. Overall, for rotator cuff tears and many other musculoskeletal injuries, exploring the timing of intervention is critical for promoting sustained tissue regeneration and improving patient prognoses.

Furthermore, it is important to consider patient to patient variability and how our treatments may differentially affect each patient. As mentioned earlier, when targeting endogenous healing mechanisms, it is important to determine the current state or health of these healing mechanisms. For elderly patients who may be in poor health, their inflammatory cell or stem cell count in the bone marrow or blood may be low, which limits the efficacy of targeting these cell populations to promote muscle regeneration in the rotator cuff. Therefore, prior screening may be required to determine the health of each patient and the potential efficacy of our treatment strategy, which would include blood analysis for inflammatory and stem cell populations as well as analysis of the muscle state within the rotator cuff. Dependent on these results, we may have a better understanding of whether each individual patient is more suited for our treatments targeting endogenous healing mechanisms, or if alternative treatment approaches may be more effective.

Lastly, though Chapter 5 and 6 have focused on muscle regeneration following rotator cuff injury, other tissue of the joint space including tendon, cartilage, and bone have all shown to be significantly affected after severe rotator cuff injury. Tendon tissue

has shown to exhibit an initial inflammatory response, followed by disorganization and fragmentation of collagen and overall degeneration [165]. Mankin scoring of cartilage tissue has indicated increased structural disorganization, hypocellularity, decreased GAG content and tide marks crossed by blood vessels, all of which are indicators of cartilage degeneration [148]. For the surrounding bone tissue, the disrupted kinematics of the glenohumeral joint after rotator cuff injury can often lead to osteoarthritis, where the subchondral bone of the humeral head collapses and the surrounding bone tissue erodes [148]. In our previous work, we have shown that drug loaded heparin-based MPs can be injected into the intra-articular joint space of rat knees, and in turn prevented cartilage degeneration in the context of post-traumatic osteoarthritis. Therefore, intra-articular injection of drug loaded MPs may be a method to treat cartilage, bone, and tendon in this context. Furthermore, we have shown that unloaded MPs can be injected directly into tendon tissue, which may offer a method to specifically target degenerating tendon tissue as well. Ultimately, as rotator cuff tear affects many tissues of the joint space, heparin-based MPs may be a method to treat multiple tissues, thereby improving the condition of the rotator cuff following injury or repair.

APPENDIX A

A.1 PicoGreen Assay for DNA quantification of C2C12 mouse myoblasts

Methods: dsDNA was quantified by Quant-iT dsDNA PicoGreen assay (Invitrogen, Grand Island, NY). After incubating C2C12 cells for 3 days at 37°C, cells were lysed with 100 µL lysis buffer and frozen, thawed and sonicated three times to completely dissociate the cells. Cell lysates and standards were incubated in PicoGreen reagent and the fluorescence (ex 485 nm, em 528 nm) was measured (n = 3-5).

Results: After 3 days of incubation, no significant differences in C2C12 dsDNA content were seen between any groups.

Discussion: Treatment with soluble BMP-2, unloaded 10 wt% Hep MPs, or BMP-2 loaded MPs did not significantly affect the total DNA content of C2C12 cells over 3 days.

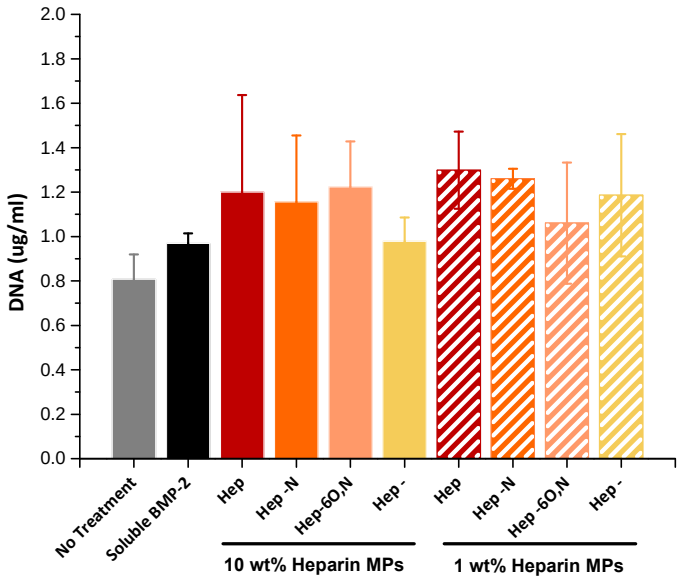

Figure A.1. PicoGreen Assay for DNA quantification of C2C12 mouse myoblasts. No significant differences between any group; $p \leq 0.05$; n = 3-5.

A.2 Detected levels of BMP-2 after incubation with soluble heparin derivatives.

Methods: 100 ng BMP-2 was incubated with 0.01 mg soluble Hep, Hep^{-N}, $Hep^{-6O,N}$, Hep-, or PEG-4Ac in 0.5 mL 0.5% v/v BSA PBS solution for 15 minutes or 24 hours at 4°C. BMP-2 was then quantified via ELISA (n = 3-5).

Results: After incubating heparin and BMP-2 for 15 minutes, the ELISA accurately detected approximately 100 ng BMP-2 in all heparin samples (Figure A.2A). After incubating for 24 hours at 4°C, the detected levels of BMP-2 remained between 90-100 ng in Hep and Hep^{-N} samples but decreased to between 40-50 ng in $Hep^{-6O,N}$, Hep-, and no heparin samples, significantly lower than Hep and Hep^{-N} (Figure A.2B).

Discussion: The ELISA accurately detected approximately 100 ng BMP-2 in samples with each heparin derivative after 15 minutes incubation, indicating that no derivative significantly interfered with the assay. After 24 hours incubation, the detected levels of BMP-2 were maintained in the more sulfated heparin samples (Hep and Hep^{-N}), indicating that these heparin derivatives protected BMP-2 over this timeframe, allowing for accurate detection via ELISA. In contrast, BMP-2 levels were significantly lower in the more desulfated heparin and no heparin samples, indicating that BMP-2 was not well protected by these derivatives.

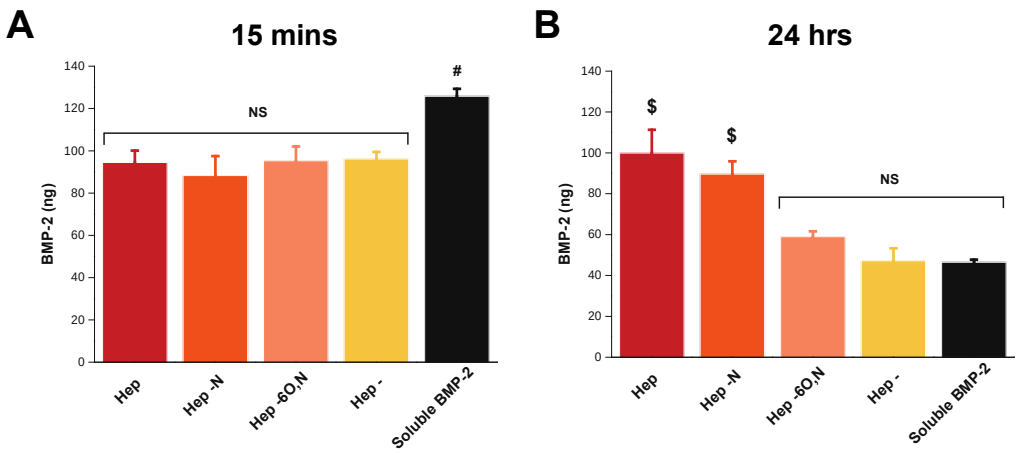

Figure A.2. Detected levels of BMP-2 after incubation with soluble heparin derivatives. (A) After 15-min incubation, there was no difference between heparin groups. (B) After 24-hr incubation, there was significantly higher detected levels of BMP-2 in more sulfated heparin groups. [#]Significantly different than all other groups at 15 mins; $p \leq 0.05$. [$]Significantly different than all other groups at 24 hrs; $p \leq 0.05$; n = 3-5.

APPENDIX B

B.1 PROTON NUCLEAR MAGNETIC RESONANCE

Methods: Proton nuclear magnetic resonance (^{1}H NMR) was performed whereby 10 mg/mL Hep^{-N} MAm and PEGDA samples were each dissolved in deuterated H_2O (Sigma), run on a Bruker Avance III spectrometer at 400 Hz, and analyzed using iNMR software [21]. Percent modification was determined by dividing the integral of the methacrylamide peak by the heparin peak for Hep^{-N} MAm and the acrylate peaks by the PEG peak for PEGDA.

Results: Using ^{1}H NMR analysis, PEGDA was determined to be ~55% functionalized (Figure B.1A) and Hep^{-N} methacrylamide was determined to be 22-28% functionalized (Figure B.1B).

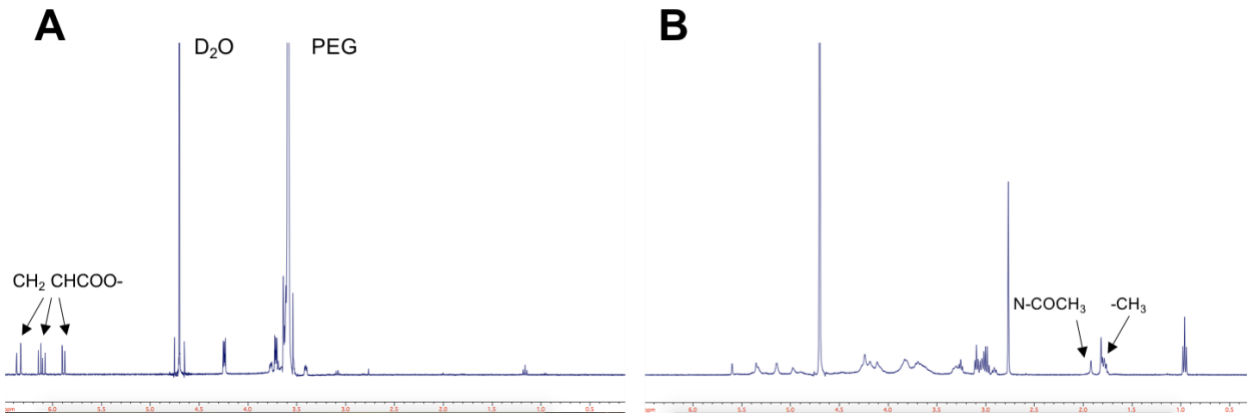

Figure B.1. ^{1}H NMR of poly (ethylene glycol) diacrylate and N-desulfated heparin methacrylamide. (A) Characteristic peaks for acrylate groups were present in the PEGDA spectra and (B) characteristic peaks for methacrylamide peaks were present in the N-desulfated heparin methacrylamide.

B.2 MICROPARTICLE SIZE AND MORPHOLOGY BEFORE AND AFTER TSG-6 LOADING

Methods: TSG-6 was loaded onto microparticles (MPs) using the same method for all other *in vitro* and *in vivo* studies. Briefly, 0.6 mg 10 wt% Hep^{-N} MPs were incubated with 1.0 ug TSG-6 for 2 hours at 4°C. Phase microscopy and ImageJ software were used to image and quantify the diameter of microparticles before and after the loading protocol.

Results: MPs appear to have the same morphology (Figure B.2A-B) and exhibit a similar size distribution (Figure B.2C) before and after loading.

Discussion: Overall, TSG-6 loading did not affect MP morphology or size, indicating that MPs from our previous *in vitro* and *in vivo* studies likely remained approximately 80 ± 60 μm in diameter before and after loading.

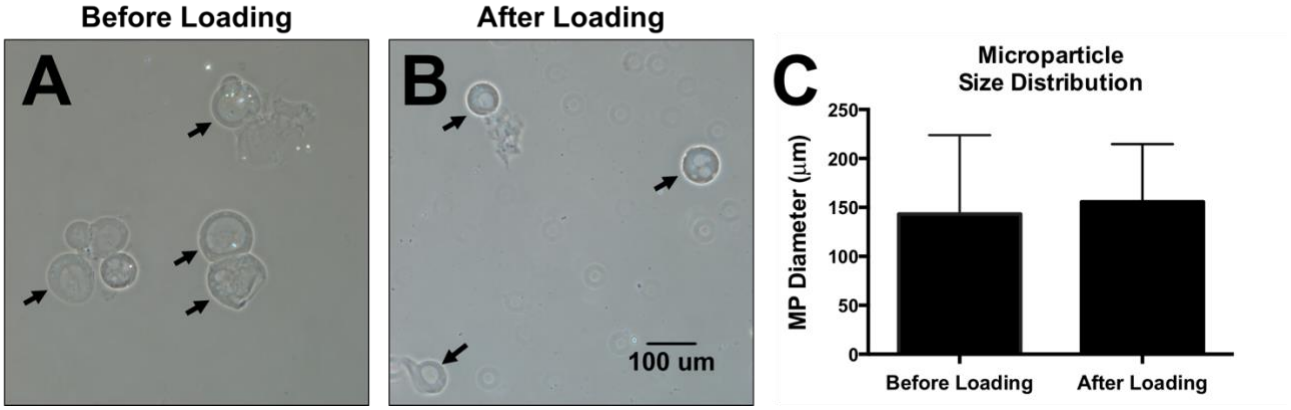

Figure B.2. Microparticle size and morphology before and after TSG-6 loading. (A-B) 10 wt% Hep^{-N} MPs qualitatively appeared similar in morphology before and after TSG-6 loading, and (C) were not significantly different in average size distribution. Before loading and after loading group were not significantly different; $p \leq 0.05$; two-tailed t-test; $n > 30$ microparticles per group; data shown as mean ± SD.

APPENDIX C

C.1 STRONG ANION EXCHANGE HIGH PERFORMANCE LIQUID CHROMATOGRAPHY

Results: SAX-HPLC analysis was used to determine Hep and Hep^{-N} disaccharide composition. For Hep, 74% of the sample was 2-sulfo unsaturated uronic acid (ΔUA(2S)) / 6-sulfo-N-sulfo glucosamine (GlcNS(6S)), which is likely the common disaccharide repeat unit of heparin, 2-O-sulfo-α-L-iduronic acid / 6-O-sulfo-N-sulfo-α-D-glucosamine (Table C.1). Additionally, 8% of the Hep sample was ΔUA / GlcNS(6S) and 6% was ΔUA(2S) / GlcNS. In the Hep^{-N} sample, however, the above N-sulfated repeat units were not detected and instead appeared to be replaced by the N-desulfated equivalents. Specifically, the Hep^{-N} sample was 72% ΔUA(2S) / 6-sulfo glucosamine (Glc(6S)), 10% ΔUA / Glc(6S), and 7% ΔUA(2S) / Glc, indicating that the sample was successfully N-desulfated. One other repeat unit, ΔUA(2S) / GlcNAc(6S) made up 2% of the Hep sample but was no longer detected in the Hep^{-N} sample which may indicate that a small amount of acetyl groups were also removed in the N-desulfation process.

Table C.1. Heparin and N-desulfated heparin disaccharide composition as determined by SAX-HPLC analysis. ΔUA=$\Delta^{4,5}$-unsaturated uronic acid; Glc= glucosamine; NS= N-sulfo; NAc=N-acetyl; ND = not detected.

	ΔUA(2S)-GLCNS(6S)	**ΔUA(2S)-GLC(6S)**	**ΔUA-GLCNS(6S)**	**ΔUA-GLC(6S)**	**ΔUA(2S)-GLCNS**	**ΔUA(2S)-GLC**	**ΔUA(2S)-GLCNAC(6S)**
Hep	74	ND	8	ND	6	ND	2
Hep^{-N}	ND	72	ND	10	ND	7	ND

C.2 MICROPARTICLE SIZE DISTRIBUTION

Methods: Prior to all *in vitro* and *in vivo* experiments, MPs were filtered with 40 μm cell strainers to remove most MPs under 40 μm in diameter. Therefore, MP sizing was completed on the filtered microparticles using phase microscopy and ImageJ analysis of MP diameter.

Results and Discussion: MPs were 62 ± 65 μm in diameter and an image of the MPs can be found in Figure C.1.

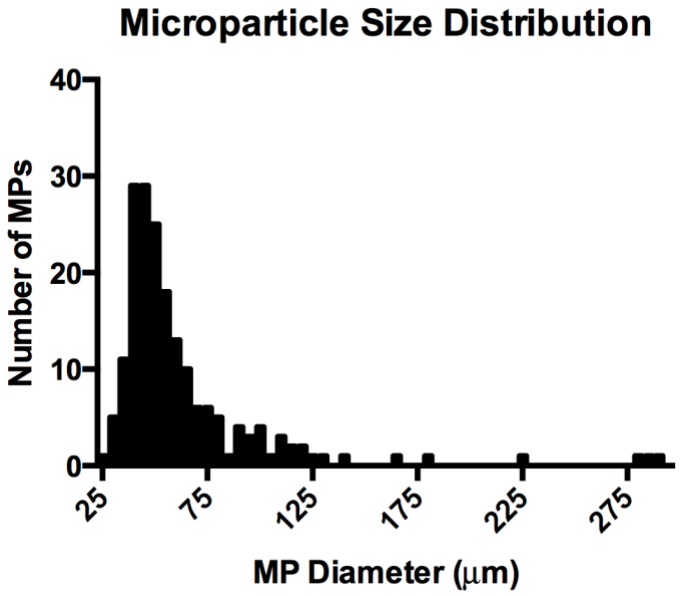

Figure C.1. Histogram of microparticle size distribution. Microparticles were found to be 62 ± 65 μm in diameter using ImageJ analysis; n > 50 microparticles.

C.3 MICROPARTICLE DEGRADATION

Methods: MP degradation *in vitro* was monitored by incubating 0.5 mg MPs in 0.5 mL 0.1 wt% BSA solution at 37°C. 30 μL of each sample was removed and imaged via phase microscopy every 2 days until complete degradation; n = 3 per MP formulation.

MP degradation was defined as the time point at which no MP were found across the entire microscope slide, at which point no image was taken.

Results and Discussion: MPs degradation varied by DTT concentration, whereby 20 mM DTT MPs degraded in 30 days, 25 mM DTT MPs degraded within 10-16 days, and 40 mM DTT MPs degraded within 8 days (Figure C.2). The incorporation of DTT within 10 wt% Hep^{-N} MPs accelerates ester hydrolysis within the PEGDA molecules [276]. Therefore, by increasing the concentration of DTT within MPs allowed for tunable degradation from within 30 days for 20 mM DTT MPs to 8 days for 40 mM DTT MPs.

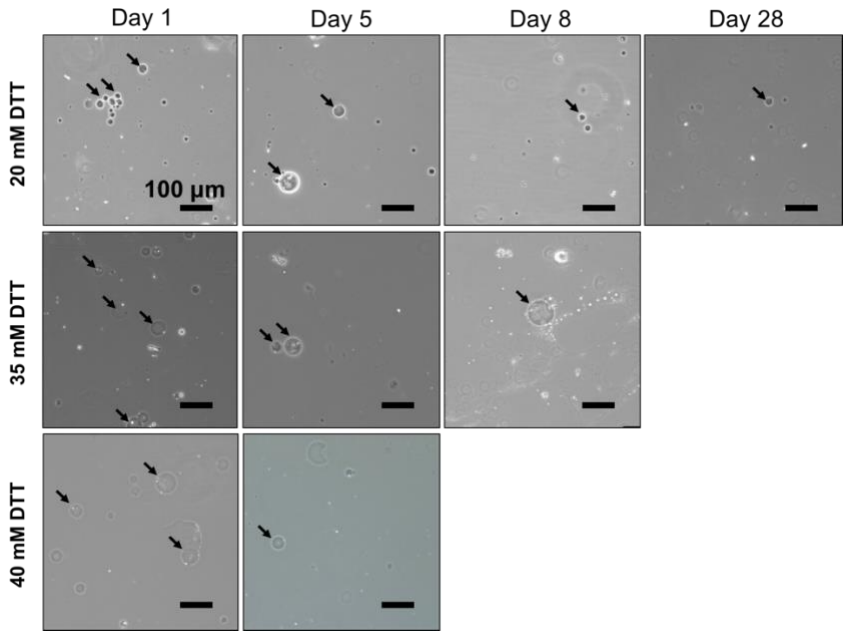

Figure C.2. 10 wt% Hep^{-N} microparticles degraded between 8 to 30 days *in vitro*. Microparticle degradation time course *in vitro* was dependent on the concentration of dithiothreitol (DTT) crosslinked within microparticles. Microparticle degradation was defined as the time point at which no microparticles were found, at which time no image was taken. Black arrows indicate microparticles; scale bar is 100 µm.

C.4 SUPRASPINATUS MUSCLE WEIGHT AND FIBROUS INFILTRATION FOLLOWING INJURY

Methods: After 1, 3, and 6 weeks following injury and treatment, animals were euthanized and the supraspinatus muscles were dissected, weighed, and fixed in 2%

paraformaldehyde solution (PFA, J.T. Baker) for 45 mins, followed by incubations in 10% v/v optimum cutting temperature (OCT, Sakura Finetek) PBS solutions with 0, 10, and 20% sucrose for 10 mins each. Muscles were placed in histology blocks with 100% OCT under vacuum overnight and then frozen in 190 proof ethanol cooled by liquid nitrogen. Muscles were sectioned with a cryostat (Thermo Scientific CryoStar NX70) into 7 μm sections perpendicular to the muscle to create tissue cross-sections. Masson's trichrome (Sigma, Fisher) was used to identify fibrous infiltrate and following staining, slides were mounted with Cytoseal 60 (Richard Allen Scientific) and cover slipped. Sections were imaged with a Nikon Eclipse 80i and analyzed using ImageJ software and color thresholding; n = 4-5 per experimental group per time point. To quantify fibrous infiltration:

$$\% \text{ of fibrous infiltration} = \frac{\text{blue pixel count}}{\text{red pixel count} + \text{blue pixel count}} \times 100$$

Results and Discussion: Though no differences were apparent after 1 week following tendon injury, supraspinatus muscle weight significantly decreased by 40 ± 9% compared to uninjured controls at week 6 (Figure C.3). Masson's trichrome showed that fibrous infiltration was significantly greater in the injured supraspinatus muscles compared to uninjured controls at both the 3 and 6 week time points (Figure C.3B-C). These results confirm that this is a model of degenerative muscle injury and thus is an appropriate *in vivo* platform to test effects of release of SDF-1α on altering the cellular milieu in a degenerative environment.

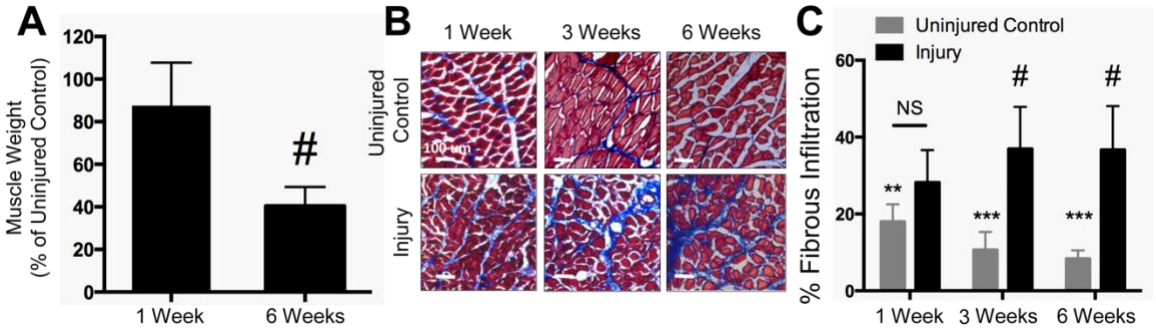

Figure C.3. Supraspinatus muscle weight significantly decreased after 6 weeks and fibrosis significantly increased after 3 weeks following injury compared to uninjured control. (A) Injured supraspinatus muscle weight was ~40% the weight of the uninjured contralateral control 6 weeks following injury; #Significantly different than uninjured control; $p \leqq 0.05$; $n = 5 \pm SD$. (B) Masson's trichrome staining was used to identify fibrous infiltrate (blue) within the supraspinatus muscle (red); scale bar is 100 μm. (C) Image analysis indicated that fibrosis was significantly greater in the injured muscle compared to the contralateral control after 3 and 6 weeks; **Significantly different than 3 and 6 week injury; $p \leqq 0.05$; ***Significantly different than 1, 3, and 6 week injury; $p \leqq 0.05$; $n = 4\text{-}5 \pm SD$.

C.5 Flow cytometry gating schemes

Methods: Single cells were identified first by gating for all cells (forward scatter vs. side scatter) followed by identifying the single cell population with forward scatter area vs. forward scatter height (Figure C.4A-B). Fluorescence minus one (FMO) controls were used to gate for all markers, including CD11b, CD68, CD163 (Figure C.5C-E), CD90, CD29, and CD44 (example not shown) and were applied to all samples, including one sample shown in Figure C.5F-H. Cell populations were identified as follows: leukocytes (CD11b+), macrophages (CD11b+CD68+), M1-like macrophages (CD11b+CD68+CD163-), M2-like macrophages (CD11b+CD68+CD163+), and MSCs (CD29+CD44+CD90+).

Results and Discussion: Overall results from these studies can be found in the main text and in Figure 5.3-4.

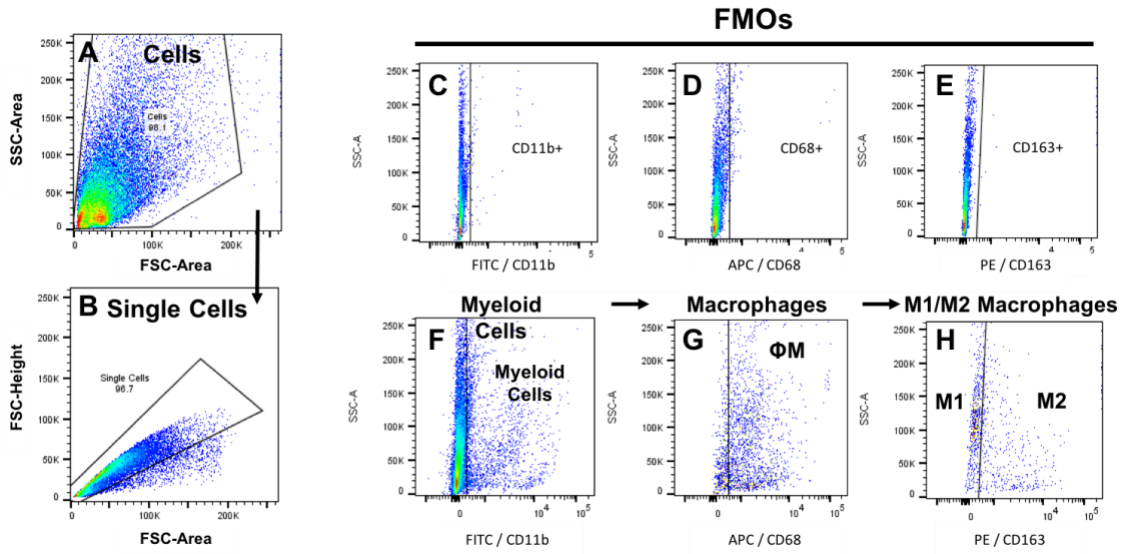

Figure C.4. Flow cytometry gating scheme for inflammatory cell populations. (A) Cells were first gated through forward scatter (FSC) area vs. side scatter (SSC) area plot, (B) then further gated through FSC-area vs. FSC-height plot to identify single cells. Fluorescence minus one (FMO)s were used to create gates for (C) CD11b+, (D) CD68+, and (E) CD163+ cells. Example data from supraspinatus muscle shows the identification of (F) leukocytes, CD11b+, (G) macrophages, CD11b+CD68+, and (H) M1 or M2 macrophages, CD11b+CD68+CD163-/+.

C.6 Fc BLOCKING OF FLOW CYTOMETRY SAMPLES

Methods: To ensure that nonspecific binding of antibodies to Fc receptors on leukocytes and macrophages did not significantly affect our flow cytometry results, infraspinatus muscles from the rotator cuff of Sprague Dawley rats that underwent tendon transection and denervation were harvested, digested with collagenase 1A (Sigma) for 45 mins at 37º C, and passed through a 40 µm cell strainer (Corning). Fc blocker (CD16/32, BioLegend) was then added to half of each sample according to the manufacturer's protocol. Briefly, 10 ug/mL Fc blocker was added to each sample and allowed to incubate for 5-10 mins on ice. Subsequently, all samples were stained with the inflammatory cell panel that included FITC-conjugated anti-CD11b (AbD Serotec), PE-conjugated anti-CD163 (BioRad), and APC-conjugated anti-CD68 (BioRad). Samples

were stained for 30 mins and fixed in 2% PFA for 20 mins, then analyzed using a FACS-AriaIIIu flow cytometer (BD Biosciences). The cell populations of interest are presented as a percentage of single cells.

Results and Discussion: No significant differences were observed in total myeloid cells, total macrophages, M2-like macrophages, or M1-like macrophages between the Fc blocked and non-Fc blocked samples (Figure C.5). As Fc blocking did not affect the inflammatory cell staining and subsequent analysis, we did not use Fc blocking for any other flow cytometry experiments presented in Chapter 5 or 6.

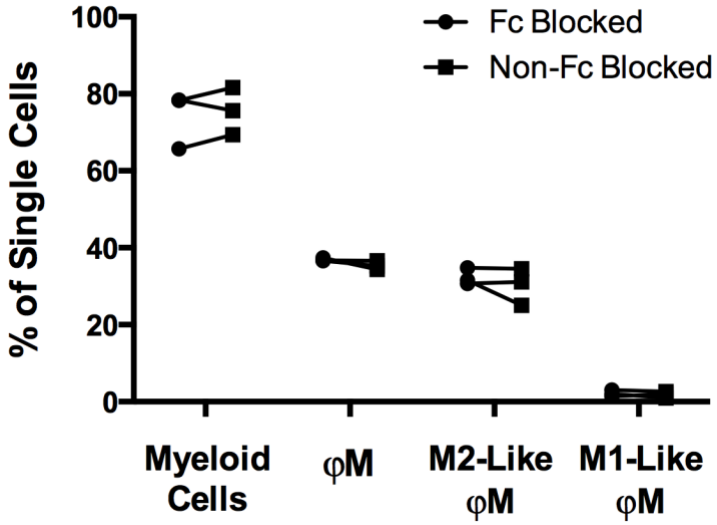

Figure C.5. Fc blocking of flow cytometry samples. No significant difference in total myeloid cells, total macrophages, M2-like macrophages, or M1-like macrophages was observed between blocked and non-blocked digested infraspinatus muscles; n = 3.

APPENDIX D

D.1 PCA ANALYSIS OF MUSCLE SECRETOME

Methods: Portions of muscle harvested at day 7 were utilized for Luminex analysis with the MILLIPLEX MAP rat cytokine/chemokine immunology magnetic bead panel (EMD Millipore). After acquisition of analyte concentrations within each sample, individual samples were normalized to total protein content (in mg/mL) which was determined using a BCA assay (Thermo Scientific). Principal component analysis (PCA) was then completed using JMP software; n = 4-6.

Results: PCA was utilized to determine if unsupervised multivariate analysis could distinguish between groups based on protein production. However, PCA was unable to distinguish between treatment, injured, or uninjured groups (Figure E.1).

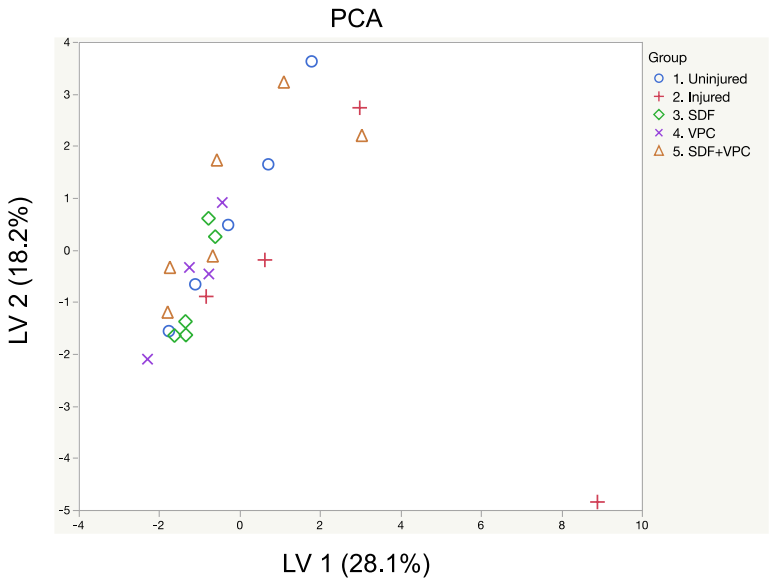

Figure D.1. Principal component analysis did not separate treated, injured, or uninjured groups across latent variable 1 or 2; n = 4-6.

APPENDIX E

IN VIVO RELEASE OF SDF-1A FROM MICROPARTICLES IN SUPRASPINATUS MUSCLE

E.1 *EX VIVO* SDF-1α LOADED MICROPARTICLE AND SOLUBLE SDF-1α DELIVERY

Methods: For *ex vivo* imaging of SDF-1α loaded MPs, infraspinatus muscles from 3 male, Sprague Dawley rats were cut in half, and one half of each muscle was used for either the SDF-1α loaded MP or soluble SDF-1α group. Each portion of muscle was weighed to ensure the same size muscles were used for each group. As the muscles were imaged *ex vivo*, 1 μg SDF-1α was loaded onto 0.6 mg MPs, the same dose used for cell recruitment studies, which was sufficient to detect the fluorescent signal using IVIS. For the soluble SDF-1α group, the same amount of SDF-1α that loaded onto 0.6 mg MPs was used. The SDF-1α loaded MPs and soluble SDF-1α were imaged prior to injection into muscles, as well as at day 0, 1, 3, and 7 after injection into the infraspinatus muscles using IVIS (Ex: 621, Em: 639).

Results: Prior to injection, the soluble SDF-1α signal was ~1.3x brighter than the SDF-1α MPs (Figure E.1A). Once injected into the muscle, the soluble SDF-1α signal was ~1.4x brighter than the SDF-1α MPs (Figure E.1B).

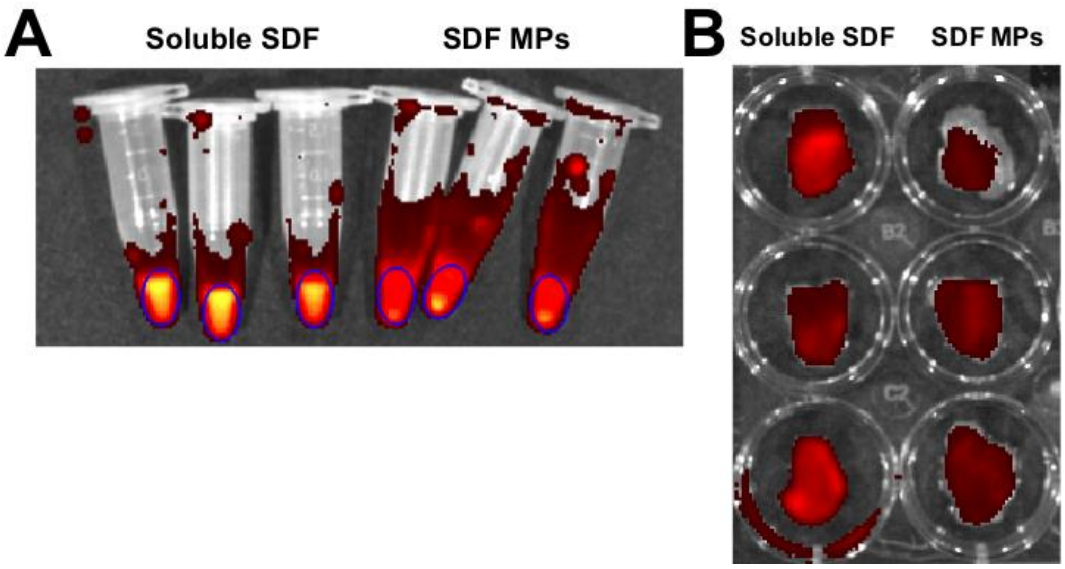

Figure E.1. Soluble SDF-1α is brighter than SDF-1α loaded MPs before and after injection into muscle; n = 3.

Between day 0 to 7, the SDF-1α signal increased in the SDF-1α loaded MP group, indicating that SDF-1α was released from MPs and subsequently diffused to the surface of the muscle (Figure E.2).

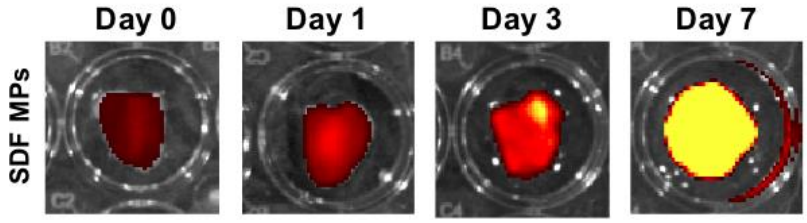

	Day 0	Day 1	Day 3	Day 7
SDF MPs	0.72 ± 0.16	1.54 ± 0.582	3.79 ± 0.65	10.40 ± 3.71

Figure E.2. SDF-1α is released from MPs within infraspinatus muscle over 7 days; n = 3.

E.2 IN VIVO SDF-1α LOADED MICROPARTICLE AND SOLUBLE SDF-1α RELEASE

Methods: For *in vivo* imaging of SDF-1α loaded MPs, 9 µg AlexaFluor633-labelled SDF-1α was loaded onto 5.4 mg MPs (9x dose compared to cell recruitment studies) to ensure that the fluorescent signal was detectable using the *In Vivo* Imaging System (IVIS, Perkin Elmer). For the soluble SDF-1α group, the same amount of SDF-1α that loaded onto 5.4 mg MPs was used. To track AF633 SDF-1α release over time, longitudinal *in vivo* imaging (Ex: 621, Em: 639) was performed with IVIS on day 0, 1, 3, and 7 following injury and injection. Radiant efficiency (photons/second * steradia * µW) was evaluated using the same-sized circular region of interest (ROI) at each time point. Background fluorescence from the skin was evaluated for each animal at each time point and subtracted from each respective ROI measurement. Fluorescent signal at each time point was normalized to the day 0 time point; n = 3.

Results: Similar to the results from our *ex vivo* study, the soluble SDF-1α signal was ~1.5x brighter than the SDF-1α MPs when injected and imaged in the supraspinatus muscles (Figure D.2A). However, the difference in fluorescent signal from each group was not statistically significant. For the SDF-1α MP group, on average the highest SDF-1α signal was observed 1 day following injury and SDF-1α MP injection (Figure D.2Ai-iv and S2B).

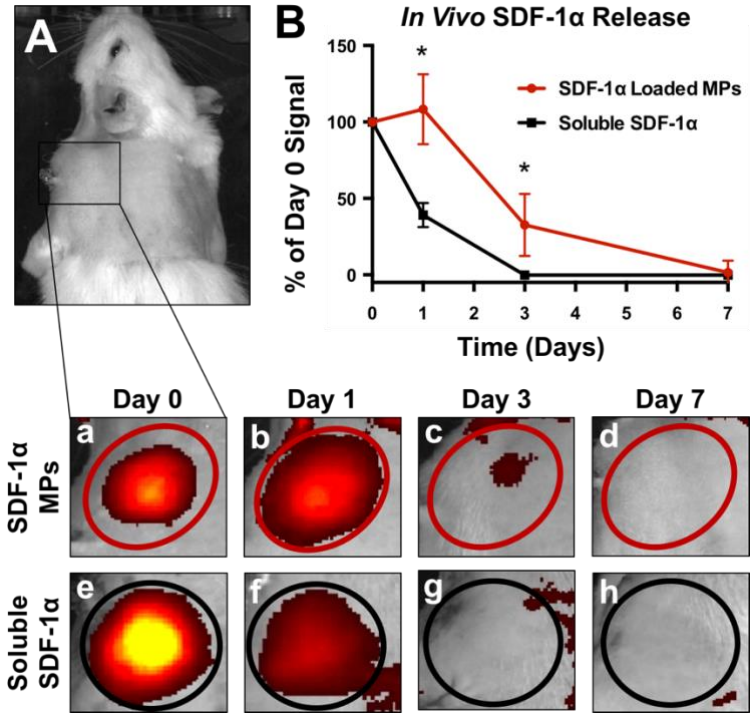

Figure E.3. SDF-1α released from MPs remained near the supraspinatus muscle for at least 3 days following injury and injection. (A) Representative images showing (i-iv) fluorescently-tagged SDF-1α released from MPs or (v-vii) soluble fluorescently-tagged SDF-1α in the supraspinatus muscle over time; red and black circles indicate the region of interest used for quantification. (B) For SDF-1α loaded MPs, the highest fluorescently-tagged SDF-1α signal was observed at day 1, and SDF-1α was still detected after at least 3 days. For soluble SDF-1α, no signal was detected by day 3 following injection. *Significantly different SDF-1α signal at designated time point; $p \leqq 0.05$; n = 3 ± SD.

Between 20-60% of the SDF-1α signal observed at day 0 was still observed by day 3, whereas little to no SDF-1α signal was observed by day 7. For the soluble SDF-1α group, the highest SDF-1α signal was observed at day 0 (Figure E.3v-viii and E.3B). By day 1, only 30-50% of the SDF-1α signal observed at day 0 was still present and by day 3, little to no SDF-1α signal was observed. Ultimately, significantly more SDF-1α signal was observed at day 1 and 3 in the SDF-1α loaded MP group compared to the soluble SDF-1α group.

Discussion: At day 0, it appeared that the soluble SDF-1α group was brighter than SDF-1α MPs, which was corroborated by our *ex vivo* findings (Figure E.1 and 2A). Collectively, these results suggest that MPs may be interfering with the fluorescent SDF-1α signal in these studies. For SDF-1α loaded MPs, the greatest AF633 SDF-1α signal was generally exhibited 1 day following injury and MP injection, which may be due to the release of AF633 SDF-1α from MPs within ~1 day (Figure E.3i-iv). Furthermore, because a high dose of MPs was used for IVIS imaging compared to our cell recruitment studies, it is also possible that the MPs shifted within the muscle over the first 24 hours, possibly resulting in the increased fluorescent signal. Despite most SDF-1α being released from MPs after ~24 hours, however, some AF633 SDF-1α was still detected near the supraspinatus muscle at least 3 days following injury and injection (Figure E.3A-B). In contrast, with soluble SDF-1α, AF633 SDF-1α signal began to decrease as early as 1 day following injection, and no AF633 SDF-1α signal was observed at day 3, indicating that at this concentration, MPs retained SDF-1α near the site of injection over a longer period of time than soluble SDF-1α alone (Figure E.3B). It is important to note, however, that due to limits in the in sensitivity of the imaging equipment, the dose employed in the IVIS imaging studies was 9x greater than the dose used for cell recruitment, meaning that the release kinetics observed may differ from the release kinetics during the cell recruitment studies (see Chapter 5 and 6). Nevertheless, our results indicate that with SDF-1α loaded MPs, SDF-1α signal was observed localized near the supraspinatus muscle for at least 3 days following injury and treatment.

REFERENCES

[1] R.C. Lawrence, C.G. Helmick, F.C. Arnett, R.A. Deyo, D.T. Felson, E.H. Giannini, S.P. Heyse, R. Hirsch, M.C. Hochberg, G.G. Hunder, M.H. Liang, S.R. Pillemer, V.D. Steen, F. Wolfe, Estimates of the prevalence of arthritis and selected musculoskeletal disorders in the United States, Arthritis Rheum. 41 (1998) 778–799. doi:10.1002/1529-0131(199805)41:5<778::AID-ART4>3.0.CO;2-V.

[2] M. Urwin, D. Symmons, T. Allison, T. Brammah, H. Busby, M. Roxby, A. Simmons, G. Williams, Estimating the burden of musculoskeletal disorders in the community: the comparative prevalence of symptoms at diVerent anatomical sites, and the relation to social deprivation, Ann Rheum Dis. 57 (1998) 649–655. doi:10.1136/ard.57.11.649.

[3] B. Vaibhav, P. Nilesh, S. Vikram, C. Anshul, Bone morphogenic protein and its application in trauma cases: a current concept update., Injury. 38 (2007) 1227–35. doi:10.1016/j.injury.2006.12.012.

[4] N. Gerwin, C. Hops, A. Lucke, Intraarticular drug delivery in osteoarthritis, Adv. Drug Deliv. Rev. 58 (2006) 226–242. doi:10.1016/j.addr.2006.01.018.

[5] S.G. Owen, H.W. Francis, M.S. Roberts, Disappearance kinetics of solutes from synovial fluid after intra-articular injection, Br. J. Clin. Pharmacol. (1994) 349–355.

[6] B. Gharaibeh, Y. Chun-Lansinger, T. Hagen, S.J.M. Ingham, V. Wright, F. Fu, J. Huard, Biological Approaches to Improve Skeletal Muscle Healing after Injury and Disease, Birth Defects Res. C Embryo Today. 96 (2012) 82–94. doi:10.1002/bdrc.21005.Biological.

[7] C.H. Evans, V.B. Kraus, L.A. Setton, Progress in intra-articular therapy, Nat. Rev. Rheumatol. 10 (2014) 11–22. doi:10.1038/nrrheum.2013.159.Progress.

[8] T. Laumonier, J. Menetrey, Muscle injuries and strategies for improving their repair., J. Exp. Orthop. 3 (2016) 15. doi:10.1186/s40634-016-0051-7.

[9] J.R. Krieger, M.E. Ogle, J. McFaline-Figueroa, C.E. Segar, J.S. Temenoff, E.A. Botchwey, Spatially localized recruitment of anti-inflammatory monocytes by SDF-1α-releasing hydrogels enhances microvascular network remodeling, Biomaterials. 77 (2016) 280–290. doi:10.1016/j.biomaterials.2015.10.045.

[10] M.E. Ogle, J.R. Krieger, L.E. Tellier, J. McFaline-Figueroa, J.S. Temenoff, E.A. Botchwey, Dual Affinity Heparin-Based Hydrogels Achieve Pro-Regenerative Immunomodulation and Microvascular Remodeling, ACS Biomater. Sci. Eng. (2017). doi:10.1021/acsbiomaterials.6b00706.

[11] S. Prokoph, E. Chavakis, K.R. Levental, A. Zieris, U. Freudenberg, S. Dimmeler, C. Werner, Sustained delivery of SDF-1a from heparin-based hydrogels to attract circulating pro-angiogenic cells, Biomaterials. 33 (2012) 4792–4800. doi:10.1016/j.biomaterials.2012.03.039.

[12] E.M. Anderson, B.J. Kwee, S.A. Lewin, T. Raimondo, M. Mehta, D.J. Mooney, Local delivery of VEGF and SDF enhances endothelial progenitor cell recruitment and resultant recovery from ischemia, Tissue Eng. Part A. 21 (2015) 1217–1227.

doi:10.1089/ten.tea.2014.0508.
[13] T.E. Rinker, B.D. Philbrick, J.S. Temenoff, Core-shell microparticles for protein sequestration and controlled release of a protein-laden core, Acta Biomater. 56 (2016) 91–101. doi:10.1016/j.actbio.2016.12.042.
[14] L.E. Tellier, T. Miller, T.C. McDevitt, J.S. Temenoff, Hydrolysis and sulfation pattern effects on release of bioactive bone morphogenetic protein-2 from heparin-based microparticles, J. Mater. Chem. B. 3 (2015) 8001–8009. doi:10.1039/C5TB00933B.
[15] M.H. Hettiaratchi, T. Miller, J.S. Temenoff, R.E. Guldberg, T.C. McDevitt, Heparin microparticles effects on presentation and bioactivity of bone morphogenetic protein-2, Biomaterials. 35 (2014) 7228–7238.
[16] X. Xu, A.K. Jha, R.L. Duncan, X. Jia, Heparin-decorated, hyaluronic acid-based hydrogel particles for the controlled release of bone morphogenetic protein 2, Acta Biomater. 7 (2011) 3050–3059. doi:10.1016/j.actbio.2011.04.018.
[17] Y. Peng, L.E. Tellier, J.S. Temenoff, Heparin-based hydrogels with tunable sulfation & degradation for anti-inflammatory small molecule delivery, Biomater. Sci. 4 (2016) 1371–1380. doi:10.1039/C6BM00455E.
[18] R. Sadir, A. Imberty, H. Lortat-Jacob, Heparan sulfate/heparin oligosaccharides protect stromal cell-derived factor-1 (SDF-1)/CXCL12 against proteolysis induced by CD26/dipeptidyl peptidase IV, J. Biol. Chem. 279 (2004) 43854–43860. doi:10.1074/jbc.M405392200.
[19] B.P. Purcell, J.A. Elser, A. Mu, K.B. Margulies, J.A. Burdick, Synergistic effects of SDF-1alpha chemokine and hyaluronic acid release from degradable hydrogels on directing bone marrow derived cell homing to the myocardium, Biomaterials. 33 (2012) 7849–7857. doi:10.1016/j.biomaterials.2012.07.005.
[20] R. Sadir, A. Imberty, F. Baleux, H. Lortat-Jacob, Heparan sulfate/heparin oligosaccharides protect stromal cell-derived factor-1 (SDF-1)/CXCL12 against proteolysis induced by CD26/dipeptidyl peptidase IV, J. Biol. Chem. 279 (2004) 43854–43860. doi:10.1074/jbc.M405392200.
[21] S.P. Seto, T. Miller, J.S. Temenoff, Effect of selective heparin desulfation on preservation of bone morphogenetic protein-2 bioactivity after thermal stress, Bioconjug. Chem. 26 (2015) 286–293. doi:10.1021/bc500565x.
[22] D.J. Mahoney, B. Mulloy, M.J. Forster, C.D. Blundell, E. Fries, C.M. Milner, A.J. Day, Characterization of the interaction between tumor necrosis factor-stimulated gene-6 and heparin: Implications for the inhibition of plasmin in extracellular matrix microenvironments, J. Biol. Chem. 280 (2005) 27044–27055. doi:10.1074/jbc.M502068200.
[23] C.D. Blundell, D.J. Mahoney, A. Almond, P.L. DeAngelis, J.D. Kahmann, P. Teriete, A.R. Pickford, I.D. Campbell, A.J. Day, The link module from ovulation- and inflammation-associated protein TSG-6 changes conformation on hyaluronan binding., J. Biol. Chem. 278 (2003) 49261–49270. doi:10.1074/jbc.M309623200.
[24] J.A. Kummer, J.J. Abbink, J. DeBoer, D. Roem, E.J. Nieuwenhuys, A.M. Kamp, T.J.G. Swaak, C.E. Hack, Analysis of intraarticular fibronolytic pathways in patients with inflammatory and noninflammatory joint diseases, Arthritis Rheum. 35 (1992) 884–893.
[25] P. Brommer, G. Dooijewaard, B. Dijkmans, F. Breedvelf, Plasminogen activators

in synovial fluid and plasma from patients with arthritis, Ann. Rheum. Dis. 51 (1992) 965–968.
[26] C. Belcher, F. Fawthrop, R. Bunning, M. Doherty, Plasminogen activators and their inhibitors in synovial fluids from normal , osteoarthritis , and rheumatoid arthritis knees, Ann. Rheum. Dis. 55 (1996) 230–236.
[27] H.K. Ronday, H.H. Smits, G.N. Van Muijen, M.S. Pruszczynski, R.J. Dolhain, E.J. Van Langelaan, F.C. Breedveld, J.H. Verheijen, Difference in expression of the plasminogen activation system in synovial tissue of patients with rheumatoid arthritis and osteoarthritis, Br. J. Rheumatol. 35 (1996) 416–423.
[28] E. Brzoska, M. Kowalewska, A. Markowska-Zagrajek, K. Kowalski, K. Archacka, M. Zimowska, I. Grabowska, A.M. Czerwińska, M. Czarnecka-Góra, W. Stremińska, K. Jańczyk-Ilach, M.A. Ciemerych, Sdf-1 (CXCL12) improves skeletal muscle regeneration via the mobilisation of Cxcr4 and CD34 expressing cells, Biol. Cell. 104 (2012) 722–737. doi:10.1111/boc.201200022.
[29] C.C. Bleul, R.C. Fuhlbrigge, J.M. Casanovas, A. Aiuti, T.A. Springer, A highly efficacious lymphocyte chemoattractant, stromal cell-derived factor 1 (SDF-1), J. Exp. Med. 184 (1996) 1101–1109.
[30] B.A. Aiuti, I.J. Webb, C. Bleul, T. Springer, The chemokine SDF-1 is a chemoattractant for human CD34+ hematopoietic progenitor cells and provides a new mechanism to explain the mobilization of CD34+ progenitors to peripheral blood, J. Exp. Med. 185 (1997) 111–120.
[31] D.P. Cross, C. Wang, Stromal-derived factor-1 alpha-loaded PLGA microspheres for stem cell recruitment, Pharm. Res. 28 (2011) 2477–2489. doi:10.1007/s11095-011-0474-x.
[32] S. Otsuru, K. Tamai, T. Yamazaki, H. Yishikawa, Y. Kaneda, Circulating bone marrow-derived osteoblast progenitor cells are recruited to the bone-forming site by the CXCR4/stromal cell-derived factor-1 pathway, Stem Cells. 26 (2008) 223–234. doi:10.1634/stemcells.2007-0515.
[33] M. Kucia, K. Jankowski, R. Reca, M. Wysoczynski, L. Bandura, D.J. Allendorf, J. Zhang, J. Ratajczak, M.Z. Ratajczak, CXCR4 – SDF-1 signalling , locomotion , chemotaxis and adhesion, J. Mol. Histol. 35 (2004) 233–245.
[34] W. Zhao, K. Jin, J. Li, X. Qiu, S. Li, Delivery of stromal cell-derived factor 1α for in situ tissue regeneration, (2017). doi:10.1186/s13036-017-0058-3.
[35] K.R. Lynch, T.L. Macdonald, Sphingosine 1-phosphate chemical biology, Biochim. Biophys. Acta - Mol. Cell Biol. Lipids. 1781 (2008) 508–512. doi:10.1016/j.bbalip.2008.06.006.
[36] M.E. Ogle, C.E. Olingy, A.O. Awojoodu, A. Das, R.A. Ortiz, H.Y. Cheung, E.A. Botchwey, Sphingosine-1-Phosphate Receptor-3 Supports Hematopoietic Stem and Progenitor Cell Residence Within the Bone Marrow Niche, Stem Cells. 35 (2016) 1040–1052.
[37] R.H. Cofield, J. Parvizi, P.J. Hoffmeyer, W.L. Lanzer, D.M. Ilstrup, C.M. Rowland, Surgical repair of chronic rotator cuff tears, J. Bone Jt. Surg. 83 (2001) 71.
[38] N.J. Willett, T. Thote, A.S. Lin, S. Moran, Y. Raji, S. Sridaran, H.Y. Stevens, R.E. Guldberg, Intra-articular injection of micronized dehydrated human amnion/chorion membrane attenuates osteoarthritis development., Arthritis Res.

Ther. 16 (2014) R47. doi:10.1186/ar4476.
[39] M.B. Goldring, Osteoarthritis and cartilage: the role of cytokines., Curr. Rheumatol. Rep. 2 (2000) 459–65. http://www.ncbi.nlm.nih.gov/pubmed/15480070.
[40] A.D. Pearle, R.F. Warren, S.A. Rodeo, Basic science of articular cartilage and osteoarthritis, Clin. Sports Med. 24 (2005) 1–12. doi:10.1016/j.csm.2004.08.007.
[41] M.B. Goldring, M. Otero, Inflammation in Osteoarthritis, Curr. Opin. Rheumatol. 23 (2011) 471–478. doi:10.1097/BOR.0b013e328349c2b1.
[42] H.G. Wisniewski, J. Vilček, TSG-6: An IL-1/TNF-inducible protein with anti-inflammatory activity, Cytokine Growth Factor Rev. 8 (1997) 143–156. doi:10.1016/S1359-6101(97)00008-7.
[43] H.G. Wisniewski, J.C. Hua, D.M. Poppers, D. Naime, J. Vilcek, B.N. Cronstein, TNF/IL-1-inducible protein TSG-6 potentiates plasmin inhibition by inter-alpha-inhibitor and exerts a strong anti-inflammatory effect in vivo., J. Immunol. 156 (1996) 1609–1615.
[44] N. Busso, V. Peclar, A. So, A.-P. Sappino, Plasminogen activation in synovial tissues: differences between normal, osteoarthritis, and rheumatoid arthritis joints., Ann. Rheum. Dis. 56 (1997) 550–7.
[45] K.A. Thomas, M.C. Gibbons, J.G. Lane, A. Singh, S.R. Ward, A.J. Engler, Rotator cuff tear state modulates self-renewal and differentiation capacity of human skeletal muscle progenitor cells, J. Orthop. Res. (2016) 12–14. doi:10.1002/jor.23453.
[46] W.E. Hennink, C.F. van Nostrum, Novel crosslinking methods to design hydrogels, Adv. Drug Deliv. Rev. 64 (2012) 223–236. doi:10.1016/j.addr.2012.09.009.
[47] D.M. Doroski, M.E. Levenston, J.S. Temenoff, Cyclic tensile culture promotes fibroblastic differentiation of marrow stromal cells encapsulated in poly(ethylene glycol)-based hydrogels., Tissue Eng. Part A. 16 (2010) 3457–66. doi:10.1089/ten.tea.2010.0233.
[48] Y. Qiu, J.J. Lim, L. Scott, R.C. Adams, H.T. Bui, J.S. Temenoff, PEG-based hydrogels with tunable degradation characteristics to control delivery of marrow stromal cells for tendon overuse injuries, Acta Biomater. 7 (2011) 959–966. doi:10.1016/j.actbio.2010.11.002.
[49] M.L. Kang, J.Y. Ko, J.E. Kim, G. Il Im, Intra-articular delivery of kartogenin-conjugated chitosan nano/microparticles for cartilage regeneration, Biomaterials. 35 (2014) 9984–9994. doi:10.1016/j.biomaterials.2014.08.042.
[50] M.H. Hettiaratchi, T. Rouse, C. Chou, L. Krishnan, H.Y. Stevens, M.A. Li, T.C. Mcdevitt, R.E. Guldberg, Enhanced in vivo retention of low dose BMP-2 via heparin microparticle delivery does not accelerate bone healing in a critically sized femoral defect, Acta Biomater. 59 (2017) 21–32. doi:10.1016/j.actbio.2017.06.028.
[51] L. Lu, G.N. Stamatas, a G. Mikos, Controlled release of transforming growth factor beta1 from biodegradable polymer microparticles., J. Biomed. Mater. Res. 50 (2000) 440–451.
[52] K. Mequanint, A. Patel, D. Bezuidenhout, Synthesis, swelling behavior, and biocompatibility of novel physically cross-linked polyurethane-block-

poly(glycerol methacylate) hydrogels, Biomacromolecules. 7 (2006) 883–891. doi:10.1021/bm0507047.
[53] H.J. Lim, H. Do Ghim, J.H. Choi, H.Y. Chung, J.O. Lim, Controlled release of BMP-2 from alginate nanohydrogels enhanced osteogenic differentiation of human bone marrow stromal cells, Macromol. Res. 18 (2010) 787–792. doi:10.1007/s13233-010-0804-6.
[54] H.-C. Lim, J.-H. Bae, S.-H. Song, Y.-E. Park, S.-J. Kim, Current treatments of isolated articular cartilage lesions of the knee achieve similar outcomes., Clin. Orthop. Relat. Res. 470 (2012) 2261–7. doi:10.1007/s11999-012-2304-9.
[55] P. Thevenot, A. Nair, J. Shen, P. Lotfi, C.Y. Ko, L. Tang, The Effect of Incorporation of SDF-1α into PLGA Scaffolds on Stem Cell Recruitment and the Inflammatory Response, Biomaterials. 31 (2011) 3997–4008. doi:10.1016/j.biomaterials.2010.01.144.
[56] S.P. Seto, M.E. Casas, J.S. Temenoff, Differentiation of mesenchymal stem cells in heparin-containing hydrogels via coculture with osteoblasts, Cell Tissue Res. 347 (2012) 589–601. doi:10.1007/s00441-011-1265-8.
[57] N.S. Gandhi, R.L. Mancera, The structure of glycosaminoglycans and their interactions with proteins, Chem. Biol. Drug Des. 72 (2008) 455–482. doi:10.1111/j.1747-0285.2008.00741.x.
[58] T. Miller, M.C. Goude, T.C. McDevitt, J.S. Temenoff, Molecular engineering of glycosaminoglycan chemistry for biomolecule delivery, Acta Biomater. 10 (2014) 1705–1719. doi:10.1016/j.actbio.2013.09.039.
[59] J.T. Gallagher, Heparan sulfate : growth control with a restricted sequence menu, 108 (2001) 357–361. doi:10.1172/JCI200113713.
[60] D.L. Rabenstein, Heparin and heparan sulfate: Biosynthesis, structure and function, Curr. Opin. Chem. Biol. 4 (2000) 626–631. doi:10.1016/S1367-5931(00)00145-9.
[61] J. Taipale, J. Keski-Oja, Growth factors in the extracellular matrix., FASEB J. Off. Publ. Fed. Am. Soc. Exp. Biol. 11 (1997) 51–9. http://www.ncbi.nlm.nih.gov/pubmed/9034166.
[62] R. Ruppert, E. Hoffmann, W. Sebald, Human bone morphogenetic protein 2 contains a heparin-binding site which modifies its biological activity., Eur. J. Biochem. 237 (1996) 295–302. doi:10.1111/j.1432-1033.1996.0295n.x.
[63] D.S.W. Benoit, K.S. Anseth, Heparin functionalized PEG gels that modulate protein adsorption for hMSC adhesion and differentiation, Acta Biomater. 1 (2005) 461–470. doi:10.1016/j.actbio.2005.03.002.
[64] A. Zieris, S. Prokoph, K.R. Levental, P.B. Welzel, M. Grimmer, U. Freudenberg, C. Werner, FGF-2 and VEGF functionalization of starPEG-heparin hydrogels to modulate biomolecular and physical cues of angiogenesis., Biomaterials. 31 (2010) 7985–94. doi:10.1016/j.biomaterials.2010.07.021.
[65] G. Tae, M. Scatena, P.S. Stayton, A.S. Hoffman, PEG-cross-linked heparin is an affinity hydrogel for sustained release of vascular endothelial growth factor, J. Biomater. Sci. Polym. Ed. 17 (2006) 187–197. doi:10.1163/156856206774879090.
[66] U. Freudenberg, A. Zieris, K. Chwalek, M. V. Tsurkan, M.F. Maitz, P. Atallah, K.R. Levental, S.A. Eming, C. Werner, Heparin desulfation modulates VEGF release and angiogenesis in diabetic wounds, J. Control. Release. 220 (2015) 79–

88. doi:10.1016/j.jconrel.2015.10.028.
[67] S.E. Sakiyama-Elbert, J.A. Hubbell, Controlled release of nerve growth factor from a heparin-containing fibrin-based cell ingrowth matrix, J. Control. Release. 69 (2000) 149–158. doi:10.1016/S0168-3659(00)00296-0.
[68] D.B. Pike, S. Cai, K.R. Pomraning, M.A. Firpo, R.J. Fisher, X.Z. Shu, G.D. Prestwich, R.A. Peattie, Heparin-regulated release of growth factors in vitro and angiogenic response in vivo to implanted hyaluronan hydrogels containing VEGF and bFGF, Biomaterials. 27 (2006) 5242–5251. doi:10.1016/j.biomaterials.2006.05.018.
[69] J. Lee, W. Il Choi, G. Tae, Y.H. Kim, S.S. Kang, S.E. Kim, S.-H. Kim, Y. Jung, S.H. Kim, Enhanced regeneration of the ligament–bone interface using a poly(l-lactide–co-ε-caprolactone) scaffold with local delivery of cells/BMP-2 using a heparin-based hydrogel, Acta Biomater. 7 (2011) 244–257. doi:10.1016/j.actbio.2010.08.017.
[70] Y.I. Chung, K.M. Ahn, S.H. Jeon, S.Y. Lee, J.H. Lee, G. Tae, Enhanced bone regeneration with BMP-2 loaded functional nanoparticle-hydrogel complex, J. Control. Release. 121 (2007) 91–99. doi:10.1016/j.jconrel.2007.05.029.
[71] O. Jeon, C. Powell, L.D. Solorio, M.D. Krebs, E. Alsberg, Affinity-based growth factor delivery using biodegradable, photocrosslinked heparin-alginate hydrogels, J. Control. Release. 154 (2011) 258–266. doi:10.1016/j.jconrel.2011.06.027.
[72] M.C. Goh, Y. Hwang, G. Tae, Epidermal growth factor loaded heparin-based hydrogel sheet for skin wound healing, Carbohydr. Polym. 147 (2016) 251–260. doi:10.1016/j.carbpol.2016.03.072.
[73] W. Choi, M. Kim, G. Tae, Y. Kim, Sustained release of human growth hormone from heparin-based hydrogel, Biomacromolecules. 9 (2008) 1698–1704.
[74] R. Jin, L.S. Moreira Teixeira, P.J. Dijkstra, C.A. Van Blitterswijk, M. Karperien, J. Feijen, Chondrogenesis in injectable enzymatically crosslinked heparin/dextran hydrogels, J. Control. Release. 152 (2011) 186–195. doi:10.1016/j.jconrel.2011.01.031.
[75] M. Kim, J.Y. Lee, C.N. Jones, A. Revzin, G. Tae, Heparin-based hydrogel as a matrix for encapsulation and cultivation of primary hepatocytes., Biomaterials. 31 (2010) 3596–603. doi:10.1016/j.biomaterials.2010.01.068.
[76] G. Tae, Y.J. Kim, W. Il Choi, M. Kim, P.S. Stayton, A.S. Hoffman, Formation of a novel heparin-based hydrogel in the presence of heparin-binding biomolecules, Biomacromolecules. 8 (2007) 1979–1986. doi:10.1021/bm0701189.
[77] H.J. Sim, T. Thambi, D.S. Lee, Heparin-based temperature-sensitive injectable hydrogels for protein delivery, J. Mater. Chem. B. 3 (2015) 8892–8901. doi:10.1039/c5tb01399b.
[78] M. Fujita, M. Ishihara, M. Simizu, K. Obara, T. Ishizuka, Y. Saito, H. Yura, Y. Morimoto, B. Takase, T. Matsui, M. Kikuchi, T. Maehara, Vascularization in vivo caused by the controlled release of fibroblast growth factor-2 from an injectable chitosan/non-anticoagulant heparin hydrogel, Biomaterials. 25 (2004) 699–706. doi:10.1016/S0142-9612(03)00557-X.
[79] M.H. Hettiaratchi, C. Chou, N. Servies, J.M. Smeekens, A. Cheng, C. Esancy, R. Wu, T.C. McDevitt, R.E. Guldberg, L. Krishnan, Competitive Protein Binding Influences Heparin-Based Modulation of Spatial Growth Factor Delivery for Bone

Regeneration, Tissue Eng. Part A. (2017). doi:10.1089/ten.tea.2016.0507.
[80] T.E. Rinker, B.D. Philbrick, M.H. Hettiaratchi, D.M. Smalley, T.C. McDevitt, J.S. Temenoff, Microparticle-mediated sequestration of cell-secreted proteins to modulate chondrocytic differentiation, Acta Biomater. 68 (2018) 125–136. doi:10.1016/j.actbio.2017.12.038.
[81] A. Zieris, R. Dockhorn, A. Ro, R. Zimmermann, M. Mu, P.B. Welzel, M. V Tsurkan, J. Sommer, U. Freudenberg, C. Werner, Biohybrid networks of selectively desulfated glycosaminoglycans for tunable growth factor delivery, Biomacromolecules. 15 (2014) 4439–4446.
[82] D. Gospodarowicz, J. Cheng, Heparin Protects Basic and Acidic FGF From Inactivation, J. Chem. Inf. Model. 53 (2013) 1689–1699. doi:10.1017/CBO9781107415324.004.
[83] J. Kan, Mikio Wang, Fen Xu, Jianming Crabb, John W. Hou, W.L. McKeehan, An Essential Heparin-Binding Domain in the Fibroblast Growth Factor Receptor Kinase, Science. (1993) 1918–1921. doi:10.1017/CBO9781107415324.004.
[84] N.S. Gandhi, R.L. Mancera, Prediction of heparin binding sites in bone morphogenetic proteins (BMPs)., Biochim. Biophys. Acta. 1824 (2012) 1374–81. doi:10.1016/j.bbapap.2012.07.002.
[85] T. Takada, T. Katagiri, M. Ifuku, N. Morimura, M. Kobayashi, K. Hasegawa, A. Ogamo, R. Kamijo, Sulfated Polysaccharides Enhance the Biological Activities of Bone Morphogenetic Proteins, J. Biol. Chem. 278 (2003) 43229–43235. doi:10.1074/jbc.M300937200.
[86] B. Zhao, T. Katagiri, H. Toyoda, T. Takada, T. Yanai, T. Fukuda, U. Il Chung, T. Koike, K. Takaoka, R. Kamijo, Heparin potentiates the in Vivo ectopic bone formation induced by bone morphogenetic protein-2, J. Biol. Chem. 281 (2006) 23246–23253. doi:10.1074/jbc.M511039200.
[87] J. Ratanavaraporn, Y. Tabata, Enhanced osteogenic activity of bone morphogenetic protein-2 by 2-O-desulfated heparin, Acta Biomater. 8 (2012) 173–182. doi:10.1016/j.actbio.2011.09.035.
[88] A.A. Parkar, A.J. Day, Overlapping sites on the link module of human TSG-6 mediate binding to hyaluronan and chondroitin-4-sulphate, FEBS Lett. 410 (1997) 413–417. doi:10.1016/S0014-5793(97)00621-2.
[89] R. Sadir, F. Baleux, A. Grosdidier, A. Imberty, H. Lortat-Jacob, Characterization of the stromal cell-derived factor-1alpha-heparin complex, J Biol Chem. 276 (2001) 8288–8296. doi:10.1074/jbc.M008110200.
[90] S. Fermas, F. Gonnet, A. Sutton, N. Charnaux, B. Mulloy, Y. Du, F. Baleux, R. Daniel, Sulfated oligosaccharides (heparin and fucoidan) binding and dimerization of stromal cell-derived factor-1 (SDF-1/CXCL 12) are coupled as evidenced by affinity CE-MS analysis, Glycobiology. 18 (2008) 1054–1064. doi:10.1093/glycob/cwn088.
[91] C.T. Veldkamp, F.C. Peterson, A.J. Pelzek, B.F. Volkman, The monomer – dimer equilibrium of stromal cell-derived factor-1 (CXCL12) is altered by pH, phosphate, sulfate, and heparin, Protein Sci. 1 (2005) 1071–1081. doi:10.1110/ps.041219505.minal.
[92] J. Luo, Z. Luo, N. Zhou, J.W. Hall, Z. Huang, Attachment of C-terminus of SDF-1 enhances the biological activity of its N-terminal peptide, Biochem. Biophys. Res.

Commun. 264 (1999) 42–47. doi:10.1006/bbrc.1999.1476.
[93] K. Uchimura, M. Morimoto-Tomita, A. Bistrup, J. Li, M. Lyon, J. Gallagher, Z. Werb, S.D. Rosen, HSulf-2, an extracellular endoglucosamine-6-sulfatase, selectively mobilizes heparin-bound growth factors and chemokines: effects on VEGF, FGF-1, and SDF-1., BMC Biochem. 7 (2006). doi:10.1186/1471-2091-7-2.
[94] B.M. Loo, J. Kreuger, M. Jalkanen, U. Lindahl, M. Salmivirta, Binding of heparin/heparan sulfate to fibroblast growth factor receptor 4., J. Biol. Chem. 276 (2001) 16868–16876. doi:10.1074/jbc.M011226200.
[95] L. Lundin, H. Larsson, J. Kreuger, S. Kanda, U. Lindahl, M. Salmivirta, L. Claesson-Welsh, Selectively desulfated heparin inhibits fibroblast growth factor-induced mitogenicity and angiogenesis, J. Biol. Chem. 275 (2000) 24653–24660. doi:10.1074/jbc.M908930199.
[96] S. Roy, H. Lai, R. Zouaoui, J. Duffner, H. Zhou, L. P Jayaraman, G. Zhao, T. Ganguly, T.K. Kishimoto, G. Venkataraman, Bioactivity screening of partially desulfated low-molecular-weight heparins: A structure/activity relationship study, Glycobiology. 21 (2011) 1194–1205. doi:10.1093/glycob/cwr053.
[97] E.L. Shipp, L.C. Hsieh-Wilson, Profiling the Sulfation Specificities of Glycosaminoglycan Interactions with Growth Factors and Chemotactic Proteins Using Microarrays, Chem. Biol. 14 (2007) 195–208. doi:10.1016/j.chembiol.2006.12.009.
[98] Y. Zhang, M.T. Hannan, C.E. CHaisson, T.E. McAlindon, S.R. Evans, P. Aliabadi, D. Levy, D.T. Felson, Bone mineral density and risk of incident and progressive radiographic knee osteoarthritis in women: the framingham study, J. Rheumatol. 27 (2000).
[99] J. Martel-Pelletier, Pathophysiology of osteoarthritis., Osteoarthritis Cartilage. 12 Suppl A (2004) S31–S33. doi:10.1053/joca.1998.0140.
[100] L.J. Sandell, T. Aigner, Articular cartilage and changes in arthritis. An introduction: cell biology of osteoarthritis., Arthritis Res. 3 (2001) 107–13.
[101] H.A. Kim, F.J. Blanco, Cell death and apoptosis in osteoarthritis cartilage, Curr. Drug Targets. 8 (2007) 333–345.
[102] J. Clouet, C. Vinatier, C. Merceron, M. Pot-vaucel, Y. Maugars, P. Weiss, G. Grimandi, J. Guicheux, From osteoarthritis treatments to future regenerative therapies for cartilage, Drug Discov. Today. 14 (2009) 913–925. doi:10.1016/j.drudis.2009.07.012.
[103] T. Aigner, J. Stöve, Collagens - Major component of the physiological cartilage matrix, major target of cartilage degeneration, major tool in cartilage repair, Adv. Drug Deliv. Rev. 55 (2003) 1569–1593. doi:10.1016/j.addr.2003.08.009.
[104] K.P.H. Pritzker, S. Gay, S.A. Jimenez, K. Ostergaard, J.P. Pelletier, K. Revell, D. Salter, W.B. van den Berg, Osteoarthritis cartilage histopathology: Grading and staging, Osteoarthr. Cartil. 14 (2006) 13–29. doi:10.1016/j.joca.2005.07.014.
[105] V.B. Kraus, J.L. Huebner, J. DeGroot, A. Bendele, The OARSI histopathology initiative - recommendations for histological assessments of osteoarthritis in the guinea pig, Osteoarthr. Cartil. 18 (2010) S24–S34. doi:10.1016/j.joca.2010.04.015.
[106] W. Zhang, R.W. Moskowitz, G. Nuki, S. Abramson, R.D. Altman, N. Arden, S. Bierma-Zeinstra, K.D. Brandt, P. Croft, M. Doherty, M. Dougados, M. Hochberg, D.J. Hunter, K. Kwoh, L.S. Lohmander, P. Tugwell, OARSI recommendations for

the management of hip and knee osteoarthritis, Part I: Critical appraisal of existing treatment guidelines and systematic review of current research evidence, Osteoarthr. Cartil. 15 (2007) 981–1000. doi:10.1016/j.joca.2007.06.014.
[107] F. Eckstein, F. Cicuttini, J.P. Raynauld, J.C. Waterton, C. Peterfy, Magnetic resonance imaging (MRI) of articular cartilage in knee osteoarthritis (OA): morphological assessment, Osteoarthr. Cartil. 14 (2006) 46–75. doi:10.1016/j.joca.2006.02.026.
[108] B.C. Vande Berg, F.E. Lecouvet, P. Poilvache, J. Jamart, R. Materne, B. Lengele, B. Maldague, J. Malghem, Assessment of knee cartilage in cadavers with dual-detector spiral CT arthrography and MR imaging., Radiology. 222 (2002) 430–436. doi:10.1148/radiol.2222010597.
[109] J.-D. Vassalli, A.-P. Sappino, D. Belin, The plasminogen activator/plasmin system, J. Clin. Invest. 88 (1991) 1067–1072.
[110] E. Superio-Cabuslay, M.M. Ward, K.R. Lorig, Patient education interventions in osteoarthritis and rheumatoid arthritis: a meta-analytic comparison with nonsteroidal antiinflammatory drug treatment, Arthritis Care Res. 9 (1996) 292–301.
[111] A. Anandacoomarasamy, L. March, Current evidence for osteoarthritis treatments, Ther. Adv. Musculoskelet. Dis. 2 (2010) 17–28. doi:10.1177/1759720X09359889.
[112] R.R. Bannuru, N.S. Natov, I.E. Obadan, L.L. Price, C.H. Schmid, T.E. McAlindon, Therapeutic trajectory of hyaluronic acid versus corticosteroids in the treatment of knee osteoarthritis: A systematic review and meta-analysis, Arthritis Rheum. 61 (2009) 1704–1711. doi:10.1002/art.24925.
[113] P.R. Fortin, J.R. Penrod, A.E. Clarke, Y. St-Pierre, L. Joseph, P. Bélisle, M.H. Liang, D. Ferland, C.B. Phillips, N. Mahomed, M. Tanzer, C. Sledge, A.H. Fossel, J.N. Katz, Timing of total joint replacement affects clinical outcomes among patients with osteoarthritis of the hip or knee, Arthritis Rheum. 46 (2002) 3327–3330. doi:10.1002/art.10631.
[114] V. Deshmukh, H. Hu, C. Barroga, C. Bossard, S. KC, L. Dellamary, J. Stewart, K. Chiu, M. Ibanez, M. Pedraza, T. Seo, L. Do, S. Cho, J. Cahiwat, B. Tam, J.R.S. Tambiah, J. Hood, N.E. Lane, Y. Yazici, A small-molecule inhibitor of the Wnt pathway (SM04690) as a potential disease modifying agent for the treatment of osteoarthritis of the knee, Osteoarthr. Cartil. 26 (2018) 18–27. doi:10.1016/j.joca.2017.08.015.
[115] M. Saito, K. a. Takahashi, Y. Arail, a. Inoue, K. Sakao, H. Tonomura, K. Honjo, S. Nakagawa, H. Inoue, Y. Tabata, T. Kubo, Intraarticular administration of platelet-rich plasma with biodegradable gelatin hydrogel microspheres prevents osteoarthritis progression in the rabbit knee, Clin. Exp. Rheumatol. 27 (2009) 201–207.
[116] A. Inoue, K. a. Takahashi, Y. Arai, H. Tonomura, K. Sakao, M. Saito, M. Fujioka, H. Fujiwara, Y. Tabata, T. Kubo, The therapeutic effects of basic fibroblast growth factor contained in gelatin hydrogel microspheres on experimental osteoarthritis in the rabbit knee, Arthritis Rheum. 54 (2006) 264–270. doi:10.1002/art.21561.
[117] K.E. Brown, K. Leong, C.H. Huang, R. Dalal, G.D. Green, H.B. Haimes, P. a. Jimenez, J. Bathon, Gelatin/chondroitin 6-sulfate microspheres for the delivery of therapeutic proteins to the joint, Arthritis Rheum. 41 (1998) 2185–2195.

[118] H. Thakkar, R.K. Sharma, a K. Mishra, K. Chuttani, R.S.R. Murthy, Enhanced retention of celecoxib-loaded solid lipid nanoparticles after intra-articular administration., J. Pharm. Pharmacol. 56 (2004) 1091–1099. doi:10.1211/0022357044166.
[119] E. Horisawa, T. Hirota, S. Kawazoe, J. Yamada, H. Yamamoto, H. Takeuchi, Y. Kawashima, Prolonged anti-inflammatory action of DL-lactide/glycolide copolymer nanospheres containing betamethasone sodium phosphate for an intra-articular delivery system in antigen-induced arthritic rabbit, Pharm. Res. 19 (2002) 403–410. doi:10.1023/A:1015123024113.
[120] R.T. Liggins, T. Cruz, W. Min, L. Liang, W.L. Hunter, H.M. Burt, Intra-articular treatment of arthritis with microsphere formulations of paclitaxel: Biocompatibility and efficacy determinations in rabbits, Inflamm. Res. 53 (2004) 363–372. doi:10.1007/s00011-004-1273-1.
[121] G. Huang, Z. Zhang, Micro- and nano-carrier mediated intra-articular drug delivery systems for the treatment of osteoarthritis, J. Nanotechnol. 2012 (2012). doi:10.1155/2012/748909.
[122] S.H.R. Edwards, Intra-articular drug delivery: The challenge to extend drug residence time within the joint, Vet. J. 190 (2011) 15–21. doi:10.1016/j.tvjl.2010.09.019.
[123] M. Tuncay, S. Calis, H. S. Kas, M., In vitro and in vivo evaluation of diclofenac sodium loaded album in microspheres, J. Microencapsul. 17 (2000) 145–155. doi:10.1080/026520400288382.
[124] R.E. Whitmire, S.D. Wilson, A. Singh, M.E. Levenston, N. Murthy, A.J. Garcia, Self-assembling nanoparticles for intra-articular delivery of anti- inflammatory proteins Rachel, Biomaterials. 33 (2012) 7665–7675. doi:10.1016/j.biomaterials.2012.06.101.
[125] N. Butoescu, C. a Seemayer, G. Palmer, P.-A. Guerne, C. Gabay, E. Doelker, O. Jordan, Magnetically retainable microparticles for drug delivery to the joint: efficacy studies in an antigen-induced arthritis model in mice., Arthritis Res. Ther. 11 (2009) R72. doi:10.1186/ar2701.
[126] N. Butoescu, O. Jordan, P. Burdet, P. Stadelmann, A. Petri-Fink, H. Hofmann, E. Doelker, Dexamethasone-containing biodegradable superparamagnetic microparticles for intra-articular administration: Physicochemical and magnetic properties, in vitro and in vivo drug release, Eur. J. Pharm. Biopharm. 72 (2009) 529–538. doi:10.1016/j.ejpb.2009.03.003.
[127] T. Thote, A.S.P. Lin, Y. Raji, S. Moran, H.Y. Stevens, M. Hart, R. V. Kamath, R.E. Guldberg, N.J. Willett, Localized 3D analysis of cartilage composition and morphology in small animal models of joint degeneration, Osteoarthr. Cartil. 21 (2013) 1132–1141. doi:10.1016/j.joca.2013.05.018.
[128] C. Guingamp, P. Gegout-Pottie, L. Philippe, B. Terlain, P. Netter, P. Gillet, Mono-iodoacetate-induced experimental osteoarthritis: A dose-response study of loss of mobility, morphology, and biochemistry, Arthritis Rheum. 40 (1997) 1670–1679. doi:10.1002/art.1780400917.
[129] Christopher B. Little and Margaret M. Smith, Little CB and Smith MM, Christopher B. Little and Margaret M. Smith, Little CB and Smith MM, Animal Models of Osteoarthritis, Curr. Rheumatol. Rev. 4 (2008) 175–182.

doi:10.2174/1573397087851335 23#sthash.OCnUaXeo.dpuf.
[130] L.M. Wancket, V. Baragi, S. Bove, K. Kilgore, P.J. Korytko, R.E. Guzman, Anatomical localization of cartilage degradation markers in a surgically induced rat osteoarthritis model., Toxicol. Pathol. 33 (2005) 484–489. doi:10.1080/01926230590965364.
[131] N.J. Willett, T. Thote, M. Hart, S. Moran, R.E. Guldberg, R. V. Kamath, Quantitative pre-clinical screening of therapeutics for joint diseases using contrast enhanced micro-computed tomography, Osteoarthr. Cartil. 24 (2016) 1604–1612. doi:10.1016/j.joca.2016.04.021.
[132] L. Xie, A.S.P. Lin, M.E. Levenston, R.E. Guldberg, Quantitative assessment of articular cartilage morphology via EPIC-??CT, Osteoarthr. Cartil. 17 (2009) 313–320. doi:10.1016/j.joca.2008.07.015.
[133] H.Y. Stevens, B.E. Shockley, N.J. Willett, A.S.P. Lin, Y. Raji, R.E. Guldberg, S.A. Labib, Particulated Juvenile Articular Cartilage Implantation in the Knee: A 3-Year EPIC-μCT and Histological Examination, Cartilage. 5 (2014) 74–77. doi:10.1177/1947603513515483.
[134] L. Xie, A.S.P. Lin, R.E. Guldberg, M.E. Levenston, Nondestructive assessment of sGAG content and distribution in normal and degraded rat articular cartilage via EPIC-μCT, Osteoarthr. Cartil. 18 (2010) 65–72. doi:10.1016/j.joca.2009.07.014.
[135] A.J. Day, S.P. Drummond, S. Anand, E. Bartnik, C.M. Milner, A novel chondroprotective property of TSG-6 has therapeutic potential for OA, Osteoarthr. Cartil. 24 (2016) S19–S20. doi:10.1016/j.joca.2016.01.064.
[136] M.T. Bayliss, S.L.T. Howat, J. Dudhia, J.M. Murphy, F.P. Barry, J.C.W. Edwards, A.J. Day, Up-regulation and differential expression of the hyaluronan-binding protein TSG-6 in cartilage and synovium in rheumatoid arthritis and osteoarthritis, Osteoarthr. Cartil. 9 (2001) 42–48. doi:10.1053/joca.2000.0348.
[137] H. Wisniewski, E. Colón, V. Liublinska, R.J. Karia, T. V Stabler, M. Attur, S.B. Abramson, P.A. Band, V.B. Kraus, TSG-6 activity as a novel biomarker of progression in knee osteoarthritis, Osteoarthr. Cartil. 22 (2014) 235–241. doi:10.1016/j.joca.2013.12.004.
[138] C. Chou, H. Wisniewski, P. Band, J. Huebner, T. Stabler, C. Lattermann, V.B. Kraus, TSG-6 activity reflects severity of inflammation in knee osteoarthritis and acute joint injury, Osteoarthr. Cartil. 24 (2016) S81–S82. doi:10.1016/j.joca.2016.01.174.
[139] T. Bárdos, R. V. Kamath, K. Mikecz, T.T. Glant, Anti-Inflammatory and chondroprotective effect of TSG-6 (Tumor Necrosis Factor-α-Stimulated Gene-6) in murine models of experimental arthritis, Am. J. Pathol. 159 (2001) 1711–1721. doi:10.1016/S0002-9440(10)63018-0.
[140] T.T. Glant, R. V. Kamath, T. Bárdos, I. Gál, S. Szántó, Y.M. Murad, J.D. Sandy, J.S. Mort, P.J. Roughley, K. Mikecz, Cartilage-specific constitutive expression of TSG-6 protein (product of tumor necrosis factor α-stimulated gene 6) provides a chondroprotective, but not antiinflammatory, effect in antigen-induced arthritis, Arthritis Rheum. 46 (2002) 2207–2218. doi:10.1002/art.10555.
[141] M.A. Ciccotti, M.C. Ciccotti, M.G. Ciccotti, A.J. Cosgarea, P.P. Castle, Rotator Cuff Injury, Orthop. Sport. Med. 2 (2005) 1–12.
[142] A.K. Saha, Dynamic Stability of the Glenohumeral Joint, Acta Orthop. 42 (1971)

491–505. doi:10.3109/17453677108989066.
[143] S.B. Lee, K.J. Kim, S.W. O'Driscoll, B.F. Morrey, K.N. An, Dynamic glenohumeral stability provided by the rotator cuff muscles in the mid-range and end-range of motion. A study in cadavera., J. Bone Joint Surg. Am. 82 (2000) 849–857. doi:10.1016/j.math.2007.07.002.
[144] G.A.C. Murrell, J.R. Walton, Diagnosis of rotator cuff tears, Lancet. 357 (2001) 769–770.
[145] A. Yamamoto, K. Takagishi, T. Osawa, Prevalence and risk factors of a rotator cuff tear in the general population, J. Shoulder Elb. Surg. 19 (2010) 116–120. doi:10.1016/j.jse.2009.04.006.
[146] L.S. Oh, B.R. Wolf, M.P. Hall, B.A. Levy, R.G. Marx, Indications for rotator cuff repair: a systematic review, Clin. Orthop. Relat. Res. 455 (2007) 52–63. doi:10.1097/BLO.0b013e31802fc175.
[147] L. Bryant, R. Shnier, C. Bryant, G.A.C. Murrell, A comparison of clinical estimation, ultrasonography, magnetic resonance imaging, and arthroscopy in determining the size of rotator cuff tears, J. Shoulder Elb. Surg. 11 (2002) 219–224. doi:10.1067/mse.2002.121923.
[148] C.S. Neer, E. V. Craig, H. Fukuda, Cuff-Tear Arthropathy, J. Bone Jt. Surg. 65 (1983) 1232–1244.
[149] C. Gerber, B. Fuchs, J. Hodler, The results of repair of massive tears of the rotator cuff., J. Bone Joint Surg. Am. 82 (2000) 505–515.
[150] J.N. Gladstone, J.Y. Bishop, I.K.Y. Lo, E.L. Flatow, Fatty infiltration and atrophy of the rotator cuff do not improve after rotator cuff repair and correlate with poor functional outcomes, Am. J. Sports Med. 35 (2007) 719–728. doi:10.1177/0363546506297539.
[151] M.D. Williams, A. Lädermann, B. Melis, R. Barthelemy, G. Walch, Fatty infiltration of the supraspinatus: A reliability study, J. Shoulder Elb. Surg. 18 (2009) 581–587. doi:10.1016/j.jse.2008.12.014.
[152] D. Laron, S.P. Samagh, X. Liu, H.T. Kim, B.T. Feeley, Muscle degeneration in rotator cuff tears, J. Shoulder Elb. Surg. 21 (2012) 164–174. doi:10.1016/j.jse.2011.09.027.
[153] C. Gerber, A.G. Schneeberger, H. Hoppeler, D.C. Meyer, Correlation of atrophy and fatty infiltration on strength and integrity of rotator cuff repairs : A study in thirteen patients, (2007) 691–696. doi:10.1016/j.jse.2007.02.122.
[154] A.R. Gillies, B.. Lieber, R.L. Lieber, Structure and Function of the Skeletal Muscle Extracellular Matrix, Muscle Nerve. 44 (2012) 318–331. doi:10.1002/mus.22094.Structure.
[155] A.C. Colvin, N. Egorova, A.K. Harrison, A. Moskowitz, E.L. Flatow, National trends in rotator cuff repair, J. Jt. Surg. Am. 94 (2012) 227–233.
[156] X. Liu, A.Y. Ning, N.C. Chang, H. Kim, R. Nissenson, L. Wang, B.T. Feeley, Investigating the cellular origin of rotator cuff muscle fatty infiltration and fibrosis after injury, Muscle, Ligaments, Tendon J. 6 (2016) 6–15.
[157] M.L. Mcmaster, S.Y. Kristinsson, I. Turesson, M. Bjorkholm, O. Landgren, Inhibition of 5-LOX, COX-1, and COX-2 Increases Tendon Healing and Reduces Muscle Fibrosis and Lipid Accumulation After Rotator Cuff Repair, Clin. Lymphoma. 9 (2010) 19–22. doi:10.3816/CLM.2009.n.003.Novel.

[158] M.E. Davis, M.A. Korn, J.P. Gumucio, J.A. Harning, A.L. Saripalli, A. Bedi, C.L. Mendias, Simvastatin reduces fibrosis and protects against muscle weakness after massive rotator cuff tear, J. Shoulder Elb. Surg. 24 (2017) 280–287. doi:10.1016/j.jse.2014.06.048.
[159] C.L. Mendias, S.M. Roche, J.A. Harning, M.E. Davis, E.B. Lynch, E.R.S. Enselman, J.A. Jacobson, D.R. Claflin, S. Calve, A. Bedi, Reduced muscle fiber force production and disrupted myofibril architecture in patients with chronic rotator cuff tears, J. Shoulder Elb. Surg. 24 (2015) 111–119. doi:10.1016/j.jse.2014.06.037.
[160] E. Maman, C. Harris, L. White, G. Tomlinson, M. Shashank, E. Boynton, Outcome of Nonoperative Treatment of Symptomatic Rotator Cuff Tears Monitored by Magnetic Resonance Imaging, J. Bone Jt. Surg. (2009). doi:10.2106/JBJS.G.01335.
[161] C.J. Fu, J.B. Sun, Z.G. Bi, X.M. Wang, C.L. Yang, Evaluation of platelet-rich plasma and fibrin matrix to assist in healing and repair of rotator cuff injuries: A systematic review and meta-analysis, Clin. Rehabil. 31 (2017) 158–172. doi:10.1177/0269215516634815.
[162] B.Y.H. Ellman, G. Hanker, M. Bayer, Repair of the Rotator Cuff, J. Bone Jt. Surg. - Br. Vol. 68A (1986) 1136–1144.
[163] A.H. Lebaschi, X.-H. Deng, C.L. Camp, J. Zong, G.-T. Cong, C.B. Carballo, Z. Album, S.A. Rodeo, Biomechanical, histologic, and molecular evaluation of tendon healing in a new murine model of rotator cuff repair, Arthrosc. Assoc. North Am. (2017).
[164] A. De Carli, M. Fabbri, R.M. Lanzetti, A. Ciompi, E. Gaj, G. Beccarini, M. Vetrano, A. Ferretti, Functional treatment in rotator cuff tears: Is it safe and effective? a retrospective comparison with surgical treatment, Muscles. Ligaments Tendons J. 7 (2017) 40–45. doi:10.11138/mltj/2017.7.1.040.
[165] T.J. Matthews, G.C. Hand, J.L. Rees, N.A. Athanasou, A.J. Carr, Pathology of the torn rotator cuff tendon: Reduction in Potential for Repair as Tear Size Increase, J. Bone Jt. Surg. - Br. Vol. 88–B (2006) 489–495. doi:10.1302/0301-620X.88B4.16845.
[166] J.P. Iannotti, M.P. Bernot, J.R. Kuhlman, M.J. Kelley, G.R. Williams, Postoperative assessment of shoulder function: a prospective study of full-thickness rotator cuff tears., J. Shoulder Elbow Surg. 5 (1996) 449–57. doi:10.1016/S1058-2746(96)80017-6.
[167] B.B. Rothrauff, T. Pauyo, R.E. Debski, M.W. Rodosky, R. Tuan, V. Musahl, The Rotator Cuff Organ: Integrating Developmental Biology, Tissue Engineering, and Surgical Considerations to Treat Chronic Massive Rotator Cuff Tears, Tissue Eng. Part B Rev. (2017) doi:10.1089/ten.TEB.2016.0446.
[168] L.M. Galatz, G.M. Ball, S.A. Teefey, W.D. Middleton, K. Yamaguchi, The Outcome and Repair Integrity of Completely Arthroscopically Repaired Large and Massive Rotator Cuff Tears, J. Bone Jt. Surg. (2004).
[169] C. Latte, M. Salvatore, P. Avanzi, A. Grasso, Treatment options for irreparable rotator cuff tears, in: Shoulder Arthrosc. Princ. Pract., 2013.
[170] L. Soslowsky, J.E. Carpenter, C.M. DeBano, I. Banerji, M.R. Moalli, Development and use of an animal model for investigations on rotator cuff disease,

J. Shoulder Elb. Surg. (1996) 383–392.
[171] J.A. Gimbel, J.P. Van Kleunen, S. Mehta, S.M. Perry, G.R. Williams, L.J. Soslowsky, Supraspinatus tendon organizational and mechanical properties in a chronic rotator cuff tear animal model, J. Biomech. 37 (2004) 739–749. doi:10.1016/j.jbiomech.2003.09.019.
[172] E.J. Kramer, B.M. Bodendorfer, D. Laron, J. Wong, H.T. Kim, X. Liu, B.T. Feeley, Evaluation of cartilage degeneration in a rat model of rotator cuff tear arthropathy, J. Shoulder Elb. Surg. 22 (2013) 1702–1709. doi:10.1016/j.jse.2013.03.014.
[173] M.R. Davies, B. Ravishankar, D. Laron, H.T. Kim, X. Liu, B.T. Feeley, Rat rotator cuff muscle responds differently from hindlimb muscle to a combined tendon-nerve injury, J. Orthop. Res. 33 (2015) 1046–1053. doi:10.1002/jor.22864.
[174] M.R. Davies, S. Garcia, S. Tamaki, X. Liu, S. Lee, A. Jose, J.H. Pomerantz, B.T. Feeley, Muscle Stem Cell Activation in a Mouse Model of Rotator Cuff Injury, J. Orthop. Res. (2017) 1–7. doi:10.1002/jor.23679.
[175] J. Gumucio, M. Flood, J. Harning, A. Phan, S. Roche, E. Lynch, A. Bedi, C. Mendias, T lymphocytes are not required for the development of fatty degeneration after rotator cuff tear., Bone Joint Res. 3 (2014) 262–72. doi:10.1302/2046-3758.39.2000294.
[176] J.P. Gumucio, M.E. Davis, J.R. Bradley, P.L. Stafford, C.J. Schiffman, E.B. Lynch, D.R. Claflin, A. Bedi, C.L. Mendias, Rotator cuff tear reduces muscle fiber specific force production and induces macrophage accumulation and autophagy, J. Orthop. Res. (2012) 1963–1970. doi:10.1002/jor.22168.
[177] X. Liu, G. Manzano, H.T. Kim, B.T. Feeley, A Rat Model of Massive Rotator Cuff Tears, J. Orthop. Res. (2011) 588–595. doi:10.1002/jor.21266.
[178] J.P. Gumucio, M.D. Flood, A. Bedi, H.F. Kramer, A.J. Russell, C.L. Mendias, Inhibition of prolyl 4-hydroxylase decreases muscle fibrosis following chronic rotator cuff tear, Bone Jt. Res. 6 (2017) 57–65. doi:10.1302/2046-3758.61.BJR-2016-0232.R1.
[179] M.E. Davis, P.L. Stafford, M.J. Jergenson, A. Bedi, C.L. Mendias, Muscle Fibers are Injured at the Time of Acute and Chronic Rotator Cuff Repair, Clin. Orthop. Relat. Res. 473 (2015) 226–232. doi:10.1007/s11999-014-3860-y.
[180] M.R. Davies, L. Lee, B.T. Feeley, H.T. Kim, X. Liu, Lysophosphatidic acid-induced RhoA signaling and prolonged macrophage infiltration worsens fibrosis and fatty infiltration following rotator cuff tears., J. Orthop. Res. (2016) 1–9. doi:10.1002/jor.23384.
[181] S.K. Joshi, X. Liu, S.P. Samagh, D.H. Lovett, S.C. Bodine, H.T. Kim, B.T. Feeley, mTOR Regulates Fatty Infiltration through SREBP-1 and PPAR g after a Combined Massive Rotator Cuff Tear and Suprascapular Nerve Injury in Rats, (2013) 724–730. doi:10.1002/jor.22254.
[182] X. Liu, S.K. Joshi, B. Ravishankar, D. Laron, H.T. Kim, B.T. Feeley, Upregulation of transforming growth factor-β signaling in a rat model of rotator cuff tears., J. Shoulder Elb. Surg. 23 (2014) 1709–16. doi:10.1016/j.jse.2014.02.029.
[183] N. Ochiai, E. Hashimoto, Y. Sasaki, K. Akimoto, H. Sugaya, N. Takahashi, K. Matsuki, Prevalence of concomitant neuropathy in large to massive rotator cuff tear using needle electromyography, J. Shoulder Elb. Surg. 26 (1826) e111.

doi:10.1016/j.jse.2016.11.023.
[184] W.J. Mallon, R.J. Wilson, C.J. Basamania, The association of suprascapular neuropathy with massive rotator cuff tears : A preliminary report, (2006) 395–398. doi:10.1016/j.jse.2005.10.019.
[185] L. V Gulotta, D. Kovacevic, J.R. Ehteshami, E. Dagher, J.D. Packer, S. a Rodeo, Application of bone marrow-derived mesenchymal stem cells in a rotator cuff repair model., Am. J. Sports Med. 37 (2009) 2126–33. doi:10.1177/0363546509339582.
[186] A. Bedi, A.J.S. Fox, D. Kovacevic, X. -h. Deng, R.F. Warren, S.A. Rodeo, Doxycycline-Mediated Inhibition of Matrix Metalloproteinases Improves Healing After Rotator Cuff Repair, Am. J. Sports Med. 38 (2010) 308–317. doi:10.1177/0363546509347366.
[187] D. Kovacevic, A.J. Fox, A. Bedi, L. Ying, X. Deng, R.F. Warren, S. a Rodeo, Calcium-Phosphate Matrix With or Without TGF- b 3 Improves Tendon-Bone Healing After Rotator Cuff Repair, (2011) 811–819. doi:10.1177/0363546511399378.
[188] C.K. Hee, J.S. Dines, D.M. Dines, C.M. Roden, L.A. Wisner-lynch, A.S. Turner, D. Acvs, K.C. Mcgilvray, A.S. Lyons, C.M. Puttlitz, B.G. Santoni, Augmentation of a Rotator Cuff Suture Repair Using rhPDGF-BB and a Type I Bovine Collagen Matrix in an Ovine Model, 39 (2011) 1630–1639. doi:10.1177/0363546511404942.
[189] C. Uggen, J. Dines, M. Mcgarry, D. Grande, D. Ph, T. Lee, D. Ph, O. Limpisvasti, The Effect of Recombinant Human Platelet-Derived Growth Factor, YJARS. 26 (2010) 1456–1462. doi:10.1016/j.arthro.2010.02.025.
[190] T. Tokunaga, T. Karasugi, H. Arimura, R. Yonemitsu, H. Sakamoto, J. Ide, H. Mizuta, Enhancement of rotator cuff tendon–bone healing with fibroblast growth factor 2 impregnated in gelatin hydrogel sheets in a rabbit model, J. Shoulder Elb. Surg. 26 (2017) 1708–1717. doi:10.1016/j.jse.2017.03.020.
[191] N.R. Oak, J.P. Gumucio, M.D. Flood, A.L. Saripalli, M.E. Davis, J.A. Harning, E.B. Lynch, S.M. Roche, A. Bedi, C.L. Mendias, Increases Tendon Healing and Reduces Muscle Fibrosis and Lipid Accumulation After Rotator Cuff Repair, Am. J. Sports Med. 42 (2014) 2860–2868. doi:10.1177/0363546514549943.
[192] S.A. Shah, I. Kormpakis, N. Havlioglu, M.S. Ominsky, L.M. Galatz, S. Thomopoulos, Sclerostin antibody treatment enhances rotator cuff tendon-to-bone healing in an animal model, J. Bone Jt. Surg. - Am. Vol. 99 (2017) 855–864. doi:10.2106/JBJS.16.01019.
[193] A. Prabhath, V.N. Vernekar, E. Sanchez, C.T. Laurencin, Growth factor delivery strategies for rotator cuff repair and regeneration, Int. J. Pharm. (2018). doi:10.1016/j.ijpharm.2018.01.006.
[194] N.A. Friel, A.G. McNickle, M.J. DeFranco, F. Wang, E.F. Shewman, N.N. Verma, B.J. Cole, B.R. Bach, S. Chubinskaya, S.M. Kramer, V.M. Wang, Effect of highly purified capsaicin on articular cartilage and rotator cuff tendon healing: An in vivo rabbit study., J. Orthop. Res. 4975 (2015) 1854–1860. doi:10.1002/jor.22971.
[195] A. J Quintero, V. J Wright, F. H Fu, J. Huard, Stem Cells for the Treatment of Skeletal Muscle Injury, Clin Sport. Med. 28 (2010) 1–11. doi:10.1016/j.csm.2008.08.009.Stem.

[196] M. Dezawa, H. Ishikawa, Y. Itokazu, T. Yoshihara, M. Hoshino, S. Takeda, C. Ide, Y. Nabeshima, Bone marrow stromal cells generate muscle cells and repair muscle degeneraiton, Science. 309 (2005) 314–317. doi:10.1126/science.1110364.
[197] C. De Bari, F. Dell'Accio, F. Vandenabeele, J.R. Vermeesch, J.M. Raymackers, F.P. Luyten, Skeletal muscle repair by adult human mesenchymal stem cells from synovial membrane, J. Cell Biol. 160 (2003) 909–918. doi:10.1083/jcb.200212064.
[198] R. Darabi, K. Gehlbach, R.M. Bachoo, S. Kamath, M. Osawa, K.E. Kamm, M. Kyba, R.C.R. Perlingeiro, Functional skeletal muscle regeneration from differentiating embryonic stem cells, Nat. Med. 14 (2008) 134–143. doi:10.1038/nm1705.
[199] H. Peng, J. Huard, Muscle-derived stem cells for musculoskeletal tissue regeneration and repair, Transpl. Immunol. 12 (2004) 311–319. doi:10.1016/j.trim.2003.12.009.
[200] D. Montarras, J. Morgan, C. Collins, Direct Isolation of Satellite Cells for Skeletal Muscle Regeneration, 309 (2005) 2064–2067.
[201] J. Huegel, D.H. Kim, J.M. Cirone, A.M. Pardes, T.R. Morris, C.A. Nuss, R.L. Mauck, L.J. Soslowsky, A.F. Kuntz, Autologous Tendon-Derived Cell-Seeded Nanofibrous Scaffolds Improve Rotator Cuff Repair in an Age-Dependent Fashion, J. Orthop. Res. (2016) 1–8. doi:10.1002/jor.23381.
[202] M.D. Kwan, B.J. Slater, D.C. Wan, M.T. Longaker, Cell-based therapies for skeletal regenerative medicine, Hum. Mol. Genet. 17 (2008) 93–98. doi:10.1093/hmg/ddn071.
[203] J. Huard, Y. Li, F.H. Fu, Muscle injuries and repair: current trends in research., J. Bone Joint Surg. Am. 84–A (2002) 822–832.
[204] J. Menetrey, C. Kasemkijwattana, C.S. Day, P. Bosch, M. Vogt, F.H. Fu, M.S. Moreland, J. Huard, Growth factors improve muscle healing in vivo, J. Bone Jt. Surg. - Ser. B. 82 (2000) 131–137. doi:10.1302/0301-620X.82B1.8954.
[205] B.T. Corona, X. Wu, C.L. Ward, J.S. McDaniel, C.R. Rathbone, T.J. Walters, The promotion of a functional fibrosis in skeletal muscle with volumetric muscle loss injury following the transplantation of muscle-ECM, Biomaterials. 34 (2013) 3324–3335. doi:10.1016/j.biomaterials.2013.01.061.
[206] B.T. Corona, M.A. Machingal, T. Criswell, M. Vadhavkar, A.C. Dannahower, C. Bergman, W. Zhao, G.J. Christ, Further Development of a Tissue Engineered Muscle Repair Construct *In Vitro* for Enhanced Functional Recovery Following Implantation *In Vivo* in a Murine Model of Volumetric Muscle Loss Injury, Tissue Eng. Part A. 18 (2012) 1213–1228. doi:10.1089/ten.tea.2011.0614.
[207] B.M. Sicari, V. Agrawal, B.F. Siu, C.J. Medberry, C.L. Dearth, N.J. Turner, S.F. Badylak, A Murine Model of Volumetric Muscle Loss and a Regenerative Medicine Approach for Tissue Replacement, Tissue Eng. Part A. 18 (2012) 1941–1948. doi:10.1089/ten.tea.2012.0475.
[208] M.T.A. Li, N.J. Willett, B.A. Uhrig, R.E. Guldberg, G.L. Warren, Functional Analysis of Limb Recovery following Autograft Treatment of Volumetric Muscle Loss in the Quadriceps Femoris, J. Biomech. 47 (2014). doi:10.1038/nature13314.A.
[209] A. Aurora, J.L. Roe, B.T. Corona, T.J. Walters, An acellular biologic scaffold does

not regenerate appreciable de novo muscle tissue in rat models of volumetric muscle loss injury, Biomaterials. 67 (2015) 393–407. doi:10.1016/j.biomaterials.2015.07.040.
[210] M. Pilia, T. McDaiel, J. S.Guda, X.K. Chen, R.P. Rhodas, R.E. Allen, B.T. Coroa, C.R. Rathbone, Transplantation and perfusion of microvascular fragments in a rodent model of volumentric muscle loss injury, Eur. Cells Mater. 28 (2014) 11–24. doi:10.22203/eCM.v028a02.
[211] K. Garg, B.T. Corona, T.J. Walters, Losartan administration reduces fibrosis but hinders functional recovery after volumetric muscle loss injury, J Appl Physiol. 117 (2014) 1120–1131. doi:DOI 10.1152/japplphysiol.00689.2014.
[212] J.M. Grasman, D.M. Do, R.L. Page, G.D. Pins, Rapid release of growth factors regenerates force output in volumetric muscle loss injuries, Biomaterials. 2 (2015) 147–185. doi:10.1515/jci-2013-0007.Targeted.
[213] N. Arsic, S. Zacchigna, L. Zentilin, G. Ramirez-Correa, L. Pattarini, A. Salvi, G. Sinagra, M. Giacca, Vascular endothelial growth factor stimulates skeletal muscle regeneration in Vivo, Mol. Ther. 10 (2004) 844–854. doi:10.1016/j.ymthe.2004.08.007.
[214] C. Borselli, H. Storrie, F. Benesch-Lee, D. Shvartsman, C. Cezar, J.W. Lichtman, H.H. Vandenburgh, D.J. Mooney, Functional muscle regeneration with combined delivery of angiogenesis and myogenesis factors, Proc. Natl. Acad. Sci. U S A. 107 (2010) 3287–3292. doi:10.1073/pnas.0903875106.
[215] J. Doukas, K. Blease, D. Craig, C. Ma, L.A. Chandler, B.A. Sosnowski, G.F. Pierce, Delivery of FGF genes to wound repair cells enhances arteriogenesis and myogenesis in skeletal muscle, Mol. Ther. 5 (2002) 517–527. doi:10.1006/mthe.2002.0579.
[216] Y. Jeong, H. Kyu, H. Hwa, Y. Chan, Direct Comparison of Human Mesenchymal Stem Cells Derived from Adipose Tissues and Bone Marrow in Mediating Neovascularization in Response to Vascular Ischemia, Cell. Physiol. Biochem. 20 (2007) 867–876.
[217] M.H. Moon, S.Y. Kim, Y.J. Kim, S.J. Kim, J.B. Lee, Y.C. Bae, S.M. Sung, J.S. Jung, Human adipose tissue-derived mesenchymal stem cells improve postnatal neovascularization in a mouse model of hindlimb ischemia, Cell. Physiol. Biochem. 17 (2006) 279–290.
[218] M.R. Davies, X. Liu, L. Lee, D. Laron, A.Y. Ning, H.T. Kim, B.T. Feeley, TGF-β Small Molecule Inhibitor SB431542 Reduces Rotator Cuff Muscle Fibrosis and Fatty Infiltration By Promoting Fibro/ Adipogenic Progenitor Apoptosis, PLoS One. (2016). doi:10.1371/journal.pone.0155486.
[219] M. D'Apuzzo, A. Rolink, M. Loetscher, J.A. Hoxie, I. Clark-lewis, F. Melchers, M. Baggiolini, B. Moser, The chemokine SDF-1 , stromal cell-derived factor 1 , attracts early stage B cell precursors via the chemokine receptor CXCR4, Eur. J. Immunol. 27 (1997) 1788–1793.
[220] I. Petit, T. Ponomaryov, D. Zipori, L. Tsvee, G-CSF induces stem cell mobilization by decreasing bone marrow SDF-1 and up-regulating CXCR4, Nat. Immunol. 3 (2002) 687–694. doi:10.1038/ni813.
[221] L.J. Bendall, K.F. Bradstock, G-CSF : From granulopoietic stimulant to bone marrow stem cell mobilizing agent, Cytokine Growth Factor Rev. 25 (2014) 355–

367. doi:10.1016/j.cytogfr.2014.07.011.
[222] T. Liu, X. Li, S. You, S.S. Bhuyan, L. Dong, Effectiveness of AMD3100 in treatment of leukemia and solid tumors: From original discovery to use in current clinical practice, Exp. Hematol. Oncol. 5 (2016) 1–11. doi:10.1186/s40164-016-0050-5.
[223] I.G. Winkler, A.R. Pettit, L.J. Raggatt, R.N. Jacobsen, C.E. Forristal, V. Barbier, B. Nowlan, A. Cisterne, L.J. Bendall, N.A. Sims, J.P. Lévesque, Hematopoietic stem cell mobilizing agents G-CSF, cyclophosphamide or AMD3100 have distinct mechanisms of action on bone marrow HSC niches and bone formation, Leukemia. 26 (2012) 1594–1601. doi:10.1038/leu.2012.17.
[224] M. Tamura, K. Hattori, H. Nomura, M. Oheda, N. Kubota, I. Imazeki, Induction of neutrophilic granulocytosis in mice by administration of purified human native granulocyte colony-stimulating factor (G-CSF), Biochem Biophys Res Commun. 142 (1987) 454–460.
[225] V.K. Singh, P.K. Singh, S.Y. Wise, T.M. Seed, Mobilized progenitor cells as a bridging therapy for radiation casualties: A brief review of tocopherol succinate-based approaches, Int. Immunopharmacol. 11 (2011) 839–844. doi:10.1016/j.intimp.2011.01.017.
[226] W.S. Chew, W. Wang, D.R. Herr, To fingolimod and beyond : The rich pipeline of drug candidates that target S1P signaling, Pharmacol. Res. 113 (2016) 521–532. doi:10.1016/j.phrs.2016.09.025.
[227] A. Olivera, S. Spiegel, Sphingosine-1-phosphate as second messenger in cell proliferation induced by PDGF and FCS mitogens., Nat. Lett. 365 (1993) 557–60. doi:10.1038/365557a0.
[228] V. Brinkmann, D. Pinschewer, K. Chiba, L. Feng, FTY720: A novel transplantation drug that modulates lymphocyte traffic rather than activation, Trends Pharmacol. Sci. 21 (2000) 49–52. doi:10.1016/S0165-6147(99)01419-4.
[229] S. Pyne, N.J. Pyne, Translational aspects of sphingosine 1-phosphate biology, Trends Mol. Med. 17 (2011) 463–472. doi:10.1016/j.molmed.2011.03.002.
[230] M. Matloubian, C.G. Lo, G. Cinamon, M.J. Lesneski, Y. Xu, V. Brinkmann, M.L. Allende, R.L. Proia, J.G. Cyster, Lymphocyte egress from thymus and peripheral lymphoid organs is dependent on S1P receptor 1, Nature. 427 (2004) 355–360. doi:10.1038/nature02284.
[231] R. Zhu, A.H. Snyder, Y. Kharel, L. Schaffter, Q. Sun, P.C. Kennedy, K.R. Lynch, T.L. Macdonald, Asymmetric synthesis of conformationally constrained Fingolimod analogues - Discovery of an orally active sphingosine 1-phosphate receptor type-1 agonist and receptor type-3 antagonist, J. Med. Chem. 50 (2007) 6428–6435. doi:10.1021/jm7010172.
[232] J.M. Selma, A. Das, A.O. Awojoodu, T. Wang, A.P. Kaushik, Q. Cui, H. Song, M.E. Ogle, C.E. Olingy, E.G. Pendleton, K.F. Tehrani, L.J. Mortensen, E.A. Botchwey, Novel Lipid Signaling Mediators for Mesenchymal Stem Cell Mobilization During Bone Repair, Cell. Mol. Bioeng. (2018). doi:10.1007/s12195-018-0532-0.
[233] W.F. McKay, S.M. Peckham, J.M. Badura, A comprehensive clinical review of recombinant human bone morphogenetic protein-2 (INFUSE Bone Graft)., Int. Orthop. 31 (2007) 729–34. doi:10.1007/s00264-007-0418-6.

[234] S.W. Kang, J.S. Kim, K.S. Park, B.H. Cha, J.H. Shim, J.Y. Kim, D.W. Cho, J.W. Rhie, S.H. Lee, Surface modification with fibrin/hyaluronic acid hydrogel on solid-free form-based scaffolds followed by BMP-2 loading to enhance bone regeneration, Bone. 48 (2011) 298–306. doi:10.1016/j.bone.2010.09.029.
[235] L. Tao, J. Liu, J. Xu, T.P. Davis, Synthesis and bioactivity of poly(HPMA)-lysozyme conjugates: the use of novel thiazolidine-2-thione coupling chemistry., Org. Biomol. Chem. 7 (2009) 3481–3485. doi:10.1039/b907061c.
[236] J.R. Lieberman, A. Daluski, T.A. Einhorn, The role of growth factors in the repair of bone, J. Bone Jt. Surg. (2002) 1032–1044.
[237] M.F. Sciadini, K.D. Johnson, Evaluation of Recombinant Human Bone Morphogenetic Protein-2 as a Bone-Graft Substitute in a Canine Segmental Defect Model, J. Orthop. Res. (2000) 289–302.
[238] I.H. Bae, B.C. Jeong, M.S. Kook, S.H. Kim, J.T. Koh, Evaluation of a thiolated chitosan scaffold for local delivery of bmp-2 for osteogenic differentiation and ectopic bone formation, Biomed Res. Int. 2013 (2013). doi:10.1155/2013/878930.
[239] Z.S. Patel, M. Yamamoto, H. Ueda, Y. Tabata, A.G. Mikos, Biodegradable gelatin microparticles as delivery systems for the controlled release of bone morphogenetic protein-2, Acta Biomater. 4 (2008) 1126–1138. doi:10.1016/j.actbio.2008.04.002.
[240] F. Wehrhan, K. Amann, A. Molenberg, R. Lutz, F.W. Neukam, K. a. Schlegel, PEG matrix enables cell-mediated local BMP-2 gene delivery and increased bone formation in a porcine critical size defect model of craniofacial bone regeneration, Clin. Oral Implants Res. 23 (2012) 805–813. doi:10.1111/j.1600-0501.2011.02223.x.
[241] Y. Tabata, M. Yamamoto, Y. Ikada, Comparison of Release Profiles of Various Growth Factors from Biodegradable Carriers, 530 (1998) 13–18.
[242] O. Jeon, S.J. Song, S.W. Kang, A.J. Putnam, B.S. Kim, Enhancement of ectopic bone formation by bone morphogenetic protein-2 released from a heparin-conjugated poly(l-lactic-co-glycolic acid) scaffold, Biomaterials. 28 (2007) 2763–2771. doi:10.1016/j.biomaterials.2007.02.023.
[243] S.W. Kang, W.G. La, J.M. Kang, J.H. Park, B.S. Kim, Bone morphogenetic protein-2 enhances bone regeneration mediated by transplantation of osteogenically undifferentiated bone marrow-derived mesenchymal stem cells, Biotechnol. Lett. 30 (2008) 1163–1168. doi:10.1007/s10529-008-9675-8.
[244] H.S. Yang, W.-G. La, S.H. Bhang, J.-Y. Jeon, J.H. Lee, B.-S. Kim, Heparin-Conjugated Fibrin as an Injectable System, Tissue Eng. Part A. 16 (2010) 1–10.
[245] G. Bhakta, B. Rai, Z.X.H. Lim, J.H. Hui, G.S. Stein, A.J. van Wijnen, V. Nurcombe, G.D. Prestwich, S.M. Cool, Hyaluronic acid-based hydrogels functionalized with heparin that support controlled release of bioactive BMP-2, Biomaterials. 33 (2012) 6113–6122. doi:10.1016/j.biomaterials.2012.05.030.
[246] M. Yamamoto, Y. Ikada, Y. Tabata, Controlled release of growth factors based on biodegradation of gelatin hydrogel., J. Biomater. Sci. Polym. Ed. 12 (2001) 77–88. doi:10.1163/156856201744461.
[247] H. Baumann, H. Scheen, B. Huppertz, R. Keller, Novel regio- and stereoselective O-6-desulfation of the glucosamine moiety of heparin with N-methylpyrrolidinone-water or N,N-dimethylformamide-water mixtures,

Carbohydr. Res. 308 (1998) 381–388. doi:10.1016/S0008-6215(98)00097-4.
[248] H. Habuchi, O. Habuchi, K. Kimata, Sulfation pattern in glycosaminoglycan: Does it have a code?, Glycoconj. J. 21 (2004) 47–52. doi:10.1023/B:GLYC.0000043747.87325.5e.
[249] G.S. Schultz, A. Wysocki, Interactions between extracellular matrix and growth factors in wound healing, Wound Repair Regen. 17 (2009) 153–162. doi:10.1111/j.1524-475X.2009.00466.x.
[250] S.E. Kim, J.H. Park, Y.W. Cho, H. Chung, S.Y. Jeong, E.B. Lee, I.C. Kwon, Porous chitosan scaffold containing microspheres loaded with transforming growth factor-β1: Implications for cartilage tissue engineering, J. Control. Release. 91 (2003) 365–374. doi:10.1016/S0168-3659(03)00274-8.
[251] J. Zhao, C. Luo, Y. Chen, D. Wu, C. Shen, W. Han, M. Tu, R. Zeng, Preparation, structure and BMP-2 controlled release of heparin-conjugated hyaluronan microgels, Carbohydr. Polym. 86 (2011) 806–811. doi:10.1016/j.carbpol.2011.05.026.
[252] S.A. Abbah, J. Liu, J.C.H. Goh, H.K. Wong, Enhanced control of in vivo bone formation with surface functionalized alginate microbeads incorporating heparin and rhBMP-2, Tissue Eng. Part A. 19 (2012) 120815214523006. doi:10.1089/ten.TEA.2012.0274.
[253] M. Bar-Ner, E. Amiram, L. Wasserman, Y. Matzner, I.R. Cohen, Z. Fuks, I. Vlodavsky, Inhibition of Heparanase-Mediated Degradation of Extracellular Matrix Heparan Sulfate by Non-anticoagulant Heparin Species, Blood. 70 (1987) 551–557.
[254] Y. Inoue, K. Nagasawa, Selective N-desulfation of heparin with dimethyl sulfoxide containing water or methanol., Carbohydr. Res. 46 (1976) 87–95. doi:10.1016/S0008-6215(00)83533-8.
[255] K. Nagasawa, Y. Inoue, T. Kamata, Solvolytic desulfation of glycosaminoglycuronan sulfates with dimethyl sulfoxide containing water or methanol, Carbohydr. Res. 58 (1977) 47–55.
[256] J.S. McGonigle, G. Tae, P.S. Stayton, A.S. Hoffman, M. Scatena, Heparin-regulated delivery of osteoprotegerin promotes vascularization of implanted hydrogels., J. Biomater. Sci. Polym. Ed. 19 (2008) 1021–1034. doi:10.1163/156856208784909381.
[257] M.S. Hahn, L.J. Taite, J.J. Moon, M.C. Rowland, K.A. Ruffino, J.L. West, Photolithographic patterning of polyethylene glycol hydrogels, Biomaterials. 27 (2006) 2519–2524. doi:10.1016/j.biomaterials.2005.11.045.
[258] T. Katagiri, A. Yamaguchi, M. Komaki, E. Abe, N. Takahashi, T. Ikeda, V. Rosen, J.M. Wozney, A. Fujisawa-Sehara, T. Suda, Bone morphogenetic protein-2 converts the differentiation pathway of C2C12 myoblasts into the osteoblast lineage, J. Cell Biol. 127 (1994) 1755–1766. doi:10.1083/jcb.127.6.1755.
[259] S. Zalipsky, Functionalized Poly(Ethylene Glycols) for Preparation of Biologically Relevant Conjugates, Bioconjug. Chem. 6 (1995) 150–165. doi:10.1021/bc00032a002.
[260] M. Roman, W.T. Winter, Effect of sulfate groups from sulfuric acid hydrolysis on the thermal degradation behavior of bacterial cellulose, Biomacromolecules. 5 (2004) 1671–1677. doi:10.1021/bm034519+.

[261] L.E. Tellier, E.A. Trevino, A.L. Brimeyer, D.R. Reece, N.J. Willett, R.E. Guldberg, J.S. Temenoff, Intra-Articular TSG-6 Delivery from Heparin-based Microparticles Reduces Cartilage Damage in a Rat Model of Osteoarthritis, Biomater. Sci. (2018).
[262] L. Baumann, S. Prokoph, C. Gabriel, U. Freudenberg, C. Werner, A.G. Beck-Sickinger, A novel, biased-like SDF-1 derivative acts synergistically with starPEG-based heparin hydrogels and improves eEPC migration in vitro, J. Control. Release. 162 (2012) 68–75. doi:10.1016/j.jconrel.2012.04.049.
[263] S. Nakamura, M. Ishihara, K. Obara, K. Masuoka, T. Ishizuka, Y. Kanatani, B. Takase, T. Matsui, H. Hattori, T. Sato, Hidemi Hattori, T. Sato, Y. Kariya, T. Maehara, Controlled release of fibroblast growth factor-2 from an injectable 6-O-desulfated heparin hydrogel and subsequent effect on in vivo vascularization, J. Biomed. Mater. Res. A. 81 (2006) 364–371. doi:10.1002/jbm.a.
[264] S. Cai, Y. Liu, X. Zheng Shu, G.D. Prestwich, Injectable glycosaminoglycan hydrogels for controlled release of human basic fibroblast growth factor., Biomaterials. 26 (2005) 6054–67. doi:10.1016/j.biomaterials.2005.03.012.
[265] M.D. Wood, G.H. Borschel, S.E. Sakiyama-elbert, Controlled release of glial-derived neurotrophic factor from fibrin matrices containing an affinity-based delivery system, J. Biomed. Mater. Res. Part A. (2008) 909–918. doi:10.1002/jbm.a.32043.
[266] L.E. Tellier, J.R. Krieger, A.L. Brimeyer, A.C. Coogan, A.A. Falis, T.E. Rinker, A. Schudel, S.N. Thomas, C.D. Jarrett, N.J. Willett, E.A. Botchwey, J.S. Temenoff, Localized SDF-1 delivery increases pro-healing bone marrow-derived cells in the supraspinatus muscle following severe rotator cuff injury, Regen. Eng. Transl. Med. (2018).
[267] A.W. Palmer, R.E. Guldberg, M.E. Levenston, Analysis of cartilage matrix fixed charge density and three-dimensional morphology via contrast-enhanced microcomputed tomography., Proc. Natl. Acad. Sci. U. S. A. 103 (2006) 19255–60. doi:10.1073/pnas.0606406103.
[268] M.B. Goldring, Chondrogenesis, chondrocyte differentiation, and articular cartilage metabolism in health and osteoarthritis., Ther. Adv. Musculoskelet. Dis. 4 (2012) 269–85. doi:10.1177/1759720X12448454.
[269] T. V Cao, M. La, S.J. Getting, A.J. Day, M. Perretti, Inhibitory effect of TSG-6 link module on leukocyte-endothelial cell interactions in vitro and in vio, Microcirculation. (2004) 615–624. doi:10.1080/10739680490503438.
[270] T. Nie, A. Baldwin, N. Yamaguchi, K.L. Kiick, Production of heparin-functionalized hydrogels for the development of responsive and controlled growth factor delivery systems, J. Control. Release. 122 (2007) 287–296. doi:10.1016/j.jconrel.2007.04.019.Production.
[271] H. Choi, R.H. Lee, N. Bazhanov, J.Y. Oh, D.J. Prockop, Anti-inflammatory protein TSG-6 secreted by activated MSCs attenuates zymosan-induced mouse peritonitis by decreasing TLR2 / NF-kB signaling in resident macrophages, Immunobiology. 118 (2016) 330–339. doi:10.1182/blood-2010-12-327353.
[272] N. Wang, Q. Li, L. Zhang, H. Lin, J. Hu, D. Li, S. Shi, S. Cui, J. Zhou, J. Ji, J. Wan, G. Cai, X. Chen, Mesenchymal stem cells attenuate peritoneal injury through secretion of TSG-6, PLoS One. 7 (2012). doi:10.1371/journal.pone.0043768.

[273] S. Torihashi, M. Ho, Y. Kawakubo, K. Komatsu, M. Nagai, Y. Hirayama, Y. Kawabata, N. Takenaka-Ninagawa, O. Wanachewin, L. Zhuo, K. Kimata, Acute and temporal expression of tumor necrosis factor-alpha-stimulated gene 6 product, TSG-6, in mesenchymal stem cells creates microenvironment required for their successful transplantation into muscle tissue, J. Biol. Chem. 290 (2015) 22771–22781. doi:10.1074/jbc.M114.629774.

[274] L.S. Sefcik, C.E. Petrie Aronin, A.O. Awojoodu, S.J. Shin, F. Mac Gabhann, T.L. MacDonald, B.R. Wamhoff, K.R. Lynch, S.M. Peirce, E.A. Botchwey, Selective Activation of Sphingosine 1-Phosphate Receptors 1 and 3 Promotes Local Microvascular Network Growth, Tissue Eng. Part A. 17 (2011) 617–629. doi:10.1089/ten.tea.2010.0404.

[275] J.R. Krieger, L.E. Tellier, M.T. Ollukaren, J.S. Temenoff, E.A. Botchwey, Quantitative analysis of immune cell subset infiltration of supraspinatus muscle after severe rotator cuff injury, Regen. Eng. Transl. Med. 3 (2017) 82–93. doi:10.1007/s40883-017-0030-2.

[276] P. Van De Wetering, A.T. Metters, R.G. Schoenmakers, J.A. Hubbell, Poly(ethylene glycol) hydrogels formed by conjugate addition with controllable swelling, degradation, and release of pharmaceutically active proteins, J. Control. Release. 102 (2005) 619–627. doi:10.1016/j.jconrel.2004.10.029.

[277] M.E. Ogle, C.E. Segar, S. Sridhar, E.A. Botchwey, Monocytes and macrophages in tissue repair: Implications for immunoregenerative biomaterial design, Exp. Biol. Med. 241 (2016) 1084–1097. doi:10.1177/1535370216650293.

[278] S.F. Badylak, J.E. Valentin, A.K. Ravindra, G.P. McCabe, A.M. Stewart-Akers, Macrophage phenotype as a determinant of biologic scaffold remodeling., Tissue Eng. Part A. 14 (2008) 1835–42. doi:10.1089/ten.tea.2007.0264.

[279] C.M. Kolf, E. Cho, R.S. Tuan, Mesenchymal stromal cells. Biology of adult mesenchymal stem cells: regulation of niche, self-renewal and differentiation., Arthritis Res. Ther. 9 (2007) 204. doi:10.1186/ar2116.

[280] J. Kreuger, M. Phillipson, Targeting vascular and leukocyte communication in angiogenesis, inflammation and fibrosis, Nat. Rev. Drug Discov. 15 (2016) 125–142. doi:10.1038/nrd.2015.2.

[281] G.A. Hudalla, T.S. Eng, W.L. Murphy, An approach to modulate degradation and mesenchymal stem cell behavior in poly(ethylene glycol) networks, Biomacromolecules. 9 (2008) 842–849. doi:10.1021/bm701179s.

[282] K.D. Held, D.C. Medler, Toxicity of the sulfhydryl-containing radioprotector dithiothreitol, Radiat. Res. Soc. 112 (1987) 544–554.

[283] M.B. Browning, S.N. Cereceres, P.T. Luong, E.M. Cosgriff-Hernandez, Determination of the in vivo degradation mechanism of PEGDA hydrogels, J. Biomed. Res. A. 102 (2014) 4244–4251. doi:10.1002/jbm.a.35096.Determination.

[284] E.M. Christenson, M. Dadsetan, M. Wiggins, J.M. Anderson, A. Hiltner, Poly (carbonate urethane) and poly (ether urethane) biodegradation : In vivo studies, Wiley Intersci. (2004). doi:10.1002/jbm.a.30002.

[285] H. Xu, Y. Deng, D. Chen, W. Hong, Y. Lu, X. Dong, Esterase-catalyzed dePEGylation of pH-sensitive vesicles modified with cleavable PEG-lipid derivatives, J. Control. Release. 130 (2008) 238–245. doi:10.1016/j.jconrel.2008.05.009.

[286] M. Zamani, M.P. Prabhakaran, E.S. Thian, S. Ramakrishna, Controlled delivery of stromal derived factor-1alpha from poly lactic-co-glycolic acid core-shell particles to recruit mesenchymal stem cells for cardiac regeneration, J. Colloid Interface Sci. 451 (2015) 144–152. doi:10.1016/j.jcis.2015.04.005.
[287] J. Yang, L. Zhang, C. Yu, X.-F. Yang, H. Wang, Monocyte and macrophage differentiation: circulation inflammatory monocyte as biomarker for inflammatory diseases., Biomark. Res. 2 (2014) 1. doi:10.1186/2050-7771-2-1.
[288] K.C. McCullough, S. Basta, S. Knotig, H. Gerber, R. Schaffner, Y.B. Kim, A. Saalmuller, A. Summerfield, Intermediate stages in monocyte – macrophage differentiation modulate phenotype and, Immunology. 98 (1999) 202–212.
[289] C.E. Olingy, C.L. San Emeterio, M.E. Ogle, J.R. Krieger, A.C. Bruce, D.D. Pfau, B.T. Jordan, S.M. Peirce, E.A. Botchwey, Non-classical monocytes are biased progenitors of wound healing macrophages during soft tissue injury, Sci. Rep. 7 (2017) 447. doi:10.1038/s41598-017-00477-1.
[290] S.K. Gupta, K. Pillarisetti, P.G. Lysko, Modulation of CXCR4 expression and SDF-1 α functional activity during differentiation of human monocytes and macrophages, J. Leukoc. Biol. 66 (1999) 135–143.
[291] J.G. Tidball, Inflammatory processes in muscle injury and repair, Am. J. Physiol. - Integr. Comp. Physiol. 288 (2005) 345–353. doi:10.1152/ajpregu.00454.2004.
[292] B. Chazaud, M. Brigitte, H. Yacoub-Youssef, L. Arnold, R. Gherardi, C. Sonnet, P. Lafuste, F. Chretien, Dual and beneficial roles of macrophages during skeletal muscle regeneration., Exerc. Sport Sci. Rev. 37 (2009) 18–22. doi:10.1097/JES.0b013e318190ebdb.
[293] F. Merly, L. Lescaudron, T. Rouaud, F. Crossin, Marie France Gardahaut, Macrophages enhnace muscle satellite cell proliferation and delay their differentiation, Muscle Nerve. (1999) 724–732.
[294] T. Kinnaird, E.S. Burnett, M. Shou, C.W. Lee, S. Barr, S. Fuchs, S.E. Epstein, Local delivery of marrow-derived stromal cells augments collateral perfusion through paracrine mechanisms, Circulation. 109 (2004) 1543–1549. doi:10.1161/01.CIR.0000124062.31102.57.
[295] K. Le Blanc, D. Mougiakakos, Multipotent mesenchymal stromal cells and the innate immune system, Nat. Rev. Immunol. 12 (2012) 383–396. doi:10.1038/nri3209.
[296] I.G. Winkler, N. a Sims, A.R. Pettit, V. Barbier, B. Nowlan, F. Helwani, J. Ingrid, Bone marrow macrophages maintain hematopoietic stem cell (HSC) niches and their depletion mobilizes HSC Bone marrow macrophages maintain hematopoietic stem cell (HSC) niches and their depletion mobilizes HSC, 116 (2010) 4815–4829. doi:10.1182/blood-2009-11-253534.
[297] I. Petit, D. Jin, S. Rafii, The SDF-1 – CXCR4 signaling pathway : a molecular hub modulating neo-angiogenesis, Trends Immunol. 28 (2007) 299–307.
[298] S.H. Schirmer, F.C. van Nooijen, J.J. Piek, N. van Royen, Stimulation of collateral artery growth: travelling further down the road to clinical application., Heart. 95 (2009) 191–7. doi:10.1136/hrt.2007.136119.
[299] N. Van Royen, M. Voskuil, I. Hoefer, M. Jost, S. De Graaf, F. Hedwig, J.P. Andert, T.A.M. Wormhoudt, J. Hua, S. Hartmann, C. Bode, I. Buschmann, W. Schaper, R. Van Der Neut, J.J. Piek, S.T. Pals, CD44 regulates arteriogenesiss in

mice and is differentially expressed in patients with poor and good collateralization, Circulation. 109 (2004) 1647–1652. doi:10.1161/01.CIR.0000124066.35200.18.
[300] T. Tobe, N. Okamoto, M.A. Vinores, N.L. Derevjanik, S.A. Vinores, D.J. Zack, P.A. Campochiaro, Evolution of neovascularization in mice with overexpression of vascular endothelial growth factor in photoreceptors, Invest. Ophthalmol. Vis. Sci. 39 (1998) 180–188.
[301] S. Jung, J. Kleinheinz, Angiogenesis — The Key to Regeneration, Regen. Med. Tissue Eng. - Chapter 19. (2013) 453–473. doi:10.5772/46192.
[302] K. Golan, Y. Vagima, A. Ludin, T. Itkin, S. Cohen-Gur, A. Kalinkovich, O. Kollet, C. Kim, A. Schajnovitz, Y. Ovadya, K. Lapid, S. Shivtiel, A.J. Morris, M.Z. Ratajczak, T. Lapidot, S1P promotes murine progenitor cell egress and mobilization via S1P1-mediated ROS signaling and SDF-1 release, Blood. 119 (2012) 2478–2488. doi:10.1182/blood-2011-06-358614.
[303] J.G. Cannon, B.A. St. Pierre, Cytokines in exertion-induced skeletal muscle injury, Mol. Cell. Biochem. 179 (1998) 159–167. doi:10.1023/A:1006828425418.
[304] C. Smith, M.J. Kruger, R.M. Smith, K.H. Myburgh, The inflammatory response to skeletal muscle injury: Illuminating complexities, Sport. Med. 38 (2008) 947–969. doi:10.2165/00007256-200838110-00005.
[305] S.J. Park, K.P. Lee, S. Kang, J. Lee, K. Sato, H.Y. Chung, F. Okajima, D.S. Im, Sphingosine 1-phosphate induced anti-atherogenic and atheroprotective M2 macrophage polarization through IL-4, Cell. Signal. 26 (2014) 2249–2258. doi:10.1016/j.cellsig.2014.07.009.
[306] J.E. Hughes, S. Srinivasan, K.R. Lynch, R.L. Proia, P. Ferdek, C.C. Hedrick, Sphingosine-1-phosphate induces an antiinflammatory phenotype in macrophages, Circ. Res. 102 (2008) 950–958. doi:10.1161/CIRCRESAHA.107.170779.
[307] J.R. Nofer, M. Bot, M. Brodde, P.J. Taylor, P. Salm, V. Brinkmann, T. Van Berkel, G. Assmann, E.A.L. Biessen, FTY720, a synthetic sphingosine 1 phosphate analogue, inhibits development of atherosclerosis in low-density lipoprotein receptor-deficient mice, Circulation. 115 (2007) 501–508. doi:10.1161/CIRCULATIONAHA.106.641407.
[308] A.O. Awojoodu, M.E. Ogle, L.S. Sefcik, D.T. Bowers, K. Martin, K.L. Brayman, K.R. Lynch, S.M. Peirce-Cottler, E. Botchwey, Sphingosine 1-phosphate receptor 3 regulates recruitment of anti-inflammatory monocytes to microvessels during implant arteriogenesis., Proc. Natl. Acad. Sci. U. S. A. 110 (2013) 13785–90. doi:10.1073/pnas.1221309110.
[309] J. Rivera, R.L. Proia, A. Olivera, The alliance of sphingosine-1-phosphate and its receptors in immunity, Nat Rev Immunol. 8 (2009) 753–763. doi:10.1038/nri2400.THE.
[310] P. Quint, M. Ruan, L. Pederson, M. Kassem, J.J. Westendorf, S. Khosla, M.J. Oursler, Sphingosine 1-phosphate (S1P) receptors 1 and 2 coordinately induce mesenchymal cell migration through s1p activation of complementary kinase pathways, J. Biol. Chem. 288 (2013) 5398–5406. doi:10.1074/jbc.M112.413583.
[311] J.A. Gracie, Interleukin-18 as a potential target in inflammatory arthritis, Clin. Exp. Immunol. 136 (2004) 402–404. doi:10.1111/j.1365-2249.2004.02475.x.
[312] P. Conti, M. DiGioacchino, MCP-1 and RANTES are mediators of acute and

chronic inflammation., Allergy Asthma Proc. 22 (2001) 133–137. doi:10.2500/108854101778148737.
[313] M. Jergenson, G. Le, D.A. Lowe, Expression of Pro-inflammatory Chemokines CXCL1 and CXCL5 is Rapidly Upregulated Following Traumatic Injury, (2015).
[314] N. Iikuni, Q.L.K. Lam, L. Lu, G. Matarese, A. La Cava, Leptin and Inflammation, Curr Immunol Rev. 4 (2008) 70–79. doi:10.2174/157339508784325046.Leptin.
[315] F.O. Martinez, S. Gordon, The M1 and M2 paradigm of macrophage activation: time for reassessment., F1000Prime Rep. 6 (2014) 13. doi:10.12703/P6-13.
[316] S. Kiriakidis, E. Andreakos, C. Monaco, B. Foxwell, M. Feldmann, E. Paleolog, VEGF expression in human macrophages is NF-kappaB-dependent: studies using adenoviruses expressing the endogenous NF-kappaB inhibitor IkappaBalpha and a kinase-defective form of the IkappaB kinase 2, J. Cell Sci. 116 (2003) 665–674. doi:10.1242/jcs.00286.
[317] R. Matsumoto, T. Omura, M. Yoshiyama, T. Hayashi, S. Inamoto, K.R. Koh, K. Ohta, Y. Izumi, Y. Nakamura, K. Akioka, Y. Kitaura, K. Takeuchi, J. Yoshikawa, Vascular endothelial growth factor-expressing mesenchymal stem cell transplantation for the treatment of acute myocardial infarction, Arterioscler. Thromb. Vasc. Biol. 25 (2005) 1168–1173. doi:10.1161/01.ATV.0000165696.25680.ce.
[318] B.R. Wamhoff, K.R. Lynch, T.L. Macdonald, G.K. Owens, Sphingosine-1-phosphate receptor subtypes differentially regulate smooth muscle cell phenotype, Arterioscler. Thromb. Vasc. Biol. 28 (2008) 1454–1461. doi:10.1161/ATVBAHA.107.159392.
[319] E.J. Gang, J.A. Jeong, S.H. Hong, S.H. Hwang, S.W. Kim, I.H. Yang, C. Ahn, H. Han, H. Kim, Skeletal myogenic differentiation of mesenchymal stem cells isolated from human umbilical cord blood., Stem Cells. 22 (2004) 617–24. doi:10.1634/stemcells.22-4-617.
[320] A.C. Drost, S. Weng, G. Feil, J. Schäfer, S. Baumann, L. Kanz, K.D. Sievert, A. Stenzl, R. Möhle, In vitro myogenic differentiation of human bone marrow-derived mesenchymal stem cells as a potential treatment for urethral sphincter muscle repair, Ann. N. Y. Acad. Sci. 1176 (2009) 135–143. doi:10.1111/j.1749-6632.2009.04610.x.
[321] N. Sevivas, F.G. Teixeira, R. Portugal, L. Araújo, L.F. Carriço, N. Ferreira, M. Vieira da Silva, J. Espregueira-Mendes, S. Anjo, B. Manadas, N. Sousa, A.J. Salgado, S.C. Serra, Mesenchymal Stem Cell Secretome: A Potential Tool for the Prevention of Muscle Degenerative Changes Associated With Chronic Rotator Cuff Tears, Am. J. Sports Med. 45 (2017) 179–188. doi:10.1177/0363546516657827.
[322] L. Pelosi, C. Giacinti, C. Nardis, G. Borsellino, E. Rizzuto, C. Nicoletti, F. Wannenes, L. Battistini, N. Rosenthal, M. Molinaro, A. Musaro, Local expression of IGF-1 accelerates muscle regeneration by rapidly modulating inflammatory cytokines and chemokines, FASEB J. 21 (2007) 1393–1402. doi:10.1096/fj.06-7690com.
[323] N.L. Millar, M. Akbar, A.L. Campbell, J.H. Reilly, S.C. Kerr, M. McLean, M. Frleta-Gilchrist, U.G. Fazzi, W.J. Leach, B.P. Rooney, L.A.N. Crowe, G.A.C. Murrell, I.B. McInnes, IL-17A mediates inflammatory and tissue remodelling

events in early human tendinopathy, Sci. Rep. 6 (2016) 1–11. doi:10.1038/srep27149.
[324] M. Saclier, S. Cuvellier, M. Magnan, R. Mounier, B. Chazaud, Monocyte / macrophage interactions with myogenic precursor cells during skeletal muscle regeneration, FEBS J. 280 (2013) 4118–4130. doi:10.1111/febs.12166.
[325] B. Chazaud, C. Sonnet, P. Lafuste, G. Bassez, A. Rimaniol, F. Poron, F. Authier, P.A. Dreyfus, R.K. Gherardi, Satellite cells attract monocytes and use macrophages as a support to escape apoptosis and enhance muscle growth, 163 (2003) 1133–1143. doi:10.1083/jcb.200212046.
[326] B. Deng, M. Wehling-Henricks, S.A. Villalta, Y. Wang, J.G. Tidball, IL-10 Triggers Changes in Macrophage Phenotype That Promote Muscle Growth and Regeneration, J. Immunol. 189 (2012) 3669–3680. doi:10.4049/jimmunol.1103180.
[327] K. -i. Kim, -Catenin Overexpression Augments Angiogenesis and Skeletal Muscle Regeneration Through Dual Mechanism of Vascular Endothelial Growth Factor-Mediated Endothelial Cell Proliferation and Progenitor Cell Mobilization, Arterioscler. Thromb. Vasc. Biol. 26 (2006) 91–98. doi:10.1161/01.ATV.0000193569.12490.4b.
[328] G.A. Meyer, A.L. Farris, E. Sato, M. Gibbons, J.G. Lane, S.R. Ward, A.J. Engler, M.E.T. Al, Muscle Progenitor Cell Regenerative Capacity in the Torn Rotator Cuff, J. Orthop. Res. (2015) 421–429. doi:10.1002/jor.22786.
[329] S.A. Shah, I. Kormpakis, L. Cavinatto, M.L. Killian, S. Thomopoulos, L.M. Galatz, Rotator cuff muscle degeneration and tear severity related to myogenic, adipogenic, and atrophy genes in human muscle, J. Orthop. Res. 35 (2017) 2808–2814. doi:10.1002/jor.23593.
[330] K.C. Loh, W. Leong, M.E. Carlson, B. Oskouian, A. Kumar, H. Fyrst, M. Zhang, R.L. Proia, E.P. Hoffman, J.D. Saba, Sphingosine-1-Phosphate Enhances Satellite Cell Activation in Dystrophic Muscles through a S1PR2 / STAT3 Signaling Pathway, 7 (2012). doi:10.1371/journal.pone.0037218.
[331] S. Calise, S. Blescia, F. Cencetti, C. Bernacchioni, C. Donati, P. Bruni, Sphingosine 1-phosphate stimulates proliferation and migration of satellite cells. Role of S1P receptors, Biochim. Biophys. Acta - Mol. Cell Res. 1823 (2012) 439–450. doi:10.1016/j.bbamcr.2011.11.016.
[332] H. Yin, F. Price, M.A. Rudnicki, Satellite Cells and the Muscle Stem Cell Niche, Physiol Rev. 93 (2013) 23–67. doi:10.1152/physrev.00043.2011.
[333] B.N. Brown, B.D. Ratner, S.B. Goodman, S. Amar, S.F. Badylak, Macrophage polarization: An opportunity for improved outcomes in biomaterials and regenerative medicine, Biomaterials. 33 (2012) 3792–3802. doi:10.1016/j.biomaterials.2012.02.034.Macrophage.
[334] C. Sunderkotter, T. Nikolic, M.J. Dillon, N. van Rooijen, M. Stehling, D.A. Drevets, P.J.M. Leenen, Subpopulations of Mouse Blood Monocytes Differ in Maturation Stage and Inflammatory Response, J. Immunol. 172 (2004) 4410–4417. doi:10.4049/jimmunol.172.7.4410.